THE UNIVERSITY
of EDINBURGH

Cellular and circuit excitability in rodent models of neurodevelopmental disorders

Laura M Simões de Oliveira, B.Sc. M.Sc.

THE UNIVERSITY *of* EDINBURGH

A thesis submitted for the degree of Doctor of Philosophy

Biomedical Sciences

College of Medicine and Veterinary Medicine

University of Edinburgh

July 2020

Abstract

Autism spectrum disorders and intellectual disabilities (ASD/ID) are estimated to affect approximately 3-5% of the population. Genetic factors constitute a major risk factor in ASD/ID, accounting for 40 to 50% of cases, with monogenic forms of syndromic ASD representing 5% of cases. Many of the genetic causes of ASD/ID are thought to share common phenotypes at the cellular level, thus animal models of monogenic forms of ASD/ID provide a valuable tool to better understand the underlying pathophysiology of these disorders.

In this thesis I examined two rodent models of monogenic forms of ASD/ID associated with developmental delay, impaired cognitive function and epilepsy, namely CDKL5 deficiency disorder (CDD) and Fragile X Syndrome (FXS). First, I examined synaptic function and intrinsic excitability in the hippocampus of a novel *Cdkl5* knockout (*Cdkl5*$^{-/y}$) rat model of CDD. I show an increase in long-term potentiation (LTP) in the hippocampus of *Cdkl5*$^{-/y}$ rats, consistent to what has previously been reported in mouse models of this disorder. I extend this finding by using a combination of electrophysiological and histological techniques to assess the properties of pre-synaptic neurotransmitter release together with multiple post-synaptic mechanisms that may contribute to the observed *Cdkl5*$^{-/y}$ phenotype. Intriguingly, I demonstrated that many of the mechanisms that have been postulated to underlie enhanced LTP are not altered in *Cdkl5*$^{-/y}$ rats when tested at the single cell level, including changes in AMPAR/NMDAR ratios and increased expression of Ca^{2+}-permeable AMPA receptors.

Second, I examined the contribution of the axon initial segment (AIS) to the cellular hyperexcitability of CA1 pyramidal cells in the *Fmr1*$^{-/y}$ mouse model of FXS. I show that increased AIS length in CA1 pyramidal cells in *Fmr1*$^{-/y}$ mice is associated with cellular hyperexcitability. I show that depolarisation induced AIS plasticity is unaltered in *Fmr1*$^{-/y}$ neurons *in vitro* and in *ex vivo* brain slices, and present data to suggest that the observed changes in cellular excitability result from homeostatic compensation for reduced entorhinal cortex (EC) inputs, in order to regulate CA1 pyramidal cell output. Indeed, CA1 pyramidal cell output is unaltered in *Fmr1*$^{-/y}$ mice, despite an observed reduction in synaptic transmission of EC inputs.

In the final chapter of this thesis, I built on my findings in the hippocampus of *Fmr1*$^{-/y}$ mice and examine the AIS developmental trajectory, as well as the regulation of intrinsic excitability and AIS plasticity *in vivo*, in the visual cortex of *Fmr1*$^{-/y}$ mice.

I found the AIS developmental trajectory to be affected in a layer specific manner, with *Fmr1*$^{-/y}$ mice exhibiting a typical developmental profile in L2/3 and 5 but altered AIS development in L4. However, I did not observe an effect of visual deprivation on AIS length or cellular excitability in either genotype.

In summary, this thesis provides insights into the cellular excitability and synaptic physiology in two rodent models of monogenic ASD/ID. I further our existing understanding of rodent models of CDD by characterising hippocampal synaptic and intrinsic physiology in a novel rat model of this disorder, highlighting the need for the identification of robust cross species phenotypes that can be used as potential biomarkers and therapeutic targets in CDD. Furthermore, I put forward the notion of AIS regulation as a contributor to the underpinning of cellular excitability in rodent models of FXS. Additionally, this work contributes to the growing body of evidence showing that compensatory mechanisms have a major contribution to the phenotypes observed in rodent models of ASD/ID, and which should be taken into consideration when developing potential treatment strategies.

Lay Summary

Autism spectrum disorders (ASD) and intellectual disability (ID) are believed to affect 3 to 5% of the population with many affected individuals at high risk of presenting with other neurological conditions such as anxiety, depression and epilepsy. Currently there are no effective treatments to improve the quality of life of severely affected individuals, and as such a better understanding of the mechanisms that give rise to these disorders is necessary so that we might be able to offer potential therapeutic interventions.

The brain is composed of a complex network of specialised cells called neurons, which controls our every action and thought. Neurons communicate with each other at specialised contact points called synapses, through electrical and chemical signals. It is thought that dysfunctions in either the signalling between neurons or in the way brain networks are formed and linked contribute to epilepsy, cognitive and social deficits in ASD/ID.

In my thesis I have studied two animal models in which genes normally expressed on the X chromosome have been genetically silenced so the proteins encoded by those genes are no longer made. These animal models represent two human conditions which are severe neurodevelopmental disorders associated with ASD/ID and epilepsy: CDKL5 deficiency disorder (CDD) and Fragile X Syndrome (FXS).

In my thesis I have examined the electrical and chemical signalling properties of both single neurons and networks of neurons that lack either CDKL5 or FMRP, the two proteins that are absent in CDD and FXS, respectively In particular, I have focused in a brain region called the hippocampus, a region that is critical for our ability to form and recall memories and which also is a region where epileptic seizures can be initiated.

In the CDD model, neurons in the hippocampus show an increased ability to change the strength of their communication. I propose that this enhanced change in communication is actually detrimental potentially contributing to abnormal memory formation.

In FXS, reduced communication between neurons led to a compensatory change in the portion of the neuron responsible for generating electrical signals, the axon initial segment (AIS). Altered AIS structure made FXS neurons more responsive than typical neurons. I propose that such a change is beneficial as it helps neurons regulate their output in a way that compensates for the reduced communication they receive.

The work presented in this thesis contributes to the understanding of the altera-

tions at the cellular level that contribute to altered cognition and epilepsy in ASD/ID. Importantly, this work shows that some of the alterations in the function of neurons in ASD/ID are compensatory rather than detrimental; this should be taken into account when developing potential treatments.

Acknowledgement

The work presented in this thesis would not have been possible without the guidance and support of all the people I have had the pleasure of working with for the past four years, all my friends and family.

First and foremost, I would like to thank my supervisors Prof David Wyllie and Prof Peter Kind for the opportunity of being part of the Kind/Wyllie lab, and for your guidance and academic support over the past four years.

I will always be grateful to Dr Sam Booker for teaching me everything and answering endless questions, for sharing with me his enthusiasm, for the all the discussions about physiology, and for all the guidance and advice. It's been a pleasure working alongside you!

I would further like to thank many others that provided me with technical support throughout my PhD: Dr Adam Jackson and Dr Emma Perkins for their patience and help with troubleshooting; Rita Loureiro for being a great slicing partner and providing all the coffee; Dr Owen Dando for his time and patience with my never-ending questions about GLMMs; Dr Paul Baxter for providing cultured neurons for my experiments and helping out with the film from the dark cabinet; Dr Anna Toft for all the help with LaTeX and proofreading parts of this thesis. Thank you Dr Alison Thomson, for constantly cheering me on, for reading parts of this thesis even when she'd left the lab, and for all the cat pictures, they made all the difference.

I would also like to thank Dr Susana Louros for introducing me to research in the first place and for her support and advice during my PhD.

A very special thanks to my PhD companions Tasha Anstey and Joanna Smith for sharing this adventure with me, for their friendship and continuous support.

A thank you to Hannah and Cate for making me feel at home in Edinburgh from the moment I arrived.

To Margarida, Mariana and Pedro, thank you for always being there despite the distance.

A huge thanks to my family, mãe, pai e Sofia, for always believing in me. I would never have made it this far without your support.

Finally, a huge thank you to Riccardo for being there for the past 3 years and especially for supporting me through the writing of this thesis, it would have been so much harder without you.

Declaration

This work was carried out in the Centre for Discovery Brain Sciences, School of Biomedical Sciences at the University of Edinburgh. I declare that this thesis was composed by myself and that the work contained herein is my own, unless otherwise stated and with exception of the following:

- LTP recordings from *Cdkl5* rats were performed by Ms Rita Loureiro
- Dissociated cultures used in Figure 4.6. were prepared by Dr Paul Baxter
- GFP mice used in chapter 4 were provided by Professor Peter Brophy's lab
- Dr Owen Dando and Dr Zrinko Kozic performed the statistical analysis for the data in chapter 4.

The data presented in chapter 4 has been accepted for publication at Cell Reports under the title "Input-output relationship of CA1 pyramidal neurons reveals intact homeostatic mechanisms in a mouse model of Fragile X Syndrome" and results from joint work between myself and Dr Sam Booker with specific contributions as follows:

- Dr Sam Booker contributed with the data in Figures 4.1, 4.4 and 4.9.
- AIS length data in Figure 4.2.C was collected and analysed by myself in collaboration with Dr Sam Booker and Ms Natasha Anstey.
- AIS length data in Figure 4.3.B was collected and analysed by myself and Ms Natasha Anstey, recordings presented in Figure 4.3. C-E were performed by myself and Dr Sam Booker.
- In Figure 4.8, I analysed the data from live imaging experiments performed by Dr Sam Booker.
- The data in Figure 4.10. was collected and analysed by myself and Dr Sam Booker.
- Dr Sam Booker helped with AIS analysis for DR AIS data presented in chapter 5.

No part of the work contained in this thesis has been submitted for any other degree or professional qualification.

Signed: Laura Helen Oliveira Date: 15/07/2020

Contents

List of Abbreviations

ACSF	Artificial cerebrospinal fluid
ADHD	Attention deficit and hyperactivity disorder
AHP	afterhyperpolarisation
AIS	Action initial segment
AMPA	α-amino-3-hydroxy-5-methyl-4-isoxazolepropionic acid
AMPAR	AMPA receptor
AnkG	Ankyrin G
AP	Action potential
ASD	Autism spectrum disorder
CA	*Cornu Ammonis*
CDD	CDKL5 Deficincy Disorder
CP-AMPAR	Calcium permeable AMPA receptor
DR	Dark rearing
EC	Entorhinal cortex
EE	Environmental enrichment
EPSC	Excitatory post-synaptic current
fEPSP	Field excitatory postsynaptic potential
fMRI	Functional magnetic resonance imaging
FXS	Fragile X Syndrome
HCN	Hyperpolarization-activated cyclic nucleotide–gated
I-V	current/voltage
ID	Intellectual disability
IF	Current/frequency
IR-DIC	Infrared differential interference contrast
ISI	Interstimulus interval
ITI	Intertrial interval
KO	Knock-out
KO	knock out
LEH	Long-Evans hooded
LTD	Long-term depression
LTP	Long-term potentiation

MD	Monocular deprivation
mEPSC	Miniature EPSC
mIPSCs	miniature inhibitory post-synaptic currents
mPFC	Medial prefrontal cortex
MRI	Magnetic resonance imaging
NGS	Normal goat serum
NMDA	N-methyl-D-aspartate
NMDAR	NMDA receptor
OD	Ocular dominance
PB	Phosphate buffer
PBS	Phosphate-buffered saline
PCR	Polymerase chain reaction
PFA	Paraformaldehyde
PL	Pre-limbic
PP	*Perforant path*
PPR	Paired pulse ratio
R_i	Input resistance
R_a	Access resistance
RMP	Resting membrane potential
S1	Primary somatosensory cortex
sEPSC	Spontaneous EPSC
SLM	*Stratum lacunosum moleculare*
SO	*Stratum oriens*
SR	*Stratum radiatum*
TTX	Tetrodotoxin
V1	Primary visual cortex
VGCC	Voltage gated calcium channel
VGSC	Voltage gated sodium channel
WT	Wild-type

List of Figures

List of Tables

Chapter 1

Introduction

1.1 Autism spectrum disorder and intellectual disability

Autism spectrum disorders (ASD) and intellectual disability (ID) are thought to affect 3 to 5% of the population worldwide, making them the most common developmental disorders in humans (Srivastava and Schwartz, 2014).

ASD/ID are highly heterogenous conditions both regarding phenotypic variability as well as etiology, with genetic, epigenetic and environmental factors all known to contribute. Single gene mutations are estimated to account for over 50% of severe ASD/ID cases (McRae et al., 2017; Sztainberg and Zoghbi, 2016). A Deciphering Developmental Disorders (DDD) whole-exome sequencing study revealed 42% of sporadic cases of ASD to result from single gene *de novo* mutations (McRae et al., 2017). However, this study only considered cases with no previously diagnosed genetic causes, leaving out patients with known monogenic causes associated with ASD, such as Fragile-X syndrome, Rett Syndrome, and Phelan-McDermid Syndrome, estimated to constitute an additional 5% of cases (Sztainberg and Zoghbi, 2016).

ASD diagnosis is made based on impairments in three behavioural domains: social interaction, communication and restricted interests and repetitive sterotypical behaviours (Bailey et al., 1996). ID is defined by an impairment in at least two adaptive behaviours and an intelligence quotient (IQ) of less than 70 by the age of 18 (van Bokhoven, 2011). ASD/ID are often co-occurring disorders with up to 70% of individuals with ASD also being affected with ID (Betancur, 2011), and an estimated 10 to 30% of individuals with ID being co-diagnosed with ASD (Srivastava and Schwartz, 2014). In addition to ASD/ID, affected individuals can present with a variety of co-morbidities, including attention deficit and hyperactivity disorder (ADHD), sensory hypo- and hyper-

sensitivities, anxiety and depression (LoVullo and Matson, 2009; Kerns et al., 2015). Furthermore, these co-occurring features appear to be more severe in individuals with ID also diagnosed with ASD (Cervantes and Matson, 2015). Epilepsy is a particularly common feature of ASD/ID individuals, with an estimated 20 to 30% of all affected individuals also presenting with seizures. Co-occurring ASD, ID and epilepsy result in severe neurodevelopmental disorders which are typically diagnosed in infancy when children present with delays in achieving developmental milestones, such as learning to speak or walk.

The diversity in etiology and manifestation of ASD/ID presents a challenge in terms of diagnosis as well as in the development of therapeutic strategies. With no current therapies to ameliorate symptoms, severe cases of ASD/ID present a burden to carers and society, as the behavioural phenotypes and co-morbidities of severely affected individuals can make it impossible to function in typical social or employment settings, rendering them dependent on families and carers throughout life. A better understanding of the underlying mechanisms of these disorders is therefore imperative in order to develop effective therapeutic interventions, that can contribute to a better quality of life. In particular, given the low frequency of individual ASD/ID causes, a better understanding of common and diverging features between different causes of ASD/ID would be invaluable when considering therapeutic strategies that can be effective in a larger proportion of ASD/ID individuals.

Given their identifiable cause, monogenic forms of ASD/ID have been at the core of research into the underlying mechanisms of these disorders, as they can be easily modelled in a laboratory setting with resort to transgenic animals. It is thought that cellular phenotypes might be shared across different forms of ASD/ID (Barnes et al., 2015), therefore the study of monogenic forms of autism might provide an insight into the pathophysiology of ASD/ID as a whole. As such, the work presented in this thesis will be focused on two models of genetic forms of ASD/ID with co-occurring epilepsy: Fragile X Syndrome (FXS) and CDKL5 deficiency disorder (CDD).

1.1.1 Fragile X Syndrome

FXS is one of the most common inherited forms of ID and a leading single gene cause of autism. FXS was initially described in 1943 by Martin and Bell as a new X-linked form of ID (Martin and Bell, 1943), and is estimated to affect 1 in 4000 males

and 1 in 8000 females (Turner et al., 1996; Crawford et al., 2001; Coffee et al., 2009). It is characterised by cognitive impairment, delayed or absent speech, autistic features, sensory hypersensitivities, ADHD and anxiety (Cordeiro et al., 2011). There is a high incidence of epilepsy amongst FXS individuals, with up to 20% exhibiting seizures (Berry-Kravis, 2002; Musumeci et al., 1999).

FXS is caused by the expansion of a trinucleotide repeat (>200 CGG repeats) on chromosome Xq27.3, upstream the promoter region of the *FMR1* gene. This ultimately leads to DNA hypermethylation, transcriptional silencing of the gene (Bell et al., 1991; Sutcliffe et al., 1992), and consequent absence of its protein product, FMRP (Pieretti et al. (1991), Figure 1.1).

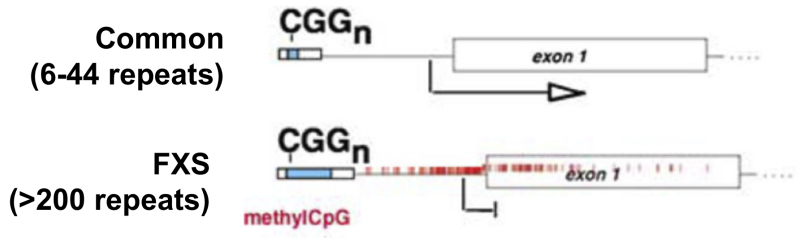

Figure 1.1: Transcriptional silencing of the *FMR1* gene in FXS. Black arrow represents transcription in typically developing individuals. Red dashes indicate methylation. Hypermethylation in individuals with >200 CGG repeats results in transciptional silencing of the gene. Figure adapted from Garber et al. (2008)

FMRP is an mRNA binding protein acting as a negative regulator of translation. FMRP is thought to associate directly with the translational machinery, thus stalling ribosomes and preventing polypeptide elongation (Darnell et al., 2011). Given FMRPs role as a translation repressor, protein synthesis is increased in the absence of FMRP (Osterweil et al., 2010; Till et al., 2015). FMRP is highly expressed in neurons, it localises to dendritic spines, and is dynamically regulated by synaptic activity (Gabel et al., 2004; Weiler and Greenough, 1999). In fact, many of its identified target mRNAs encode synaptic proteins, with as many as 30% of post-synaptic density (PSD) proteins and 30% of pre-synaptic proteins being under FMRP regulation (Brown et al., 2001; Darnell et al., 2011). Therefore, loss of FMRP can have a great impact on synaptic function and plasticity (Till, 2010; Sidorov et al., 2013).

The well described monogenic cause of FXS has allowed modelling of the human disorder in rodents. The first *Fmr1* knock out (KO, $Fmr1^{-/y}$) mouse model of FXS was generated by The Dutch-Belgian Fragile X Consortium in 1994 and has since been

widely used to study the pathophysiology of FXS (reviewed in Kazdoba et al. (2014)). Whilst this mouse model does not express FMRP, *Fmr1* mRNA is still present in KO mice, as such a second mouse model (*Fmr1* KO2) was generated whereby deletion of the *Fmr1* promoter and first exon results in the absence of both FMRP and *Fmr1* mRNA (Mientjes et al., 2006). $Fmr1^{-/y}$ mice recapitulate some of the features of the human condition including higher seizure susceptibility, hypersensitivity to sensory stimuli, heightened anxiety and learning impairments (Musumeci et al., 2000; Van Dam et al., 2000; D'Hooge et al., 1997; Gaudissard et al., 2017). More recently, rat models of FXS have been generated and despite differences at the behaviour level, rats appear to share phenotypes with the mouse model of FXS at the cellular level, including enhanced long-term depression in the hippocampus and enhanced protein synthesis (Till et al., 2015; Asiminas et al., 2019).

1.1.2 CDKL5 Deficiency Disorder

CDD is a severe neurological disorder caused by mutations in the X-linked cyclin-dependent kinase-like 5 gene (*CDKL5*; MIM: 300203). CDD individuals were initially diagnosed as atypical cases of Rett syndrome, due to the manifestation of stereotypical behaviours, sleep disturbances, and severe cognitive deficits characteristic of Rett's (Bahi-Buisson and Bienvenu, 2012). However, early onset epilepsy is a defining feature of CDD, with 90% of individuals presenting with seizures by 3 months of age. As many as 80% of children with CDD have daily seizures, which become resistant to treatment. Other common features of the disorder include severe developmental delay, intellectual disability, autistic features and motor impairments (Bahi-Buisson and Bienvenu, 2012; Fehr et al., 2016; Olson et al., 2019).

Mutations in the *CDKL5* gene were first identified in two patients by Kalscheuer et al. (2003), from then on the number of people diagnosed with CDD has grown as genetic testing becomes more frequent. Nonetheless, CDD is a rare genetic condition with recent estimates suggesting an incidence of 1 in 42400 live births (Symonds et al., 2019). Females are estimated to represent 80% of cases, as pathogenic mutations in *CDKL5* are thought to impact male fetal viability (Olson et al., 2019).

CDKL5 is a serine/threonine kinase, with 5 known human (*hCdkl5*) and mouse (*mCdkl5*) isoforms and 4 isoforms identified in the rat (*rCdkl5*). Importantly, the N-terminus of the protein, which includes the catalytic domain of CDKL5, is highly

conserved across mice, rats and humans (Hector et al., 2017b, 2016). Isoform 1 of CDKL5 is highly expressed in the brain, including in the cortex and hippocampus and its expression is developmentally regulated, increasing post natally both in mouse and human brain tissue (Hector et al., 2016).

Although pathogenic mutations in CDKL5 can be detected across the majority of the coding regions of the gene, missense mutations predicted to result in loss of catalytic function preferably cluster in the catalytic domain (Figure 1.2, Hector et al. (2017b)). Given the relevance of the catalytic domain in CDD, recent efforts have been made to identify CDKL5 phosphorylation targets. Phophoproteomic studies have highlighted proteins involved in cytoskeleton regulation and DNA damage as potential CDKL5 substrates, however the vast majority of the substrates are yet to be validated (Baltussen et al., 2018; Muñoz et al., 2018). Other suggested roles for CDKL5 include cell proliferation, neuronal differentiation (Fuchs et al., 2014) and synaptogenesis (Mari et al., 2005).

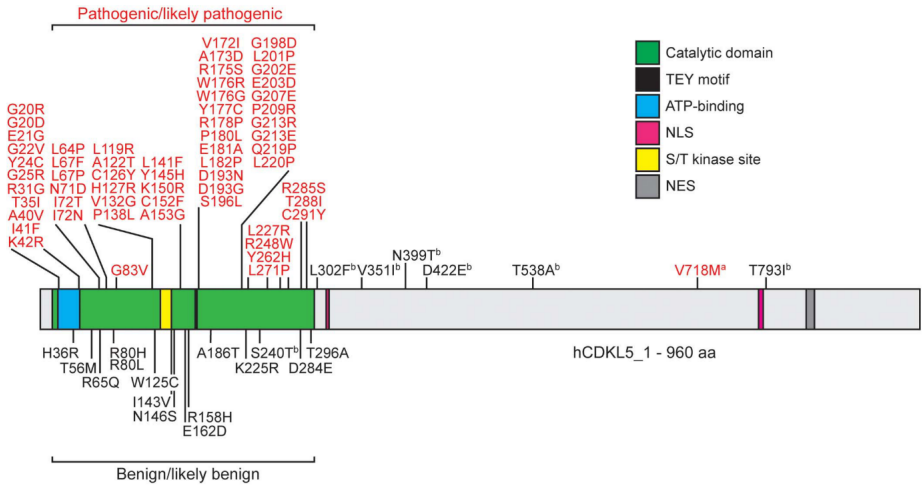

Figure 1.2: Schematic representation of pathogenic missense mutations (red) localised to the catalytic domain (green) of CDKL5. Figure adapted from Hector et al. (2017b)

Given the monogenic nature of CDD, transgenic mice have so far been the model of choice to study CDD. The number of mouse models available to study CDD has grown since the first KO mouse model of CDD (*Cdkl5*$^{-/y}$) was generated by Wang et al. (2012). Several other mouse models have now been created either by knocking out the *Cdkl5* gene (Wang et al., 2012; Amendola et al., 2014; Okuda et al., 2017) or knocking in pathogenic mutations identified in CDD patients (Yennawar et al., 2019; Tang et al., 2019). In contrast to the human condition, mouse models of CDD do not present

with spontaneous seizures (Amendola et al., 2014; Wang et al., 2012; Okuda et al., 2017). However, new evidence from Liao et al. (2020) suggests that neonatal mice (up to P12) exhibit spontaneous seizures and that this phenotype would have been missed in earlier studies examining adult mice. Motor and learning impairments have been reported in mouse models of CDD (Amendola et al., 2014; Okuda et al., 2018; Tang et al., 2019). There are conflicting reports on the prevalence of anxiety like-behaviours in mouse models of CDD, with one showing increased prevalence (Okuda et al., 2018) and another reporting unaltered anxiety (Tang et al., 2019) depending on the mouse model studied. With many phenotypic discrepancies across mouse models, it has been challenging to identify biomarkers that might translate to the human condition. As such, in this thesis I have used a *Cdkl5*$^{-/y}$ rat model of CDD in order to identify potential cross species phenotypes that can be used as reliable markers of the disorder. Similar to the mouse, the rat model does not exhibit spontaneous seizures, but it exhibits motor impairments and impaired hippocampal dependent learning when tested on an active-place avoidance task (Vijay Kumar, Shashank Tiwari, *unpublished*, see Appendix A).

1.2 Brain areas affected in ASD/ID

Given the sphere of co-occurring conditions in ASD/ID, a number of brain regions involved in cognitive function, anxiety, and sensory processing have been implicated in the pathophysiology of these disorders.

Work in our lab has taken an comprehensive approach examining a wide range of brain areas and circuits, from the somatosensory cortex (Till et al., 2012; Domanski et al., 2019; Booker et al., 2019), to the hippocampus (Barnes et al., 2015; Till et al., 2015; Asiminas et al., 2019) as well as other brain areas involved in emotional processing (on going), in order to understand the underlying mechanisms contributing to sensory, emotional processing, and cognitive phenotypes in ASD/ID. The work presented in this thesis has focused on hippocampal and cortical function in rodent models of two monogenic forms of ASD/ID with co-occurring epilepsy, as such the following section will give an account of hippocampal and cortical organisation.

Hippocampal function has been widely studied in the context of ASD/ID. Structural MRI has revealed abnormal hippocampal structure in ASD individuals (Dager et al.,

2007). FXS individuals in particular exhibit impaired performance in spatial memory tasks (Cornish et al., 1999; Kemper et al., 1988). Impaired spatial performance is shared by the rodent models of FXS, with the FXS mouse model exhibiting impaired spatial representation (Arbab et al., 2018) and the rat model exhibiting altered developmental trajectory of hippocampal-dependent memory tasks (Asiminas et al., 2019). Hippocampal function has not been studied in detail in CDD patients however, the selective absence of CDKL5 in forebrain excitatory neurons results in impaired hippocampal dependent learning and memory (Tang et al., 2017). Impaired acquisition and retention of spatial memory has also been reported in *Cdkl5*$^{-/y}$ mice (Okuda et al., 2018), indicating a role for CDKL5 in cognitive function and in particular in hippocampal-dependent learning and memory.

Altered cortical function is though to underlie abnormal sensory processing as well as cognitive impairments in ASD/ID, with both sensory and integrative cortical areas being implicated in the pathophysiology of these disorders. Sensory cortical areas such as the primary visual (V1), somatosensory (S1) and auditory cortices, are responsible for integration of sensory inputs. Altered auditory, tactile and visual processing have all been identified in FXS individuals (Kogan et al., 2004b; Ethridge et al., 2017). These are mirrored by altered cortical function and development in the mouse model of FXS (Domanski et al., 2019; Zhang et al., 2014; Chen and Toth, 2001; Harlow et al., 2010; Till et al., 2012). Cortical visual impairment is common amongst CDD patients, affecting at least 75% of individuals (Olson et al., 2019). Mouse models of CDD have shown altered sensory processing, including altered visual and auditory processing, as well as atypical whisker responses (Wang et al., 2012; Mazziotti et al., 2017; Pizzo et al., 2019).

Integrative cortical areas such as the medial prefrontal cortex (mPFC) are involved in higher executive function (reviewed in Miller et al. (2001), Euston et al. (2012)). The mPFC is responsible for integrating information arriving from other cortical and subcortical areas to exert top-down control of behaviour. As such, it is involved in cognitive processes, including working memory, as well as in processing internal states. Given the role of mPFC in cognition and emotion, mPFC function has been widely studied in ASD/ID individuals. MRI studies report reduced long range connectivity between mPFC and other cortical areas (Yerys et al., 2015; Doyle-Thomas et al., 2015; Washington et al., 2014). Rodent models of FXS exhibit impairments in mPFC dependent behaviours (Sidorov et al., 2014; Gantois et al., 2013; Kramvis et al., 2013)

accompanied by cellular level phenotypes (Krueger et al., 2011; Meredith et al., 2007; Martin et al., 2015; Asiminas et al., 2019). In rodent models of CDD, altered anxiety-like behaviours and impaired fear memory acquisition have been reported (Okuda et al., 2018).

1.2.1 Hippocampal anatomy and connectivity

The hippocampus is one of the most widely studied structures in the mammalian CNS. Its role in memory and learning was first identified by Scoville and Milner through lesion studies (Scoville and Milner, 1957). Following the discovery of place cells in rodents (O'Keefe and Dostrovsky, 1971), O'Keefe and Nadel suggested the hippocampus as a cognitive map, establishing the importance of this structure in spatial representation of the environment (O'Keefe and Nadel (1978), reviewed in Eichenbaum et al. (1999)). Functional magnetic resonance imaging (fMRI) studies have revealed the role of the hippocampus in spatial memory to be conserved in humans (Maguire et al. (1996, 1998), reviewed in Burgess et al. (2002)). The low seizure threshold in the hippocampus (Green, 1964) also makes this a brain region of interest in the study of epilepsy. Indeed, hippocampal neuronal loss and atrophy are characteristic of temporal lobe epilepsy patients (Dam, 1980; Cook et al., 1992; Cendes et al., 1993), and it is not yet clear whether these are causative or a result of epileptic activity. Importantly, plasticity of the hippocampal microcircuit makes it particularly susceptible to epileptogenesis. Goddard et al. (1969) have shown that repeated electrical stimulation gradually resulted in increased seizure susceptibility and spontaneous seizures. Given the roles of the hippocampus in cognitive function and epilepsy, the study of this structure is of particular interest in the context of ASD/ID.

The hippocampal formation is part of the limbic system. It consists of a group of structures, including the hippocampus, dentate gyrus (DG), subiculum, presubiculum, parasubiculum, and entorhinal cortex (EC) (Lorente De Nó, 1934; Blackstad, 1956). Similar to cortical regions, the hippocampus is composed mainly of excitatory pyramidal cells, which account for approximately 90% of hippocampal neurons. Inhibitory interneurons make up 10% of hippocampal neurons and are highly diverse (for review see Booker and Vida (2018); Klausberger (2009)).

The hippocampus is a laminated structure (Lorente De Nó, 1934; Blackstad, 1956). The most superficial of its layers is the *alveus* which contains the axons of pyramidal

cells that leave the hippocampus and project to other brain areas. Next, the *stratum oriens* (*SO*) contains the basal dendrites of pyramidal cells, whose cell bodies constitute the *stratum pyramidale* (*SP*). The more proximal apical dendrites of pyramidal neurons are located in the *stratum radiatum* (*SR*) and bifurcate into the more distal tuft dendrites in the *stratum lacunosum moleculare* (*SLM*). The hippocampus is divided into *Cornu Ammonis* (CA) regions, with subregions from CA1 to CA3, based on the diversity of morphological and connectivity properties of pyramidal cells (Ramon y Cajal, 1911; Lorente De Nó, 1934). A schematic representation of the different hippocampal subregions and laminar structure is shown in Figure 1.3.

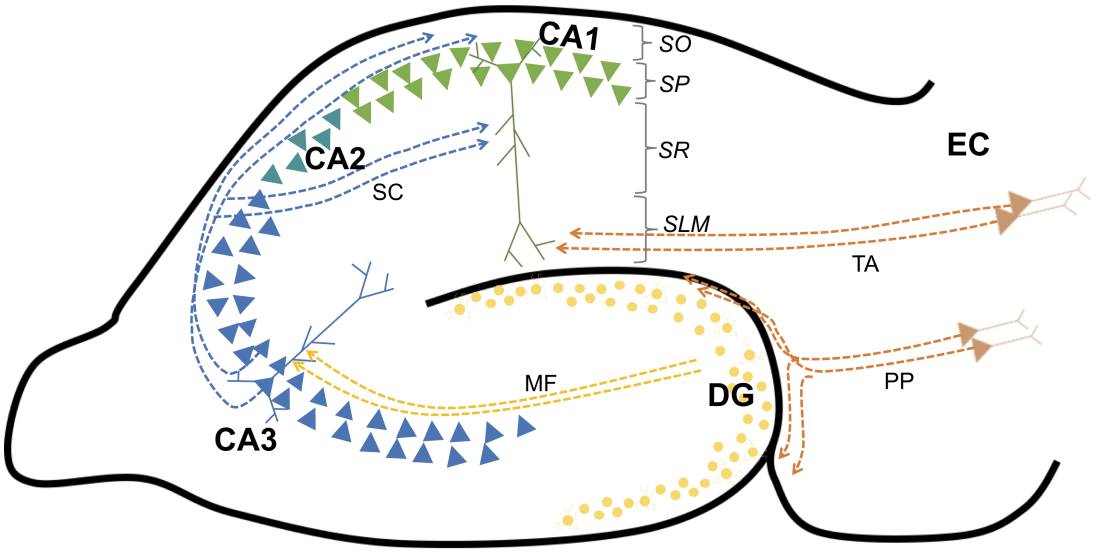

Figure 1.3: Schematic representation of excitatory synaptic connectivitity in the hippocampus, showing areas of hippocampal formation CA1 (light green), CA2 (teal), CA3 (blue), dentate gyrus (DG, yellow) and enthorhinal cortex (EC, orange). Pyramidal cells are represented as triangles, color coded by region and DG granule cells as circles. Dashed lines represent axons for the different hippocampal afferent pathways: perforant path (PP), mossy fibres (MF), Schaffer collaterals (SC) and temporoammonic (TA), with arrows indicating the direction of AP propagation. Hippocampal layer boundaries are indicated by grey brakets (from superficial to deep *stratum oriens (SO)*, *stratum pyramidale (SP)*, *stratum radiatum (SR)*, *stratum lacunosum-moleculare (SLM)*.

Transmission of excitatory inputs is thought to be unidirectional in the hippocampus, and is classicaly described as the tri-synaptic loop (reviewed in Amaral and Witter (1989), Figure 1.3), with extrinsic information arriving from the EC into the DG via the perforant path (PP) afferents. DG granule cells then connect to the apical dendrites of CA3 pyramidal neurons via mossy fibre axons. CA3 pyramidal neurons are highly interconnected, forming a recurrent network. CA3 pyramidal neurons also project to

CA1 via the Schaffer collateral (SC) pathway. CA3 axons form synaptic connections onto the apical dendrites of CA1 pyramidal neurons in the *SR*. CA3 axons can also branch and form synapses onto the basal dendrites of CA1 pyramidal cells in the *SO*. In addition to CA3 inputs, CA1 pyramidal cells receive direct extrahippocampal inputs from the EC. Layer 3 pyramidal cells from the EC project to CA1 and synapse onto the distal apical dendrites of CA1 pyramidal neurons in the *SLM* constituting the temporoammonic (TA) pathway. The loop of synaptic transmission is closed by CA1 axons projecting back to the EC.

1.2.2 Canonical cortical column

Cortical brain areas exhibit a canonical column organisation (Figure 1.4), with L4 and L6 being the main input layers of the cortex (Crocker-Buque et al., 2014; Crandall et al., 2017). L4 receives direct inputs from the thalamus, with excitatory neurons connecting to superficial layers (Shepherd and Svoboda, 2005). Pyramidal neurons in the superficial layers of the cortex then project to pyramidal neurons in the deeper layers (L5, L6, Olivas et al. (2012)) which constitute the main output neurons in the cortex, sending long range projections to other cortical or subcortical areas. L4 is more pronounced in the granular cortex which constitutes sensory areas, and less pronounced in the integrative cortex. (for review see Harris and Mrsic-flogel (2013); Bannister (2005). Pyramidal neurons are the main excitatory neurons in the cortex. Representing approximately two thirds of all neurons in the cortex, pyramidal neurons are found through all cortical layers except layer 1. Despite sharing morphological features such as a long apical dendrite that extends through the cortical layers above the cell body, specific morphology and physiological characteristics differ across pyramidal cells located in different cortical layers and with distinct projection targets (Aerde and Feldmeyer, 2015; Connors and Gutnick, 1990; Schubert et al., 2001). In addition to pyramidal cells, spiny stellate cells are excitatory neurons found exclusively in L4 of S1. These are characterised by the radial disposition of their dendrites and absence of an apical dendrite. Similar to the hippocampus inhibitory interneurons comprise a small proportion of cortical neurons, approximately 20% and are highly diverse (Bannister, 2005).

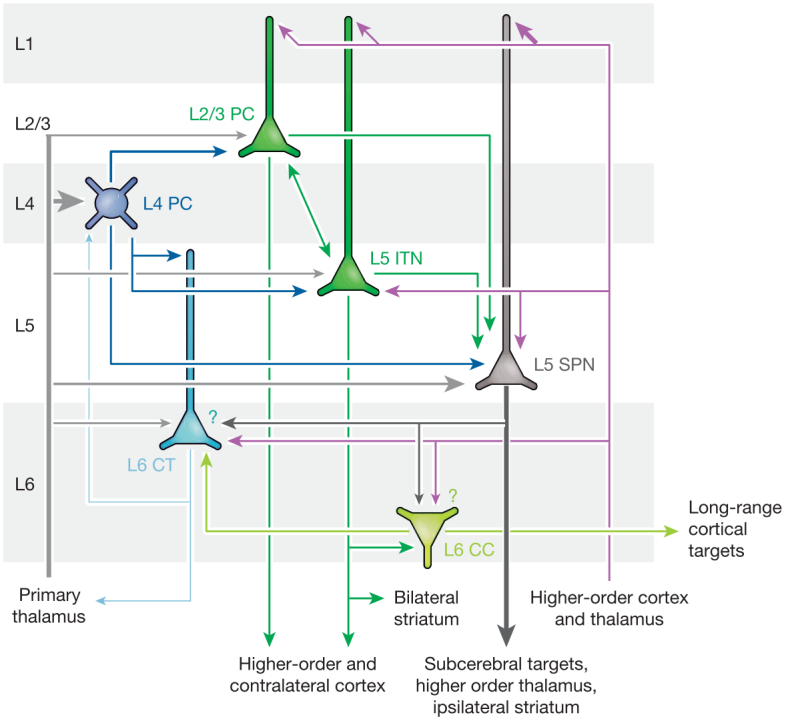

Figure 1.4: Schematic representation of connectivity in cortical columns (image from Harris and Mrsic-flogel (2013)) Arrows indicate direction of synaptic transmission, with line thickness representing strength of synaptic connections. Question marks indicate projections that are predicted but not yet confirmed. Different cell types are colour coded based on projection targets: light blue - primary thalamus; dark blue - local cortical targets; green - local cortical connections and contralateral cortex; light green - long-range cortical targets; gray - subcerebral targets, higher-order thalamus and striatum. Light gray lines indicate synaptic input from the primary thalamus and purple lines indicate synaptic input from higher-order cortex and thalamus.

1.3 Shared pathophysiology in ASD/ID

A variety of genes with known roles in chromatin remodelling, protein synthesis and degradation, cytoskeleton dynamics and synaptic transmission have been strongly associated with ASD/ID (Srivastava and Schwartz, 2014; Bourgeron, 2015). Despite the diversity of biological processes in which ASD-risk genes are involved, synaptic dysfunction is common to many monogenic forms of ASD/ID and believed to contribute to behavioural aspects of these disorders (Zoghbi and Bear, 2012; Volk et al., 2015). In addition to synaptic mechanisms, altered cellular excitability is suggested to underlie hyperexcitability of neuronal circuits, thus contributing to common co-occurring conditions in ASD/ID, such as sleep abnormalities, sensory hypersensitivities and epilepsy (Contractor et al., 2015; Nelson and Valakh, 2015). As such, for the remainder of this chapter I will provide a description of the synaptic and intrinsic excitability mechanisms known to contribute to the circuit dysfunction in FXS and CDD.

1.4 Synaptic Function

1.4.1 Excitatory synapses

Glutamate is the most abundant excitatory neurotransmitter in the CNS, as such glutamatergic synapses are responsible for most of the fast excitatory neurotransmission. Glutamatergic synapses are typically assymetrical and located on dendritic spines. They are composed of pre- and post-synaptic compartments separated by the synaptic cleft.

Pre-synaptic boutons are found in the axon terminals, and are highly enriched in synaptic vesicles containing glutamate. Membrane depolarisation at the nerve terminal triggered by an action potential results in calcium influx through voltage gated calcium channels (VGCCs). Intracellular calcium signalling cascades then lead to the mobilisation of the pre-synaptic machinery and ultimately to the release of glutamate at the active zone (Murthy and Camilli, 2003). Glutamate release into the synaptic cleft then activates receptors on the post-synaptic membrane, eliciting excitatory synaptic events. As such, synaptic vesicle release probability, the kinetics of vesicle recycling and the glutamate content of pre-synaptic vesicles can all influence the synaptic response in the post-synaptic cell. Pre-synaptic release probability is typically assessed by examining paired pulse ratio (PPR) of synaptic responses. PPR is inversely correlated with release

probability, with low release probability synapses exhibiting high PPR and vice-versa (Millar et al., 2002; Zucker and Regehr, 2002). In the hippocampus, SC synapses onto CA1 pyramidal cells exhibit variable probability of release but are generally facilitating (*i.e.* PPR>1), reflecting low release probability (Dobrunz and Stevens, 1997; Hanse and Gustafsson, 2001a).

The post synaptic compartment of glutamatergic synapses is typically located in dendritic protrusions called spines. The postsynaptic density (PSD) is located in the spine head, opposite the pre-synaptic bouton. It is composed of a dense network of scaffolding proteins, neutransmitter receptors, and signaling molecules (Sheng and Hoogenraad, 2007).

Glutamate can bind to both metabotropic (mGluRs) and ionotropic receptors in the post-synaptic membrane. Intracellular signalling downstream of mGluRs has major roles in synaptic function and plasticity. Indeed, abnormal mGluR signaling and mGluR dependent synaptic plasticity is a hallmark of the mouse model of FXS (for review see Bear et al. (2004)).

Ionotropic glutamate receptors include α-amino-3-hydroxy-5-methyl-4-isoxazolepropionic acid (AMPA), N-methyl-D-aspartate (NMDA), and kainate (KA) receptors (AMPARs, NMDARs, and KARs, respectively). All ionotropic glutamate receptors are transmembrane tetrameric protein complexes with their subunit composition determining channel conductance, kinetics, and signaling (Henley and Wilkinson, 2016).

AMPARs are typically heterotetramers composed of subunits GluA1-4. The GluA2 subunit is particularly important in regulating receptor conductance, kinetics and cation permeability. GluA2-containing receptors exhibit low calcium permeability, low conductance and open probability (Jonas et al., 1994). On the other hand, GluA-2 lacking AMPARs are modulated by intracellular polyamines and have high calcium permeability, high conductance and open probability and exhibit inward rectification (Kamboj et al., 1995; Jonas et al., 1994). Therefore, AMPAR receptor subunit composition, particularly regarding GluA2 presence, can greatly affect AMPAR function and, consequently, synaptic transmission.

NMDARs are heterotetrameric cation channels composed of two GluN1 subunits and two GluN2A/B/C/D or GluN3A/B subunits, with GluN1/GluN2A and GluN1/GluN2B being the most common combinations (reviewed in Sanz-Clemente et al. (2013)). As is the case for AMPARs, NMDAR subunit composition modulates channel properties.

GluN2A or GluN2B containing diheteromeric NMDARs exhibit high-conductance, high sensitivity to voltage dependent extracellular Mg^{2+} block, while GluN2C or GluN2D containing receptors have lower channel conductance, and lower sensitivity to extracellular Mg^{2+}. The voltage-dependent Mg^{2+} block of NMDARs means their activation requires the presence of glutamate and post-synaptic depolarisation simultaneously, therefore NMDARs act as coincidence detectors at the synapse. In contrast to AMPARs, GluN2 subunit composition does not have a large impact on the Ca^{2+} permeability of NMDARs. However, GluN2A and GluN2B subunits have an important role in determining channel kinetics and pharmacology, with GluN2A containing receptors exhibiting faster kinetics and lower ifenprodil sensitivity relative to GluN2B containing receptors (Williams, 1993; Gallagher et al., 1996). In CA1 of the hippocampus, the expression of NMDAR subtype is pathway specific, with SC synapses onto CA1 pyramidal cells expressing more GluN2B containing receptors, relative to PP synapses (Arrigoni and Greene, 2004).

1.4.2 Development of synapse composition

The composition of the post-synaptic membrane changes throughout development. In early postnatal development, excitatory synapses containing NMDAR and no AMPAR are thought to be functionally silent (Liao et al., 1995; Isaac et al., 1995), due to the voltage dependent Mg^{2+} block of NMDARs. Once AMPAR receptors are recruited to the PSD, these synapses become active and produce a post-synaptic response upon neurotransmitter release. Indeed, using minimal stimulation of thalamocortical synapses, Isaac et al. (1997) reported a reduction in functionally silent synapses in the mouse somatosensory cortex during the first 10 postnatal days. Consistent with this idea, immuno-electron microscopy studies have reported an increase in expression of AMPARs over the first 5 postnatal weeks in CA1 (Petralia et al., 1999), whilst NMDAR expression remained stable. This is functionally reflected in increase AMPAR/NMDAR ratio during postnatal development (Crair and Malenka, 1995; Hsia et al., 1998).

Specific subunit composition of neurotransmitter receptors is also developmentally regulated. During early development NMDAR receptors are mainly composed of GluN2B whilst at the end of the first post natal week, NMDARs containing the GluN2A subunit are widely expressed, resulting in faster NMDAR mediated synaptic events (Williams, 1993). Indeed, this is the case in CA1 pyramidal cells too, where ifenprodil sensitivity is reduced in the first post-natal week, reflective of a lower con-

tribution of GluN2B to synaptic transmission (Kirson et al., 1999). Ca^{2+} permeable GluA2-lacking AMPARs (CP-AMPARs) are expressed in early development and are replaced by Ca^{2+} impermeable GluA2-containing AMPARs by the second post-natal week (Kumar et al., 2002). Indeed, the GluA2 subunit is highly expressed in mature CA1 pyramidal cells (He et al., 1998). The expression and composition of glutamate receptors has therefore a crucial role in the development and maintenance of synaptic transmission and consequently shaping circuit function.

1.4.3 Synaptic plasticity

Synapses are dynamic structures that undergo both structural and functional plasticity throughout development and altered activity states. Major forms of synaptic plasticity in the brain include Hebbian (or associative) forms of plasticity, which is thought to be the cellular correlate for learning and memory (Bliss and Collingridge, 2013), and homeostatic plasticity, which is crucial to stabilise network activity (Turrigiano and Nelson, 2004).

The interplay of diverse forms of plasticity is complex and thought to be crucial to appropriate circuit function (Turrigiano, 2017; Vitureira and Goda, 2013).

1.4.3.1 Hippocampal Synaptic Plasticity

Initially postulated by Hebb, Hebbian plasticity is a positive-feedback process whereby strong synaptic connections are strengthened further ("cells that fire together, wire together" Hebb (1949)). Later on Stent suggested a converse mechanism whereby weak synapses are weakened further, making them less effective ("cells that fire out of sync lose their link", Stent (1973)). These processes result in long-term potentiation (LTP) or depression (LTD) of synaptic connections respectively and are believed to represent cellular correlates for learning and memory.

Electrophysiological studies in *ex vivo* tissue have been the gold standard to examine the mechanisms of synaptic plasticity. Bliss and Lomo initially described synaptically induced LTP in hippocampal slices (Bliss and Lømo, 1973). In this study tetanic stimulation induced strengthening of the synaptic response in the PP pathway whilst a control pathway was unaffected, showing input specificity of LTP induction, in line with Hebb's postulate.

The CA3-CA1 synapse in the hippocampus is possibly the most extensively studied

in the context of synaptic plasticity. Tetanic stimulation of the SC axons is known to result in LTP in postsynaptic CA1 pyramidal cells. LTP induction with this protocol is dependent on NMDAR function. Depolarisation of the postsynaptic cell, with coincident glutamate binding to NMDARs, leads to fast, large Ca^{2+} influx through NMDARs. Ca^{2+} then acts a second messenger activating signalling cascades that result in LTP (Malenka and Bear, 2004). On the other hand, low frequency stimulation of presynaptic axons with no activation of the postsynaptic cell, leads to a prolonged and slow Ca^{2+} influx and induces LTD (Yang et al. (1999), for review see Malenka and Bear (2004); Luscher and Malenka (2012)).

The mechanisms resulting in LTP expression are numerous with evidence of altered pre- and post-synaptic function upon LTP induction depending on cell type and developmental stage studied (reviewed in Bliss and Collingridge (2013)). Post-synaptic mechanisms include AMPAR insertion at the post-synaptic membrane, which is thought to result in strengthening of the post-synaptic response (Figure 1.5). This was first observed in early development, where a reduction synaptic transmission failures post LTP induction was suggested to result from AMPAR insertion at initially silent synapses (Isaac et al., 1995; Liao et al., 1995). This finding was later on supported by the results of Lledo et al. (1998) demonstrating for the first time that post-synaptic membrane fusion events are required for LTP expression. Additionally, Lüscher et al. (1999) showed that manipulating endocytosis and exocytosis affects AMPAR mediated currents and disrupts synaptic plasticity. A large body of evidence has grown since supporting the hypothesis of post-synaptic expression of LTP, giving notorious attention to AMPAR receptor expression and trafficking (reviewed in Collingridge et al. (2004); Huganir and Nicoll (2013)). AMPAR subtype also has been suggested to contribute to LTP, it is thought that a transient increase in synaptic CP-AMPARs contributes to LTP maintenance (Appleby et al., 2011; Guire et al., 2008; Plant et al., 2006). Indeed, mice lacking the GluA2 subunit of AMPAR exhibit enhanced LTP in the CA1 region of the hippocampus (Jia et al., 1996).

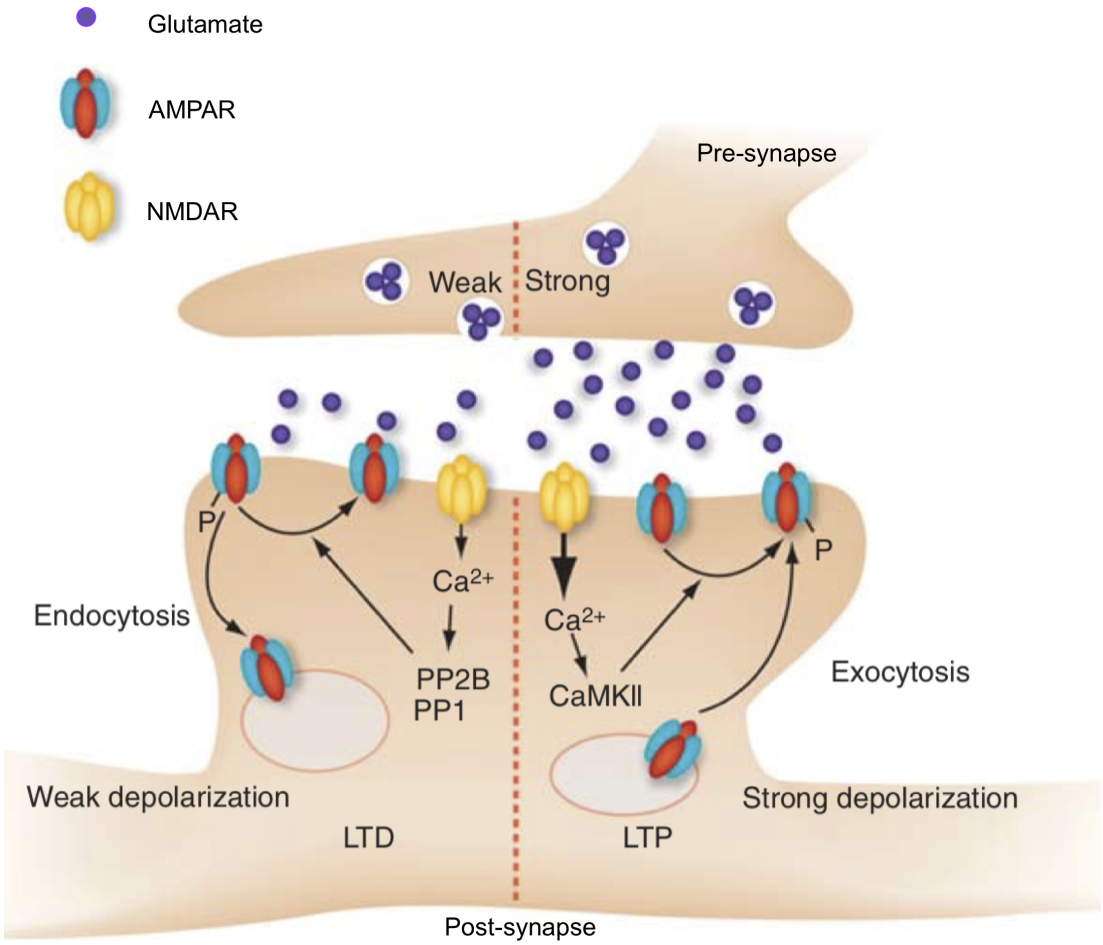

Figure 1.5: Schematic representation of post-synaptic expression of LTD and LTP (adapted from Luscher and Malenka (2012)). LTD induction results in endocytosis of AMPAR and consequent weakening of synaptic strength. LTP induction leads to AMPAR insertion at the post-synaptic membrane and consequent strengthening of the synaptic response.

1.4.3.2 Experience dependent plasticity in the cortex

Experience dependent plasticity has a particularly important role in the maturation and refinement of sensory systems (Sengpiel and Kind, 2002). Critical periods for experience dependent plasticity in sensory systems have been described across a variety of species and represent windows of opportunity during which neuronal circuits are particularly susceptible to being shaped by experience, such that early life experience helps shaping circuit function, permanently altering its performance (Hensch, 2005).

Initial studies by Hubel and Wiesel (1970) described a time-window, or critical period, for experience dependent plasticity in the kitten visual cortex during which monocular deprivation (MD) in early post-natal life leads to a reduction in the number of neurons that respond to visual input from the deprived eye, resulting in an ocular dominance (OD) shift. Importantly, disruption of visual input during this critical period has long lasting effects, affecting circuit function in later life.

In addition to Hebbian plasticity mechanisms, different types of homeostatic plasticity contribute to maintain network activity within a dynamic range (Burrone and Murthy, 2003; Turrigiano and Nelson, 2004; Marder and Goaillard, 2006), these include activity dependent changes in threshold for plasticity induction (Abraham and Bear, 1996) and synaptic scalling (Turrigiano, 2008).

Bienenstock, Cooper and Munro first put forward the idea that synaptic strength is determined by the magnitude of the post-synaptic response relative to a sliding modification threshold, formalised as the BCM theory. The modification threshold determines the stimulation intensity at which there is no LTP/LTD induction (with LTP and LTD being induced above and below that threshold, respectively), and is itself regulated by experience and previous activity state of the post-synaptic neuron (Bienenstock et al., 1982). The ability of past experience to induce changes in threshold for subsequent plasticity induction, represents a homeostatic mechanism designated metaplasticity (Abraham and Bear, 1996), whereby increased neuronal activity increases the modification threshold thus promoting LTD over LTP, whilst reduced neuronal activity results in the opposite effect. In line with this idea, dark rearing results in enhanced LTP and reduced LTD in rat cortical slices, an effect that is reversed when rats are exposed to light for 2 days prior to slice preparation (Kirkwood et al., 1996).

Homeostatic scaling of synaptic responses was first described by Turrigiano et al. (1998) in dissociated cultures of neocortical neurons. Activity blockade with TTX or

CNQX for 48 hours led to increased AMPAR mediated synaptic transmission. Conversely, blocking GABA-A receptor mediated inhibition with bicuculine resulted in a compensatory reduction in excitatory synaptic transmission (Turrigiano et al., 1998). In the visual cortex, homeostatic scaling of post-synaptic neurotransmitter receptors results in altered E/I balance towards increase excitation following reduction of visual inputs through lid suture or intraocular injection of TTX (Maffei and Turrigiano, 2008). Interestingly, Goel and Lee (2007) have shown that 2 days of visual deprivation is sufficient to enhance AMPAR mediated synaptic transmission in L2/3 of the mouse visual cortex, even in adult mice, suggesting that homeostatic plasticity of synaptic inputs can have a role in regulating circuit function *in vivo* not only during development but also throughout life.

Experience dependent plasticity has also been well described in the mouse primary somatosensory cortex. In the barrel cortex experience dependent plasticity occurs during a narrow time window, decreasing between birth and P4 (Fox, 1992). This aligns with the critical period for LTP and LTD induction at thalamocortical synapses (Crair and Malenka, 1995). Additionally, Stern et al. (2001) have shown that receptive field organisation can be disrupted by sensory deprivation between P12 and P14. Interestingly, similar to homeostatic plasticity in the visual cortex, plasticity windows are layer specific, closing earlier in L4 and with L2/3 remaining plastic for longer (Desai et al., 2002; Goel and Lee, 2007; Stern et al., 2001).

Altered critical periods of plasticity have been suggested to contribute to abnormal circuit development in ASD/ID, as abnormal experience dependent plasticity during these time windows can have life long impact on the wiring of neuronal networks. Indeed, altered critical period plasticity has been reported in mouse models of ASD/ID, including FXS, Rett Syndrome and Angelman Syndrome (reviewed in Fagiolini and Leblanc (2011)).

1.4.4 Synaptic physiology in FXS

FMRP is known to regulate AMPAR trafficking and therefore has a crucial role in regulating excitatory neurotransmission. In the absence of FMRP, AMPAR internalisation is increased (Nakamoto et al., 2007). In line with FMRP's role in AMPAR trafficking, hippocampal neurons in culture exhibit abnormal homeostatic scaling following activity blockade, as treatment with TTX and APV fails to increase the amplitude

of mEPSC as seen in WT (Soden and Chen, 2010). Consistent with reduced surface expression of AMPAR reported in culture (Nakamoto et al., 2007; Soden and Chen, 2010), amplitude of spontaneous EPSCs is reduced in CA1 pyramidal cells (Meredith et al., 2011). However this phenotype is age dependent, emerging during the second post-natal week and returning to typical values by 8 weeks of age, potentially reflecting compensatory mechanisms at the circuit level throughout development.

Enhanced mGluR dependent hippocampal LTD is a hallmark of the mouse model of FXS (Bear et al., 2004). Unaltered NMDAR dependent LTP in the mouse model of FXS has been reported by Godfraind et al. (1996) and Larson et al. (2005), whilst Pilpel et al. (2009) report an age dependent increase in LTP in $Fmr1^{-/y}$ mice. Additionally, Lauterborn et al. (2007) have shown that deficits in LTP in young $Fmr1^{-/y}$ mice are revealed when using a weaker LTP induction protocol and occluded when using stronger stimulation paradigms, indicating that differences in induction protocol can significantly contribute to the discrepancies in phenotypes reported across different studies. Interestingly, Talbot et al. (2018) reported altered LTP following a hippocampal dependent learning paradigm, as *ex vivo* hippocampal slices from trained $Fmr1^{-/y}$ mice exhibited reduced hippocampal LTP, reflecting enhanced experience-dependent plasticity *in vivo*.

In addition to the hippocampal plasticity phenotypes described above, altered critical periods have been reported for experience dependent plasticity in the visual cortex (Dölen et al., 2007) and the auditory cortex (Kim et al., 2013) of $Fmr1^{-/y}$. In the somatosensory cortex, Harlow et al. (2010) reported a delay in the critical period for LTP induction at thalamocortical synapses of $Fmr1^{-/y}$ mice. This delay in maturation of thalamocortical synapses is followed by a delay in the maturation of translaminar connectivity, as $Fmr1^{-/y}$ mice exhibit weaker connectivity between L2/3 and L4 during the second post-natal week which returns to WT levels by the third postnatal week (Bureau et al., 2008).

Other synaptic phenotypes in the somatosensory cortex include a reduction in excitatory inputs onto interneurons leading to disinhibition of L4 stellate cells and consequent circuit hyperexcitability (Gibson et al., 2008). Domanski et al. (2019) revealed reduced connectivity between fast-spiking interneurons and stellate cells in early post-natal development and altered thalamocortical feed-forward inhibition. Interestingly, a recent study by Antoine et al. (2019) suggests that altered E/I balance itself results from

homeostatic compensation in rodent models of ASD/ID including in the *Fmr1*$^{-/y}$ mouse model of FXS. Antoine et al. (2019) showed that enhanced E/I ratio in L2/3 pyramidal neurons in the somatosensory cortex of mouse models of ASD/ID is associated with typical spontaneous firing in response to network activity, rather than circuit hyperexcitability. This study raises two interesting points: firstly neuronal networks in ASD/ID are capable of homeostatic compensation and secondly it raises the possibility that other phenotypes observed in ASD/ID, beyond synaptic E/I balance, might result from homeostatic compensation.

1.4.5 Synaptic physiology in CDD

In the hippocampus, abnormal expression of glutamate receptor subunits is suggested to contribute to altered synaptic plasticity in mouse models of CDD. Yennawar et al. (2019) have reported increased early phase LTP (<30 min) suggested to result from an increase in CP-AMPARs, consistent with the transient role of these receptors in LTP expression (Appleby et al., 2011; Plant et al., 2006). Okuda et al. (2017) suggest increased LTP, due to altered NMDAR function and increased GluN2B expression, as a mechanism contributing to higher sensitivity to chemically induced seizures in *Cdkl5*$^{-/y}$ mice. Indeed, blocking GluN2B containing NMDARs with ifenprodil reduced seizure susceptibility to WT levels.

In transgenic mice lacking CDKL5 in excitatory neurons, Tang et al. (2017) reported trends towards increased frequency of mEPSCs and mIPSCs in CA1 pyramidal cells, and significantly increased inhibitory charge transfer. These data should be considered with caution as they represent recordings from only 3 mice per genotype, however it provides some evidence supporting a role of CDKL5 in synaptic transmission and E/I balance in particular. Indeed, these cellular level phenotypes are reflected at the local circuit level, with altered temporal dynamics of synaptic transmission in the hippocampus, assessed with voltage sensitive dye imaging experiments (Tang et al., 2017). In KO mouse models of CDD, evidence from anatomical studies suggests that E/I balance might be altered in sensory brain areas. In the visual cortex, Pizzo et al. (2016) reported increased density of parvalbumin positive interneurons in L5 (Pizzo et al., 2016). In L4 of the mouse barrel cortex, absence of CDKL5 resulted in reduced density of cortico-cortical excitatory synapses and unaltered inhibitory synapse density, potentially resulting in altered E/I ratio. Furthermore, Pizzo et al. (2019) suggest that the reduction in density of cortico-

cortical synapses might reflect an homeostatic compensation for reduced thalamic input. Nonetheless, these anatomical studies are yet to be supported by functional assessment of synaptic transmission. In contrast with the findings in L4, Della Sala et al. (2016) showed a reduction in spine density accompanied by reduced mEPSC frequency in L5 of the somatosensory cortex in $Cdkl5^{-/y}$ mice.

1.5 Regulation of Cellular Excitability

Pyramidal cells receive thousands of excitatory and inhibitory synaptic inputs. The integration of synaptic inputs occurs along the dendritic tree and in the somatic compartment and is highly dependent on the biophysical properties of the cell membrane (Magee, 2000; Branco and Häusser, 2011). Ion channel composition of the neuronal membrane is therefore crucial in determining cellular excitability (Hodgkin and Huxley, 1952; Turrigiano et al., 1995). In addition to the synaptic mechanisms mentioned previously, intrinsic excitability too can have a large impact on circuit function. Interestingly, intrinsic excitability can also be modulated during learning and in response to altered activity states (Debanne et al., 2019).

Persistent changes in cellular excitability are known to accompany long term synaptic plasticity (LTP/LTD). Indeed, in the hippocampus LTP is accompanied by increased excitability of the post-synaptic neurons (Bliss and Lømo, 1973; Andersen et al., 1980). In CA1 pyramidal cells, synaptic LTP is accompanied by a reduction in AP threshold mediated by a shift in the activation curve of VGSCs, resulting in increased excitability (Xu et al., 2005). Potentiation of intrinsic excitability appears to share some of the mechanisms of synaptic LTP in that it is NMDAR dependent and Ca^{2+} dependent and is suggested to be a cellular correlate for learning and memory. Indeed, changes in cellular excitability during learning have been reported in the hippocampus. Learning of a conditioned eye blink task resulted in a transient increase in cellular excitability in the rabbit hippocampus, mediated by a reduction in K^+ channel mediated afterhyperpolarisation (AHP) and consequent reduction in spike accommodation (Moyer Jr. et al., 1996). In the rat dorsal hippocampus intrinsic excitability increases following learning a spatial memory task (Oh et al., 2003).

In addition to learning and memory, modulation of intrinsic excitability has an important role in regulating neuronal activity in an homeostatic manner. Turrigiano

et al. (1994) first described modulation of intrinsic excitability in response to altered synaptic input in lobster somatogastric ganglion neurons. When isolated in culture these cells exhibit tonic firing, and transition to burst firing mode similar to their *in vivo* behaviour after 4 days in culture, indicating they have the ability to adapt ionic conduction in order to normalise their activity pattern. In cultured hippocampal neurons, chronic depolarisation leads to a reduction in input resistance and consequently to a homeostatic reduction in cellular excitability. This effect is mediated by an increase in leak K^+ current and dependent on NMDAR and L-type Ca^{2+} channels (O'Leary et al., 2010). Importantly, depolarisation induced reduction in excitability is reversible, showing the homeostatic nature of this phenomenon, as neurons are able to return their initial state once the depolarising stimulus is removed.

In addition to the synaptic mechanisms already described, altered cellular excitability is believed to contribute to circuit dysfunction in ASD/ID (Contractor et al., 2015). Thus, an understanding of the mechanisms regulating neuronal excitability is key in order to identify potential therapeutic targets that act to normalise circuit function.

1.5.1 The axon initial segment

If the integration of synaptic inputs reaches the threshold for action potential (AP) firing, APs are initiated at the axon initial segment (AIS) (Kole et al., 2008; Kole and Stuart, 2012), and then travel down the axon until they reach the pre-synaptic terminal and results in neurotransmitter release (Figure 1.6A). The AIS is therefore a key regulator of cellular excitability. Additional functions of the AIS include acting as a diffusion barrier and maintaining cellular polarity. Whilst these functions are important for axonal specification and function these will not be discussed in detail (for review see Leterrier (2018)). Instead I will focus on the role of the AIS as AP initiation site and its influence on cellular excitability.

1.5.1.1 Structure and function

Historically, the AIS has been defined as the initial non-myelinated portion of the axon. Whilst functional studies suggested the initial portion of the axon as the potential site for spike initiation as early as in 1953 (Brock et al., 1953), a morphological characterisation of the AIS was not achieved until 1968 when the studies of Palay et al. (1968) and Peters et al. (1968) used electron microscopy (EM) to describe the

AIS. These early morphological studies described three distinctive features of the AIS: closely apposed bundles of 3 to 10 microtubules (fascicles), a 50 nm thick undercoat lining of the plasma membrane, and an almost complete absence of ribosomes (Palay et al., 1968; Peters et al., 1968). Since then, the study of the molecular composition, as well as structural organisation of the AIS has grown revealing a complex network of scaffolding proteins and ion channels (for review see Leterrier (2018), Figure 1.6B).

Ankyrin G (AnkG) is an AIS specific scaffolding protein. It is often referred to as the "master-organiser" of the AIS, as it has a fundamental role in recruiting other scaffolding proteins, such as βIV-spectrin and neurofascin-186, as well as ion channel to the AIS during its formation. AnkG clusters at the AIS during early development (between E13.5 and P1 *in vivo* or 3-4 days *in vitro* in dissociated cultures), and in its absence AIS development is halted (Zhou et al., 1998).

The structure of AnkG includes a membrane binding domain in its N-terminal, a spectrin binding domain, a serine rich domain, an unstructured tail and a carboxyl-terminal. AnkG's membrane-binding domain is responsible for anchoring ion channels and cell adhesion molecules, including neurofascin-186 (NF-186) and Neuronal-CAM (Nr-CAM) to the membrane. AnkG binds to the underlying actin/spectrin sub-membrane complex through its spectrin binding domain. Super-resolution microscopy studies have shown that AnkG's molecular structure leads to the periodic organisation of structural elements of the AIS (Leterrier et al., 2015). Periodic organisation of structural elements is thought to contribute to robustness and stability of axonal structure, whilst periodicity of ion channel distribution is hypothesised to influence action potential generation and propagation, though this has yet to be tested experimentally.

The high density of voltage gated sodium, potassium and calcium channels is crucial for its role as the site of AP initiation. Ion channels bind to AnkG through their ankyrin targeting motiffs. Moreover, comparative studies show that these binding motifs are highly conserved in vertebrates (Hill et al., 2008), and suggest that the appearance of the AIS in evolution coincided with the development of complex sensory systems.

Voltage gated sodium channels (VGSCs) are responsible for the local depolarising current at the AIS, contributing to the initiation and rise phase of APs (Hodgkin and Huxley, 1952). Kole et al. (2008) have elegantly shown using a combination of electrophysiology and computational modelling that high density of VGSCs at the AIS is required for AP initiation in cortical pyramidal neurons. In line with those findings,

Na^+ imaging studies have subsequently shown high Na^+ influx localised to the AIS (Fleidervish et al., 2010; Bender and Trussell, 2009). VGSC in the brain contain one of four α subunits ($Na_v1.1$, $Na_v1.2$, $Na_v1.3$ and $Na_v1.6$), with subunits $Na_v1.1$, $Na_v1.2$ and $Na_v1.6$ localising to the AIS in a developmental and cell type specific manner. Of these $Na_v1.6$ is the main isoform expressed in the adult CNS and preferentially localises to the distal end of the AIS, with electron microscopy studies estimating the density of $Na_v1.6$ channels in the AIS to be 35 fold higher than that at the soma (Lorincz and Nusser, 2010). The high density of these channels combined with their relatively hyperpolarised activation voltage (15-20 mV) compared to other isoforms (Rush et al., 2005; Hu et al., 2009) contributes to the lower AP threshold at this site. The differential expression of $Na_v1.1$ and 1.2 is thought to shape firing behaviour of different neurons. With $Na_v1.1$ being preferentially expressed in the proximal AIS of GABAergic interneurons (Lorincz and Nusser, 2008). $Na_v1.2$ is expressed as the main AIS VGSC in unmyelinated axons during early development. Upon axon myelination $Na_v1.2$ is gradually replaced by $Na_v1.6$, so that in mature pyramidal cells in the cortex and hippocampus the expression of $Na_v1.2$ is restricted to the proximal portion of the AIS, where it is suggested to contribute to AP back-propagation (Hu et al., 2009). Indeed, a recent study by Spratt and colleagues reported impaired AP backpropagation in a adult transgenic mice that lack $Na_v1.2$ expression (Spratt et al., 2019).

K^+ channel opening after AP initiation contributes to the repolarising phase of APs. Channels of the K_v1 subtype are the most abundantly expressed at the AIS typically localising to the distal end, with both $K_v1.1$ and $K_v1.2$ being present in most neuronal cell types (Lorincz and Nusser, 2008), including cortical and hippocampal pyramidal cells. The high density of K^+ channels regulates AP waveform, with K^+ channel blocking leading to an increase in the half width of axonal APs and consequent increase in neurotransmitter release and synaptic efficacy (Kole et al., 2007). Additionally, blockade of K_v1 channels specifically at the AIS influences intrinsic excitability and firing properties measured in the somatic compartment, resulting in hyperexcitability of CA3 pyramidal cells (Rama et al., 2017), in line with previous studies reporting hyperexcitability in mice lacking $K_v1.1$ (Lopantsev et al., 2003).

KCNQ2 and KCNQ3 ($K_v7.2$ and $K_v7.3$ respectively) mediate the M current. $K_v7.2$ and $K_v7.3$ are localised to the AIS by AnkG (Pan et al., 2006) and generate a slow voltage dependent current that is activated just below spike threshold. In hippocampal

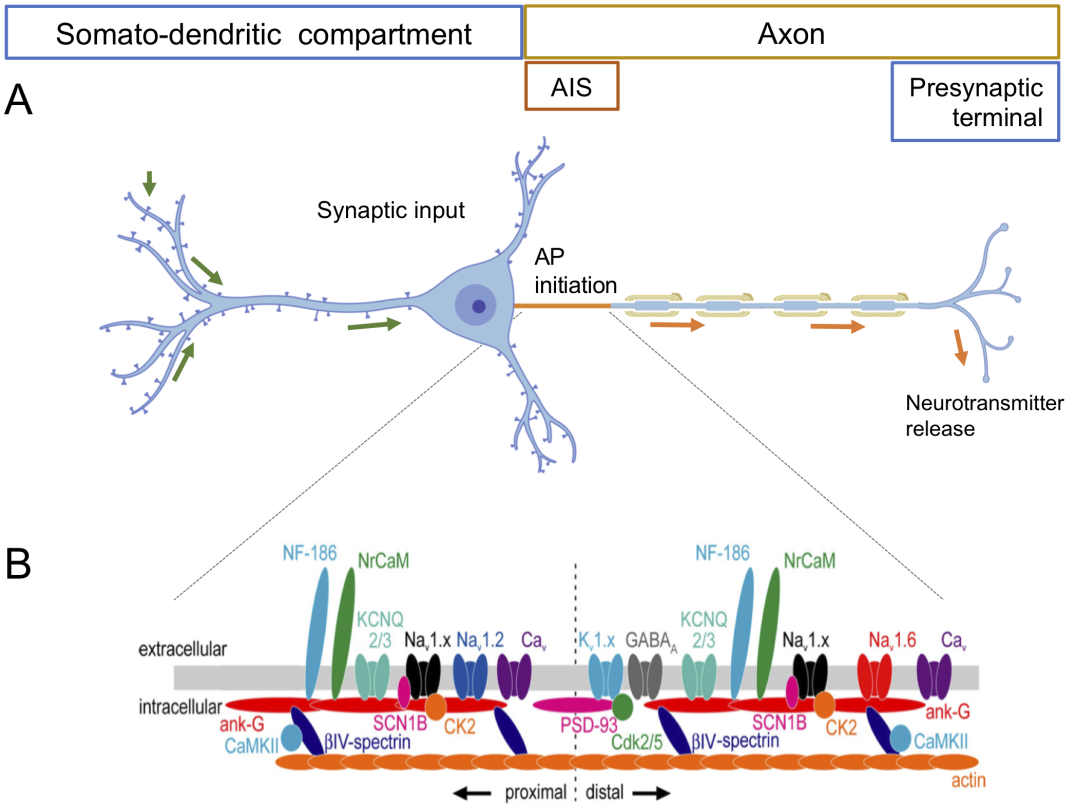

Figure 1.6: Schematic representation of AIS location and molecular composition. A - Schematic representation of a neuron with AIS represented in orange. Green arrows represent synaptic inputs being received and integrated along the somatodendritic compartment, leading to AP initiation at the AIS. Orange arrows represent APs traveling down the axon until reaching the pre-synaptic termninal thus resulting in neurotransmitter release. (Schematic made using Biorender, based on Leterrier and Dargent (2014). B - Schematic representation of AIS molecular composition adapted from Grubb et al. (2011).

pyramidal cells, blocking KCNQ leads to increased cellular excitability (Shah et al., 2008; Lezmy et al., 2017), due to a lower spike threshold and enhanced spontaneous AP firing. Disruption of the interaction of the channel with Ank-G results in a similar effect to that observed by channel blocking (Shah et al., 2008), suggesting that axonal localisation is crucial to determine KCNQ function in the regulation of cellular excitability.

In addition to Na^+ and K^+ channels, voltage gated calcium channels (VGCCs) are also expressed at the AIS though their functional role is not as well understood. Using calcium imaging and selective pharmacology, Bender and Trussell (2009) have shown that T and R type VGCCs are codistributed with Na^+ channels at the AIS and suggest Ca^{2+} influx through these channels is essential to the generation and timing of complex spikes, in interneurons of the dorsal cochlear nucleus. In cortical pyramidal neurons, Yu et al. (2010) suggest that P/Q VGCCs modulate AP kinetics and consequently cellular excitability, as channel blocking resulted in slower AP decay through a reduction of Ca^{2+}-activated K^+current.

1.5.1.2 AIS Plasticity

The AIS is a dynamic structure and it is known to undergo functional and morphological changes in response to neuronal activity (Grubb and Burrone, 2010; Grubb et al., 2011). AIS structural plasticity occurs during development and is believed to be a homeostatic mechanism in order to maintain neuronal activity (Kuba et al., 2006; Gutzmann et al., 2014). Indeed, evidence from computational modelling studies suggests that modulating AIS length and position allows neurons to optimise their excitability (Gulledge and Bravo, 2016), with the effect of AIS length and position on cellular excitability depending on somatodendritic morphology. While small neurons (*e.g.* DGCs) exhibit maximum excitability with more proximal AISs of intermediate length, in larger neurons (*e.g.* pyramidal neurons) longer AISs were associated with increased cellular excitability (Gulledge and Bravo, 2016).

Structural modulation of the AIS was initially described in *nucleus magnocellularis* and *nucleus laminaris* of the avian auditory system by Kuba et al. (2006). In these regions, neurons respond to sounds of a characteristic frequency (CF), and are arranged in a tonotopic manner. Neurons with a low-CF exhibit longer AISs positioned closer to the soma, compared to shorter AISs positioned more distally from the soma in high-CF neurons. Computational modelling showed that AIS length and position were

optimised in order to reduce AP threshold and increase sensitivity to interaural time difference at each specific frequency. Therefore AIS morphology has a crucial role in the estimation of sound source location for a range of different frequencies in chicks. In a subsequent study, Kuba et al. (2010) showed that AIS length in the chick auditory system is directly modulated by neuronal activity in a compensatory manner. Loss of auditory input achieved by cochlear ablation resulted in progressively longer AISs and a concomitant increase in cellular excitability. It is now known that frequency tuning during development in this system relies on the activity dependent modulation of the AIS (Kuba et al., 2014).

Since Kuba et al. (2006) original study, AIS structural plasticity during development has been reported in other systems. Gutzmann et al. (2014) first described the developmental trajectory of the AIS in the mouse visual cortex. In this brain region, AIS length increases until eye opening around post-natal day (P) 14 and decreases shortly after by P28. This is an activity dependent phenomenon as this transition no longer occurs when mice are visually deprived from birth or for 2 weeks after eye opening. The activity dependent nature of this developmental shift appears to be dependent on Ca^{2+} signalling, as in mice lacking synaptopodin, a marker for the cisternal organelle, AIS development appears to be independent of visual activity (Schlüter et al., 2018). However further studies are needed to establish the precise role of Ca^{2+} signalling in activity dependent development of the AIS.

The developmental trajectory of the AIS is thought to reflect a compensatory mechanism in response to changes in neuronal activity, whereby an increase in visually driven neuronal activity upon eye opening results in shorter AISs and consequently reduced cellular excitability (Gutzmann et al., 2014). However, a direct link between cellular excitability and AIS length during development has not been established in this particular system. Whilst there is evidence from homeostatic plasticity studies of compensatory changes in synaptic transmission and cellular excitability upon visual deprivation (Brown et al., 2019; Keck et al., 2013; Maffei et al., 2004), these have not been causally linked to AIS plasticity.

More recently, Jamann et al. (2020) have described the developmental trajectory of AISs in the somatosensory cortex. In line with the previous studies in the visual system, Jamann et al. (2020) showed an increase in AIS length during early development up until P15. After the end of the second postnatal week, active whisking results in a

reduction in AIS length by P21. This is also dependent on sensory activity as whisker trimming prevents this AIS shortening.

Additionally, environmental factors such as environmental enrichment (EE) are known to modulate AIS plasticity and development across a range of brain areas including the mPFC (Nozari et al., 2016), the DG (Bolos et al., 2019) and somatosensory cortex (Jamann et al., 2020). The precise effect of EE on AIS length appears to be dependent on brain area, perhaps reflecting differences at the local circuit level. EE results in longer AISs in the mPFC (Nozari et al., 2016), while it leads to AIS shortening in the DG (Bolos et al., 2019). In L2/3 of the somatosensory cortex, AIS reduces in length in a transient manner during the first 3 hours of exposure and returns to baseline length at the end of 6 hours, reflecting an increase in exploratory activity when the mice are first exposed to the novel environment that wears off by the 6 hours of maximum exposure (Jamann et al., 2020). This effect is thought to represent an homeostatic compensation to the increase in neuronal activity, measured as an increase in c-Fos positive cells during the first 3 hours of exposure that also returns to baseline after 6 hours.

AIS plasticity on shorter timescales has been studied in *in vitro* systems which allow for the dissociation of the cellular mechanisms involved. Grubb and Burrone (2010) first described an activity dependent relocation of the AIS in dissociated hippocampal neurons. In this system, depolarisation with 15 mM KCl or optogenentic stimulation in bursts resulted in distal relocation of the AIS relative to the soma over the course of 2 days. AIS plasticity under these conditions is independent from AP firing but dependent on L type Ca^{2+} channel activity and downstream intracellular activation of calcineurin (Evans et al., 2013; Grubb and Burrone, 2010). The more distal location of the AIS was associated with a reduction in cellular excitability, observed as an increase in AP current threshold. In a subsequent study, Evans et al. (2015) showed that DG granule cells (DGCs) can undergo rapid AIS plasticity, with 3 hours of optogenetic stimulation in bursts or depolarisation with KCl being sufficient to induce AIS plasticity. Rather than a distal shift in AIS position, short-term plasticity (i.e. 3 h) results in a shortening of the AIS. AIS shortening was measured both based on AnkG immunolabelling as well as VGSCs labelling, indicating that both structural and functional elements of the AIS undergo activity dependent remodelling. AIS shortening results in reduced cellular excitability, an effect that was dependent on VGSC phosphorylation state

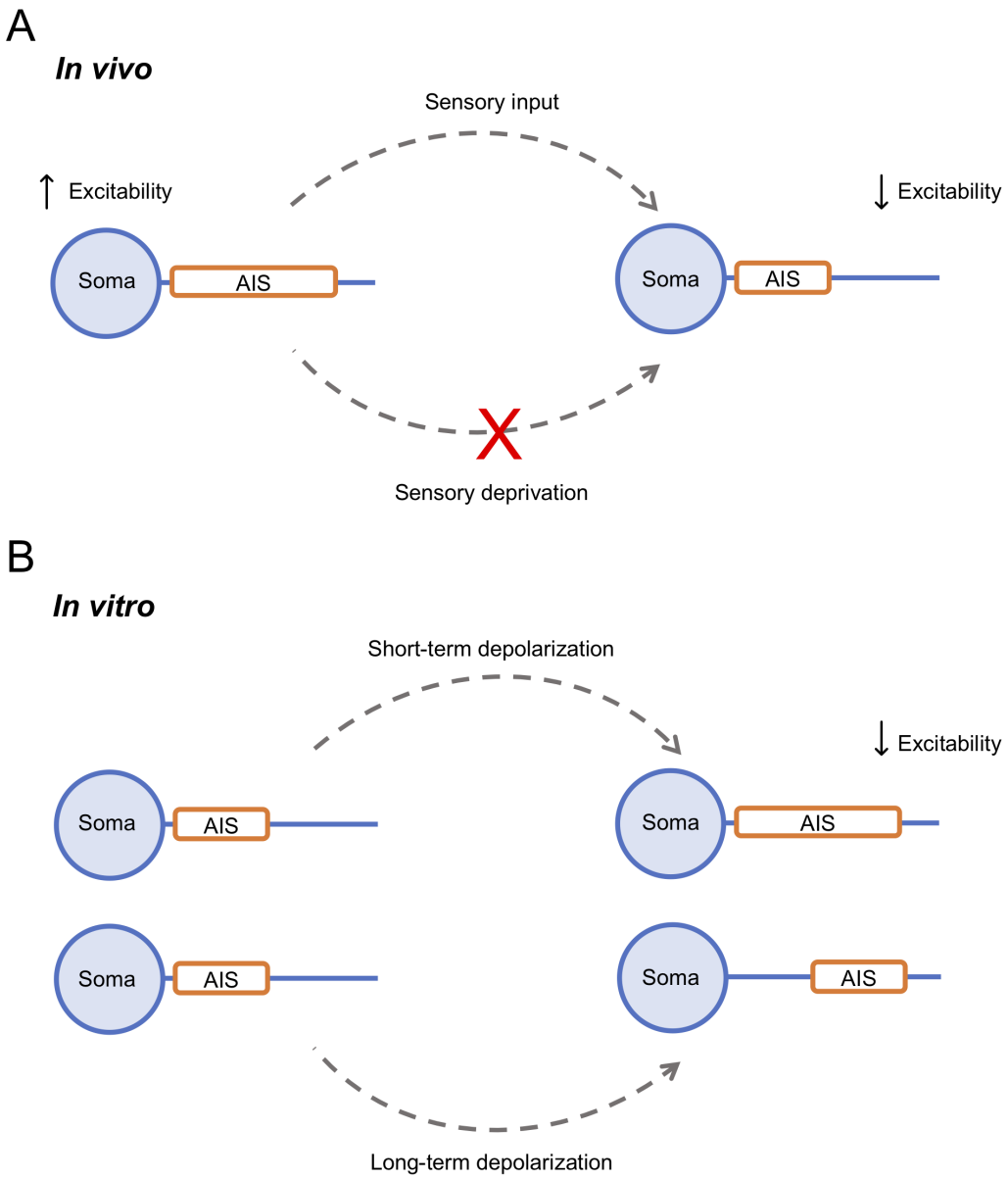

Figure 1.7: Schematic representation of AIS plasticity *in vivo* and *in vitro*. A - Sensory input leads to AIS shortening *in vivo* in the chick auditory system (Kuba et al., 2006), in the somatosensory cortex (Jamann et al., 2020) and visual cortex (Gutzmann et al., 2014) of the mouse. Sensory deprivation prevents activity dependent AIS shortening. B - Depolarisation of neurons in culture leads to distal AIS relocation (long term - 48 h) or AIS shortening (short-term, 3 h) (Grubb and Burrone, 2010; Evans et al., 2015).

modulated by calcineurin (Evans et al., 2015). Other suggested mechanisms for short term AIS plasticity include neuromodulatory factors. An increase in extracellular BDNF or NT3 concentrations has been shown to lead to proximal relocation of the AIS and increased cellular excitability in hippocampal cultures whilst in the absence of neurotrophin receptors TrkB and TrkC, AISs relocated more distally leading to a reduction in neuronal excitability (Guo et al., 2017). A schematic representation of AIS plasticity in response to altered neuronal activity is shown in Figure 1.7.

1.5.1.3 AIS in ASD/ID and epilepsy

Given the role of the AIS in the regulation of cellular excitability, it is perhaps not surprising that abnormal structure and function of the AIS have been linked to pathological conditions associated with altered network activity, including stroke, epilepsy, schizophrenia and neurodevelopmental disorders (Wimmer et al., 2010; Kaphzan et al., 2011; Buffington and Rasband, 2011). As epilepsy is a common comorbidity in ASD/ID, the role of the AIS in epilepsy is of particular interest in the context of this thesis.

A variety of ion channels expressed at the AIS have been implicated in the pathophysiology of epilepsy. Mutations in the SCN1A gene encoding VGSC $Na_v1.1$ are the most commonly associated with epilepsy (for review see Catterall et al. (2010)). Loss of function mutations result in a severity spectrum of epilepsy ranging from mild febrile seizures (Sugawara et al., 2001) to severe myoclonic epilepsy of infancy (or Dravet syndrome) (Mantegazza et al., 2005). Consistent with the known interneuron specific expression of $Na_v1.1$, loss of function of this channel in mouse models of Dravet syndrome leads to reduced AP firing of interneurons and consequent disinhibition of pyramidal cells, leading to network hyperexcitability (Ogiwara et al., 2007).

Interestingly, the genes encoding Nav1.2 channels have been implicated in epilepsy as well as ASD/ID. Whilst gain of function mutations are associated with epilepsy, loss of function mutations are associated with ASD/ID and absence seizures (Scalmani et al., 2006; Ben-Shalom et al., 2017). Nav1.2 haploinsufficency results in impaired AP backpropagation resulting in impaired dendritic excitability, in line with the proximal AIS location of this channel. This is suggested as a potential cellular mechanism underlying cognitive deficits in ASD/ID (Spratt et al., 2019).

Similar, to $Na_v1.2$ mutations, $Na_v1.6$ gain of function is associated with epilepsy whilst loss of function mutations are linked to ID (reviewed in O'Brien and Meisler

(2013)). Gain of function *de novo* mutations in the SCN8A gene encoding $Na_v1.6$, have been associated with epileptic encephalopathy (Estacion et al., 2014; Veeramah et al., 2012). While, in the mouse hippocampus and EC, up regulation of $Na_v1.6$ during epileptogenesis is known to contribute to circuit hyperexcitability further seizure generation (Hargus et al., 2013; Blumenfeld et al., 2009). Interestingly, reducing $Na_v1.6$ expression in haploinsufficient mice has a protective effect, resulting in reduced seizure susceptibility (Blumenfeld et al., 2009). Furthermore, seizure severity and viability are improved in the mouse model of Dravet syndrome when these are haploinsufficient for $Na_v1.6$ (Martin et al., 2007).

Mutations in AIS K^+ channels have also been associated with epilepsy. Kv1.1 mutations have been associated with episodic ataxia and epilepsy (Zuberi et al., 1999) and loss of Kv1.1 results in spontaneous seizures in mice (Smart et al., 1998). Mutations that enhance Kv7.2 and Kv7.3 channel function are associated with epilepsy (Devaux et al., 2016; Miceli et al., 2015). Interestingly, the channel location is just as important for its role regulating cellular excitability, with mutations that disrupt cellular distribution of Kv channels without impairing channel conductance also being associated with epilepsy (Abidi et al., 2015). *De novo* loss of function mutations in Kv7.3 have also been identified in an ASD cases (Gilling et al., 2013), while loss of Kv7.2 in rodents results in impaired social interaction and repetitive behaviours (Kim et al., 2020).

The study of the AIS in the context of ASD/ID is still at its early stages. In addition to the implication of AIS ion channels in ASD/ID mentioned above, the work of Kaphzan et al. (2011) is the only study to date reporting altered AIS morphology in a mouse model of ASD/ID. In this study, increased AIS length and Nav1.6. expression was associated with a more hyperpolarised AP threshold and enhanced intrinsic excitability in CA1 pyramidal cells in a mouse model of Angelman Syndrome.

1.5.2 Cellular Excitability in CDD and FXS

How loss of CDKL5 affects cellular excitability is largely unknown, with most studies attributing synaptic mechanisms for circuit dysfunction in mouse models of CDD (Tang et al., 2019, 2017; Della Sala et al., 2016; Yennawar et al., 2019; Okuda et al., 2017).

However, in the mouse model of FXS, cellular hyperexcitability has been reported in multiple brain areas and attributed to a variety of mechanisms (Contractor et al., 2015). In particular hyperexcitability in the somatosensory cortex has long been suggested as a

mechanism contributing to sensory hypersensitivities (Gibson et al., 2008; Booker et al., 2019; Domanski et al., 2019). Voltage sensitive dye imaging experiments showed that the spread or activity in the cortical surface occurs faster and with greater intensity in *Fmr1*$^{-/y}$ mice upon whisker stimulation and this is associated with increased cellular excitability (Zhang et al., 2014). In addition to synaptic phenotypes, Domanski et al. (2019) reported hyperexcitability of L4 SCs, accompanied by altered AP firing properties in fast-spiking interneurons. Booker et al. (2019) have shown that hyperexcitability of L4 stellate cells is mediated by a reduction in hyperpolarization-activated cyclic nucleotide–gated (HCN) channels mediated current (I_h).

I_h is a non-inactivating cation conductance activated by hyperpolarisation of the neuronal membrane. As HCN channels are also active at rest, I_h can have an impact on resting membrane potential and input resistance (Shah, 2014). Consistent with the dendritic expression of HCN1/2, altered HCN channel expression has also been associated with altered dendritic excitability in the hippocampus and mPFC (Brager et al., 2012; Kalmbach et al., 2015). In CA1 pyramidal cells of *Fmr1*$^{-/y}$ mice, I_h is increased resulting in reduced input resistance and consequently reduced dendritic excitability (Brager et al., 2012). In contrast, mPFC L5 pyramidal neurons show reduced dendritic I_h resulting in increased dendritic excitability in *Fmr1*$^{-/y}$ mice (Kalmbach et al., 2015). The bidirectional nature of HCN expression in *Fmr1*$^{-/y}$ mice suggests it might reflect a compensatory mechanism rather than a direct consequence of the lack of FMRP. Indeed, HCN channel expression can be regulated by network activity activity in *ex vivo* tissue (Fan et al., 2005) and in epileptic states *in vivo* (Jung et al., 2011; Richichi et al., 2008). In addition to HCN channels, K^+ channels have been implicated in the excitability of pyramidal cells in the hippocampus of *Fmr1*$^{-/y}$ mice. $K_v4.2.$ mediates the A-type K^+ current and its translation is regulated by FMRP (Darnell et al., 2011). Expression of $K_v4.2.$ increases along the dendrites with distance from the soma, and it has an important role in mediating dendritic excitability (Kerti et al., 2012). Routh et al. (2013) have reported reduced A-type current in the dendrites of CA1 pyramidal cells contributing to hyperexcitability of the dendritic compartment. Deng et al. (2013) reported increased AP broadening during repetitive firing in CA3 pyramidal cells of *Fmr1*$^{-/y}$ mice mediated by increased BK channel activation in the absence of FMRP. In CA1 pyramidal cells, Luque et al. (2017) reported increased excitability in CA1 pyramidal cells, reflected as an increase in AP firing in response

to depolarising current steps, an effect that appears to be mediated by an increase in input resistance. Additionally, Luque et al. (2017) observed broader APs in *Fmr1*$^{-/y}$ mice which is attributed to altered BK channel as previously reported in CA3 (Deng et al., 2013), however, this was never confirmed with pharmacology. Other suggested mechanisms underlying hyperexcitability in FXS include increased persistent sodium current in EC L3 pyramidal neurons, which leads to a more hyperpolarised AP threshold (Deng and Klyachko, 2016).

In addition to altered ion channel function, altered homeostasis of cellular excitability has recently been suggested as a potential mechanism contributing to cortical hyperexcitability (Bülow et al., 2019). WT neurons show enhanced cellular excitability following blocking of synaptic transmission with TTX and APV, this effect is exaggerated in *Fmr1*$^{-/y}$ neurons (Bülow et al., 2019), potentially contributing to hyperexcitability of cortical networks. Interestingly, the work of Domanski et al. (2019) suggests that opposition of synaptic and cellular excitability phenotypes might represent compensatory mechanisms of neuronal circuits in FXS. Therefore homeostatic regulation of intrinsic excitability might play an important role in regulating neuronal function in ASD/ID that is yet to be explored. Furthermore, with many studies focusing on dendritic excitability phenotypes in FXS, the role of the AIS in regulating cellular excitability is poorly understood in the context of FXS and ASD/ID more generally.

1.6 Aims

This introduction has summarised different aspects involved in neurotransmission, from pre-synaptic neurotransmitter release, to synaptic plasticity and regulation of cellular excitability. Given the large body of evidence implicating these processes in the pathophysiology of ASD/ID and epilepsy, the overarching aim of this thesis is to further our understanding of synaptic transmission and cellular excitability in the context of ASD/ID, focusing in particular in rodent models of CDD and FXS.

Chapter 3: In this chapter I addressed the hypothesis that loss of CDKL5 results in altered synaptic function and cellular excitability in *Cdkl5*$^{-/y}$ rats. I used electrophysiological recordings to examine hippocampal synaptic plasticity, and pre- and post-synaptic function and cellular excitability in CA1 and mPFC. I provide evidence that CDKL5 plays a role in synaptic plasticity in the hippocampus. Synaptic function

and excitability in the mPFC were unaffected in *Cdkl5*$^{-/y}$ rats.

Chapter 4: I hypothesised that altered AIS morphology contributes to altered cellular excitability in *Fmr1*$^{-/y}$ mice. I used a combination of histology and electrophysiology to examine cellular excitability, AIS plasticity and synaptic inputs to CA1. I found cellular hyperexcitability of CA1 pyramidal cells to be associated with increased AIS length in *Fmr1*$^{-/y}$ mice. The data in this chapter provide evidence that changes in AIS length homeostatically normalise cellular excitability to compensate for altered synaptic inputs to CA1 in *Fmr1*$^{-/y}$ mice.

Chapter 5: In this chapter I addressed the hypothesis that regulation of AIS structure by experience is intact in *Fmr1*$^{-/y}$ mice. I examined the developmental trajectory of AIS length across cortical layers in the primary visual cortex of *Fmr1*$^{-/y}$ and WT mice and used a visual deprivation paradigm to assess *in vivo* AIS plasticity and regulation of cellular excitability. I provide evidence for altered AIS developmental trajectory in a cortical layer specific manner in *Fmr1*$^{-/y}$ mice. However, I failed to observe AIS plasticity in response to visual deprivation in either genotype.

Chapter 2

Materials and Methods

2.1 Animal husbandry

All procedures were performed in accordance with Home Office (ASPA, 2013; HMO license: P1351480E) and institutional guidelines. Animals were housed with littermates on a 12 h light/dark cycle with food and water *ad libitum*, unless otherwise stated. As FXS and CDD are X-linked disorders, only male mutant and WT littermate animals were used for experiments. All experiments and data analysis were performed blinded to genotype (and treatment where applicable).

2.1.1 *CDKL5* rats

The *CDKL5* knock out (KO) rat was generated by Horizon Discovery (St. Louis, Missouri, USA). A 10 bp deletion in exon 8 of the *Cdkl5* gene leads to a null allele and, consequently, absence of CDKL5 protein expression. Rats were bred in house on the LEH (Jackson Laboratories) background.

2.1.2 *Fmr1* mice

Fmr1 KO mice were obtained from the Dutch-Belgium Consortium (Jackson Laboratories, 003025, The Dutch-Belgian Fragile X Consorthium et al. (1994)) and bred in-house onto the C57/Bl6J/Crl background.

2.1.3 Generation of β1-Na$_v$-GFP - *Fmr1* mice

β1-Na$_v$-GFP mice were generated by Dr Diane Sherman and Professor Peter Brophy. Briefly, the β1-Na$_v$-GFP cDNA (McEwen et al., 2009) was cloned into the blunted XhoI

site of the pTSC21k vector and released using the restriction enzyme Not I (Zonta et al., 2011). This construct was used for pronuclear injection (Sherman and Brophy, 2000), generating transgenic mice that express the β1 subunit of the sodium channel (β1-Na$_v$) fused to the C-terminus of GFP, under the control of the Thy1.2 promoter (Caroni, 1997).

The mice used for the work in this thesis result from backcrossing male β1-Na$_v$-GFP with female *Fmr1*$^{+/-}$ C57/BL6J/Crl mice in order to obtain β1-Na$_v$-GFP-Fmr1 WT and β1-Na$_v$-GFP-Fmr1$^{-/y}$ mice for genotype comparisons. Mice were backcrossed for at least six generations before data collection.

2.2 Genotyping

Tissue biopsies that were collected at weaning for the purpose of animal identification or at the time of the experiments (for animals used prior to weaning) were used for genotyping. Genotyping for the *Fmr1* mouse lines was carried out in house as detailed in the following section. Genotyping for the *Cdkl5* rat line was outsourced to Transnetyx (Cordova, TN, USA).

2.2.1 *Fmr1* mice

2.2.1.1 DNA extraction

For DNA extraction, tissue samples were digested in 600 μL NaOH (50 mM) for 1 h at 100°C (inverted every 20 min). The pH was neutralised with 50 μL Tris-HCl (1 M) for 2 min at 100°C. The samples were then centrifuged at 14,000 rpm for 10 min, leaving the DNA in the supernatant to use in the polymerase chain reaction (PCR) protocol.

2.2.1.2 Polymerase Chain Reaction

For individual PCR reactions, 1 μL of DNA was added to 6 μL of GoTaq master mix (2x stock, Promega) and specific primers (Table 2.1), at a final concentration of 1 or 2 μM for forward and the reverse primers respectively. The PCR protocol used is detailed in Table 2.2.

The PCR products were loaded on a 2% agarose gel (50 mL) containing SYBRSafe (1:50000, Invitrogen) for 20 min at 100 mV. WT samples were identified by the presence

of a single band corresponding to 85 kb and *Fmr1* KOs by a band at 105 kb.

Table 2.1: Primer sequences for *Fmr1* mice

***Fmr1* Primers**	**Sequence - 5'-3'**
Forward primer (WT)	TGT GAT AGA ATA TGC AGC ATG TGA
Forward primer (KO)	CTT CTG GCA CCT CCA GCT T
Reverse primer (common)	CAC GAG ACT AGT GAG ACG TG

Table 2.2: Thermocycling conditions for *Fmr1* primers

Step	**Temperature** (°C)	**Time**	
1	94	3 min	
2	94	1 s	} x 35 cycles
3	63	1 s	
4	72	1 s	
5	72	2 min	
6	10	∞	

2.3 Electrophysiology

2.3.1 Solutions

Table 2.3: Composition of extracellular solutions used in electrophysiology experiments

	Cutting ACSF	**Recording ACSF**
	Concentration (mM)	
NaCl	86	124
NaH_2PO_4	1.2	1.2
KCl	2.5	2.5
$NaHCO_3$	25	25
D-glucose	25	20
Sucrose	75	-
$CaCl_2$	0.5	2
$MgCl_2$	7	1

Table 2.4: Composition of the potassium gluconate based intracellular solutions used in current clamp recordings

	8mM Cl^-	**24mM Cl^-**
	Concentration (mM)	
K-Gluconate	142	120
KCl	4	20
HEPES	10	10
Na_2GTP	0.3	0.3
pCreatine	1	10
Na_2ATP	2	-
EGTA	0.5	-
$MgCl_2$	2	-
NaCl	-	4
Mg-ATP	-	4

Table 2.5: Composition of the cesium gluconate based intracellular solution used in voltage clamp recordings

	Concentration (mM)
CsOH	110
D-Gluconic Acid	110
CsCl	20
HEPES	10
NaCl	4
MgATP	4
Na_2GTP	0.3
EGTA	0.2
pCreatine	10
$QX314Cl^-$	5

The pH of all intracellular solutions (Tables 2.4, 2.5) was adjusted to 7.3 and osmolarity was 290-300 $mOsm.L^{-1}$. In a subset of recordings 0.1-0.2% biocytin (Sigma) was added to the intracellular solution to allow post-hoc labelling and morphological characterisation of the cell recorded.

2.3.2 Acute slice preparation

Mice and rats were deeply anesthetised with isofluorane and then decapitated. The brain was rapidly removed and placed in carbogenated (95% O_2 / 5% CO_2) ice-cold sucrose-modified artificial cerebrospinal fluid (cutting ACSF, Table 2.3). 400 μm-thick slices containing the brain region of interest were cut coronally (mPFC, hippocampus, primary visual cortex) or horizontally (hippocampus) on a Vibratome (VT1200s, Leica, Germany). Slices were transferred to a storage chamber and allowed to recover submerged in cutting-ACSF at 35°C for 30 min. Slices were kept at room temperature thereafter until used for electrophysiological recordings.

2.3.3 Extracellular field recordings

Extracellular field recordings to assess hippocampal synaptic plasticity were performed by Rita Loureiro, when she was a research assistant in the lab.

Slices were transferred to a submerged recording chamber perfused with warm carbogenated recording ACSF (Table 2.3) at a flow rate of 3-4 mL/min. Temperature was maintained at 31 ± 1°C throughout the recordings. Recording pipettes (1-3 MΩ resistance) were pulled from borosilicate glass capillaries (1.5 mm outer / 0.86 mm inner diameter, Harvard Apparatus, UK) on a horizontal electrode puller (P-97, Sutter Instruments, CA, USA), and filled with recording ACSF. The stimulating electrode was placed in the *stratum radiatum* (SR) to stimulate the Schaffer collateral (SC) pathway and evoke synaptic responses in CA1 (Figure 2.1 A). Single pulses of electric stimulation (200 μs) were delivered every 30 s through a bipolar electrode (Ni:Cr) connected to a constant current stimulator (DS3, Digititmer Ltd, UK). Stimulus intensity was set to produce 50% of the maximum field excitatory post-synaptic potential (fEPSP) amplitude, and kept constant thereafter. After 20 min of stable baseline, tetanic stimulation (two trains of 1 s 100 Hz stimulation, 20 s inter-train interval) was used to induce LTP (Komiyama et al., 2002). fEPSP were recorded for 1 h after LTP induction. fEPSP slopes were normalised to baseline values and LTP magnitude reported as the average fEPSP slope in the final 10 min of the recording divided by the average fEPSP slope during the baseline period. LTP was quantified based on the slope of the fEPSP rise phase rather than peak amplitude, as the slope is linearly correlated with synaptic conductance, while peak amplitude can be contaminated by the presence of population-spikes (Johnston, Daniel and Wu, 1994). Data acquisition and analysis were performed

in WinLTP Software (University of Bristol, UK).

2.3.4 Patch-clamp recordings

Whole-cell patch-clamp recordings were used to assess excitatory synaptic transmission and cellular excitability. Slices were transferred to a submerged recording chamber perfused with warm carbogenated recording ACSF (Table 2.3) at a flow rate of 5-6 mL/min. All recordings were performed at a near physiological temperature (31° ± 1°C) maintained with an in-line heater (HPT-2, ALA Scientific, NY, USA). Recordings were obtained with a Multiclamp 700B (Molecular Devices) amplifier, signals were Bessel filtered online at 10 kHz (for current clamp recordings) or 2 kHz (for voltage clamp recordings) and digitized at 20 kHz (Digidata1440, Molecular Devices). Trace files were recorded with pCLAMP^{TM} Software (Molecular Devices). Recording pipettes (3-5 MΩ resistance) were pulled from borosilicate glass capillaries (1.5 mm outer / 0.86 mm inner diameter, Harvard Apparatus, UK) on a horizontal electrode puller (P-97, Sutter Instruments, CA, USA). Infrared differential interference contrast (IR-DIC) microscopy, using a digital camera (QIMAGING) mounted on an upright microscope (Olympus BX51WI) and a 40x (0.8 NA) water immersion objective was used for visual guidance.

Pyramidal cells were identified based on the teardrop shaped somas, a prominent apical dendrite, their location in the slice and firing properties. Once a cell of interest (CA1 pyramidal cell, mPFC L5 pyramidal cell, V1 L2/3 pyramidal cell) was identified, whole cell patch clamp recordings were performed. Positive pressure was applied, and the electrode was moved through the tissue using a micromanipulator (Patchstar, Scientifica, UK). A 10 mV (100 Hz) seal-test was used to monitor pipette resistance. Once a dimple in the cell membrane was visible, positive pressure was released. Cell attached configuration was achieved once a seal resistance higher than 1 GΩ was reached. Once sealed, a -70 mV holding potential was applied and small pulses of negative pressure were used to rupture the cell membrane and achieve whole cell configuration. Access resistance (R_a) was monitored throughout the experiment and recordings where R_a changed more than 20% were discarded. Cells with a zero current potential more depolarised than -50 mV or R_a greater than 25 MΩ were discarded.

2.3.4.1 Evoked EPSCs

I used extracellular electrical stimulation to assess the functional properties of excitatory synaptic transmission in the hippocampus. Synaptic inputs to CA1 pyramidal cells were stimulated by placing a stimulating bipolar electrode (Ni:Cr) in the *Stratum radiatum* (SR), *Stratum oriens* (SO) or *Stratum lacunosum-moleculare* (SLM) in horizontal hippocampal slices (Figure 2.1). Stimulation site for each particular experiment will be detailed in the respective results section. The CA3 containing portion of these slices was cut off to prevent the recruitment of recurrent network activity, and allow the recording of monosynaptic responses.

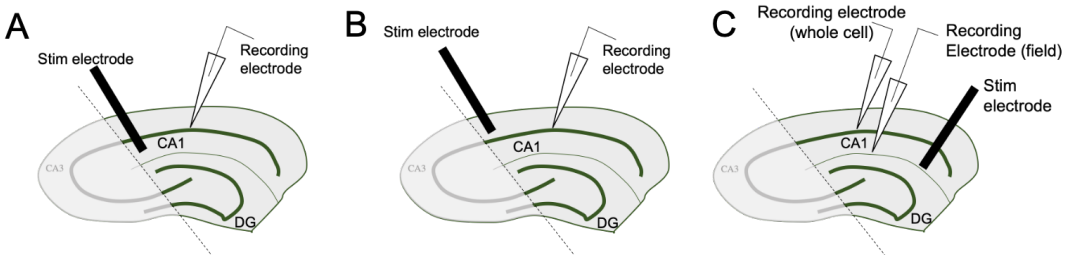

Figure 2.1: Schematic representation of recording configuration of evoked EPSCs in the hippocampus. A - Stimulation electrode placed in the *Stratum radiatum* and recording electrode in the *Stratum pyramidale*, used for field LTP recordings and whole cell paired pulse, AMPAR/NMDAR ratios and minimal stimulation recordings in *CDKL5* rats. B - Stimulation electrode was placed in the *Stratum oriens* and recording electrode in the pyramidal cell layer for minimal stimulation and paired pulse ratio recordings in *CDKL5* rats. C - Stimulation electrode placed in the *SLM* and whole cell recording electrode in the pyramidal cell layer and field recording electrode in the *SLM* used to assess enthorinal cortex inputs to CA1 in *Fmr1* mice.

In all recordings, EPSCs were pharmacologically isolated by adding 50 μM picrotoxin (HelloBio) to the recording ACSF (Table 2.3), thus blocking $GABA_A$ receptor mediated inhibition. Single pulses were delivered by an isolated constant current stimulator (DS3, Digitimer.Ltd, Cambridge, UK). Stimulation intensity was adjusted in order to obtain an EPSC amplitude of approximately 100 pA, while holding the cell at -70 mV in voltage clamp with a cesium gluconate based intracellular solution (Table 2.5).

Paired pulse ratio

Paired pulse stimulation was used to assess pre-synaptic release probability. After setting the appropriate stimulus intensity as described above, a pair of stimuli was delivered with 20, 50 or 100 ms interstimulus interval (ISI), and a 10 second inter-trial interval. In order to obtain paired pulse ratio (PPR) values for each ISI, 10 sweeps were averaged per cell and the peak amplitudes of the first and second evoked EPSCs were

determined on Stimfit, for each of the ISIs tested. PPR was determined dividing the amplitude of the second EPSC by the first.

NMDAR/AMPAR ratio

AMPAR-mediated EPSCs were recorded at -70 mV. Following the recording of AMPAR-mediated EPSCs, ACSF containing 50 μM picrotoxin (HelloBio) and 10 μM CNQX (HelloBio), a AMPAR antagonist, was washed in and EPSC amplitude was monitored until the response at -70 mV was fully blocked. The same cell was then held at +40 mV to record pharmacologically isolated NMDAR-mediated EPSCs. AMPAR and NMDAR-mediated EPSC peak amplitude was determined from an average of 10 and 20 traces per cell, respectively. NMDAR/AMPAR ratios were obtained by dividing peak amplitude of NMDAR mediated EPSC by the peak amplitude of the AMPAR mediated EPSC.

Calcium permeable AMPAR mediated EPSCs

To examine the presence of CP-AMPARs, AMPAR-mediated EPSCs were evoked by placing the stimulating electrode in the SR (Figure 2.1 A). Recordings were performed in the presence of 50 μM picrotoxin, to block $GABA_A$ receptor currents, and 50 μM AP-5 (Tocris), a NMDAR antagonist, in order to isolate AMPAR-mediated EPSCs. EPSCs were recorded over a range of voltages from -80 mV to +40 mV, in 20 mV increments. The rectification index was calculated dividing peak EPSC amplitude at -60 mV over peak EPSC amplitude at +40 mV, from an average of 10 traces per cell. In these recordings, the same cesium based intracellular solution (Table 2.5) was used with added 0.1 mM spermine (HelloBio) to ensure the presence of intracellular polyamines that confer rectification of GluA2-lacking AMPARs (Kamboj et al., 1995).

Minimal stimulation

I used a minimal stimulation paradigm to investigate the presence of silent synapses in CA1 pyramidal cells. Low intensity electrical stimulation was used to activate a single synapse or a small number of synapses. Once a reliable EPSC was identified at -70 mV, stimulus amplitude was reduced until the synaptic response would fail in some of the trials. Following recording of 50 trials at a holding potential of -70 mV, corresponding to AMPAR mediated EPSCs, the cell was depolarised to -40 mV, to reveal mixed AMPAR and NMDAR mediated EPSCs and an additional 50 trials were recorded. To determine response probability the traces for each holding potential were visually inspected and the number of traces with a visible EPSC was divided by the

total number of traces for each cell. I compared the event probability at a holding potential of -70 mV relative to +40 mV, and calculated the ratio of response probability at +40 mV divided by response probability at -70 mV, with a ratio >1 corresponding to the presence silent synapses (Isaac et al., 1997).

Temporammonic inputs to CA1 and CA1 pyramidal cell spiking

To assess the strength of entorhinal cortex inputs to CA1, the temporoammonic (TA) pathway was activated by placing the stimulating electrode in the *SLM* at the border of CA1 and subiculum (Figure 2.1 C). fEPSPs were recorded with a second electrode (patch pipette filled with recording ACSF) placed in the *SLM* and a CA1 pyramidal cell was recorded in cell-attached or whole-cell configurations. A constant-voltage stimulation box (Digitimer Ltd., Cambridge, UK) was used to deliver a train of 5 stimuli (20 Hz, 200 μs each) over a range of stimulation intensities (0, 30, 60 and 90 V). To assess the strength of TA inputs to CA1, EPSP amplitude was measured for the first EPSP in a train of 5 stimuli both for the field EPSP and the whole cell recordings. To assess CA1 pyramidal cell spiking in response to TA input, I recorded from CA1 PCs in cell attached mode in voltage clamp. To quantify the proportion of cells that spiked in response to TA stimulation, spiking cells were defined as cells that spiked at least once in any of the 5 stimulus in a train. To compare probability of cell spiking across genotypes, spike probability was calculated for each of the 5 stimuli in the train separately and for each stimulation intensity tested. Spike probability was calculated and plotted including all cells or spiking cells only (detailed in the figure legends).

2.3.4.2 Spontaneous and miniature EPSCs

I recorded spontaneous EPSCs (sEPSCs) and miniature EPSCs (mEPSCs) to assess excitatory neurotransmission under basal conditions. EPSCs were recorded in voltage clamp while holding the cell at -70 mV, using a cesium gluconate based internal solution (Table 2.5) to improve space clamp. Cells were allowed to stabilise for 5 min, while ACSF with 50 μM picrotoxin or 50 μM picrotoxin and 300 nM TTX washed in. EPSCs were then recorded for 5 min. Recordings of sEPSCs were performed in recording ACSF (Table 2.3) in the presence of 50 μM picrotoxin to block $GABA_A$ receptors and allow the isolation of excitatory synaptic events. In addition to picrotoxin, mEPSC recordings were performed in the presence of 300 nM TTX to block VGSCs, allowing to isolate

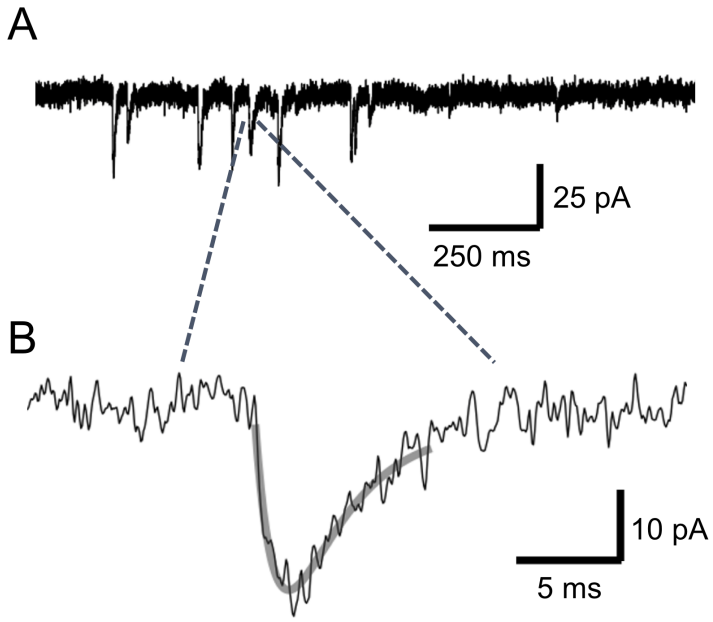

Figure 2.2: Detection of EPSCs with template matching algorithm in Stimfit A - Example trace of mEPSC recording on a larger timescale. B - Example of template matching to a single mEPSC event.

events resulting from the stochastic release of glutamate independently from AP firing.

Analysis of spontaneous and mEPSC frequency and amplitude was performed using a template matching algorithm, and filtering out of events with amplitude smaller than 2x the standard deviation of baseline noise (Clements and Bekkers (1997), Figure 2.2). All events detected were extracted to Microsoft Excel. EPSC frequency and average EPSC amplitude were then calculated for each cell recorded.

2.3.4.3 Intrinsic physiology

In order to assess cellular excitability, passive and active membrane properties of neurons were assessed as follows. A potassium gluconate-based internal solution (Table 2.4) was used and the protocols described below were run in current clamp mode, with bridged balance. Recordings in slices from the *Fmr1* mouse line were performed using the 8 mM Cl^- internal solution, whereas those from *Cdkl5* rat were performed using the 24 mM Cl^- internal solution. This was done to allow the data to be directly comparable to that collected on other mouse/rat lines by other members of the lab.

Passive membrane properties

Resting membrane potential (RMP) was determined as the mean zero current po-

tential over the first 10 s following break-through, by recording the cell in gap free I=0 mode. Following measurement of resting membrane potential all other recordings were performed at -70 mV, held by injection of a bias current throughout the recording. Input resistance, membrane time constant and capacitance were determined from the voltage response to a 500 ms, hyperpolarising -10 pA step (Figure 2.3 A). Input resistance (R_i) was calculated according to Ohm's Law (Equation 2.1), where V is the average voltage response during the last 100 ms of the 500 ms step and I is the amount of current injected.

$$R = \frac{V}{I} \tag{2.1}$$

Membrane time constant (τ_m) was determined by fitting a monoexponential curve to the initial voltage response, and estimated as the time needed to reach 63% of the maximum response. Capacitance was calculated by dividing the membrane time constant by the input resistance.

Active membrane properties

Families of 500 ms current injection steps, from -100 pA up to a maximum of 400 pA in 25 pA increments were performed to examine AP discharge, rheobase current, as well as AP properties (amplitude, maximum rise and decay rates, half-height duration). The protocol was run in triplicate for each cell and the values reported represent average values of the three repetitions. Rheobase current is reported as the smallest current step to result in firing of at least one AP. AP properties were measured from the first AP elicited. AP amplitude and AP rise time were measured from threshold, set as dV/dt=20mV.ms^{-1}, and AP half-height duration was taken as the width at $\frac{1}{2}$ the maximum AP amplitude. Maximum rates of rise and decay were measured as the maximum slopes (dV/dt) during the depolarising and repolarising phase of the AP, respectively (Figure 2.3 B).

All analysis of electrophysiological data was performed on Stimfit (Gutzmann et al., 2014).

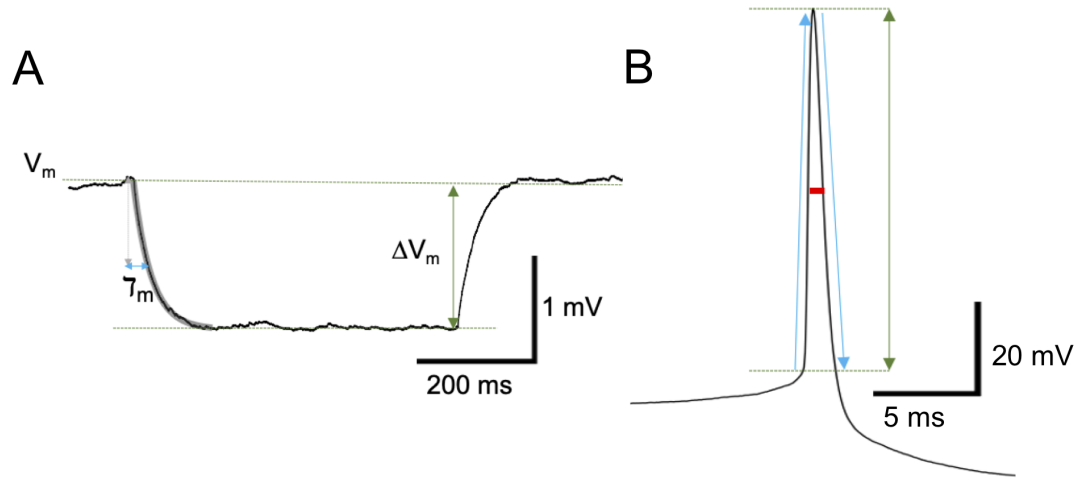

Figure 2.3: Measurement of passive membrane and active membrane properties A - Example trace of the voltage response to a hyperpolarising 10 pA step with fitted monoexponential curve used to determine membrane time constant (τ_m), given as 63% of the maximum voltage response (ΔV_m). B - Example measurement of AP properties. Red line indicates half-height duration, vertical double-headed arrow (green) indicates AP amplitude from threshold, blue arrows indicate rise (upwards) and decay (downwards) phase of AP where rise and decay rates were estimated.

2.4 Cell morphology

2.4.1 Streptavidin labelling

To visualise recorded neurons in slices used for electrophysiology experiments, cells were resealed using the outside-out patch configuration following recording and immersion fixed in 4% paraformaldehyde (PFA) in 0.1 M phosphate buffer (PB: 75 mM NaH_2PO_4, 25 mM Na_2HPO_4), pH 7.35, over night. Slices were stored in PBS (0.1 M PB + 0.9% NaCl) at 4°C thereafter until used for histology. Overnight incubation with Alexa488 or 568-conjugated streptavidin (1:500 dilution, Molecular probes, Invitrogen) in PBS with 0.3% triton-X, allowed for fluorescent labelling of biocytin filled cells. Slices were then thoroughly washed in 0.1 M PB and mounted on glass slides using Vectashield Hardset mounting medium (H-1400, Vector Labs).

2.4.2 Imaging and image analysis

2.4.2.1 Cell morphology

To examine neuronal morphology, the biocytin-filled cells were imaged on a inverted confocal microscope (Axiovert LSM510, Zeiss) under a 20x Plan Neofluar (NA 0.5) objective (Zeiss). Multiple Z-stacks (1 μm steps, 2048x2048, 2x average line scan) per

cell were taken in order to capture the entire cell.

All image processing and analysis for cell morphology was performed using the software package FIJI (ImageJ, Schindelin et al. (2012)). The Z-stacks obtained for a given cell were stitched using the 3D stitching plug in (Preibisch et al., 2009), and the cell was reconstructed using a semi automated method with the Simple Neurite Tracer plug in (Longair et al., 2011). The reconstructed paths were rendered and Sholl analysis (Ferreira et al., 2014) was performed in order to examine dendritic complexity, this also allowed to determine dendritic length, both total dendritic length and dendritic length for distinct dendritic domains (e.g. basal vs apical dendrites).

2.4.2.2 Spine density

To examine spine distribution in biocytin-filled cells, high resolution Z-stacks were taken from basal and apical (oblique and tuft) dendrites (2-3 dendrite sections per dendrite type per cell). Spines were imaged under a 63x Plan Apochromat (NA 1.4) oil immersion objective on an inverted confocal microscope (Axiovert LSM510, Zeiss), with a 2.8x zoom, 2x average line scan and 1024x1024 resolution, 0.14 μm Z step. The images obtained were then deconvolved using the Huygens Essential software (Scientific volume imaging, Netherlands).

The deconvolved images were used for analysis on FIJI (ImageJ, Schindelin et al. (2012)). Z-projections of the deconvolved Z-stacks were used to manually count spines using the cell counter tool. The number of spines was normalised to the dendritic length of the respective imaged dendrite section.

2.5 Axon initial segment plasticity paradigms

2.5.1 Depolarising stimulus

2.5.1.1 Dissociated hippocampal cultures

Hippocampal neuronal cell cultures were prepared by members of the Hardingham lab as described previously (Baxter et al., 2015). Hippocampi were dissected from embryonic day 17.5 wild-type and *Fmr1*$^{-/y}$ male mice. Neurons were dissociated in 36000 USP units/mL papain, and plated at a density of 1315 cells/mm^2 on poly-L-lysine coated glass-coverslips. Cells were grown in Neurobasal A culture medium supplemented with B-27 (Invitrogen, Carlsbad), 1 mM glutamine, 1% rat serum (Harlan

Laboratories), at 37°C until 10 days *in vitro* (DIV). The mitotic inhibitor cytosine β-D-arabino-furanoside hydrochloride (4.8 μM) was applied to the culture at DIV 4 to limit astrocyte proliferation.

To induce AIS plasticity, 15 mM KCl or NaCl was added to conditioned media at DIV 10, and the cells were returned to the incubator for 3h at 37°C (Evans et al., 2015). At the end of the 3 h treatment, the cultured cells were fixed in 4% PFA for 20 minutes at room temperature and then used for immunohistochemical labelling.

2.5.1.2 Acute hippocampal slices

Hippocampal slices were obtained according to the procedure described for slice preparation for electrophysiology experiments (see section 2.3.2). Following the 30 minute recovery at 35°C, slices were transferred to a holding chamber containing recording ACSF (Table 2.3) with added 15mM of KCl or NaCl, where they were kept for 3 h at 35°C, mimicking the experimental conditions known to induce AIS plasticity in dissociated cultures (Evans et al., 2015). At the end of the treatment period, slices were immersion fixed in 4% PFA for 1 h at room temperature. Following fixation, slices were stored at 4°C in PBS until used for immunohistochemical labelling.

2.5.1.3 Two photon live imaging

To measure potential changes in AIS length in real time, we performed live imaging of β-1-Na_v-GFP mice. Live imaging was performed on 400 μm thick horizontal, hippocampal slices (see section 2.3.2). A custom built galvanometric scanning 2-photon microscope (Femto2D-Galvo, Femtonics, Budapest, Hungary) fitted with a tuneable wavelength Ti:Sapphire laser (Chameleon, Coherent, CA, USA), with laser power controlled by a Pockels cell (Conoptics, CT, USA) was used to image the GFP labelled AISs. Photomultiplier tubes were used for signal detection through the MES microscope software (Femtonics, Hungary).

As the same slices were used to assess plasticity of intrinsic excitability, whole-cell patch clamp recordings of CA1 pyramidal cells were performed. Once whole cell configuration was achieved, CA1 PCs were dye filled (Alexafluor 594 hidrazyde, Thermofisher Scientific was added to the 8 mM Cl^- K-gluconate internal solution 2.4), and baseline intrinsic physiology recordings were collected (see section 2.3.4.3). A small region of interest (ROI) was selected, including the dye filled cell and proximal SO of CA1, cap-

turing the full extent of the AISs from CA1 pyramidal cells. A Z-stack of the top 50 μm of the slice (1 μm steps) was acquired and the slice was transferred to a holding chamber containing recording ACSF (Table 2.3) with added 15 mM NaCl or 15 mM KCl for 3 h. Slices were transferred back to the recording chamber at the end of the 3 h treatment period, in order to image the initial ROI under the same conditions, using the filled cell as a landmark. At this point, whole cell patch clamp recordings were performed in the dye filled cell to assess intrinsic excitability after treatment in a pairwise manner.

2.5.2 Visual deprivation

Dark rearing (DR) of mice for 4 weeks (P0-P28) or 2 weeks (P14-P28) has previously been described to result in AIS plasticity *in vivo* (Gutzmann et al., 2014). At birth or at P14 mouse pups and the dam were put in a dark cabinet, in their home cage with food and water *ad libitum* and checked daily for 4 or 2 weeks, respectively. Complete darkness was controlled for by monitoring the exposure of photographic film placed in the cabinet throughout the experiments. At P28 the mice were perfusion fixed and brain tissue was processed for immunocytochemistry. Alternatively, mice were decapitated and used for acute slice preparation for electrophysiology. A schematic representation of the experimental timeline is shown in Figure 2.4.

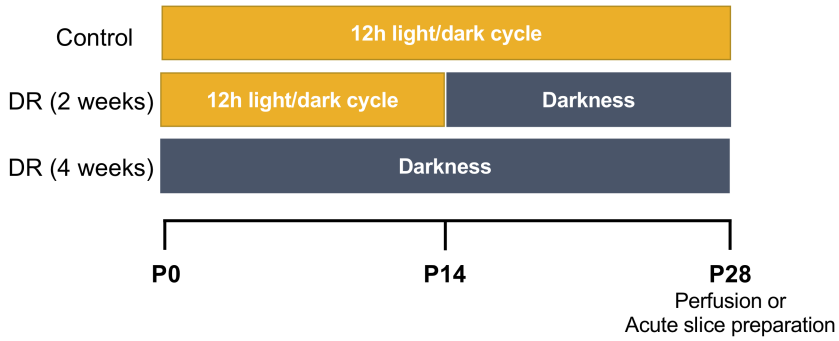

Figure 2.4: Schematic representation of experimental timeline for dark rearing experiments. Control animals were kept in a normal 12h light/dark cycle, animals were dark reared (DR) for 2 weeks (from P14 to P28) or for 4 weeks (from birth to P28).

2.6 Histology

2.6.1 Perfusion fixation

Mice and rats were sedated with isofluorane, followed by terminal anaesthesia with sodium pentobarbital (27.5 g/kg body weight) via intraperitoneal injection. Mice were then transcardially perfused with 20 mL PBS, followed by 20 mL of 4% PFA in 0.1 M PB (pH 7.4). The brain was removed and post-fixed in 4% PFA for 1 h. Rats were transcardially perfused with 20 mL PBS, followed by 30-40 mL of 4% PFA in 0.1 M PB (pH 7.4). The brain was removed and post-fixed in 4% PFA for 2h30min, and stored at 4°C in PBS after that until sectioning. Solutions used for perfusions were chilled and filtered prior to use.

Perfusion fixed brains were sectioned coronally in 50-55 μm thick sections using a vibratome (Leica VT 1000S). Sections containing the brain region of interest (dorsal hippocampus from *Fmr1* mice and *Cdkl5* rats and visual cortex from *Fmr1* mice used for dark rearing experiments and respective controls) were kept at 4°C in PBS until used for immunohistochemical labelling.

2.6.2 Immunohistochemistry

Acute slices used for AIS plasticity paradigms or sections of perfusion fixed brains were used for immunohistochemical labelling. Following blocking of non specific labelling in 10% normal goat serum (NGS, Vector Labs), 0.3% Triton-X100, 0.05% NaN_3 in PBS (Sigma-Aldrich, UK) for 1 h at room temperature, slices/sections were incubated at 4°C for 24 to 72 hours with primary antibodies (Table 2.6) diluted in 5% NGS, 0.3% Triton-X100 and 0.05% NaN_3 in PBS. Slices were then washed in PBS and incubated with secondary antibodies for 24 h at 4°C (diluted in PBS containing 3% NGS, 0.1% triton-X and 0.05% NaN_3). A list of the secondary antibodies and respective dilution used is provided in table 2.7. Slices were rinsed twice in PBS and three times in 0.1 M PB, before mounting in glass slides with Vectashield Hardset mounting medium (H-1400, Vector Labs).

The immunocytochemistry protocol described above was adjusted for use in dissociated hippocampal culture. The duration of the blocking step was reduced to 10 minutes. Coverslips were incubated with primary antibodies over-night at 4°C and secondary antibodies for 1 hour at room temperature. The composition of primary and secondary

antibody solutions was identical to that used in slices, but without Triton-X100.

Table 2.6: Primary antibodies used in immunohistochemical labelling

Antigen	Host	Dilution	Supplier	Catalog ID
Ankyrin G	Mouse	1:1000	Neuromab	N106/36
Ankyrin G	Rabbit	1:500	Santa Cruz	sc-28561
NeuN	Rabbit	1:1000	Merk Millipore	ABN78
NeuN	Mouse	1:1000	Merk Millipore	MAB377

Table 2.7: Secondary antibodies used in immunohistochemical labelling

Antibody	Alexa conjugate	Dilution	Supplier
Goat anti-mouse	488	1:500	Themofisher Scientific
	568		
Goat anti-rabbit	488		
	568		

2.6.3 Imaging and analysis for AIS length measurements

2.6.3.1 Confocal imaging

Images were acquired on inverted confocal microscope (Axiovert LSM 510, Zeiss), under a 63x/1.4 oil immersion objective. Z-stacks of 1 μm steps and 1024x1024 resolution were taken. For acute hippocampal slices used for AIS plasticity experiments, images of the hippocampal subfield CA1 were taken through the top 20 to 30 μm of the slices. Two Z-stacks of CA1 were taken per experimental condition for each animal.

For cell culture experiments I imaged 3 non-overlapping fields of view per coverslip, Z-stacks of 1 μm steps were taken from the top to bottom of the monolayer of cells.

For visual cortex sections, from dark rearing experiments, 2 Z-stacks were taken for each of the cortical layers in primary visual cortex. A schematic representation of the brain areas imaged is represented in Figure 2.5.

2.6.3.2 AIS length measurements

Image analysis was performed on FIJI (Image J), AISs were manually traced from their most proximal to distal end through the 3D image stack using the segmented line tool in FIJI, based on AnkyrinG labelling or β-Na_v-GFP signal (for live imaging experiments). Individual AIS lengths were exported to an Excel file and averaged per

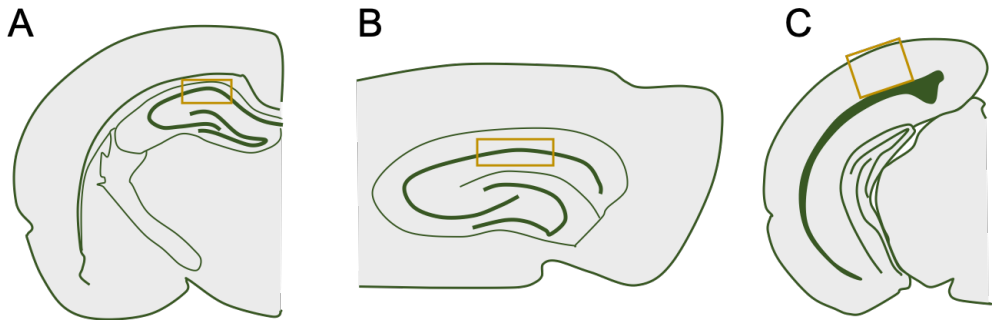

Figure 2.5: Schematic representation of brain areas imaged for AIS analysis. A - Coronal section containing dorsal hippocampus, Z-stacks including the pyramidal cell layer of hippocampus were taken to assess baseline AIS length in *Fmr1* mice; B - CA1 pyramidal cell layer was imaged in horizontal sections to assess AIS plasticity in acute hippocampal slices; C - All cortical layers in the primary visual cortex (V1) were imaged in sections from dark reared and control animals. Yellow boxes highlight the region of interest (A,B - CA1; V1 - C).

animal. For hippocampal slices and visual cortex sections 50 to 100 AISs were measured per animal for each experimental condition. For cell culture experiments, 10 to 15 AISs were measured per coverslip and averaged per embryo, for each experimental condition. For live imaging experiments, the same 10 to 15 AISs were measured per slice at the start and end of the 3 h treatment period. To validate the β1-NaV-GFP AIS labelling, I measured AIS length based on GFP signal and Ankyrin G labelling on the same AISs.

2.7 Statistical analysis

Graphpad prism 7 was used to perform statistical comparisons across groups using two-tailed unpaired T-test, repeated measures two-way ANOVA, or non-parametric tests as appropriate, using animal numbers as the experimental unit. Details on sample size and statistical test used are presented in the figure legends. For a subset of data, the R package lme4 (Bates et al., 2014) was used to fit mixed effects models (GLMM for data fitting a gamma distribution or LMM for normal and log-normal distributed data) to compare across groups, using genotype, age or treatment (or combinations of these where relevant) as fixed effects and animal, slice (and cell where relevant) as random effects. Where mixed effects models were used the experimental unit was cells, except for quantification of dendritic spine density (Figure 3.7) where dendrite section was used as the experimental unit. This approach avoids pseudoreplication, whilst taking into consideration the wealth of data that comes from multiple measurements per animal, which is lost when using animal averages. For all data $p<0.05$ was used as the criteria

for significance and defined throughout as *p<0.05, **p<0.01, ***p<0.001.

Chapter 3

Cellular excitability and synaptic physiology in a rat model of CDKL5 deficiency disorder

3.1 Introduction

CDKL5 deficiency disorder (CDD) is a severe neurological disorder caused by mutations in the X-linked gene cyclin-dependent kinase-like 5 (*CDKL5*; MIM: 300203) (Bahi-Buisson and Bienvenu, 2012). It is estimated to affect 1 in 41 000 live births (Symonds et al., 2019), with patients typically presenting with early onset seizures, sleep disturbances, motor impairments, autistic features and severe intellectual disability (ID) (Fehr et al., 2013; Olson et al., 2019).

Pathogenic mutations in the *CDKL5* gene are predicted to result in loss of protein function and predominantly cluster in the catalytic domain of CDKL5 (Hector et al., 2017b), which is highly conserved across mice, rats and humans (Hector et al., 2017a, 2016). Identification of physiological substrates of CDKL5 has suggested a role in cytoskeleton organisation (Baltussen et al., 2018; Muñoz et al., 2018) which appears to be NMDAR dependent (Baltussen et al., 2018). In line with this role in cytoskeletal organisation, reduced dendritic complexity and altered spine distribution have been repeatedly reported in mouse models of CDD (Amendola et al., 2014; Della Sala et al., 2016; Fuchs et al., 2014; Tang et al., 2017; Okuda et al., 2018). These anatomical phenotypes are frequently associated with abnormal synaptic function. In fact, altered cellular and synaptic physiology has been reported in the hippocampus of a variety of mouse models (Tang et al., 2017; Okuda et al., 2017; Yennawar et al., 2019), with enhanced long-term potentiation (LTP), attributed to increased expression of GluA2 lacking CP-AMPARs by Yennawar et al. (2019) and, alternatively, to NMDAR dys-

function by (Okuda et al., 2017). These phenotypes are thought to underlie seizure susceptibility, as well as hippocampal dependent learning deficits (Okuda et al., 2017, 2018; Tang et al., 2017).

Mouse models of CDD display not only impaired short-term hippocampal dependent learning (Fuchs et al., 2014; Okuda et al., 2018) but also long term spatial memory impairments (Okuda et al., 2018). The consolidation of spatial memory is known to be dependent on mPFC, and, in particular, on the connection between hippocampus and mPFC (Binder et al., 2019; Backus et al., 2016). Moreover hippocampus-mPFC connectivity is also involved in anxiety related behaviour (Adhikari et al., 2010; Padilla-Coreano et al., 2016), shown to be altered in mouse models of CDD (Okuda et al., 2018; Wang et al., 2012; Jhang et al., 2017). However, the precise role of CDKL5 in anxiety related behaviour remains unclear, with studies showing either increased (Okuda et al., 2018) or reduced (Wang et al., 2012) anxiety-like behaviour depending on the mouse model used.

Given conflicting reports from the different mouse models it is imperative to identify robust physiological phenotypes that cross the species barrier in order to identify disease mechanisms and therapeutic strategies which might translate to the human condition. For this reason, I have used an outbred rat model of CDD to determine whether previously published phenotypes are robustly expressed, independent of species. Given that the behavioural domains affected in mouse models of CDD can be explained by alterations to the limbic system, I hypothesise that loss of CDKL5 leads to impaired synaptic function in the hippocampus and mPFC of *Cdkl5*$^{-/y}$ rats. To address this, I have examined neuronal excitability, synaptic physiology and plasticity, and cellular morphology of neurons in these regions using a combination of extracellular and whole cell electrophysiological recordings and histology

3.2 Results

3.2.1 Typical cellular excitability but reduced AP amplitude in CA1 pyramidal cells from P28 *Cdkl5*$^{-/y}$ rats

Cellular excitability can have a large impact on circuit function and information processing as it determines how neurons respond to synaptic inputs. Indeed, altered cellular excitability is a feature common to a variety of rodent models of ASD/ID, and it is thought to contribute to abnormal circuit function and behavioural phenotypes (Contractor et al., 2015; Zhang et al., 2014; Clement et al., 2012). Mouse models of CDD show impairments in hippocampal dependent behavioural tasks (Okuda et al., 2018). I have examined cellular excitability of CA1 pyramidal cells by performing whole cell electrophysiological recordings in current clamp mode, using a 24 mM Cl^- K-gluconate based internal solution (Table 2.4).

Firstly, I assessed passive membrane properties, as membrane time constant and input resistance determine how membrane potential changes in response to synaptic input, and are therefore important in regulating cellular excitability. CA1 pyramidal cells from WT rats exhibited a hyperpolarised resting membrane potential, fast membrane time constant and low input resistance (Table 3.1), consistent with earlier studies (Spruston and Johnston, 1992; Staff et al., 2000). I found these properties to be unchanged in *Cdkl5*$^{-/y}$ neurons relative to WT controls (Table 3.1).

Next, I examined firing properties of these cells in response to depolarising current steps (-100 to +400 pA, in 25 pA steps). WT neurons required 206 ± 20 pA of current injection to elicit the first AP (rheobase, Figure 3.1 C), the number of APs fired increased with current injection thereafter until reaching a firing frequency of 22 ± 2 Hz in response to the maximum current injection step (400 pA). The overall firing response to increasing current steps was unchanged in cells from *Cdkl5*$^{-/y}$ rats (Two-Way ANOVA $F_{16,208}$=0.12, genotype effect: p=0.66, Figure 3.1, B), as was the rheobase current (LMM, p=0.91, Figure 3.1 C).

The properties of single APs reflect the function of specific ionic conductances. Whilst the rise phase of the AP is determined by the activation of VGSCs, the decay phase of the AP is determined by the inactivation of VGSCs and activation of voltage gated potassium channels. When examining the AP properties of the first AP elicited, all AP kinetic properties in WT neurons were consistent with what has been previously

Table 3.1: Passive membrane properties of CA1 pyramidal cells

Physiological property	**WT**	***Cdkl5*$^{-/y}$**	**Stats test**	**p value**
Resting membrane potential (mV)	-69.8 ± 1.2	-69.2 ± 1.1	LMM	0.56
Input resistance (MΩ)	68.1 ± 6.8	65.4 ± 3.0	LMM	0.64
Membrane time constant (ms)	19.1 ± 1.0	20.7 ± 2.1	LMM	0.64
Capacitance (pF)	299 ± 23	331 ± 35	LMM	0.69

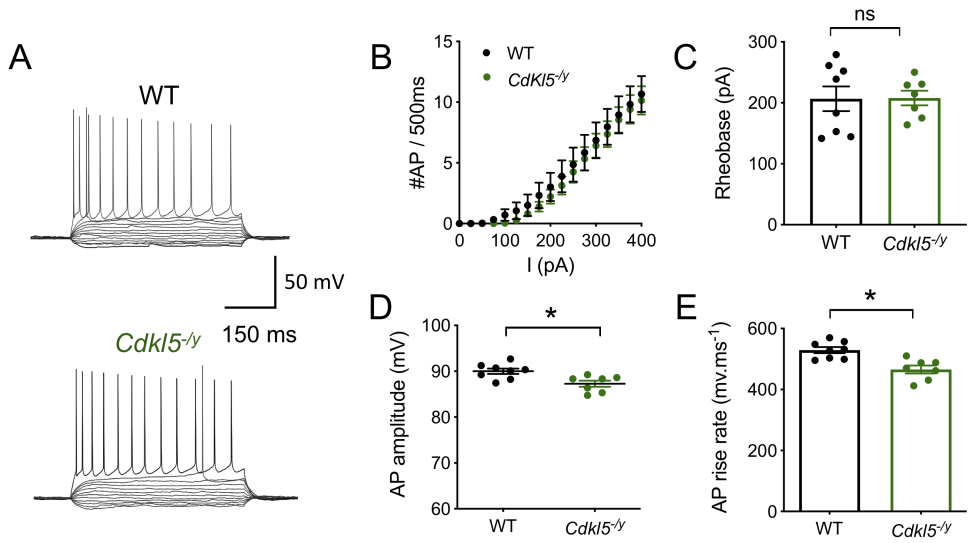

Figure 3.1: Typical excitability but reduced AP amplitude in CA1 pyramidal cells A - Representative traces of whole cell recordings from CA1 pyramidal cells in response to subsequent 25 pA steps. Traces shown from -100 pA to rheobase-1 and for the maximum firing frequency (I = 400 pA). B - Action potential discharge in response to 500 ms long 25 pA current steps up to 400 pA (Two-way ANOVA genotype effect $F_{16,208}$=0.12, p = 0.66). C - Rheobase current (LMM, p=0.91).D - Reduced AP amplitude in *Cdkl5*$^{-/y}$ rats (LMM, p=0.008) and slower rise rate (LMM, p=0.0001, measured from the first AP fired) Data shown as mean ± SEM (WT – n = 26 cells/8 rats, *Cdkl5*$^{-/y}$ – n = 24 cells/7 rats, dots represent animal averages. Statistics shown: *p<0.05, ns - p>0.05, GLMM

reported (Spruston and Johnston, 1992; Staff et al., 2000). However, I found APs to have a smaller amplitude and slower rise rate in *Cdkl5*$^{-/y}$ neurons (Figure 3.1, Table 3.2). All other AP kinetic properties examined were unchanged relative to WT (Table 3.2). Importantly, the change in AP amplitude and rise rate I observed was not due to differences in access resistance across recordings from different genotypes, as this was also unaltered (Table 3.2).

Table 3.2: Action potential properties of CA1 pyramidal cells

Physiological property	**WT**	***Cdkl5***$^{-/y}$	**Stats test**	**p value**
Voltage threshold (mV)	-44.2 ± 0.5	-43.7 ± 0.5	LMM	0.56
Half height duration (ms)	0.76 ± 0.02	0.78 ± 0.03	LMM	0.54
Amplitude (mV)	90.0 ± 0.6	87.3 ± 0.7	LMM	*0.008
Max rise rate (mV.ms^{-1})	529 ± 10	466 ± 13	LM	*0.001
Max decay rate (mV.ms^{-1})	103 ± 3	99 ± 5	LMM	0.56
Access resistance (MΩ)	11.28 ± 0.86	11.36 ± 0.76	LM	0.72

These data suggest that intrinsic excitability is largely unaltered in CA1 pyramidal neurons of *Cdkl5*$^{-/y}$ rats, however the altered AP amplitude and kinetics here described may have a wider impact in neuronal function (Spratt et al., 2019).

3.2.2 Unaltered AIS length in *Cdkl5*$^{-/y}$ rats

The AIS is the site of AP initiation and altered AIS structure can contribute to altered cellular excitability and in particular, altered AP waveform (Kole et al., 2007; Evans et al., 2015). Indeed increased AIS length has been associated with cellular hyperexcitability of CA1 pyramidal cells in mouse models of Angelman Syndrome (Kaphzan et al., 2011) and FXS (Chapter 4 of this thesis).

To address the hypothesis that altered AIS length contributes to the altered AP waveform observed in *Cdkl5*$^{-/y}$ rats, I used immunohistochemistry to label AISs in hippocampal sections from P28 perfusion fixed rats. Using the scaffolding protein AnkyrinG as an AIS marker allowed to reliably visualise AISs of CA1 pyramidal cells, which emerged from the *str. pyramidale* into the *str oriens*.

By measuring AISs from their proximal to distal end, I found AIS length in the CA1 area of the hippocampus to be unaltered in *Cdkl5*$^{-/y}$ rats (Figure 3.2). In *Cdkl5*$^{-/y}$ rats, AISs measured on average 34.02 ± 0.72 μm, not different from those of WT (33.75 ± 0.62 μm, Two-Tailed T test: T_8=0.28, p=0.79, Figure 3.2B). This is also

reflected in the overlapping cumulative distribution of AIS length from both genotypes (Figure 3.2C). This data suggests the reduced AP amplitude observed in CA1 pyramidal cells does not result from abnormal AIS structure.

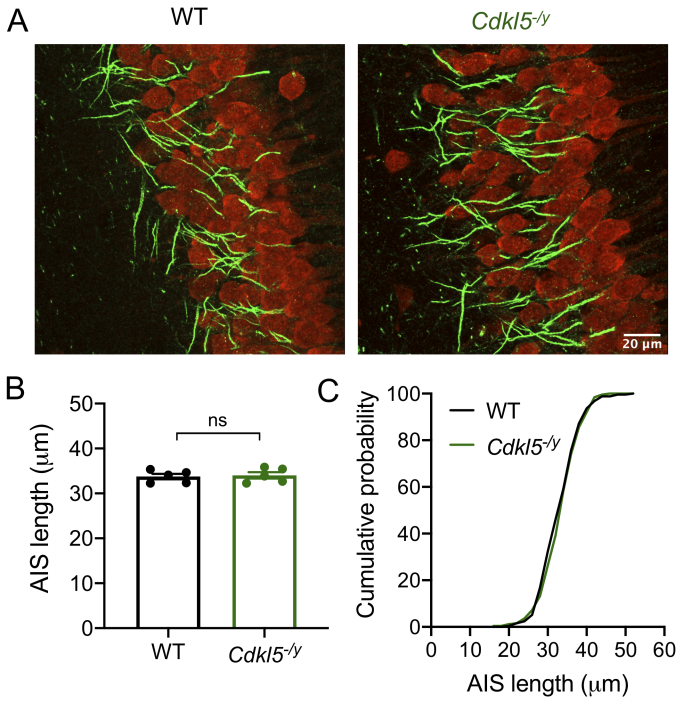

Figure 3.2: Unaltered AIS length in CA1 of *Cdkl5*$^{-/y}$ *rats* A - Representative images of CA1 sections labelled for the neuronal marker NeuN (red) and the AIS scaffolding protein AnkyrinG (green). B – AIS length in WT and *Cdkl5*$^{-/y}$ *rats* (data shown as mean ± SEM, dots represent animal averages), C – cumulative distribution of AIS length (WT n= 250 AISs / 5 rats, *Cdkl5*$^{-/y}$ n= 250 AISs / 5 rats), ns - p>0.05 Two-tailed T test

3.2.3 Synaptic physiology in the hippocampus of *Cdkl5*$^{-/y}$ *rats*

3.2.3.1 Enhanced hippocampal LTP in *Cdkl5*$^{-/y}$ rats

To examine synaptic plasticity in the hippocampus of *Cdkl5*$^{-/y}$ rats we performed extracellular field recordings in horizontal hippocampal slices from *Cdkl5*$^{-/y}$ rats and their WT littermate controls aged P28 to P35. fEPSPs were evoked by placing a stimulation electrode in the *SR*, activating the SC pathway (Figure 3.3A). Electrical stimulation reliably produced a synaptic response consisting of an afferent fibre volley followed by the fEPSP, with a smooth rise, a peak, and decay phases (Figure 3.3B). To assess hippocampal LTP, the slope of the rise phase of the fEPSP was measured over a baseline period of 20 minutes and for 1 h following tetanic stimulation (2 trains

of 100 Hz stimulation for 1 s). In line with previous studies (Komiyama et al., 2002), tetanic stimulation reliably induced potentiation of the post-synaptic response which was maintained for up to 1 h in WT rats. Indeed, fEPSP slope was 138.3 ± 5.8% of baseline in the final 10 min of the recordings Analysis of the LTP time course (Figure 3.3C) revealed enhanced LTP in *Cdkl5*$^{-/y}$ rats (Two-way ANOVA Interaction: $F_{79,1501}$=7.76, p<0.0001, genotype effect p<0.0001). The increase in post-synaptic response after LTP induction was consistently higher in *Cdkl5*$^{-/y}$ throughout the recording (p<0.05 for every minute post-tetanus, post-hoc Sidak's multiple comparison test), indicating enhanced post-tetanic potentiation as well as enhanced LTP. In the final 10 min of the 1 h recording *Cdkl5*$^{-/y}$ rats fEPSP slope was 176.1 ± 5.6% of baseline, significantly higher than that observed in WT (Two tailed T test, T_{19}=4.45, p=0.0003, Figure 3.3D).

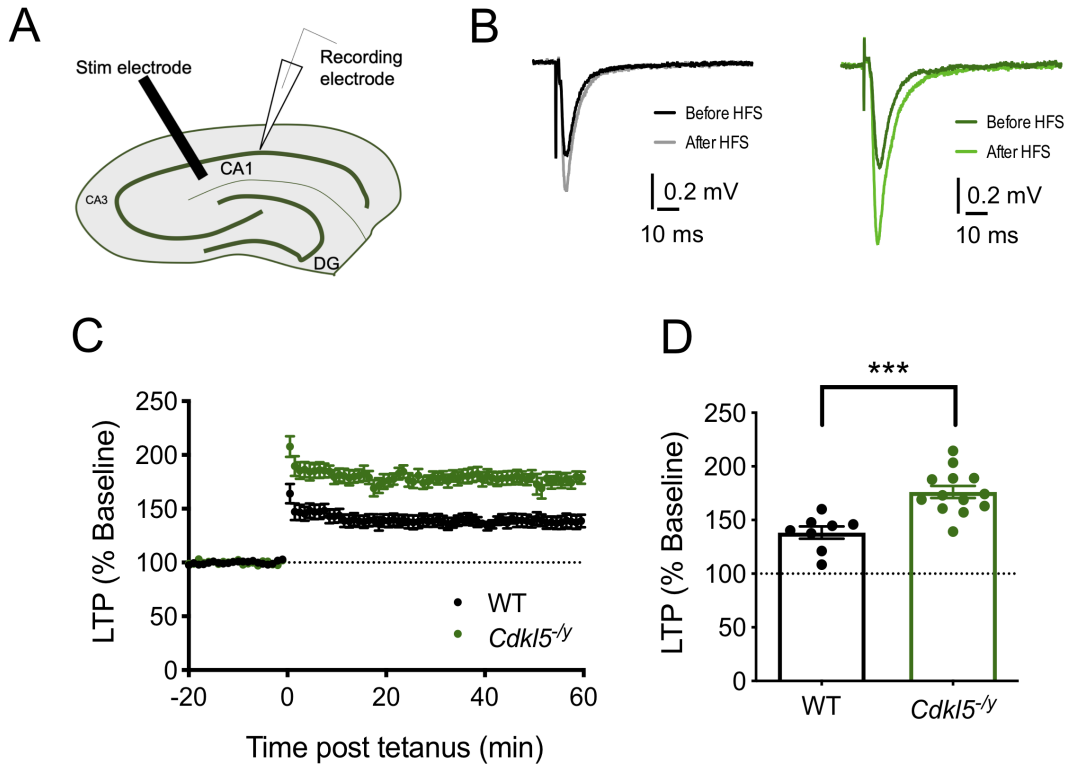

Figure 3.3: Enhanced hippocampal LTP in *Cdkl5*$^{-/y}$ rats. A – recording setup schematic. B – Representative WT (left, black) and *Cdkl5*$^{-/y}$(right, green) fEPSP traces before and after tetanic stimulation (HFS). C - Time-course showing LTP in the hippocampal CA1 induced by two trains with 100 pulses at 100 Hz (20 seconds apart), resulting in a significant increase in LTP in *Cdkl5*$^{-/y}$ rats when compared to WT rats (Two-way ANOVA Interaction: $F_{79,1501}$=7.76, p<0.0001, genotype effect p<0.0001, ***p<0.001 Two tailed T test). D - LTP as percentage of baseline fEPSP slope in the final 10 minutes. (WT n = 8 rats; *Cdkl5*$^{-/y}$: n = 13 rats; , data shown as mean ± SEM, dots represent average of 2 slices per animal). Data collected and analysed by Rita Loureiro.

3.2.3.2 Unaltered NMDAR and AMPAR function in *Cdkl5*$^{-/y}$ rats

Both AMPAR and NMDAR dysfunction and altered subunit composition have been suggested to contribute to abnormal LTP in mouse models of CDD (Okuda et al., 2017; Yennawar et al., 2019). Therefore, I assessed the NMDAR/AMPAR ratios of synaptic responses at the Schaffer collateral synapse of CA1, to test whether NMDAR receptor function was altered in *Cdkl5*$^{-/y}$ rats, possibly contributing to the enhanced LTP phenotype observed. AMPAR-mediated currents were recorded at a holding potential of -70 mV, whilst NMDAR-mediated EPSCs were recorded at +40 mV in the presence of the AMPAR antagonist CNQX (Figure 3.4A). WT neurons exhibited NMDAR/AMPAR ratio of 0.62 ± 0.08 (Figure 3.4B) and an average NMDAR-mediated EPSC decay time of 85.69 ± 5.07 ms (Figure 3.4C), consistent with the values reported in the literature (Arrigoni and Greene, 2004; Otmakhova et al., 2002). NMDAR/AMPAR ratio (Figure 3.4B) was unaltered in *Cdkl5*$^{-/y}$ rats (0.84 ± 0.14, GLMM: p=0.31). NMDAR mediated EPSC decay time was also unchanged in *Cdkl5*$^{-/y}$ rats (105.3 ± 16.50 ms, p=0.78 Mann-Whitney test). These data suggest that NMDAR receptor function is unaltered in *Cdkl5*$^{-/y}$ rats.

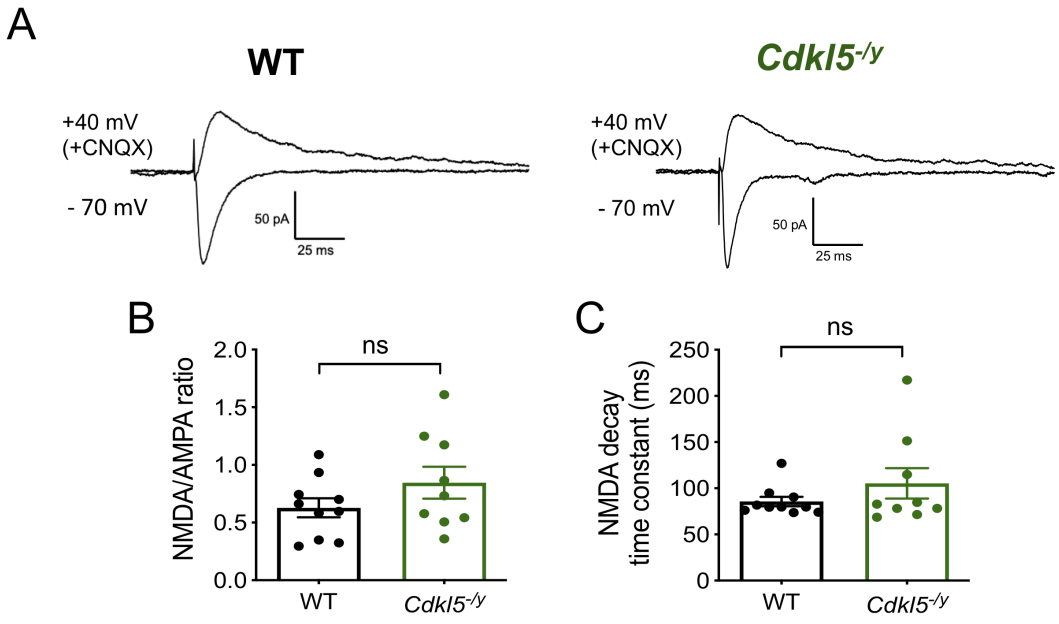

Figure 3.4: Unaltered NMDAR/AMPAR ratio in *Cdkl5*$^{-/y}$ rats. A – Representative traces of AMPAR and NMDAR mediated currents evoked by stimulating Schafer collateral inputs to CA1 via *str radiatum*. B – NMDAR/AMPAR ratio (p=0.31 GLMM), C – Pharmacologically isolated NMDA mediated EPSC decay time (p=0.78 Mann-Whitney U test performed on animal averages). Data shown as mean ± SEM (WT n = 10 rats / 14 cells; *Cdkl5*$^{-/y}$: n = 9 rats / 18 cells), dots represent animal averages

An increase in expression of CP-AMPARs has been suggested to contribute to enhanced LTP in *Cdkl5*$^{-/y}$ mice (Yennawar et al., 2019). Therefore, I tested the hypothesis that increased Ca^{2+} influx through CP-AMPAR contributes to the enhanced LTP phenotype observed in *Cdkl5*$^{-/y}$ rats. I recorded AMPAR-mediated EPSCs by stimulating the Schaffer collateral pathway, as described for the LTP recordings, and performing whole-cell recordings in voltage clamp from CA1 pyramidal cells in the presence of AP-5 and picrotoxin to block NMDAR and GABA-A receptor mediated currents, respectively. The intracellular solution in the recording pipette contained 0.1 mM of spermine to maintain the intracellular polyamine block, which leads to rectification of GluA2-lacking AMPARs (Kamboj et al., 1995). EPSCs were recorded over a range of holding potentials from -80 mV to +40 mV, in 20 mV increments (Figure 3.5 A).

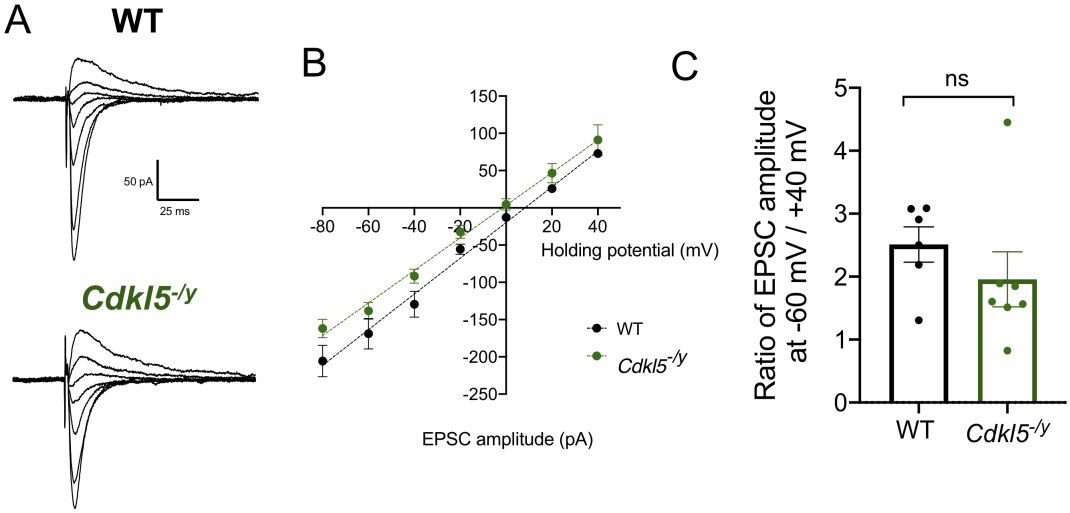

Figure 3.5: AMPAR-mediated EPSC IV relationship in *Cdkl5*$^{-/y}$ rats. A – Representative traces of AMPAR-mediated currents recorded over a range of holding potentials (-80mV to +40 mV) in the presence of 0.1 mM spermine in the intracellular solution. B – IV relationship of AMPAR-mediated EPSC amplitude with linear regression (dashed line) ($F_{1,87}$=1.54, p = 0.22, Sum-of-least squares F-test) C – Rectification index calculated as the ratio of EPSC amplitude at -60 mV over +40 mV (p=0.29, GLMM). Data shown as mean ± SEM (WT n = 6 rats / 12 cells; *Cdkl5*$^{-/y}$: n = 7 rats / 16 cells), dots represent animal averages.

AMPAR mediated EPSCs exhibited a linear current-voltage (I-V) relationship in WT neurons (r^2=0.90, linear regression), indicating no inward rectification and consistent with the high GluA2 expression in CA1 pyramidal cells (He et al., 1998). The I-V relationship of AMPAR receptor mediated EPSCs was also linear in *Cdkl5*$^{-/y}$ rats (r^2=0.89, linear regression, Figure 3.5B). The slope of the linear I-V relationship in

Cdkl5$^{-/y}$ rats did not differ to that of WT rats ($F_{1,87}$=1.54, p = 0.22, Sum-of-least squares F-test), in line with the unaltered rectification index calculated as the ratio of EPSC amplitude at the holding potentials of -60 mV and +40 mV (Figure 3.5 C, WT: 2.51 ± 0.28, *Cdkl5*$^{-/y}$: 1.96 ± 0.44, p=0.29 GLMM).

Together, these data suggest that alterations to NMDAR and AMPAR-mediated synaptic transmission do not contribute to the enhanced LTP that is observed in *Cdkl5*$^{-/y}$ rats, as I've found unaltered NMDAR/AMPAR ratios and typical AMPAR I-V relationship in the rat model of CDD.

3.2.3.3 Typical CA1 pyramidal cell morphology but altered spine density in *Cdkl5*$^{-/y}$ rats

Altered dendritic morphology has previously been reported in mouse models of CDD (Okuda et al., 2018; Tang et al., 2017; Amendola et al., 2014). As dendritic morphology can have profound effects on how synaptic inputs are processed (Vetter et al., 2001; Mainen and Sejnowski, 1996), I next reconstructed biocytin filled neurons from whole cell recordings in order to examine dendritic arborisation and spine density across different dendritic domains.

In WT rats, reconstructed neurons exhibited typical CA1 pyramid morphology (Amaral and Witter, 1989; Ishizuka et al., 1995; Bannister and Larkman, 1995), with a large calibre apical dendrite extending through the *SR*, which ramified into thinner oblique dendrites along the *SR* and bifurcates forming tuft dendrites in the *SLM*. Basal dendrites extended from the soma into the the *SO*. Example reconstruction of CA1 pyramidal cells from both genotypes can be found in Figure 3.6A. I found a significant interaction of Sholl radius and genotype when examining the Sholl profile (Figure 3.6A, Two-way ANOVA on animal averages, Interaction: F 76,912 = 2.094, p<0.001, genotype effect: p=0.38), indicating altered dendritic distribution in *Cdkl5*$^{-/y}$ rats. Nonetheles, total dendritic length (WT: 9882 μm ± 707 μm, *Cdkl5*$^{-/y}$: 9455 μm ± 610 μm, Two-tailed T Test: T=0.46, df=12, p=0.66) as well as total length of apical (WT: 6622 μm ± 520 μm,*Cdkl5*$^{-/y}$: 5795 μm ± 519 μm, Two-tailed T Test: T=1.12, df=12, p=0.28) and basal dendrites (WT: 3260 μm ± 257 μm, *Cdkl5*$^{-/y}$: 3660 μm ± 275 μm, Two-tailed T Test: T=1.06, df=12, p=0.31) were unchanged (Figure 3.6C-E), indicating that overall dendritic complexity is not affected by the lack of CDKL5.

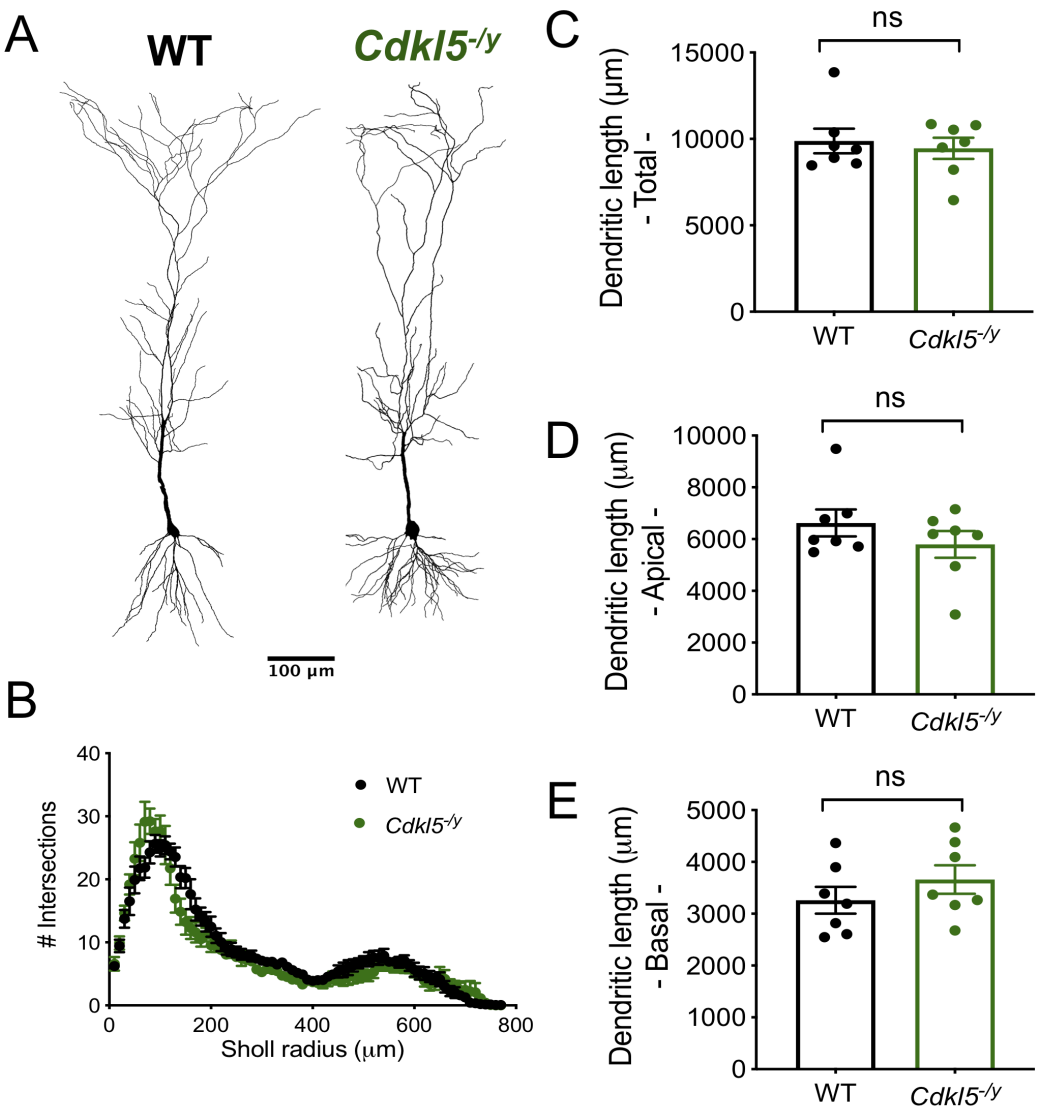

Figure 3.6: CA1 pyramidal cell morphology in *Cdkl5*$^{-/y}$ rats. A – Example reconstruction of CA1 pyramidal cells from WT and *Cdkl5*$^{-/y}$ rats filled with biocytin during whole cell patch clamp recordings. B – Sholl analysis of the dendritic arborisation (Two way ANOVA: Interaction: F 76,912 = 2.094, p<0.001, genotype effect p = 0.38) . C – Total dendritic length, D – total length of basal dendrites, E – total length of apical dendrites. Data shown as mean ± SEM (WT - n=14 cells/7 rats, *Cdkl5*$^{-/y}$ - n=14 cells/7 rats, dots represent animal averages, all p values > 0.05, Two tailed t-test on animal averages).

WT CA1 pyramidal cells exhibited a characteristic high density of dendritic spines (Megıas et al., 2001; Bannister and Larkman, 1995), with oblique dendrites showing the highest spine density (20.02 ± 1.76 spines/10 μm), followed by basal dendrites (16.08 ± 0.98 spines/10 μm) and the lowest spine density in tuft dendrites (8.71 ± 0.78 spines/10μm, Figure 3.7). Despite no overall changes in gross dendritic morphology, I found a 19% increase in spine density in the basal dendrites of CA1 pyramidal cells from *Cdkl5*$^{-/y}$ rats (19.18 ± 1.18 spines/10 μm, LMM p=0.04, Figure 3.7B). In *Cdkl5*$^{-/y}$ rats, spine density was unaltered in the two domains of apical dendrites examined (Figure 3.7C,D): oblique (18.30 ± 0.92 spines/10 μm, LMM p=0.71) and tuft (8.26 ± 0.82 spines/10 μm LMM p=0.71). These data suggest that excitatory synaptic inputs might be altered in *Cdkl5*$^{-/y}$ in a dendritic domain specific manner.

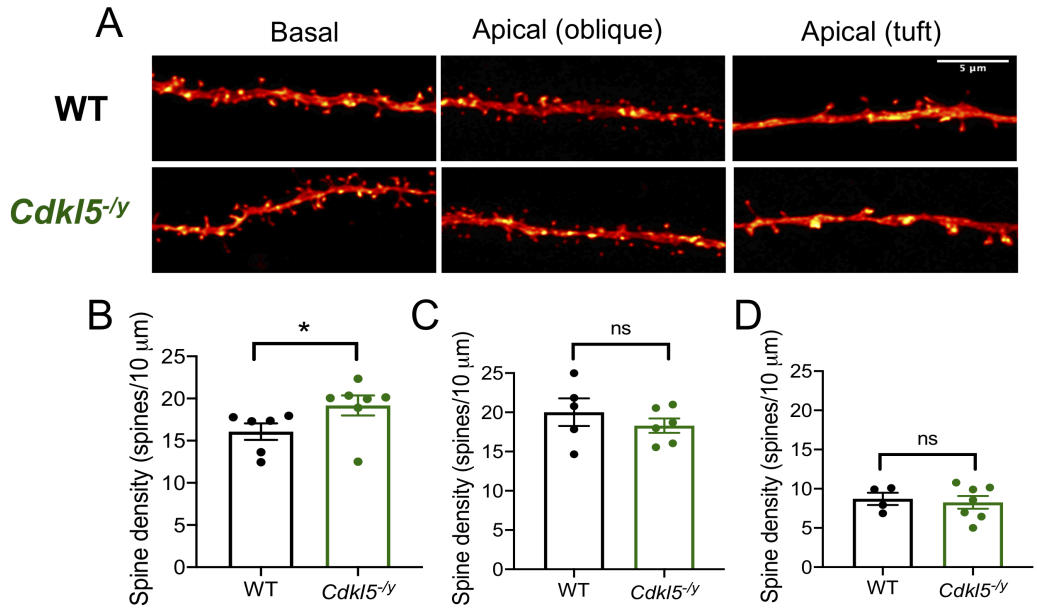

Figure 3.7: Spine density across dendritic compartments of CA1 pyramidal cells in *Cdkl5*$^{-/y}$ rats. A – Representative segments of basal and apical (oblique and tuft) dendrites from CA1 pyramidal cells filled during whole cell patch clamp recordings. B – Spine density in basal dendrites (WT: n = 12 cells/6 rats, *Cdkl5*$^{-/y}$: n = 12 cells/7 rats). C – Spine density in apical oblique dendrites (WT: n = 9 cells/6 rats, *Cdkl5*$^{-/y}$: n = 12 cells/6 rats). D – Spine density in apical tuft dendrites (WT: n = 7 cells/4 rats, *Cdkl5*$^{-/y}$: n = 11 cells/7 rats). Data shown as mean ± SEM, dots represent animal averages. *p<0.05, ns p>0.05 LMM

3.2.3.4 Excitatory synaptic function in *Cdkl5*$^{-/y}$ rats

Dendritic spines are the typical site of excitatory synapse formation, therefore I used whole cell patch clamp recordings to examine mEPSCs in CA1 pyramidal cells, as a functional correlate for the increased spine density (Figure 3. A). I found mEPSC amplitude to be unchanged (WT: 11.51 ± 0.82 pA, *Cdkl5*$^{-/y}$: 10.88 ± 0.69 pA, LMM p=0.64) and a 30% reduction in mEPSC frequency in CA1 pyramidal cells from 5.43 ± 0.49 Hz in WT to 3.78 ± 0.34 Hz in *Cdkl5*$^{-/y}$ rats (GLMM p=0.06). The difference in mEPSC frequency between genotypes was significant when using normal parametric statistics (Two tailed T-test on animal averages p=0.02) and a linear model fitted with a log-normal distribution (p=0.02), however when using a GLMM with a gamma distribution p=0.06. I tested both distributions when using mixed effects models as the data fit similarly both distributions (further details on the statistical analysis for this data set is given in Appendix B). Given these statistical results and the effect size, I believe this to be a biologically relevant effect and will discuss it as such for the remaining of this chapter.

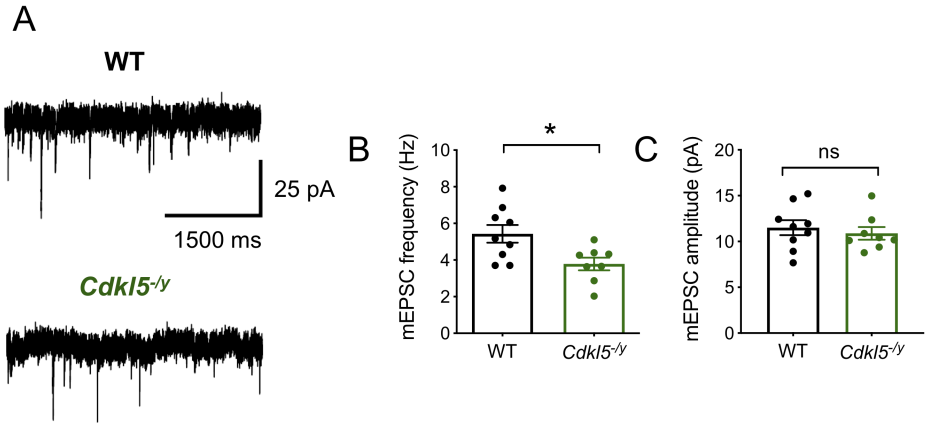

Figure 3.8: Reduced mEPSC frequency in *Cdkl5*$^{-/y}$ rats. Representative traces of mEPSC recordings from CA1 pyramidal cells from WT and *Cdkl5*$^{-/y}$ rats (A). mEPSC frequency (B, p=0.06 GLMM) and mEPSC amplitude (C, p=0.64 LMM): WT n = 24 cells / 9 rats, *Cdkl5*$^{-/y}$ n = 20 cells / 8 rats. Data shown as mean ± SEM, dots represent animal averages.

This reduction in mEPSC frequency is not consistent with the increased spine density I observed. As such, it is possible that the alterations in mEPSC frequency and synaptic plasticity may be a consequence of altered pre-synaptic function; particularly given that CDKL5 phosphorylates the pre-synaptic protein amphiphysin-1 (Sekiguchi et al., 2013).

Paired pulse ratio (PPR) has traditionally been used to assess pre-synaptic release probability (Debanne et al., 1996; Dobrunz et al., 1997). To determine whether the

decrease in mEPSC frequency resulted from a reduction in pre-synaptic release probability I assessed PPR by evoking two EPSCs 50 ms apart and calculating the ratio of the amplitude of the second EPSC relative to the first EPSC. Unlike the mEPSC recordings, this approach also allowed me to tap into the dendritic domain specific synaptic transmission. EPSCs were evoked by placing a stimulating electrode in the *SR* (Figure 3. F-G), preferentially activating synapses in the apical oblique dendrites or *SO*, preferentially activating synapses in the basal dendrites of CA1 pyramidal cells (Figure 3. H-I, Ishizuka et al. (1990) to address the hypothesis that synaptic inputs to CA1 pyramidal cells are altered in a dendritic domain dependent manner.

I found that in both cases synapses were facilitating (i.e. PPR>1) but observed no difference between *Cdkl5*$^{-/y}$ rats and WT controls. Stimulating CA1 inputs in the *SR* resulted in a postsynaptic response with a PPR of 1.71 ± 0.11 in WT and 1.97 ± 0.18 in *Cdkl5*$^{-/y}$ rats (LMM p=0.33). Stimulating CA1 inputs in the *SO* resulted in a postsynaptic response with a PPR of 1.60 ± 0.10 in WT and 1.60 ± 0.10 in *Cdkl5*$^{-/y}$ rats (LM p=0.62). In a subset of recordings I also tested a PPR over a range of ISIs (Figure 3.9 D and H) and found no significant effect of genotype in either the *SR* (Two-way ANOVA on animal averages interaction: $F_{2,20}$=1.01, p=0.38, genotype effect: p=0.30) or *SO* (Two-way ANOVA on animal averages interaction: $F_{2,10}$=0.7, p=0.52, genotype effect: p=0.48) stimulation paradigms.

This data suggests that pre-synaptic release probability is unaltered in *Cdkl5*$^{-/y}$ rats, both in synapses onto the basal dendrites and synapses onto the apical-oblique dendrites.

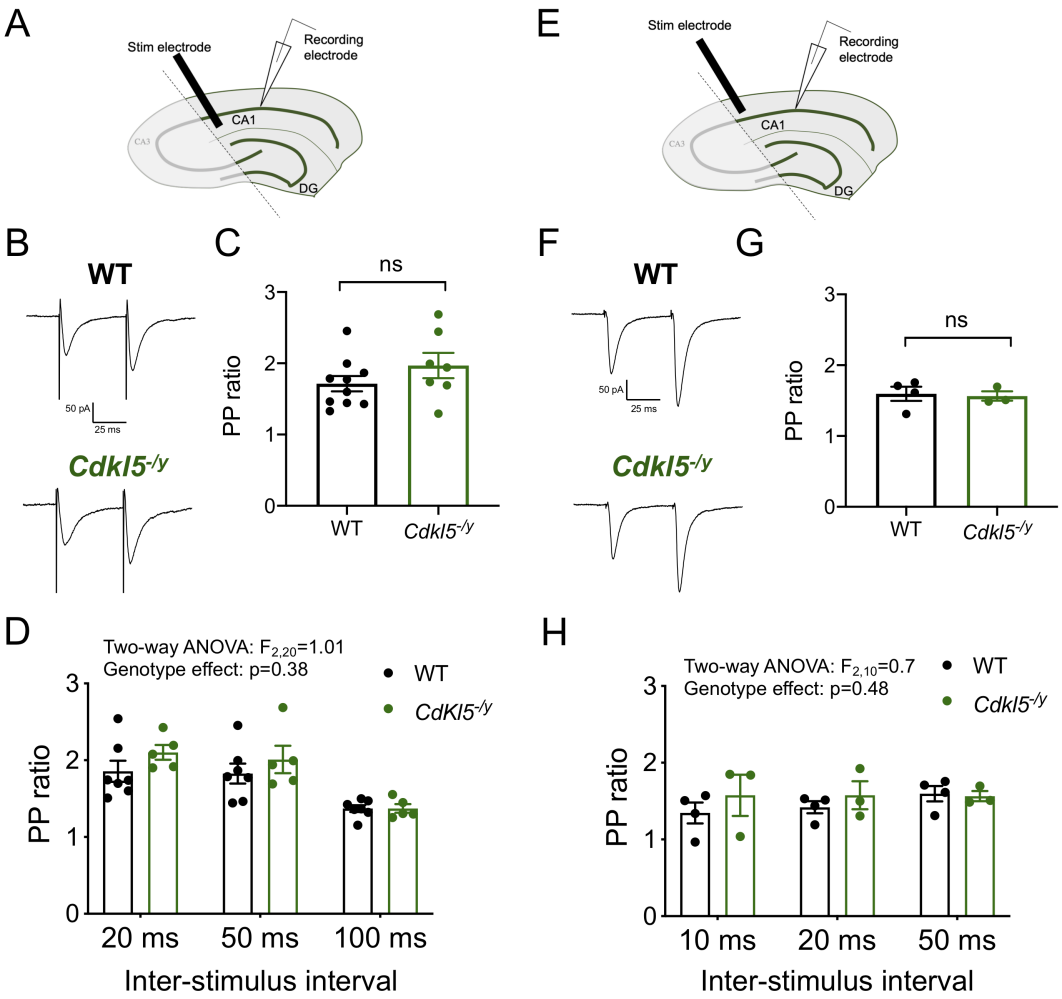

Figure 3.9: Typical paired pulse facilitation in *Cdkl5*$^{-/y}$ rats. Schematic representation of recording configuration: stimulation of CA3 inputs to CA1 via *Stratum radiatum* (A) and *Stratum oriens* (E). Representative traces of EPSCs evoked by paired pulse stimulation (50 ms ISI) of *Stratum radiatum* (B) and *Stratum oriens* (F) and respective paired pulse ratio (C: WT n= 20 cells / 10 rats, *Cdkl5*$^{-/y}$ n= 10 cells / 7 rats; I: WT 12 cells / 4 rats, *Cdkl5*$^{-/y}$ n= 6 cells / 3 rats). PP ratio over a range of ISIs (D, H). Data shown as mean ± SEM, dots represent animal averages, ns-p>0.05 LMM

3.2.3.5 Minimal stimulation of CA3 inputs to CA1 pyramidal cells

Synapses containing NMDARs but no AMPARs are thought to be functionally silent, as the voltage dependence of NMDAR activation means these synapses would be inactive at resting membrane potential (Isaac, 2003; He et al., 1998). Moreover, AMPAR insertion at silent synapses is a crucial process in LTP expression (Isaac et al., 1995; Wyllie et al., 1994; Kullmann and Nicoll, 1992). Given the increase in spine density in basal dendrites accompanied by a reduction in mEPSC frequency, I next asked whether *Cdkl5*$^{-/y}$ rats rats exhibit a greater abundance of silent synapses. I used a minimal stimulation paradigm to elicit on-or-off EPCSs in CA1 pyramidal cells and compared the event probability at a holding potential of -70 mV, when AMPAR containing synapses would be activated, relative to +40 mV, when synapses containing both AMPAR and NMDAR or only NMDAR would be activated. Placing the stimulating electrode in the *SR* mirrored the stimulation used during the field LTP recording (Figure 3.10 A) and would reveal silent synapses present in the oblique dendrites. On the other hand, placing the stimulating electrode in the *SO* (Figure 3.10F) would reveal a potential increase in silent synapses in the basal dendrites, where I observe an increase in spine density in *Cdkl5*$^{-/y}$ rats.

Regarding *SR* stimulation, response probability was of 0.66 ± 0.02 in WT and it was unchanged in *Cdkl5*$^{-/y}$ rats (0.73 ± 0.03) when recording at -70 mV (LMM, p=0.63). When recording at +40 mV, response probability increased to 0.79 ± 0.03 in WT and 0.89 ± 0.02 in *Cdkl5*$^{-/y}$ rats (LMM p=0.21, Figure 3.10 D), reflecting the activation of silent synapses. Additionally, I calculated the ratio between response probability at +40 mV and at -70 mV. A ratio greater than one would indicate the presence of silent synapses, and a difference in the probability ratio would be indicative of altered relative abundance of silent synapses in *Cdkl5*$^{-/y}$ rats. I found the ratio of response probability to be unaltered in *Cdkl5*$^{-/y}$ rats (WT: 1.23 ± 0.07, *Cdkl5*$^{-/y}$: 1.21 ± 0.08, GLMM p=0.83, Figure 3.10E), consistent with the unchanged response probability across the holding potentials tested. Whilst, an increased number of silent synapses could contribute to the enhanced LTP phenotype, no difference revealed with these minimal stimulation experiments is in line with my finding of unaltered NMDAR/AMPAR ratio in *Cdkl5*$^{-/y}$ rats.

Regarding *SO* stimulation, response probability was similar for WT (0.58 ± 0.03) and *Cdkl5*$^{-/y}$ (0.59 ± 0.04) rats when recording at -70 mV (LMM p=0.99) and increased

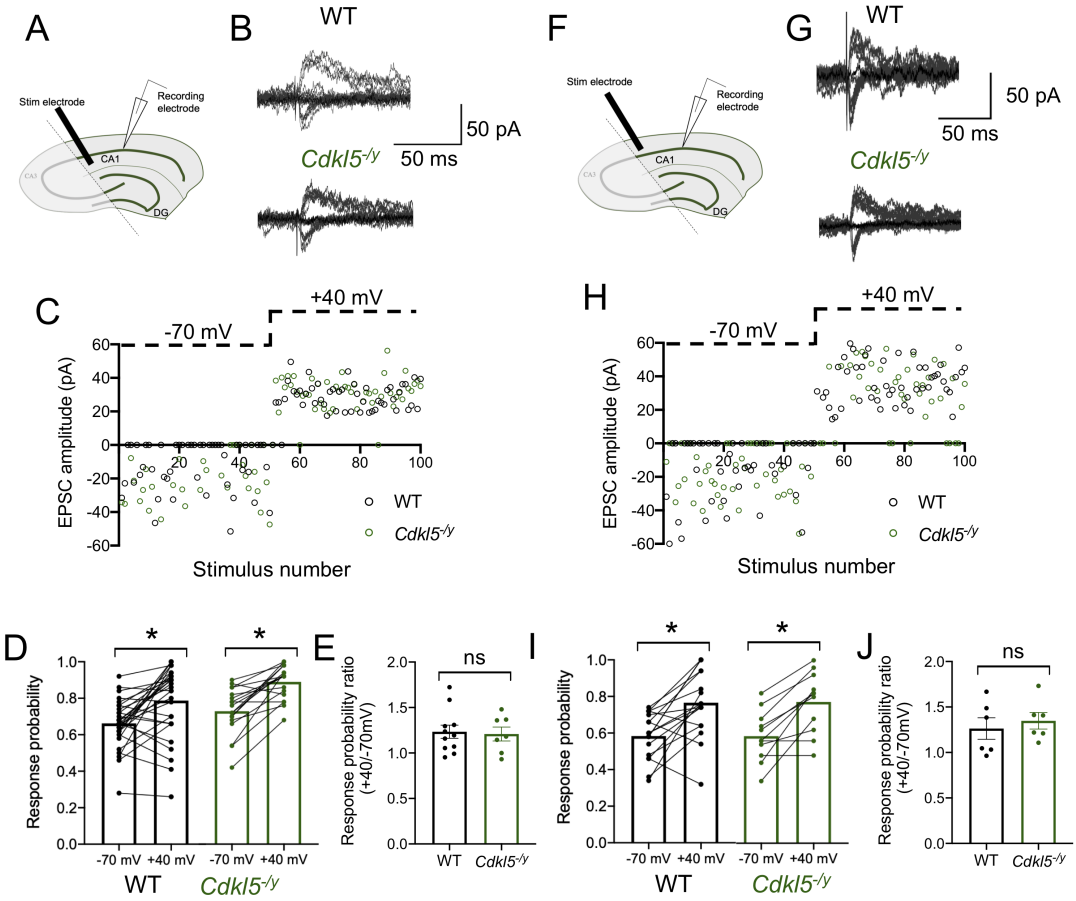

Figure 3.10: Minimal stimulation of CA3 inputs to CA1. Schematic representation of recording configuration for minimal stimulation of CA3 inputs to CA1 via *SR* (A) or *SO* (F) and respective representative traces of EPSCs recorded at -70 mV (down deflecting) and +40 mV (up deflecting) (B, G). Example of timecourse synaptic responses throughout a single WT and *Cdkl5*$^{-/y}$ recording upon *SR* (C) and *SO* stimulation (H). Response probability at -70 mV and +40 mV resulting from *SR* stimulation (D, data shown as cells, values for each cell connected by a black line) and respective ratio of the response probability (E, WT n= 30 cells / 11 rats, *Cdkl5*$^{-/y}$ n=18 cells / 7 rats, data shown as mean ± SEM, dots represent animal averages). Response probability at -70 mV and +40 mV resulting from *SO* stimulation (I, shown as cells, values for each cell connected by a black line) and respective ratio of the response probability (J, WT n= 17 cells / 6 rats, *Cdkl5*$^{-/y}$ n=11 cells / 6 rats, data shown as mean ± SEM, dots represent animal averages). Statistics shown: *p<0.05, ns p>0.05, GLMM

equally in both genotypes when recording at +40 mV (WT: 0.77 ± 0.04 , *Cdkl5*$^{-/y}$ 0.77 ± 0.05, LMM p=0.93, Figure 3.10D). This is reflected in the similar ratio of response probability between genotypes (WT: 1.26 ± 0.12, *Cdkl5*$^{-/y}$ 1.35 ± 0.09, GLMM p=0.61, Figure 3.10J).

Overall these data suggest, that *Cdkl5*$^{-/y}$ rats do not show increased numbers of silent synapses in their oblique or basal dendrites, and therefore does not support my initial hypothesis that an increase in silent synapses contributes to the enhanced LTP and reduced mEPSC phenotypes observed in *Cdkl5*$^{-/y}$ rats.

3.2.4 Physiology and morphology of mPFC L5 pyramidal cells in *Cdkl5*$^{-/y}$ rats

The mPFC is part of the limbic system and is involved in anxiety related behaviours and fear learning (Adhikari et al., 2010; Sierra-Mercado et al., 2011; Tovote et al., 2015), both of which are altered in mouse models of CDD (Okuda et al., 2018; Tang et al., 2019). Furthermore, the pre-limbic (PL) region of the mPFC in particular has an important role in fear expression (Sotres-Bayon and Quirk, 2010; Sierra-Mercado et al., 2011), which is altered in *Cdkl5*$^{-/y}$ rats (Vijay Kumar, Shashank Tiwari, unpublished). Therefore, I hypothesised that loss of CDKL5 would result in altered cellular excitability and/or excitatory synaptic transmission in L5 pyramidal cells in the PL-mPFC of *Cdkl5*$^{-/y}$ rats underlying the behavioural phenotype.

3.2.4.1 Typical intrinsic excitability in L5 pyramidal cells in the PL-mPFC

To examine cellular excitability of L5 pyramidal cells in the PL-mPFC, I used whole cell patch clamp recordings of mPFC in acute slices from P28-35 rats. L5 was identified by the position in the slice and the sparse cell density, with L5 pyramidal neurons exhibiting a large tearshaped cell body and a visible thick apical dendrite.

L5 pyramidal neurons from WT rats exhibited an hyperpolarised membrane potential, fast membrane time constant and low input resistance (Table 3.3). Upon injection of depolarising current steps, WT neurons required a current of 183 ±22 pA to elicit the first AP, and increased thereafter until reaching 10 ± 2 APs/500 ms for the maximum current injection step tested (400 pA). Analysis of AP properties, revealed a slightly depolarised voltage threshold, fast rise until reaching a peak amplitude of 77.7±2.0 mV followed by a slow decay phase (Table 3.4). All electrophysiological properties are within

the expected values according to previous studies (Dembrow et al., 2010; Aerde and Feldmeyer, 2015).

I found excitability of L5 pyramidal cells in mPFC to be unaltered in *Cdkl5*$^{-/y}$ rats. All passive membrane properties examined were comparable to WT controls (Table 3.3). All AP properties were similar across genotypes (Table 3.4). The number of APs fired in response to current injection was also unaltered in *Cdkl5*$^{-/y}$ rats (Two-way ANOVA genotype effect $F_{1,40}$=0.25, p = 0.62, Figure 3.11B), as was the rheobase current (LMM, p=0.97, Figure 3.11C).

Table 3.3: Passive membrane properties of mPFC L5 pyramidal cells in P28-35 rats

Physiological property	**WT**	***Cdkl5***$^{-/y}$	**Stats test**	**p value**
Resting membrane potential (mV)	-73.4 ± 0.8	-74.1 ± 0.79	LMM	0.51
Input resistance (MΩ)	98.4 ± 10.6	102.0 ± 8.8	LMM	0.93
Membrane time constant (ms)	21.0 ± 1.2	23.2 ± 1.4	LMM	0.32
Capacitance (pF)	233 ± 18	240 ± 15	LMM	0.65

Table 3.4: Action potential properties of mPFC L5 pyramidal cells in P28-35 rats

Physiological property	**WT**	***Cdkl5***$^{-/y}$	**Stats test**	**p value**
Voltage threshold (mV)	-38.2 ± 0.5	-37.9 ± 1.1	LMM	0.61
Half height duration (ms)	0.76 ± 0.03	0.76 ± 0.03	LMM	0.94
Amplitude (mV)	77.7 ± 2.0	77.8 ± 2.3	LMM	0.84
Max rise rate (mV.ms^{-1})	367 ± 19	378 ± 24	LMM	0.75
Max decay rate (mV.ms^{-1})	104 ± 8	98 ± 5	LMM	0.98

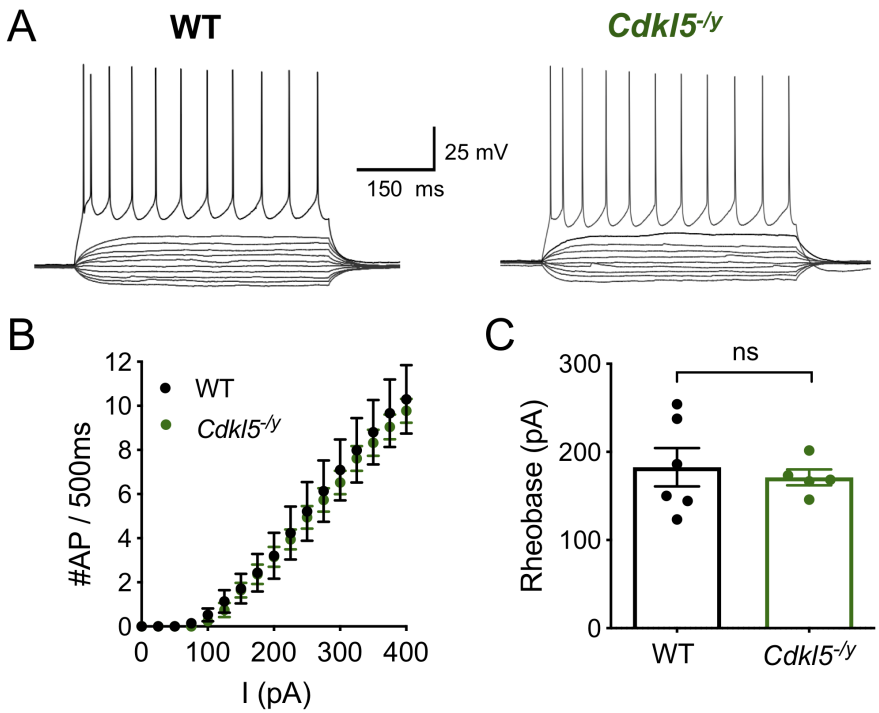

Figure 3.11: Unaltered excitability of L5 pyramidal cells in juvenile *Cdkl5*$^{-/y}$ *rats* A - Representative traces of whole cell recordings from CA1 pyramidal cells in response to subsequent 25 pA steps. Traces shown from -100 pA to rheobase-1 and for the maximum firing frequency (I = 400pA). B - Action potential discharge in response to 500 ms long 25 pA current steps up to 400 pA (Two-way ANOVA genotype effect $F_{1,40}$=0.25, p = 0.62). C = Rheobase current (LMM, p=0.97). Data shown as mean ± SEM, WT – n = 21 cells/6 rats, *Cdkl5*$^{-/y}$ – n = 21 cells/5 rats, dots represent animal averages.

3.2.4.2 Unaltered excitatory synaptic transmission

Altered synaptic transmission has been reported across different brain regions in mouse models of CDD (Della Sala et al., 2016; Tang et al., 2017, 2019). To test whether basal synaptic transmission was altered in the PL-mPFC, I recorded sEPSCs and mEPSCs from L5 pyramidal cells. Whole-cell electrophysiology recordings were performed in voltage clamp at a holding potential of -70 mV in the presence of the GABA-A receptor blocker picrotoxin in order to isolate excitatory events and record sEPSCs. mEPSC recordings were performed in the additional presence of TTX, to block AP dependent neurotransmitter release.

WT neurons exhibited sEPSC with an average amplitude of 16.52 ± 0.87 pA, at a frequency of 12.54 ± 1.30 Hz (Figure 3.12 B). These were unaltered in *Cdkl5*$^{-/y}$ neurons (sEPSC amplitude: 15.84 ± 1.05 pA, p=0.48, LMM; sEPSC frequency: 11.58 ± 1.03 Hz, p=0.49, LM). As a result of blocking AP dependent neurotransmitter, mEPSC frequency was lower than that observed for sEPSCs. WT neurons exhibited mEPSC events at a frequency of 8.80 ± 0.84 Hz, which was unaltered in *Cdkl5*$^{-/y}$ cells (8.37 ± 1.23 Hz, p=0.9, LMM). mEPSCs had an amplitude of 13.42 ± 0.67 pA in WT neurons, also unaltered in *Cdkl5*$^{-/y}$ rats (14.87 ± 0.88 pA, p=0.35, LMM). This data suggests that loss of CDKL5 does not affect basal excitatory synaptic transmission in L5 pyramidal cells in the mPFC.

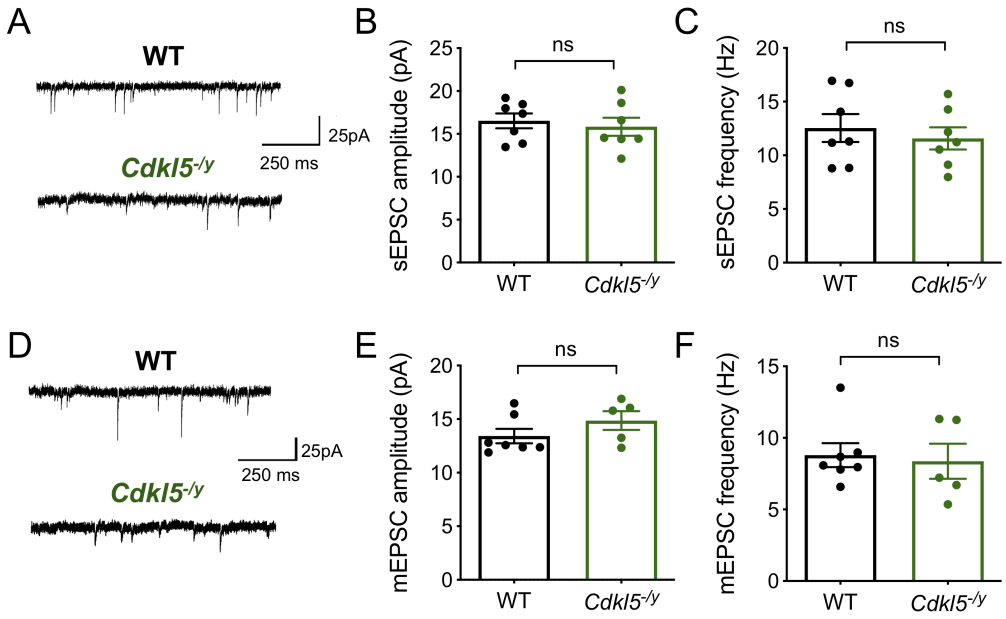

Figure 3.12: Unaltered excitatory synaptic transmission in L5 pyramidal cells of juvenile *Cdkl5*$^{-/y}$ *rats*. Representative traces of spontaneous (A) and mini (D) EPSC recordings from mPFC L5 pyramidal cells. sEPSC amplitude (B, LMM p=0.48) and frequency (C, LMM p=0.49) (WT: 21 cells/7rats, *Cdkl5*$^{-/y}$: 23 cells/7 rats). mEPSC amplitude (E, LMM p=0.35) and frequency (F, LMM p=0.90), (WT: 18 cells / 7 rats, *Cdkl5*$^{-/y}$: 15 cells / 5 rats) Data shown as mean ± SEM, dots represent animal averages.

3.2.4.3 Typical L5 pyramidal cell morphology in *Cdkl5*$^{-/y}$ rats

Reduced dendritic arborisation has been reported in mouse models of CDD across a variety of brain regions. However, I did not find that to be the case in the hippocampus of *Cdkl5*$^{-/y}$ rats. I biocytin-filled L5 pyramidal cells during electrophysiological recordings in order to recover their morphology (Figure 3.13 A). WT pyramidal cells exhibited a long apical dendrite, that reached L1 and ramified into tuft dendrites, characteristic of tufted L5 pyramidal cells in mPFC (Aerde and Feldmeyer, 2015; Dembrow et al., 2010). Though I only recovered a small number of cells from each genotype, my data suggests that cell morphology is unaltered in the absence of CDKL5, with the sholl profile not being significantly different between genotypes (Two way ANOVA interaction: $F_{122,488} = 0.48$, $p > 0.99$; genotype effect: $F_{1,4} = 0.32$, p=0.60, Figure 3.13B). Total dendritic length was comparable between genotypes (WT: 12498 ± 2122 μm, *Cdkl5*$^{-/y}$: 11337 ± 974 μm, Two-tailed T test, T_4=0.50, p=0.64, Figure 3.13E). Total length of apical dendrites was also unaltered in *Cdkl5*$^{-/y}$ rats (7040 ± 1172 μm) relative to WT (7947 ± 1744 μm, Two-tailed T test, T_4=0.43, p=0.69, Figure 3.13C). In WT neurons,

basal dendrites measured 5195 ± 702 μm, and this was not significantly different in *Cdkl5*$^{-/y}$ neurons (3996 ± 367 μm, Two-tailed T test, T_4=1.5, p=0.20, Figure 3.13D). Based on the current data, power analysis (α=0.05, 80% power) indicated a sample size of 89 cells per group would be needed to reveal a significant effect on length of basal dendrites.

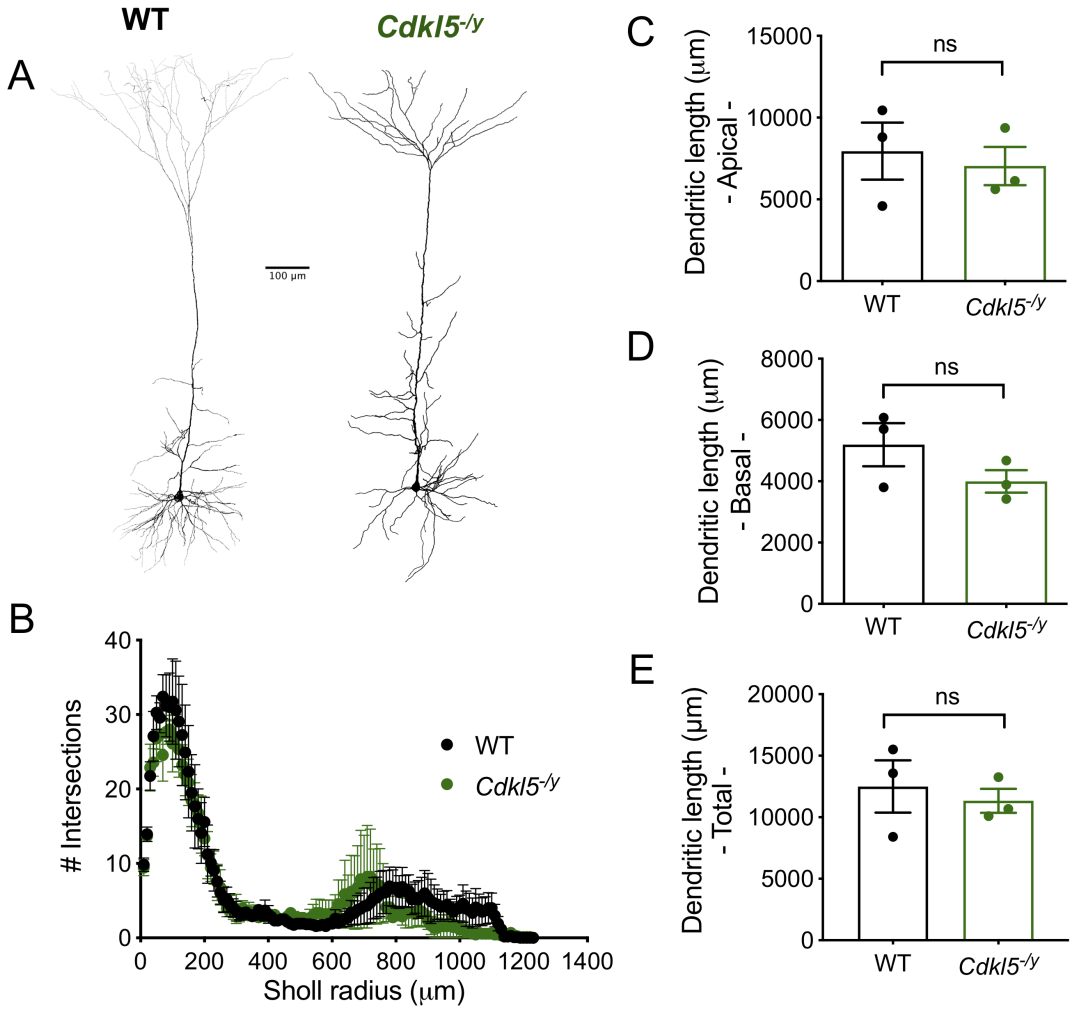

Figure 3.13: Unaltered morphology of L5 pyramidal cells in L5 pyramidal cells of juvenile *Cdkl5*$^{-/y}$ rats. A – Example reconstruction of L5 pyramidal cells from WT and *Cdkl5*$^{-/y}$ rats filled with biocytin during whole cell patch clamp recordings. B – Sholl analysis of the dendritic arborisation (Two way ANOVA interaction: $F_{122,488}$ = 0.48, p > 0.99; genotype effect: $F_{1,4}$ = 0.32, p=0.60). Total length of apical (C) and basal (D) dendrites. E - Total dendritic length WT - n=8 cells/3 rats, *Cdkl5*$^{-/y}$ - n=6 cells/3 rats)

3.3 Discussion

3.3.1 Functional implications of reduced AP amplitude in CA1 pyramidal cells

CA1 pyramidal cells exhibit typical cellular excitability in *Cdkl5*$^{-/y}$ rats. However, AP waveform is altered, with reduced AP amplitude and slower rise rate. While I do not observe a difference in AIS length that can explain the altered AP waveform. It is possible that altered density of sodium channels at the AIS rather than altered AIS length can contribute to the effect I observe. Indeed, Spratt et al. (2019) observe reduced AP amplitude and rise rate in $Na_v1.2$ haploinsufficient mice, with no change in firing pattern or AP threshold, similar to my observations in *Cdkl5*$^{-/y}$ rats. Further investigation of sodium conductances would be necessary to provide insight into the underlying mechanism resulting in altered AP waveform, as the cell membrane properties described in this chapter cannot explain this phenotype.

Whilst the effect on AP kinetics I observe does not appear to affect somatic firing in response to increasing current steps, it can nonetheless have implications in neuronal function. Spratt et al. (2019) show that small differences in somatic AP amplitude can result in drastic impairment of backpropagating APs in distal dendrites. Backpropagating APs have an important role in spike-timing dependent plasticity (Koester and Sakmann, 1998), a form of plasticity thought to underlie associative learning (reviewed in Caporale and Dan (2008)). Therefore, reduced AP amplitude can not only influence other cellular properties but also contribute to behavioural phenotypes. Interestingly, CDKL5 rats show learning deficits in the active place avoidance task (Vijay Kumar, Shashank Tiwari, *unpublished*), a hippocampal dependent spatial memory task (Cimadevilla et al., 2000). The findings presented in this section raise the possibility that dendritic excitability might be altered in *Cdkl5*$^{-/y}$ rats, interestingly this has been reported in other models of ASD/ID (Booker et al., 2019; Spratt et al., 2019; Brager et al., 2012). Two-photon calcium imaging experiments would allow to image calcium transients in dendrites while eliciting somatic APs and assess whether backpropagating APs are affected in the absence of CDKL5.

3.3.2 Mechanisms underlying enhanced hippocampal LTP are not conserved across mouse and rat models of CDD

In this chapter I show evidence for a role of CDKL5 in synaptic plasticity in the hippocampus. *Cdkl5*$^{-/y}$ rats exhibit enhanced LTP, in agreement with what has been previously described in a mouse models of CDD (Yennawar et al., 2019; Okuda et al., 2017). However, the mechanisms previously suggested to contribute to enhanced LTP in mouse models of CDD are not translated to the rat model used in this study.

Whilst Okuda et al. (2017) suggest an increase in NMDAR/AMPAR ratio and in GluN2B containing NMDA receptors as a potential mechanism underlying LTP, this is not the case in *Cdkl5*$^{-/y}$ rats. I did not observe a difference in NMDAR/AMPAR ratio or NMDAR-mediated EPSC decay time constant. Consistent with this finding, my minimal stimulation experiments did not reveal a difference in silent synapses in CA1 pyramidal cells. Furthermore, post-natal development and ifenprodil sensitivity of NMDARs appears unaltered in the same *Cdkl5*$^{-/y}$ rat model (Caballes, Benke, *unpublished*).

Alternatively, Yennawar et al. (2019) suggest that a greater content of GluA2-lacking AMPARs contributes to enhanced early phase LTP (15 min post induction). This potential mechanism also cannot explain the enhanced LTP observed in the rat model, as I observed a linear I-V relationship of AMPAR mediated EPSCs in WT and *Cdkl5*$^{-/y}$ rats. This observation is consistent with the known high expression of GluA2 AMPAR subunit in CA1 pyramidal cells (He et al., 1998), which confers low calcium permeability and no inward rectification (Jonas and Sakmann, 1992; Jonas et al., 1994). As ionotropic glutamate receptor function appears to be intact in *Cdkl5*$^{-/y}$ rats, other mechanisms might be contributing to the enhanced LTP.

Work elucidating CDKL5 targets is still in its early stages, and there is no evidence of CDKL5 directly regulating signalling cascades downstream from LTP induction. However, downregulation of the mTOR signalling pathway has been reported across different mouse models of CDD (Schroeder et al., 2019; Amendola et al., 2014; Wang et al., 2012). mTOR is a key regulator of cell growth and proliferation, and it has important roles in neuronal development and plasticity (Hoeffer and Klann, 2010). Namely, mTOR signaling is required for NMDAR dependent late phase LTP (4 h post induction) in the hippocampus (Vickers et al., 2005; Cammalleri et al., 2003; Tang et al., 2002). Furthermore, altered mTOR signalling has been implicated in various other models of ASD/ID which also present with synaptic plasticity phenotypes (reviewed in Winden

et al. (2018)), so examination of this pathway might provide insight into a potential mechanism for the synaptic plasticity phenotype in *Cdkl5*$^{-/y}$ rats.

Alternatively, as reduced long-range connectivity has been reported in ASD/ID (Zerbi et al., 2018), it is plausible that enhanced LTP arises as a compensatory reduction in threshold for LTP in response to reduced extra-hippocampal inputs (Abraham et al., 2001). Nonetheless, long-range connectivity has not been assessed in rodent models of CDD, therefore future studies should look at functional connectivity across brain areas in order to test this hypothesis. Importantly, as enhanced LTP appears to be conserved across species is might present a robust assay to test novel therapeutic strategies for CDD.

3.3.3 Excitatory synaptic transmission in the hippocampus of *Cdkl5*$^{-/y}$ rats

I observed a dendritic compartment specific increase in spine density in CA1 pyramidal cells which led me to investigate potential functional correlates. mEPSCs are synaptic events resulting from the stochastic release of a single vesicle of neurotransmitter. mEPSC amplitude gives information about the number of receptors in the post synaptic membrane, while mEPSC frequency reflects release probability and can also be a correlate for synapse numbers. Therefore, I expected an increase in mEPSC frequency in *Cdkl5*$^{-/y}$ rats, indicative of a greater abundance of excitatory synapses in line with the spine phenotype I observed. Intriguingly, I observed a reduction of mEPSC frequency instead. This phenotype could either be explained by a reduction in pre-synaptic release probability or by a reduction in the number of functional synapses, leading to fewer synaptic events.

To address the hypothesis that pre-synaptic release probability is reduced in *Cdkl5*$^{-/y}$ rats, I examined PPRs. PPRs are traditionally used to infer about pre-synaptic release probability (Debanne et al., 1996; Dobrunz et al., 1997), with PPR >1 indicating facilitating synapses, with a low release probability, as is the case in the Schaffer collateral synapses. However, the relationship between PPR and release probability is complex. Manita et al. (2007) have shown that PPR can be maintained even when release probability is altered. Indeed, more recent studies show that neuromodulatory mechanisms can result in altered release probability that does not manifest itself as a change in short-term plasticity (Burke et al., 2018). So, whilst a change in PPR could indicate altered

release probability, based on my data I cannot firmly conclude that pre-synaptic release probability is unaltered in *Cdkl5*$^{-/y}$ rats. More sophisticated experimental approaches, such as optical quantal analysis (Padamsey et al., 2019) currently allow more precise estimates of release probability at single synapses and would be useful to determine whether release probability is altered in *Cdkl5*$^{-/y}$ rat. Importantly, such an approach would also allow to study release probability at synapses onto the different dendritic domains, allowing for detection of domain specific phenotypes that might align with the spine phenotype described in this chapter.

On the other hand, if the miniEPSC phenotype results from a reduction in the number of functional synapses I would expect to observe an increase in silent synapses in *Cdkl5*$^{-/y}$ rats. Typically, the number of silent synapses decreases during early post-natal development, these comprise 20% of synapses in CA1 pyramidal cells by the end of the first post-natal week (Durand et al., 1996), and 10 to 15% remain silent into adulthood rats (Racca et al., 2000). Interestingly, increased prevalence of silent synapses has been reported in other models of ASD/ID (Harlow et al., 2010), and is thought to reflect a developmental delay. When I used a minimal stimulation paradigm to address the hypothesis that *Cdkl5*$^{-/y}$ rats exhibit a greater abundance of silent synapses, I found no genotypic differences. Firstly, my results showing a ratio of response probability slightly over 1 in WT rats (1.23 $\pm$0.07 in *Str radiatum* and 1.26 $\pm$0.12 *Str oriens*) aligns with the prevalence of silent synapses expected for CA1, based on anatomical studies (Racca et al., 2000). Furthermore, my data regarding unaltered abundance of silent synapses as revealed by *str radiatum* stimulation is in agreement with my findings regarding unchanged NMDAR/AMPAR ratio in *Cdkl5*$^{-/y}$ rats, at this same stimulation site.

Minimal stimulation of synaptic inputs allows the stimulation of a single synapse or small number of synapses, and is typically used to study quantal synaptic events as well as the presence of silent synapses (Hanse and Gustafsson, 2001b; Isaac et al., 1997). The use of minimal stimulation to study quantal events is limited by the fact that it is difficult to ensure that only one axon is being activated in response to electrical stimulation. This is particularly challenging in the hippocampus, where axons from CA3 can make more than one synapse onto the post-synaptic CA1 cell (Andersen et al., 1990). Nonetheless, in order to detect silent synapses, guaranteeing the stimulation of a single synaptic site is not crucial. It is sufficient to stimulate a small number of

synapses, producing a failing response, as the relative probability of failure or response across hyperpolarised and depolarised membrane potentials is the parameter used as an indicator of silent synapses (Isaac et al., 1997). By measuring relative abundance of silent synapses rather than an absolute number, this caveat should not influence the interpretation of my data.

Having considered potential experimental limitations, my data suggests that the presence of silent synapses is unaltered in CA1 pyramidal cells from *Cdkl5*$^{-/y}$ rats, both in their basal and apical dendrites. Recording NMDAR/AMPAR ratios upon *SO* stimulation would be a useful additional confirmation that silent synapses onto the basal dendrites of CA1 pyramidal cells are unaltered in *Cdkl5*$^{-/y}$ rats, as suggested by the minimal stimulation data.

3.3.4 Typical L5 mPFC physiology and cell morphology

I found cellular excitability and synaptic transmission to be unaltered in L5 pyramidal cells in the PL-mPFC of *Cdkl5*$^{-/y}$ rats. It is important to consider that I took a blanket approach, recording from a random sample of L5 pyramidal cells and not taking into account the different cell types making up the L5 pyramidal cell population in mPFC. L5 pyramidal cells in the mPFC are known to exhibit different morphology, excitability and connectivity patterns depending on their projecting targets (Dembrow et al., 2010; Brown and Hestrin, 2009; Molnár and Cheung, 2006). Therefore, they have the potential to be differentially affected in rodent models of neurodevelopmental disorders. Cell type specific excitability phenotypes in L5 mPFC have been reported in the *Fmr1*$^{-/y}$ mouse and rat models of FXS (Kalmbach et al., 2015; Jackson, 2016). Furthermore, social experience modulates excitability of L5 pyramidal cells in a cell type specific manner (Yamamuro et al., 2018). In the future, the study of different cell populations in mPFC might be of value to understand the physiological underpinnings of behavioural phenotypes. In particular, PL-mPFC cells projecting to the amygdala have an important role in the behavioural response to fearful stimuli (Knapska et al., 2012; Orsini et al., 2011) and should therefore be given special attention in the rat model of CDD, as *Cdkl5*$^{-/y}$ rats exhibit increased freezing in a cued fear conditioning paradigm (Vijay Kumar, Shashank Tiwari, *unpublished*, Appendix A).

3.3.5 Considerations for future work

My data provides an insight into hippocampal and mPFC synaptic physiology and cellular excitability in the absence of CDKL5. Even though intrinsic excitability and synaptic transmission appear largely unaffected in the hippocampus and mPFC, communication between these two regions is crucial for cognitive function, and was not assessed in this study. Hippocampal-mPFC connectivity is particularly important for memory consolidation and retrieval (Binder et al., 2019; Backus et al., 2016; Sang Jo et al., 2007) and is also implicated in anxiety related behaviours (Padilla-Coreano et al., 2016). In the future, *in vivo* electrophysiology or fMRI can be used to further assess larger scale circuit function. As long range hypoconnectivity appears to be a hallmark of ASD/ID both in rodent models and patients (Di Martino et al., 2014; Zerbi et al., 2018; Haberl et al., 2015), it would be of interest to establish whether those findings are common to CDD, as they could provide biomarkers of the condition that could be used to test therapeutic approaches.

Furthermore, the data presented in this chapter has focused on excitatory synaptic transmission and cellular excitability of pyramidal cells. However, as circuit hyperexcitability in ASD/ID arises many times as an imbalance of excitation and inhibition, a characterisation of interneuron function in the rat model of CDD could contribute to a better understanding of circuit function. Indeed, loss of CDKL5 is know to affect inhibitory synaptic transmission in the cerebellum (Sivilia et al., 2016), and anatomical studies suggest altered connectivity between interneurons and pyramidal cells in sensory cortical areas (Pizzo et al., 2016) in mouse models of CDD.

Chapter 4

Mechanisms of cellular excitability plasticity in the hippocampus of a mouse model of Fragile X Syndrome

4.1 Introduction

Fragile X Syndrome (FXS) is the most common inherited form of ASD/ID. It results from the transcriptional silencing of the *FMR1* gene and consequent absence of its protein product, FMRP. Patients often present with co-occurring hyperactivity, sensory hypersensitivities and epilepsy.

Altered cellular and circuit excitability are believed to contribute to many of the behavioural phenotypes observed in rodent models of FXS (reviewed in Contractor et al. (2015)), including higher susceptibility to seizures (Dölen et al., 2007; Musumeci et al., 2000) and learning deficits (Asiminas et al., 2019; Till et al., 2015; Brennan et al., 2006). FMRP is known to regulate cellular excitability through its direct interaction with ion channels (Deng et al., 2013; Deng and Klyachko, 2016; Zhang et al., 2012). Given FMRP's role as a regulator of translation, its' loss can also impact cellular excitability and synaptic transmission through deregulation of its target mRNAs, many of which encode ion channel subunits and synaptic proteins (Darnell et al., 2011). Interestingly, recent evidence suggests that cellular excitability phenotypes seen in rodent models of FXS might result from compensatory changes rather than a direct consequence of the absence of FMRP. In particular, Antoine et al. (2019) suggest that altered E/I balance across models of ASD/ID, including the *Fmr1*$^{-/y}$ mouse, arise as a mechanism to normalise cellular excitability. In line with this idea, Domanski et al. (2019) show that, in the somatosensory cortex of *Fmr1*$^{-/y}$ mice, the cellular and synaptic phenotypes observed have opposite effects, potentially reflecting an homeostatic compensation at

the circuit level.

A variety of mechanisms can contribute to the regulation of cellular excitability, from ion channels to synaptic changes, as well as AP regulation at the AIS. The role of the AIS as the site of AP initiation makes this structure a major regulator of cellular excitability. Whilst altered AIS structure and function has been reported in models of neurological disorders, including schizophrenia and epilepsy (Harty et al., 2013; Wimmer et al., 2010), it has never been studied in the context of FXS. However, cellular hyperexcitability has been associated with increased AIS length in a mouse model of Angelman's Syndrome (Kaphzan et al., 2011), a monogenic form of ASD/ID with similar excitability phenotypes to those observed in FXS, suggesting that the AIS may play an important role in cellular excitability in the context of neurodevelopmental disorders.

The AIS is a dynamic structure and it can respond to altered states of neuronal activity by regulating its length and position in an homeostatic manner. Depolarisation has been reported to result in AIS shortening in dissociated cultures (Grubb and Burrone, 2010; Evans et al., 2015). The plastic nature of the AIS raises the possibility that potential alterations to the AIS and, consequently, cell excitability can arise as a compensatory mechanism resulting from altered circuit function. Even though recent studies have reported altered excitability of CA1 pyramidal cells in *Fmr1*$^{-/y}$ mice (Luque et al., 2017; Talbot et al., 2018), no long-term alterations in neuronal activity, which could result in AIS remodelling, have yet been observed in the hippocampus of *Fmr1*$^{-/y}$ mice.

In this chapter, I examined intrinsic excitability of CA1 pyramidal cells and addressed the hypothesis that altered AIS morphology and/or plasticity contribute to changes in excitability in *Fmr1*$^{-/y}$ mice. Furthermore, I examined extrahippocampal inputs to CA1 to understand if circuit dysfunction leads to compensatory changes in AIS morphology and cellular excitability in *Fmr1*$^{-/y}$ mice. I used a combination of electrophysiology, immunohistochemistry and two-photon imaging, to assess AIS morphology and plasticity as well as cellular excitability and local circuit function in the hippocampus of *Fmr1*$^{-/y}$ mice and WT littermates.

4.2 Results

4.2.1 Hyperexcitability of CA1 pyramidal cells in *Fmr1*$^{-/y}$ mice is associated with increased AIS length

I performed whole cell patch clamp recording to assess cellular excitability of CA1 pyramidal cells in acute hippocampal slices from 28-35 day-old mice. Depolarising current steps (25 pA steps up to +400 pA, 500 ms) were used to elicit APs and examine AP discharge and AP kinetic properties. WT neurons started firing APs at a rheobase current of 157.1 ± 9.8 pA (Figure 4.1 C). Thereafter, depolarising current steps elicited an increasing number of action potentials until the maximum firing frequency of 35.9 ± 2.3 Hz was reached, this is reflected in the current-frequency (IF) plot in Figure 4.1 B. By comparison, I found CA1 pyramidal cells from *Fmr1*$^{-/y}$ mice to be hyperexcitable relative to WT when examining AP discharge in response to depolarising current steps. This is reflected in the leftward shift in the IF plot (Figure 4.1 B, Two way ANOVA on animal averages: interaction: $F_{16,432}$=2.34, p=0.005, genotype effect p=0.04) and the reduced rheobase current in *Fmr1*$^{-/y}$ (106.8 ± 7.0 pA) compared to WT (Figure 4.1C, p= 4x10^{-5}, GLMM). This did not result in a change in the firing frequency in response to the maximum current injection step (400 pA), as the peak firing frequency in *Fmr1*$^{-/y}$ (41.0 ± 9.6 Hz) was comparable to that of WT neurons (p=0.15, GLM).

When assessing passive membrane properties, there was no difference in input resistance that could explain the difference in excitability between genotypes (WT: 164.0 ± 14.8 MΩ, *Fmr1*$^{-/y}$: 170.5 ± 13.5 MΩ, p=0.37 GLMM, Figure 4.1 F). However, resting membrane potential was more hyperpolarised in *Fmr1*$^{-/y}$ mice (-65.3 ± 1.9 mV) compared to WT (-59.5 ± 1.5 mV, p=0.003 GLMM, Figure 4.1 E). This finding is unlikely to contribute to the difference in AP discharge as this was controlled for by holding the membrane potential at -70 mV for all recordings. Instead, the hyperexcitability observed results from a more hyperpolarised AP threshold in *Fmr1*$^{-/y}$ mice (-45.3 ± 0.9 mV) relative to WT (-42.4 ± 0.5 mV, p=0.0002, GLMM, Figure 4.1 D). No difference was found between genotypes in the AP kinetic properties analysed, including amplitude, rise and decay rates and half-height duration (Table 4.1).

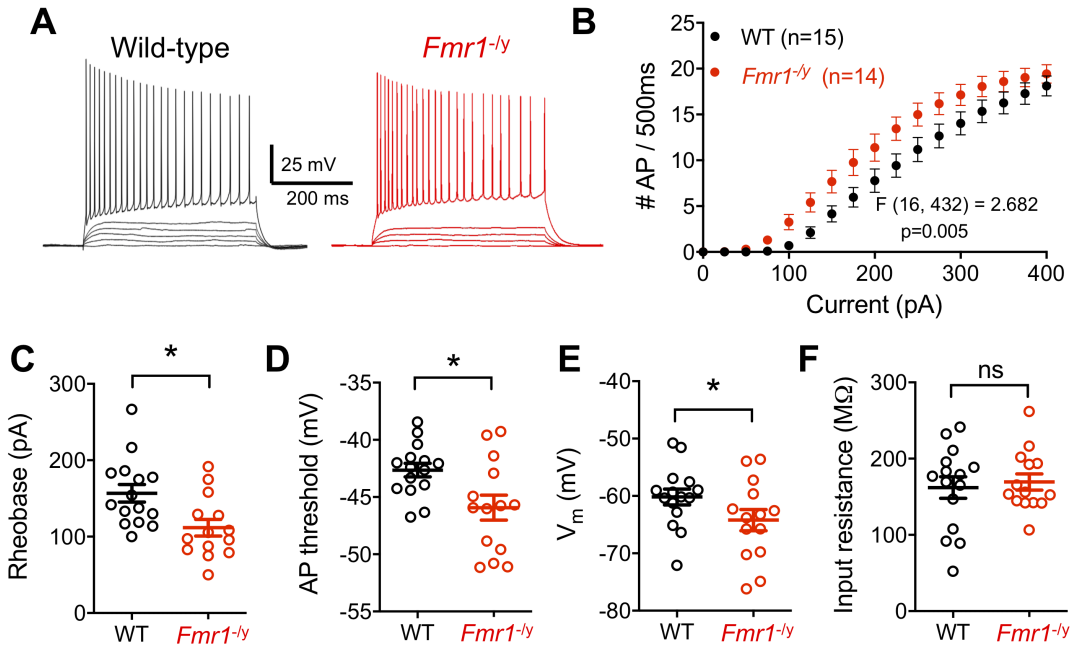

Figure 4.1: Increased CA1 PC excitability and AIS length in *Fmr1*$^{-/y}$ mice. A - Representative traces of voltage responses to 500 ms long depolarising current steps (0 to rheobase-1 in 25 pA steps, and +400 pA) from WT (left, black) and *Fmr1*$^{-/y}$(right, red) cells. B - AP discharge in response to depolarising current steps. C-F Quantification of rheobase, voltage threshold, resting membrane potential and input resistance from both genotypes. (A-F, WT n= 33 cells / 15 mice, *Fmr1*$^{-/y}$ n= 29 cells / 14 mice) All data shown as averages average of individual mice (dots). Statistics shown: ns – $p > 0.05$, $*$ - $p < 0.05$ from 2-way RM ANOVA (B) and GLMM (C-F)

Table 4.1: Action potential properties of CA1 pyramidal cells in WT and *Fmr1*$^{-/y}$ mice

Physiological property	**WT**	***Fmr1*$^{-/y}$**	**Stats test**	**p value**
Voltage threshold (mV)	-42.4 ± 0.5	-46.1 ± 0.7	GLMM	*0.002
Half height duration (ms)	0.90 ± 0.03	0.84 ± 0.02	GLMM	0.56
Amplitude (mV)	116 ± 1	114 ± 2	GLMM	0.44
Max rise rate (mV.ms^{-1})	428 ± 19	448 ± 16	GLMM	0.34
Max decay rate (mV.ms^{-1})	102 ± 4	112 ± 3	GLMM	0.55

Given the high density of VGSCs at the AIS, and its role in regulating AP threshold (Kole et al., 2008), I hypothesised that longer AISs in *Fmr1*$^{-/y}$ mice would contribute to the hyperexcitability observed. To address this hypothesis, I used immunohistochemistry to label AISs in hippocampal sections from perfusion fixed mice. The scaffolding protein Ankyrin G was used as an AIS marker, this allowed for reliable identification of AISs (Figure 4.2 A), the majority of which emerged from the soma (80%) and a smaller percentage emerged from proximal dendrites (20%) of CA1 pyramidal cells, and entered the *SO*. I found AISs to be 20% longer in *Fmr1*$^{-/y}$ mice (30.8 ± 1.3 μm) relative to the average AIS length of 26.2 ± 0.7 μm in WT mice (Figure 4.2 B, C, p=0.0046, GLMM), consistent with the altered AP threshold and rheobase observed. In a subset of mice, I measured distance between the start of the AIS and the soma, as it can also influence cell excitability. This was unaltered in *Fmr1*$^{-/y}$ mice (2.7 ± 0.2 μm) relative to WT (3.2 ± 0.2 μm, p=0.30, LMM, Figure 4.2 D).

To determine whether the AIS phenotype observed is specific to CA1 or widespread across the brain, I assessed cellular excitability and AIS length in L5 pyramidal cells in the mPFC. I found a 12% increase in AIS length from 23.7 ± 1.6 μm in WT to 26.4 ± 1.6 μm in *Fmr1*$^{-/y}$ mice (p<0.001, LMM, Figure 4.3 B). However, the hyperexcitability of L5 pyramidal cells (Figure 4.3C, Two-way ANOVA: $F_{16,288}$=3.43, genotype effect p<0.001) was not associated with altered rheobase current or AP threshold (Figure 4.3D, E, p>0.05 Two tailed T-test), as observed in CA1 pyramidal cells, indicating that other mechanisms than the AIS are contributing to this phenotype.

This data suggest that increased AIS length contributes to cellular hyperexcitability in *Fmr1*$^{-/y}$ mice in a brain region specific manner. While increased AIS length is accompanied by a hyperpolarised AP threshold in CA1 pyramidal cells, other mechanisms must be contributing to the hyperexcitability observed in L5 pyramidal cells in mPFC.

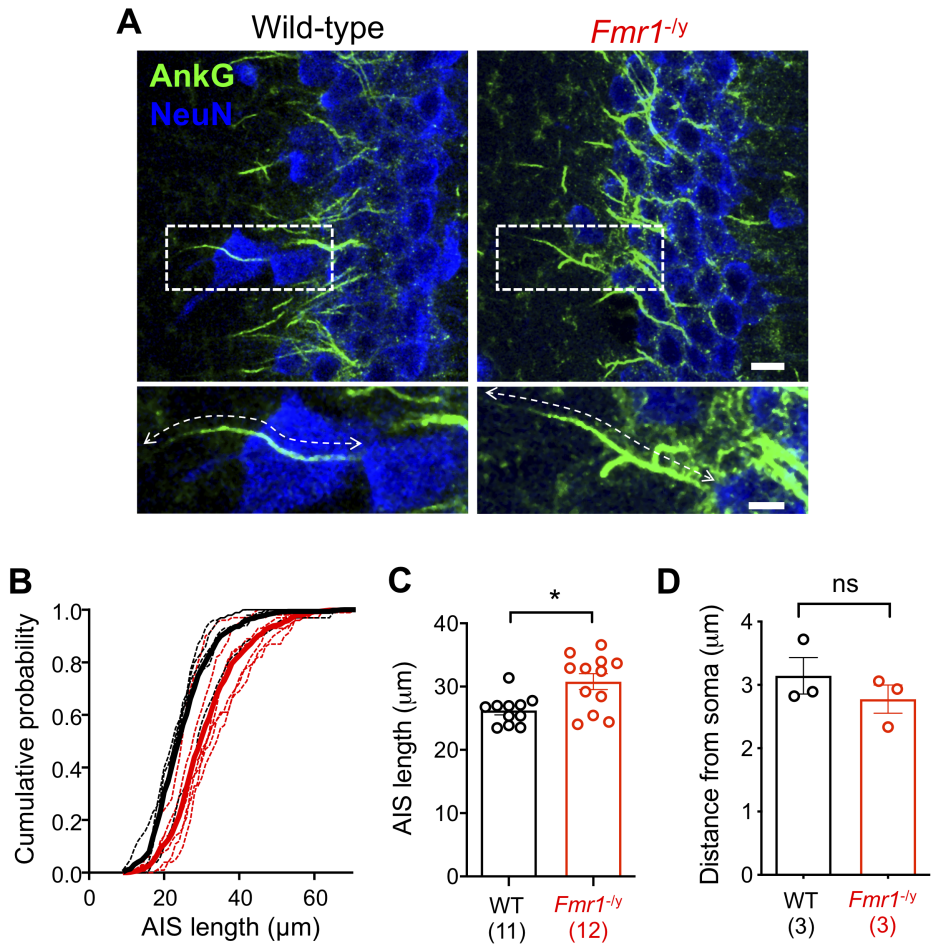

Figure 4.2: Increased AIS length in CA1 of *Fmr1*$^{-/y}$ mice. A - flattened confocal stacks of CA1 overview (top, scale bar: 20 μm) and high-power magnification of single AIS (bottom, scale bar: 5 μm) labelled for Ankyrin G (green) and NeuN (blue). The dashed line indicates the total extent of the AIS. B - Average cumulative distributions (thick lines) of AIS length across all mice examined (WT - black, *Fmr1*$^{-/y}$-red). Cumulative distributions for individual mice shown underlain (thin lines). C - Quantification of AIS length for each genotype (WT: 750 AISs from 11 mice; *Fmr1*$^{-/y}$: 946 AISs from 12 mice). D - Quantification of distance from soma in a subset of the animals analysed. All bar chart data shows averages of individual mice (dots), with total mice analysed in parenthesis. Statistics shown: ns – $p > 0.05$, $*$ - $p < 0.05$ GLMM

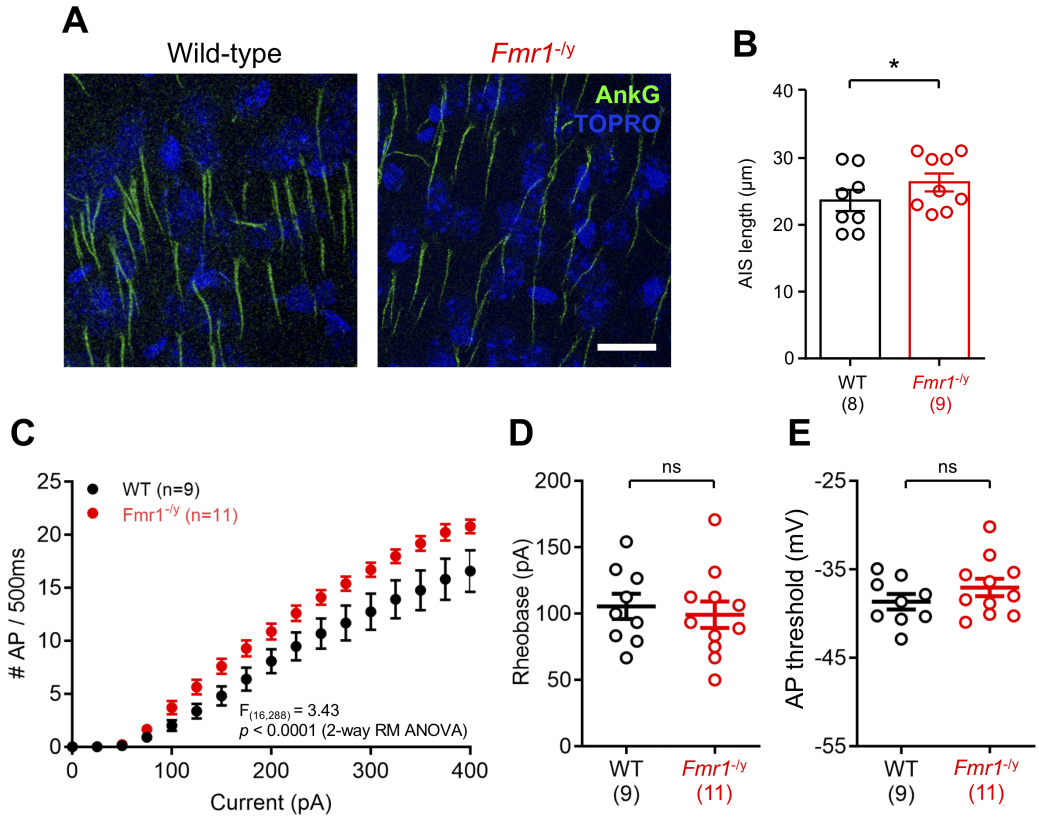

Figure 4.3: Increased AIS length and cellular excitability in mPFC L5 pyramidal cells *Fmr1*$^{-/y}$ mice. A – Representative flattened confocal stack of L5 PL-mPFC from WT (left) and *Fmr1*$^{-/y}$ (right) mice, with AISs labelled with Ankyrin G (green) and cell nuclei labelled with To-PRO (blue). B - Quantification of AIS length in mice from both genotypes. C - AP discharge in response to depolarising current steps. D, E - Quantification of rheobase and AP voltage threshold. Data shown as mean ± SEM, averages of individual mice are shown as dots, with total mice analysed in parenthesis. Statistics shown: ns – p>0.05, from LMM (B), 2-way RM ANOVA (C) and Two-tailed T-test (D,E)

4.2.2 Activity dependent regulation of cellular excitability in CA1 pyramidal cells is enhanced in *Fmr1*$^{-/y}$ mice

The ability of neurons to modulate their intrinsic excitability is crucial to maintain network function (Golowasch et al., 1999). Homeostatic regulation of intrinsic excitability is known to be altered in cultured neurons in the absence of FMRP. Indeed, Bülow et al. (2019) show that *KO* neurons exhibit an exacerbated response when neuronal activity in culture is blocked with TTX. Therefore, we asked whether the hyperexcitability observed in *Fmr1*$^{-/y}$ mice results from abnormal plasticity of intrinsic excitability, using an experimental paradigm previously described to modulate cellular excitability over short (Evans et al., 2015) and long timescales (O'Leary et al., 2010; Grubb and Burrone, 2010) *in vitro*.

We tested the effect of depolarisation on cellular excitability in a cell-wise manner by performing whole-cell patch-clamp recordings from the same CA1 pyramidal cell, thus assessing intrinsic excitability before and after 3 h depolarisation with 15 mM KCl, or treatment with 15 mM NaCl as osmotic control. The inclusion of Alexa-fluor 488 hydrazide in the patch pipette was used to allow the identification and targeting of the same cell at the end of the 3 h treatment period. As expected, the 3 h treatment with 15 mM NaCl did not alter excitability of CA1 pyramidal cells in WT or *Fmr1*$^{-/y}$ mice as seen by the overlap of the IF plots before (control) and after treatment (Figure 4.4C and D left, Two-way RM ANOVA WT: $F_{16,352}$=0.40, treatment effect p=0.34; *Fmr1*$^{-/y}$: $F_{16,102}$=0.40, treatment effect p=0.37). However, treatment with 15 mM KCl for 3 hours resulted in a small but significant decrease in excitability of WT neurons as seen by the rightward shift in the IF plot (Figure 4.4C, left, Two-way RM ANOVA $F_{16,288}$=6.37, treatment effect p=0.02) and a 39% increase in the amount of current required to elicit one AP (Figure 4.4E) from 159 ± 13 pA in control to 221 ± 24 pA after KCl (LMM, p=0.002). We observed a 23% reduction in input resistance (Figure 4.4G, p=0.05, LMM) accompanied by a 14% slowing of the maximum AP decay rate from 76.9 ± 3.4 mV.ms^{-1} prior to treatment to 65.8 ± 2.8 mV.ms^{-1} after 3 h KCl (Figure 4.4H, p=0.05 LMM). However, no effect of KCl treatment on AP threshold was found (Figure 4.4F, p=0.91, LMM). These data suggest that the reduction in cellular excitability we observe is most likely due to altered K^+ channel function (O'Leary et al., 2010; Kole et al., 2007), rather than related to AIS structural changes.

When examining the effect of depolarisation on the excitability of CA1 pyramidal

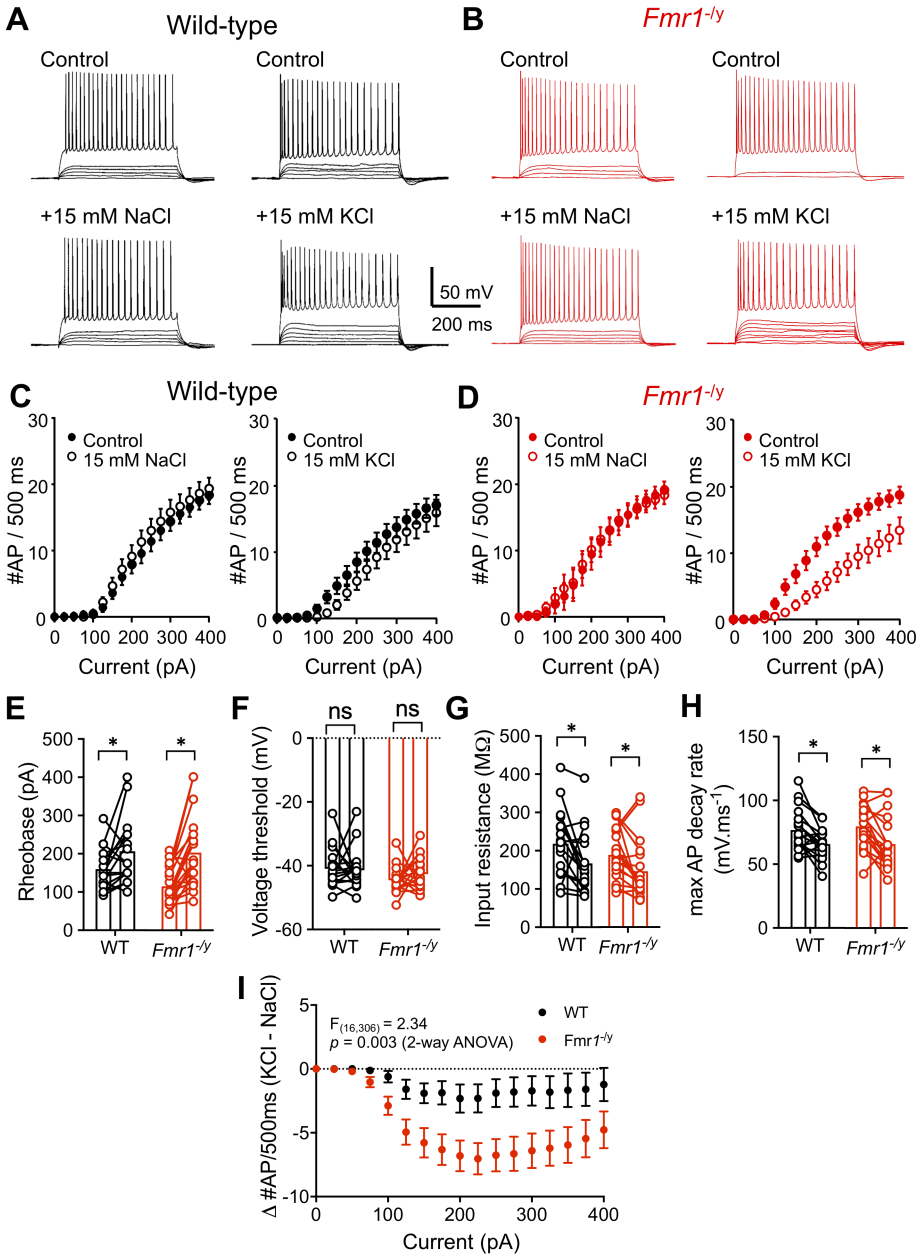

Figure 4.4: Intrinsic physiological plasticity and homeostatic responses in WT and *Fmr1*$^{-/y}$ mice. A, B Representative voltage responses from WT (black) and *Fmr1*$^{-/y}$ (red) CA1 PCs to 500 ms long depolarising current steps (0 - 400 pA, 25 pA steps). AP discharge in response to current injection from the same CA1 PCs from WT (C) and *Fmr1*$^{-/y}$ (D) mice, before (top) and after (bottom) 3 h NaCl or KCl treatment. Pairwise analysis of rheobase current (E), voltage threshold (F), input resistance (G) and AP decay rate (H) before and after KCl treatment. I - Subtracted AP discharge after KCl treatment across the range of injected current steps given to CA1 PCs. Statistics shown: ns – $p > 0.05$, $*$ $p < 0.05$ from GLMM (E-H) and 2-way RM ANOVA (C,D,I). Dots represent individual cells, with line connecting values from the same cell before and after treatment. (E-H). NaCl - WT: 10 cells / 5 mice, *Fmr1*$^{-/y}$: 10 cells/ 4 mice; KCl - WT: 18 cells / 9 mice, *Fmr1*$^{-/y}$: 19 cells / 8 mice. Experiments performed by Dr Sam Booker.

cells from *Fmr1*$^{-/y}$ mice, the 3 h treatment with 15 mM KCl resulted in a reduction in AP discharge (Figure 4.4 D right, $F_1, 17$=21.95, p=0.0002 Two-way RM ANOVA). The other parameters examined also followed the same pattern as seen in WT mice. Rheobase current was increased by 66% from 113 ± 11 pA to 188 ± 18 pA (Figure 4.4 E, p=0.004, LMM). AP threshold was unchanged (Figure 4.4F, p=0.95 LMM). I observed a tendency for reduced input resistance from 197 ± 22 MΩ to 167 ± 20 MΩ (-14%, p=0.17, LMM) and a slowing of the maximum AP decay rate (Figure 4.4H, p=0.008, LMM), suggesting a role for K^+ channels in this form of plasticity, as observed in WT mice. Interestingly, depolarisation appears to have a greater effect on the excitability of neurons in *Fmr1*$^{-/y}$ mice relative to WT. Figure 4.4I shows the difference in AP discharge before and after treatment, for the range of current injection steps tested, in WT and *Fmr1*$^{-/y}$ mice. I observed a greater decrease in the number of APs fired in *Fmr1*$^{-/y}$ mice relative to WT (Interaction: $F_{1,35}$ = 2.225, p=0.0052; Bonferroni post-hoc tests: $T_{17,20}$ = 3.0, 3.0, 3.2, 3.3, 3.3, 3.2; p= 0.05, 0.04, 0.03, 0.02, 0.02, 0.03). Importantly, the physiological parameters affected by KCl treatment were unchanged after 3 h treatment with 15 mM NaCl (Table 4.2).

Table 4.2: Intrinsic excitability of CA1 pyramidal cells before (Ctr) and after 3 h treatment with 15 mM NaCl

Physiological property	**WT Ctr**	**WT NaCl**	***Fmr1*$^{-/y}$ Ctr**	***Fmr1*$^{-/y}$ NaCl**
Membrane potential (mV)	-62.2 ± 2.55	-60.9 ± 2.55	-60.9 ± 5.56	-62.9 ± 2.56
Input resistance (MΩ)	157 ± 22	156 ± 22	144 ± 24	157 ± 22
Rheobase (pA)	158 ± 21	162 ± 21	140 ± 22	139 ± 22
Voltage threshold (mV)	-40.7 ± 1.47	-40.0 ± 1.47	-42.8 ± 1.51	-41.9 ± 1.51
Max rise rate (mV.ms^{-1})	385 ± 24	348 ± 24	374 ± 24	381 ± 24
Max decay rate (mV.ms^{-1})	78.9 ± 5.33	73.2 ± 5.33	82.4 ± 5.64	80.1 ± 5.64
All Ctr vs NaCl comparisons p>0.99, LMM				

Together these data show that prolonged depolarisation results in compensatory changes to cellular excitability in CA1 pyramidal cells from WT and *Fmr1*$^{-/y}$ mice. However, the magnitude of this effect is greater in *Fmr1*$^{-/y}$ mice, resulting in a stronger reduction in AP discharge.

4.2.3 Short-term depolarisation results in AIS shortening in cultured hippocampal neurons, but lengthening in acute slices of WT and *Fmr1*$^{-/y}$ mice.

I have shown that depolarisation of neurons in acute slices results in reduced cellular excitability. Previous studies have shown that treatment of cultured primary neurons with 15 mM KCl leads to a reduction in AIS length over short time scales (Grubb et al., 2011; Evans et al., 2015). I hypothesised that AIS structural plasticity might be altered in *Fmr1*$^{-/y}$ neurons, potentially explaining the difference in baseline AIS length and cellular excitability we observe. To address this hypothesis I used the same depolarisation paradigm described in the previous section (15 mM KCl as depolarising stimulus condition vs 15 mM NaCl osmostic control for 3 h). Following treatment, slices were fixed in 4% PFA and immunolabelled for Ankyrin G (Figure 4.5 A).

Following KCl treatment, I observed a 11% increase in AIS length relative to the NaCl control, from 25.8 ± 1.4 μm to 28.7 ± 1.7 μm (Figure 4.5B, p<0.001 GLMM). A similar 11% increase was observed in slices from *Fmr1*$^{-/y}$ mice, with AISs measuring 29.4 ± 1.9 μm following KCl treatment compared to 26.6 ± 1.6 μm in NaCl control (Figure 4.5C, p<0.001, GLMM). These data clearly show that AIS shortening following depolarisation, as has been described in cultured neurons, does not occur in *ex vivo* neurons from WT or *Fmr1*$^{-/y}$ mice. Instead, prolonged depolarisation results in AIS lengthening in acute hippocampal slices from both genotypes.

As AIS plasticity under the conditions I tested has only been reported in dissociated cultures so far, I next asked whether I could reproduce the AIS shortening others have observed, and whether this was also observed in *Fmr1*$^{-/y}$ neurons. To examine AIS plasticity in dissociated hippocampal cultures, I fixed coverslips prior to and at the end of 3 h treatment with 15 mM KCl, or 15 mM NaCl as a control, at DIV10. Ankyrin G immunolabelling was used to visualise AISs and allow their measurement.

In untreated hippocampal neurons, AISs of *Fmr1*$^{-/y}$ neurons (32.1 ± 0.7 μm) were on average 7% longer than those of WT neurons (29.9 ± 1.0 μm, p<0.001 LMM, Figure 4.6B), similar to the relationship observed in perfusion-fixed tissue sections. KCl treatment resulted in AIS shortening in both WT (NaCl: 31.1 ± 1.2 μm, KCl: 28.1 ± 1.2 μm, p<0.001 LMM, Figure 4.6 C) and *Fmr1*$^{-/y}$ neurons (NaCl: 32.7 ± 1.1 μm, KCl: 30.3 ± 0.8 μm, p<0.001 LMM, Figure 4.6 D). The magnitude of this change was similar between genotypes (Figure 4.6E, T_{29}=0.82 p=0.42, Two-tailed T test).

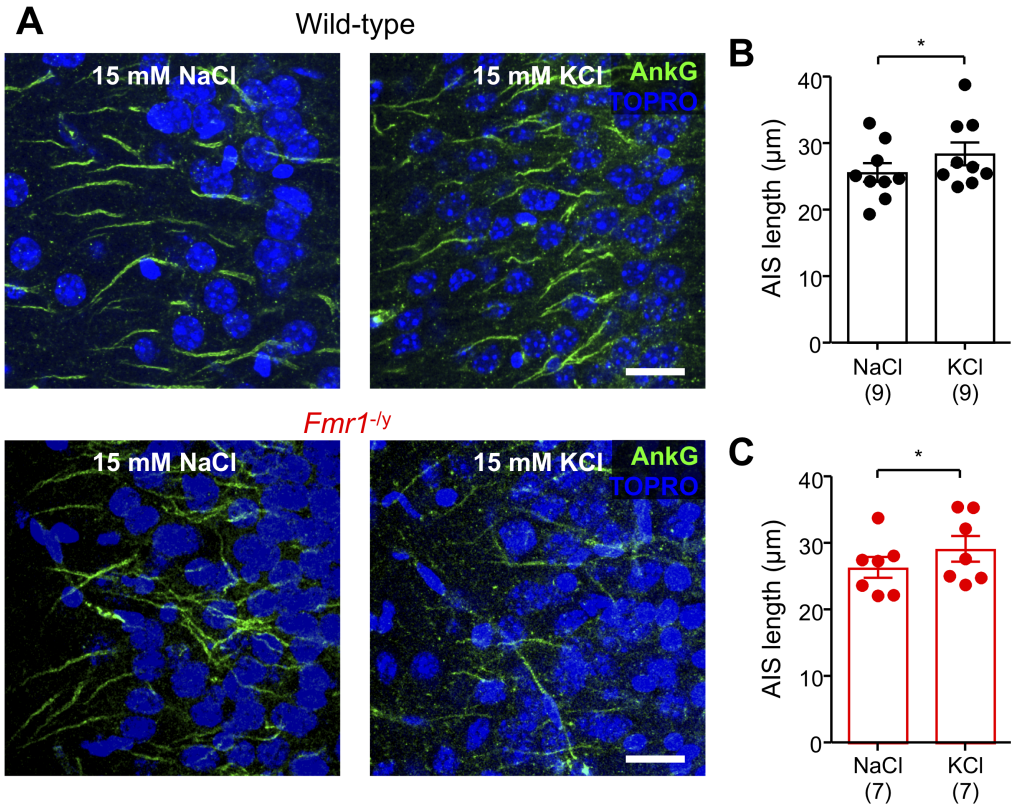

Figure 4.5: Short-term AIS shortening is absent in acute slices following sustained depolarisation A - Representative confocal stack of AISs labelled in acute hippocampal slices from WT (upper) and $Fmr1^{-/y}$, following 3 h treatment with KCl (right) or NaCl osmotic control (left). AIS were visualised with Ankyrin G (green pseudocolour) and measured in neurons labelled with NeuN (blue pseudocolor). Scale bars: 20 μm. AIS length following 3 h application of 15 mM KCl, compared to NaCl in WT (B) and $Fmr1^{-/y}$ (C) mice. Dots represent animal averages (number of mice tested in parenthesis). Statistics shown: ns – $p > 0.05$, * $p < 0.05$, from LMM.

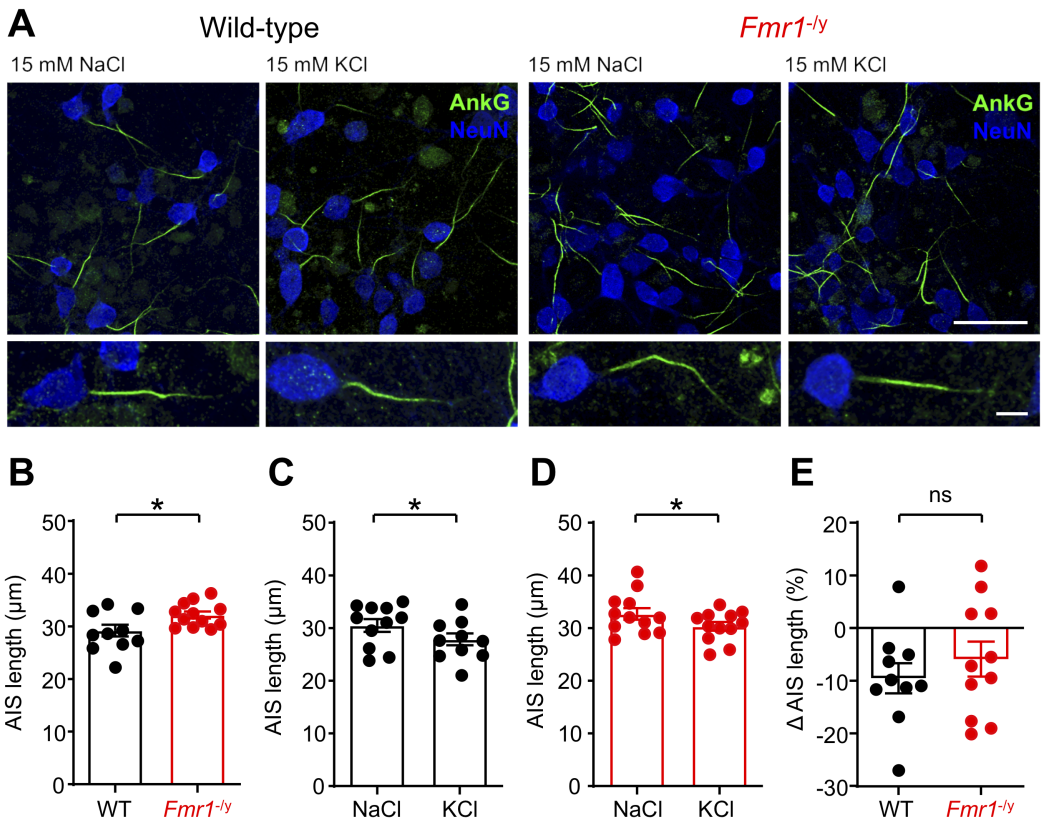

Figure 4.6: Short-term AIS shortening is present in dissociated cultures of hippocampal neurons following sustained depolarisation A - Representative images of AIS labelling (Ankyrin G, green) in primary dissociated hippocampal cell-cultures produced from WT (left) and *Fmr1*$^{-/y}$ mice following 3 h treatment with NaCl or KCl (Scale bars: 20 μm (top), 10 μm (bottom). B - AIS length under control conditions from WT (black) and *Fmr1*$^{-/y}$ (red) single mouse cultures. AIS length plotted for WT (C) and *Fmr1*$^{-/y}$ (D) mouse cultured neurons following 3 h treatment with 15 mM KCl or NaCl. H - Comparative difference in AIS length (KCl length – NaCl length). Average AIS length per mouse (from 2 coverslips) as individual data points. Statistics shown: ns – $p > 0.05$, * $p < 0.05$, from LMM (B-D) and Two-tailed Unpaired t-test (E).

The detection of AIS plasticity in the data presented above is limited by the fact that I have compared AIS length across different slices/coverslips. This approach did not allow the detection of within-cell AIS shortening, and was confounded by potential baseline differences in AIS length in slices subjected to different treatments. To circumvent these shortcomings, two-photon imaging experiments were performed in acute slices from a new transgenic mouse expressing GFP fused to the sodium channel $\beta 1$ subunit ($\beta 1$-Na$_v$-GFP), which reliably labelled the AIS.

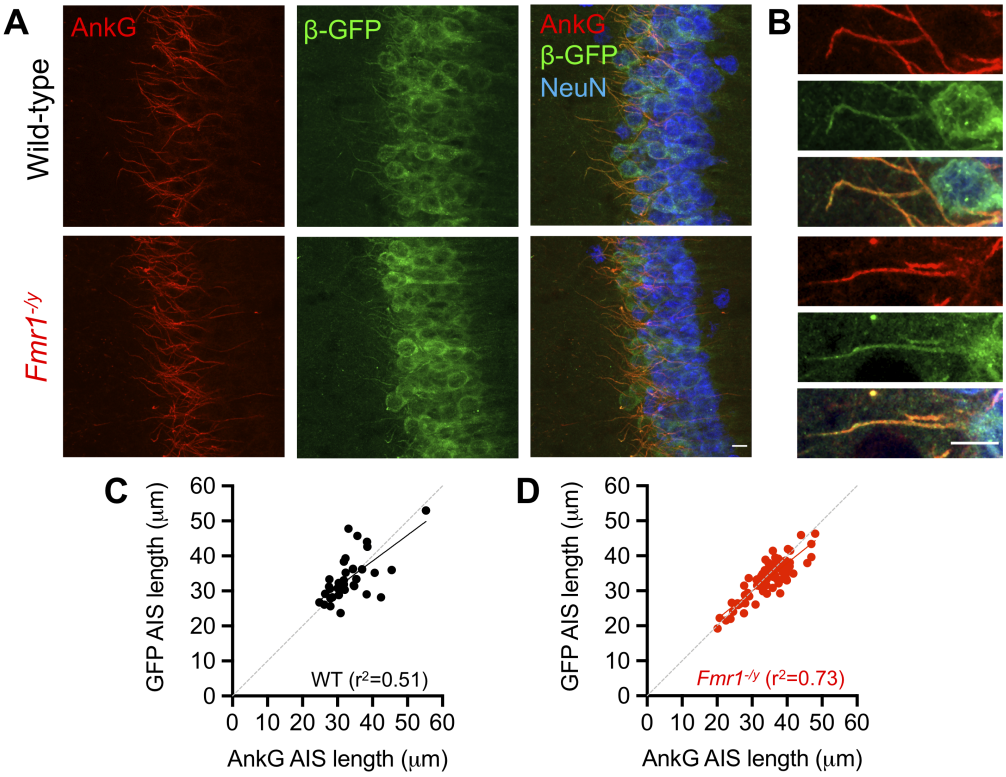

Figure 4.7: Validation of $\beta 1$-Na$_v$-GFP mice A - Flattened confocal stacks of CA1 of the hippocampus triple labelled for AnkyrinG (AnkG, red), $\beta 1$-Na$_v$-GFP (β-GFP, green), and NeuN (blue) from WT (top) and *Fmr1*$^{-/y}$ mice (bottom). B - High power micrographs showing colocalisation of AnkG (red) and $\beta 1$-Na$_v$-GFP (green) and merged (lower panel). Quantification of AnkG AIS length (x-axis) vs $\beta 1$-Na$_v$-GFP AIS length (y-axis) for WT (C, n=2 mice) and *Fmr1*$^{-/y}$ mice (D, n=3 mice), dots represent individual AISs. Note the high degree of overlap with unity (grey dotted line).

The high degree overlap between the $\beta 1$-Na$_v$-GFP expression and AnkG labelling was used as a confirmation that the GFP signal detected in the two-photon imaging experiments accurately represents the extent of the AIS (Figure 4.7). Indeed, AIS length as measured by Ankyrin G labelling highly correlated with AISs measured based on GFP expression in hippocampal sections from perfusion fixed WT and *Fmr1*$^{-/y}$ mice (WT $r^2 = 0.51$; *Fmr1*$^{-/y}$ $r^2 = 0.73$, linear regression, Figure 4.7 C, D). Importantly the

linear relationship between GFP and Ankyrin G AIS length was not different between genotypes (WT $y = 0.7x + 8.9$; *Fmr1*$^{-/y}$ $y = 0.8x + 5.9$, $F_{1,121}$=0.28, p=0.6, sum-of-least-squares F-test).

Using two-photon live imaging in acute slices allowed to answer the question of whether AISs of individual CA1 pyramidal cells would undergo plasticity following KCl treatment, as we could reliably identify the same AIS before and after the 3 h treatment period (Figure 4.8A). AIS length after treatment with NaCl or KCl was plotted as function of starting AIS length for individual AISs (Figure 4.8 B, C). The relationship between initial and final length was similar between NaCl and KCl treatment in both WT (Figure 4.8B, $F_{1,158}$=0.62, p=0.43, sum-of-least-squares F-test) and *Fmr1*$^{-/y}$ (Figure 4.8C, $F_{1,85}$=1.63, p=0.21, sum-of-least-squares F-test) mice. The difference in AIS length produced by each treatment is represented in Figure 4.8D. In WT mice, the 3 hour 15 mM NaCl treatment resulted in an average increase in length of 1.6 ± 1.0 μm, not different from the 1.1 ± 1.0 μm increase produced by the 15 mM KCl treatment (p=0.67, LMM). In slices from *Fmr1*$^{-/y}$, NaCl treatment resulted in a 1.6 ± 1.3 μm shortening of the AIS, not different from the 2.1 ± 2.0 μm shortening observed following KCl treatment (p=1.0, LMM). However, this difference was not significantly different from zero for either treament (NaCl or KCl) in either genotype (One tailed T-test p>0.05 for all groups) These data confirm that short-term, depolarisation-induced AIS shortening is absent in *ex vivo* tissue, even when measured in real time at the single-cell level.

These data suggest that short-term AIS plasticity is present in dissociated hippocampal cultures of WT and *Fmr1*$^{-/y}$ neurons, to a similar extent. However, distinct or additional factors may regulate structural plasticity following sustained depolarisation in acute hippocampal slices. Furthermore, these findings suggest a functional disconnect between cellular excitability and AIS length following sustained depolarisation.

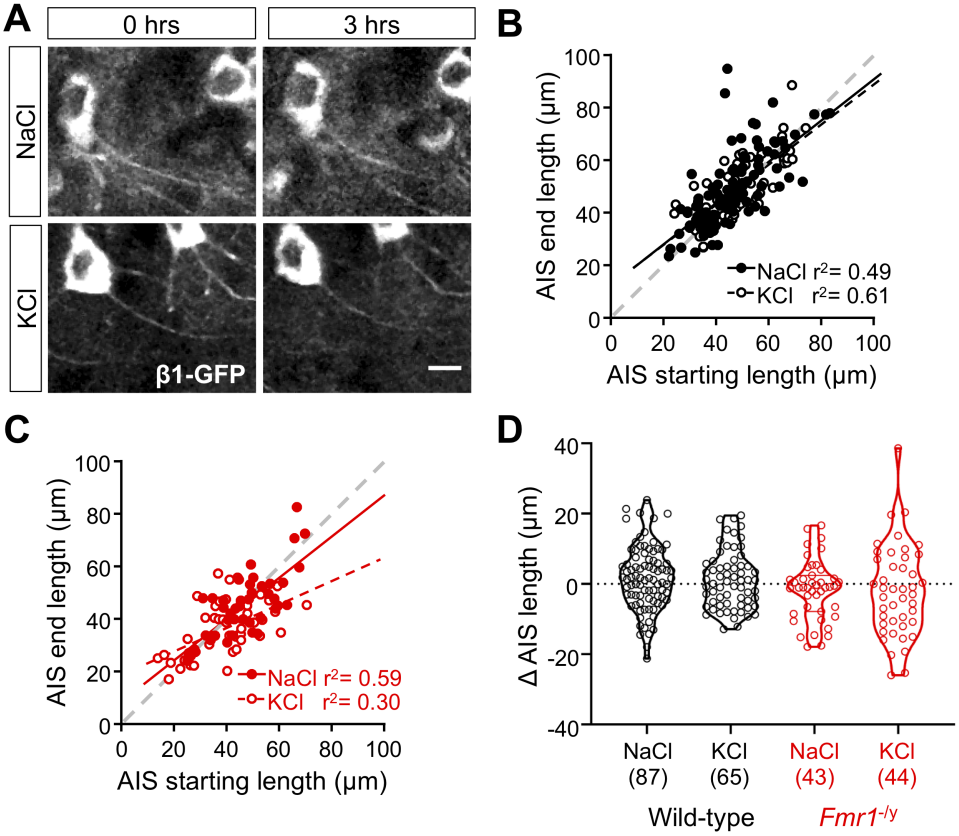

Figure 4.8: Live imaging of the AIS fails to reveal short term structural plasticity A - representative 2-photon images of the same AIS in CA1 showing β1-Na$_v$-GFP labelling under control conditions (0 hrs) compared to 3 hours of treatment with 15 mM NaCl (top) or KCl (bottom). B - Comparison of AIS length at the before (x-axis) to the AIS length 3 hours later for 15 mM NaCl (filled circles) and 15 mM KCl (open circles), in WT CA1 PCs. Data is shown for 99 AIS treated with NaCl and 65 AISs treated with KCl from 7 WT mice and fitted with linear regression (solid line – NaCl, dashed line – KCl). C - the same data as B but plotted for 44 AIS treated with NaCl and 45 AISs treated with KCl from 5 *Fmr1*$^{-/y}$ mice. D - Difference in AIS length (end - initial length) for NaCl and KCl treatments in WT and *Fmr1*$^{-/y}$ mice.

4.2.4 CA1 pyramidal cells receive reduced input from the entorhinal cortex in *Fmr1*$^{-/y}$ mice

The data presented so far suggest that hyperexcitability of CA1 pyramidal cells of *Fmr1*$^{-/y}$ mice results from structural changes of the AIS. Given that the effect of depolarisation on AIS length in *Fmr1*$^{-/y}$ cells is comparable to that of WT neurons, I hypothesised that the hyperexcitability phenotype observed could reflect homeostatic remodelling of the AIS of CA1 pyramidal cells, and consequently of membrane excitability, in response to reduced excitatory synaptic input.

To determine whether the strength of entorhinal cortex (EC) inputs to CA1 pyramidal cells is reduced in *Fmr1*$^{-/y}$ mice, we used extracellular field and whole cell patch-clamp recordings combined with electrical stimulation of the temporoammonic (TA) afferents. A bipolar stimulating electrode was placed in the distal *SLM* and used to deliver trains of stimuli (5 stimuli at 20 Hz, 200 μs each, Figure 4.9 A).

Analysis of the afferent fibre volley of field EPSP recordings allowed to assess TA recruitment in slices from both genotypes. Fibre volley amplitude increased linearly with the intensity of constant-voltage stimuli. This linear relationship was similar between WT and *Fmr1*$^{-/y}$ mice ($F_{1,348}$=2.12, p=0.15, Sum-of-least squares F-test), indicating that recruitment of entorhinal fibres is unaltered in *Fmr1*$^{-/y}$ mice, as previously described (Wahlstrom-Helgren and Klyachko, 2015). To assess the strength of synaptic inputs to CA1 via TA afferents, the dendritic fEPSPs and the somatic whole-cell EPSPs were measured simultaneously and normalised to fibre volley amplitude (Figure 4.9 B). The input-output relationship was reduced in slices from *Fmr1*$^{-/y}$ mice relative to WT when analysing both field (Figure 4.9 D, $F_{1,348}$ = 33.7, p<0.0001, Sum-of-least squares F-test) and whole cell EPSP amplitude (Figure 4.9 E, $F1, 346$=5.55, p=0.019, Sum-of-least squares F-test), indicating that dendritic filtering is insufficient to compensate for reduced synaptic inputs (Brager et al., 2012).

These data show that the strength of TA synaptic inputs to CA1 is reduced in *Fmr1*$^{-/y}$ mice, potentially resulting in homeostatic compensation of AIS length and intrinsic excitability during postnatal development.

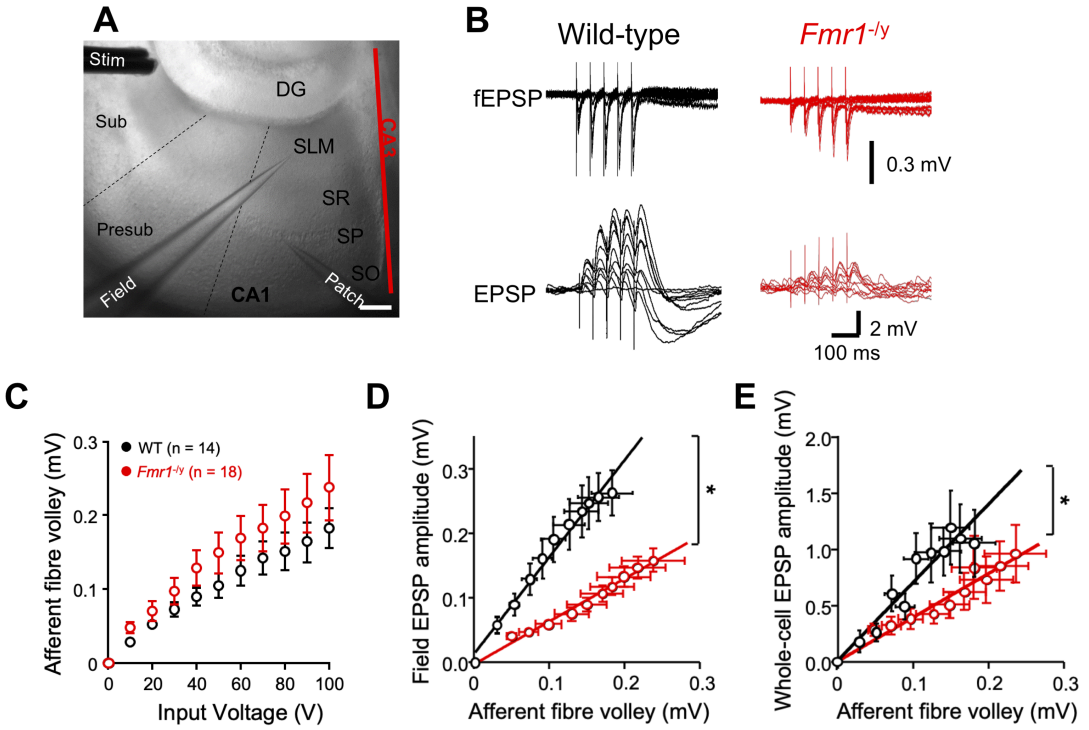

Figure 4.9: Reduced TA inputs to the CA1 region of *Fmr1*$^{-/y}$ mice A - Recording configuration showing the stimulation electrode (Stim) placed in the perforant path, extracellular field electrode (Field) placed in SLM and the whole-cell patch-clamp electrode (Patch) in *Stratum pyramidale* (Pyr). B - Representative extracellular fEPSP (top) and whole-cell EPSP (bottom), recorded in response to increasing voltage stimulation (0 – 100 V), from WT (black) and *Fmr1*$^{-/y}$ (red) mice. C - Input-output relationship for the afferent fibre volley amplitude in WT (black) and *Fmr1*$^{-/y}$ (red) mouse slices. Number of slices indicated in parenthesis. D - fEPSP amplitude recorded in SLM, plotted as a function of afferent fibre volley amplitude. E - Whole-cell EPSP amplitude plotted as a function of afferent fibre volley amplitude. Data is plotted with linear regression (straight lines, D,E). Statistics shown: * - $p<0.05$, Sum-of-least-squares F-test (D-E)). Experiments and data analysis performed by Dr Sam Booker

4.2.5 CA1 pyramidal cell spiking in response to TA stimulation is unaltered in *Fmr1*$^{-/y}$ mice

I tested the hypothesis that the hyperexcitability of CA1 pyramidal cells in *Fmr1*$^{-/y}$ reflects a homeostatic compensation for reduced synaptic input by assessing the probability of CA1 pyramidal cells spiking in response to TA stimulation, using cell-attached voltage clamp recordings. If indeed, CA1 pyramidal cells from *Fmr1*$^{-/y}$ are hyperexcitable to compensate for reduced synaptic input, probability of spiking in response to TA stimulation should be similar to that of WT neurons. Therefore, I hypothesised that CA1 pyramidal cell output would be unaltered in *Fmr1*$^{-/y}$ mice.

Using the same electrical stimulation protocol as described in the previous section, I examined the probability of spiking over a range of stimulation voltages. I found that only a small percentage of cells responded with firing at any of the stimulation voltages tested (30, 60 ad 90 V) or any of the 5 stimuli in a train (Figure 4.10 B). The percentage of firing cells was slightly higher in *Fmr1*$^{-/y}$ mice, with 37% of *Fmr1*$^{-/y}$ cells firing at least once relative to 23% in WT (p=0.04 Fisher's exact test). Taking into account all cells, the overall probability of CA1 pyramidal cells spiking in response to TA stimulation on the first stimulus in the train was similar in both genotypes across the range of stimulation voltages tested (Figure 4.10 C, Two-way ANOVA $F_{3,157}$=0.32, genotype effect: p=0.47). *Fmr1*$^{-/y}$ neurons had a probability of firing in response to the maximum stimulation intensity tested (90 V) of 0.29 ± 0.08 comparable to that of WT cells (0.21 ± 0.09). The difference between genotypes in the proportion of cells spiking is not masking an effect in overall spike probability, as this is also unchanged when assessing spike probability only in spiking cells (Figure 4.10 D, Two-way ANOVA $F_{3,43}$=1.24, genotype effect: p=0.78). When taking into account only the small percentage of spiking cells, almost all of these spiked in response to TA stimulation for the maximum voltage tested, with a spike probability of 0.98 ± 0.02 in WT and 0.85 ± 0.09 in *Fmr1*$^{-/y}$ neurons. Furthermore, repetitive stimulation of TA inputs at 20 Hz revealed no difference in CA1 pyramidal cell spike output at any of the stimulation intensities tested (Figure 4.10 E-F, Two-way ANOVA 30 V: $F_{4,224}$=0.94, genotype effect: p=0.76; 60 V: $F_{4,220}$=0.91, genotype effect: p=0.39; 90 V: $F_{4,208}$=0.28, genotype effect: p=0.47).

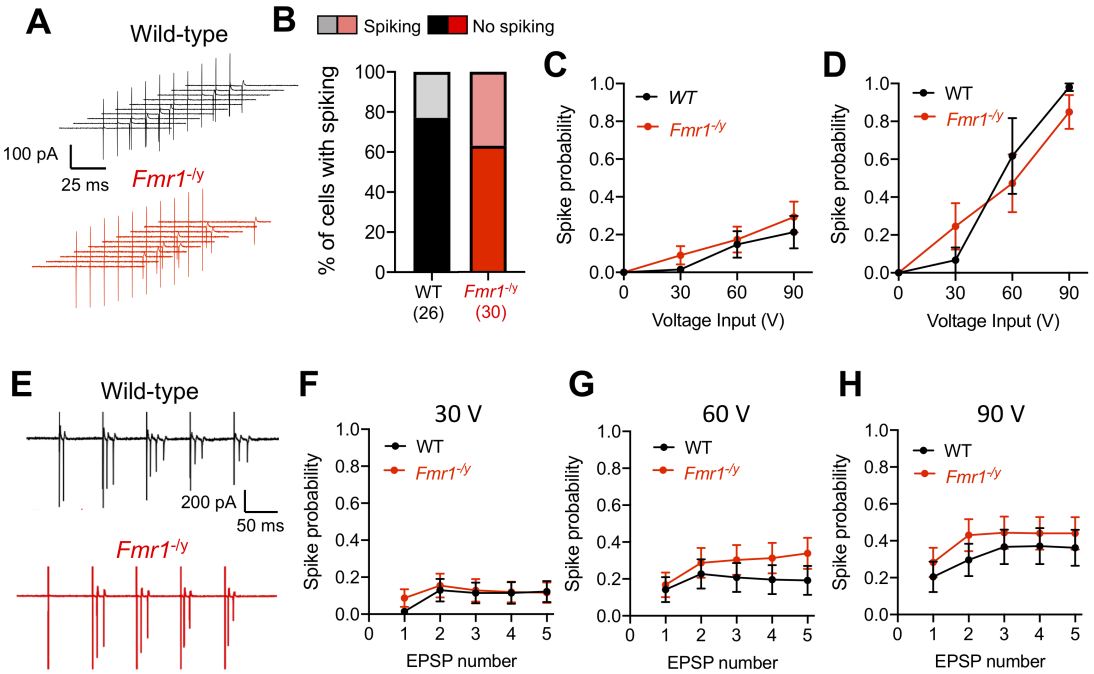

Figure 4.10: Typical cell spiking in response to TA stimulation in *Fmr1*$^{-/y}$ mice A - Example trace of multiple sweeps of cell-attached recordings from CA1 PCs following stimulation of SLM, overlaid and showing cell spiking for WT (black) and *Fmr1*$^{-/y}$ (red) neurons. Total number of cells tested shown in parenthesis (WT: 26 cells / 7 mice; *Fmr1*$^{-/y}$ 30 cells / 9 mice). B - Quantification of the % of CA1 PCs that responded to TA stimulation with a spike, in cell attached mode, at any stimulation voltage (light shading), compared to those that did not spike (dark shading). C - Measured spike probability of all CA1 PCs during the first EPSP at each stimulus intensity for WT (black) and *Fmr1*$^{-/y}$ CA1 PCs (red). D - Spike probability of spiking cells at each stimulus intensity for WT (black) and *Fmr1*$^{-/y}$ CA1 PCs (red). E - Example trace of CA1 PC spiking in response to 20 Hz stimulation of SLM. Recorded spike probability of CA1 PCs following repetitive stimulation at 30 (F), 60 (G) and 90 (H) V stimulation intensities.

These data support the idea that hyperexcitability of CA1 pyramidal cells *Fmr1*$^{-/y}$ mice is likely to be an homeostatic compensation for reduced synaptic input, resulting in similar spike output.

4.3 Discussion

In this chapter, I show that an increase in AIS length contributes to the hyperexcitability of CA1 pyramidal cells in a mouse model of FXS. This altered AIS length is not due to a lack of AIS plasticity in *Fmr1*$^{-/y}$ neurons as short-term AIS plasticity is present to the same extent in cultured neurons from both genotypes. Whilst AIS plasticity in slices appears to follow different rules to that previously described in cultured neurons (I observed an increase in AIS length rather than a decrease), prolonged depolarisation resulted in a reduction of cellular excitability, which was exacerbated in *Fmr1*$^{-/y}$ neurons. The work here presented suggests that the changes in cellular excitability observed result from homeostatic compensation for reduced entorhinal cortex inputs, in order to regulate CA1 pyramidal cell output. Indeed, reduced strength of synaptic transmission from TA inputs to CA1 is accompanied by unaltered CA1 pyramidal cell spiking in cell-attached recordings in response to the same stimulation paradigm.

4.3.1 Hyperexcitability and increased AIS length in CA1 pyramidal cells of *Fmr1*$^{-/y}$ mice

Hyperexcitability of local circuits is a hallmark feature of the mouse model of FXS (Contractor et al., 2015; Gibson et al., 2008; Zhang et al., 2014). Indeed, increased cellular excitability has been reported across multiple brain regions, from hippocampal CA1 (Luque et al., 2017) and CA3 (Deng et al., 2013) neurons, as well as entorhinal cortex (Deng and Klyachko, 2016) and neocortex (Zhang et al., 2014; Routh et al., 2017). A range of mechanisms have been suggested to underlie cellular hyperexcitability in the absence of FMRP. For instance, the interaction of FMRP with K^+ channels modulates AP kinetics, which is altered in *Fmr1*$^{-/y}$ neurons (Brown et al., 2010; Deng et al., 2013; Deng and Klyachko, 2016). Other studies show that altered ion channel expression contributes to cellular excitability phenotypes (Brager et al., 2012; Routh et al., 2017; Zhang et al., 2014), perhaps due to altered mRNA translation or homeostatic mechanisms. The downstream effects of altered cellular excitability on circuit function could contribute to a range of phenotypes, from cognitive function to sensory hypersensitivities (Biane et al., 2015; Breton and Stuart, 2009; Marder and Goaillard, 2006). The work presented in this chapter suggests that increased AIS length constitutes a potential additional mechanism contributing to cellular hyperexcitability in CA1

pyramidal cells in the absence of FMRP. This data is supported by computational modelling, showing that the change in AIS length we observe is sufficient to produce the effects on AP threshold and rheobase current seen experimentally, without affecting maximum firing rate. Interestingly, altered AIS length has previously been associated with cellular hyperexcitability in a mouse model of Angelman's Syndrome (Kaphzan et al., 2011), suggesting the AIS as a potential convergent mechanism for hyperexcitability in monogenic forms of ASD/ID.

4.3.2 Depolarisation-induced plasticity of the AIS and intrinsic excitability

The data presented here confirms that short-term AIS plasticity in response to sustained depolarisation is present in cultured neurons, as previously described (Evans et al., 2015). Importantly, this form of plasticity is unaltered in *Fmr1*$^{-/y}$ neurons, suggesting that the regulation of AIS length in response to altered neuronal activity is independent of FMRP expression. In acute hippocampal slices, I did not observe a shortening of AISs in CA1 in response to depolarising stimuli. Instead, I observed an increase in AIS length following KCl treatment, which was similar in both genotypes. Importantly, this effect is not observed when examining AIS length in live imaging experiments, indicating the lengthening observed in fixed sliced is potentially confounded by baseline differences in AIS length across slices used for the different treatments. Given that I observed the AIS shortening previously reported in cultured neurons from the same mouse colony, our data casts doubt on the ability of neurons in *ex vivo* tissue to undergo this form of plasticity on the same timescales described in cell culture. However, as I have only tested one time-point (i.e. 3 hours post stimulation), it is possible that transient changes in AIS length could occur over a shorter or longer time-window, or may be age dependent (Jamann et al., 2020). Morever, it is possible that the contribution of different cell types to the culture preparation used in my experiments explains why AIS shortening is present in this preparation and not when I look exclusively at CA1 pyramidal neurons in slice, as Evans et al. (2015) have previously shown that the AIS shortening following depolarisation is more pronounced in DGCs. Nonetheless, it is clear that the changes in excitability in response to KCl treatment observed cannot be mediated by changes in AIS length.

Whilst I did not observe AIS shortening in acute hippocampal slices, KCl treatment

resulted in a decrease in excitability of CA1 pyramidal cells, in line with the observations of Evans et al. (2015) and O'Leary et al. (2010) in cell culture. As the increase in AIS length we observe cannot account for the changes in cellular excitability following KCl treatment, other mechanisms must be involved. Altered K^+ channel function or expression can present a potential explanation. The observed slowing of AP decay kinetics is consistent with altered Kv1.1. function, which is known to be modulated by neuronal activity (Kole et al., 2007). On the other hand, the reduction in input resistance we observe could result from increased leak potassium currents (O'Leary et al., 2010; Yue and Yaari, 2006), altered M-channel activity (Yue and Yaari, 2006; Zhang et al., 2012), or altered tonic GABAA receptor activation (Curia et al., 2009). Additionally other studies have suggested activity dependent function of $K_v2.1$ as an important mechanism regulating intrinsic excitability of CA1 pyramidal cells (Du et al., 2000; Mohapatra et al., 2009). Furthermore, if this is indeed a K^+ channel dependent mechanism, the altered K^+ channel function and expression seen in the mouse model of FXS (Brown et al., 2010; Deng et al., 2013; Deng and Klyachko, 2016) could potentially explain the difference in the magnitude of the change in excitability in response to depolarisation in *Fmr1*$^{-/y}$ neurons. However, further experiments would be required to isolate the precise mechanism underlying this compensatory response. The exaggerated reduction in excitability of *Fmr1*$^{-/y}$ neurons in response to depolarisation is in line with recent studies reporting that homeostasis of cellular excitability is enhanced following dampening of activity in *Fmr1*$^{-/y}$ cultured neurons (Bülow et al., 2019). Furthermore, enhanced *in vivo* experience dependent plasticity has also been reported at the CA3-CA1 synapse (Talbot et al., 2018). However, the finding that CA1 neuronal output is normal despite the decrease in synaptic input from EC suggests that homeostatic mechanisms are able to reset neuronal firing in *Fmr1*$^{-/y}$ neurons, consistent with recent findings from somatosensory cortex (Antoine et al., 2019).

4.3.3 Network level homeostatic compensation in the hippocampus of *Fmr1*$^{-/y}$ mice

Altered long range connectivity has been suggested as a mechanism underlying cognitive impairment in the mouse model of FXS (Haberl et al., 2015) as well as in patients (Wang et al., 2017; van der Molen et al., 2014). Deficits in hippocampal function have been reported in the mouse and rat model of FXS, particularly in spatial

learning and episodic memory tasks (Asiminas et al., 2019; Talbot et al., 2018; Till et al., 2015; D'Hooge et al., 1997). However, the study of synaptic function and plasticity in the hippocampus has been restricted to specific synapses, namely the Schaffer collateral pathway connecting CA3 to CA1 (Talbot et al., 2018; Klemmer et al., 2011; Huber et al., 2002). The EC makes synaptic connections with CA1 via the TA pathway (Amaral and Witter, 1989), and it has an important role driving spatial information to CA1 (Brun et al., 2008; Fyhn et al., 2004; Miller and Best, 1980). Therefore, the reduced synaptic input we observe upon stimulation of TA afferents in hippocampal slices, may present a functional correlate for impaired spatial performance in *Fmr1*$^{-/y}$ mice. EC inputs to dentate gyrus are also reduced in FXS mice (Yun and Trommer, 2011), raising the possibility that pre-synaptic domain is responsible for this phenotype, as altered pre-synaptic function has previously been observed in the Schaffer collateral pathway (Klemmer et al., 2011). However, pre-synaptic release probability is unaltered at the TA pathway in *Fmr1*$^{-/y}$ mice (Wahlstrom-Helgren and Klyachko, 2015). In fact, my data shows that repetitive TA stimulation does not differentially affect spike probability in *Fmr1*$^{-/y}$ mice, consistent with normal pre-synaptic function. Therefore, post-synaptic mechanisms are more likely to explain the reduced EPSP amplitude I observe, as absence of FMRP is known to cause abnormal AMPA receptor trafficking and enhanced receptor internalisation even under basal conditions (Nakamoto et al., 2007; Muddashetty et al., 2007).

Additionaly, these data raise the possibility that other phenotypes previously described in *Fmr1*$^{-/y}$ mice result from compensatory mechanisms. Given the role of HCN channels in reducing dendritic gain (Magee et al., 1998) and enhancing dendritic supralinearity (Branco and Häusser, 2011), it is plausible that increased HCN channels expression is regulated by reduced TA input, representing an additional homeostatic mechanism in FXS. Indeed, this is supported by the fact that altered HCN expression in FXS is biderectional depending on the cell type (Booker et al., 2019; Kalmbach et al., 2015). Furthermore, HCN channel expression is regulated by manipulating network activity activity in *ex vivo* tissue (Fan et al., 2005) and in epileptic states *in vivo* (Jung et al., 2011; Richichi et al., 2008).

In summary, the data presented in this chapter suggest that increased AIS length and hyperexcitability of CA1 pyramidal cells arise from reduced excitatory synaptic input during development, in order to normalise neuronal output. My data suggest

that local circuit dysfunction arises as a compensatory mechanism for reduced long range connectivity in FXS, whereby absence of FMRP disrupts neuronal migration and circuit assembly during early development (La Fata et al., 2014), triggering adaptive responses that shape local circuit function throughout life. In the future, studying *in vivo* connectivity between EC and CA1 throughout development might provide valuable insight into spatial learning deficits in FXS and a better understanding of the interaction between circuit development and cellular excitability in *Fmr1*$^{-/y}$ mice.

Chapter 5

In vivo AIS plasticity in a mouse model of Fragile X Syndrome

5.1 Introduction

In Chapter 4, I show that AIS length in CA1 pyramidal neurons is increased in *Fmr1*$^{-/y}$ mice and postulate that this is a homeostatic response to reduced TA synaptic input. While my data show that AISs from *Fmr1*$^{-/y}$ mice undergo activity dependent plasticity *in vitro* and in *ex vivo* tissue, *in vivo* plasticity of the AIS has not yet been examined in *Fmr1*$^{-/y}$ mice. Furthermore, demonstrating *in vivo* AIS plasticity would strengthen the idea that the phenotype observed in the hippocampus is a compensatory response.

Neurodevelopmental disorders, and in particular FXS, are frequently associated with altered critical periods during development. Indeed, disrupted critical periods for synapse development have been reported across sensory circuits, from somatosensory (Bureau et al., 2008; Harlow et al., 2010) to auditory cortex (Kim et al., 2013). However, critical periods for AIS development and plasticity have not yet been examined in the context of FXS.

The primary visual cortex (V1) is the main brain area responsible for processing of visual information and it has long been used as a model system to study activity dependent phenomena (Wiesel and Hubel, 1965; Gordon and Stryker, 1996; Espinosa and Stryker, 2012). Visual experience plays a critical role in shaping circuit function in the visual cortex, modulating synaptic function and connectivity, as well as cellular excitability. Indeed, visual deprivation as short as 2 days is sufficient to reconfigure local circuits, which are restored once visual input is reestablished (Maffei et al., 2004).

More recently, Brown et al. (2019) have shown that visual deprivation for up to 5 weeks following eye opening results in increased cellular excitability of layer L2/3 pyramidal neurons *in vivo*, but preserves orientation selectivity, indicating that regulation of intrinsic excitability plays an important role in preserving circuit function. Interestingly, critical periods for homeostatic and hebbian forms of plasticity seem to be specific to each cortical layer (Goel and Lee, 2007; Jiang et al., 2007). With the plasticity window closing earlier in L4 (Jiang et al., 2007), the main input layer in V1, whilst L2/3 remains plastic into adulthood (Goel and Lee, 2007; Desai et al., 2002).

Sensory experience is known to modulate the AIS throughout development. Kuba et al. (2014) have shown that AISs are developmentally regulated by auditory input in the chick's *nucleus laminaris*. Additionally, the AIS exhibits an experience dependent developmental trajectory within the mouse visual cortex, with its length increasing up to P15 and then shortening by P28 in L2/3 and L5 (Gutzmann et al., 2014). This is an activity dependent phenomenon, as it does not occur when mice are visually deprived from birth or after eye opening.

Given the evidence for abnormal critical periods in FXS, I hypothesised that AIS developmental trajectory would be altered the *Fmr1*$^{-/y}$ mouse. Additionally, based on my findings in the hippocampus, I hypothesised that the AIS of *Fmr1*$^{-/y}$ mice undergoes plasticity in response to visual deprivation to the same extent as WT neurons and that compensatory changes to intrinsic excitability will be exacerbated in *Fmr1*$^{-/y}$ neurons. In this chapter, I examined the developmental trajectory of AIS length across cortical layers in the primary visual cortex of *Fmr1*$^{-/y}$ and WT mice, to assess whether this was disrupted in FXS. I used a visual deprivation paradigm to assess *in vivo* AIS plasticity and regulation of cellular excitability in *Fmr1*$^{-/y}$ mice.

5.2 Results

5.2.1 AIS development and plasticity in the visual cortex of WT and *Fmr1*$^{-/y}$ mice

I used immunolabelling for the AIS scaffolding protein Ankyrin G in sections of perfusion fixed mice to visualise AISs in the V1 binocular region of WT and *Fmr1*$^{-/y}$ mice, and examine their developmental trajectory and plasticity in response to visual deprivation across L2/3 (Figure 5.1) and L5 (Figure 5.2).

I assessed AIS length in L2/3 of the primary visual cortex in P14 and P28 mice, firstly to confirm the reduction in AIS length between these two ages that has previously been reported in WT mice (Gutzmann et al., 2014), and secondly to determine whether a similar developmental trajectory occurs in *Fmr1*$^{-/y}$ mice. In WT mice, AISs measured on average 27.6 ± 0.8 μm at P14, AIS length decreased by P28 to 22.9 ± 0.8 μm, reflecting an 18% reduction (p=0.0004 LMM, Figure 5.1 B, left). A similar decrease in AIS length over development was observed in *Fmr1*$^{-/y}$ mice, with average AIS length decreasing by 17% between P14 (27.2 ±1.0 μm) and P28 (22.6 ± 0.7 μm, p<0.0001 LMM, Figure 5.1 B, right). The average AIS length at the ages tested did not differ between genotypes (P14: p>0.99 P28: p>0.99, LMM). The shortening of AISs over development can also be observed by the similar leftward shift in the cumulative distribution of AIS length at P14 relative to P28 in both genotypes (Figure 5.1C, Kolmogorov-Smirnov test to compare cumulative distributions: K-S$_D$ = 0.21, p <0.0001).

I used a dark rearing paradigm to assess *in vivo* AIS plasticity in response to sensory deprivation. Two weeks of dark rearing from P14 to P28 has previously been shown to result in longer AISs at P28 relative to control (Gutzmann et al., 2014), as the typical AIS shortening over development is prevented by loss of visual input. WT and *Fmr1*$^{-/y}$ mice were dark reared for 2 weeks (from P14 to P28) or for 4 weeks (from birth to P28) and AIS length at the end of dark-rearing period was compared to that in control P28 mice, kept in a 12 h light/dark cycle. Dark rearing mice for either 2 or 4 weeks did not result in a significant change in AIS length relative to control in WT mice (DR (2 weeks) vs P28 (Ctr) p>0.99, DR (4 weeks) vs P28 (Ctr) p>0.99, LMM, Figure 5.1 D). In *Fmr1*$^{-/y}$ mice, there was also no effect of dark rearing mice for 2 or 4 weeks, as AIS length following visual deprivation was comparable to that of P28 control animals (DR (2 weeks) vs P28 (Ctr): p>0.99, DR (4 weeks) vs P28 (Ctr): p>0.99, LMM, Figure 5.1 E).

I performed the same analysis described above in L5 of the primary visual cortex. Similar to my findings in L2/3, AISs were longer at P14 (29.1 ± 0.7 μm) relative to P28 (20.3 ± 0.8 μm) in WT mice (p<0.0001, LMM, Figure 5.2 B). A similar developmental pattern was observed in L5 of *Fmr1*$^{-/y}$ mice, where at P14 AISs measured on average 27.4 ± 0.8 μm compared to 20.7 ± 0.8 μm at P28 (p<0.0001, LMM, Figure 5.2 B). Average AIS length at P14 and P28 under control conditions did not differ between genotypes (P14: p=0.74, P28: p>0.99, LMM). Here too, I found no effect of dark

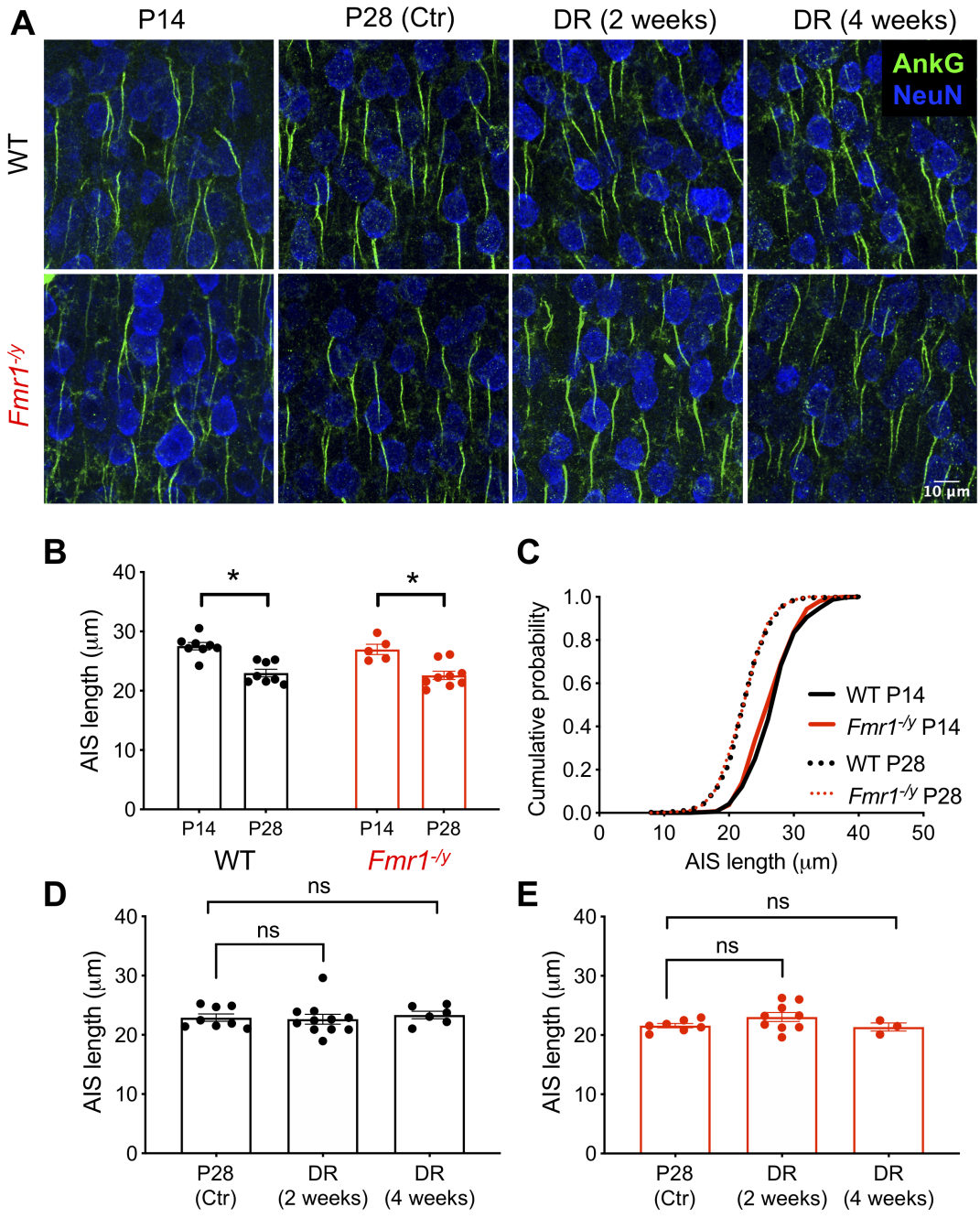

Figure 5.1: AIS length over development and following visual deprivation in L2/3 of primary visual cortex A - Flattened confocal stacks of L2/3 of the primary visual cortex from P14 and P28 mice as well as P28 mice dark reared (DR) for 2 and 4 weeks, labelled for the AIS scaffolding protein Ankyrin G (green) and the neuronal marker NeuN (blue). Average AIS length (B) and respective cumulative distribution (C) in control P14 and P28 WT and *Fmr1*$^{-/y}$ mice. Average AIS length following 2 or 4 weeks of visual deprivation (DR) compared to control AIS length in P28 WT (D) and *Fmr1*$^{-/y}$ (E) mice. All bar chart data shown as animal averages, dots represent individual animals. P14 WT: n= 390 / 8 mice *Fmr1*$^{-/y}$: n= 250 AISs / 5 mice; P28 (ctr) WT: n= 551 AISs/8 mice *Fmr1*$^{-/y}$: n= 600 AISs / 7 mice; DR 2 weeks WT: n= 950 / 11 mice *Fmr1*$^{-/y}$: n= 783 / 9 mice; DR 4 weeks WT: n= 600 AISs / 6 mice *Fmr1*$^{-/y}$: n= 300 AISs / 3 mice. Statistics shown: * $p<0.05$, ns $p>0.05$, LMM

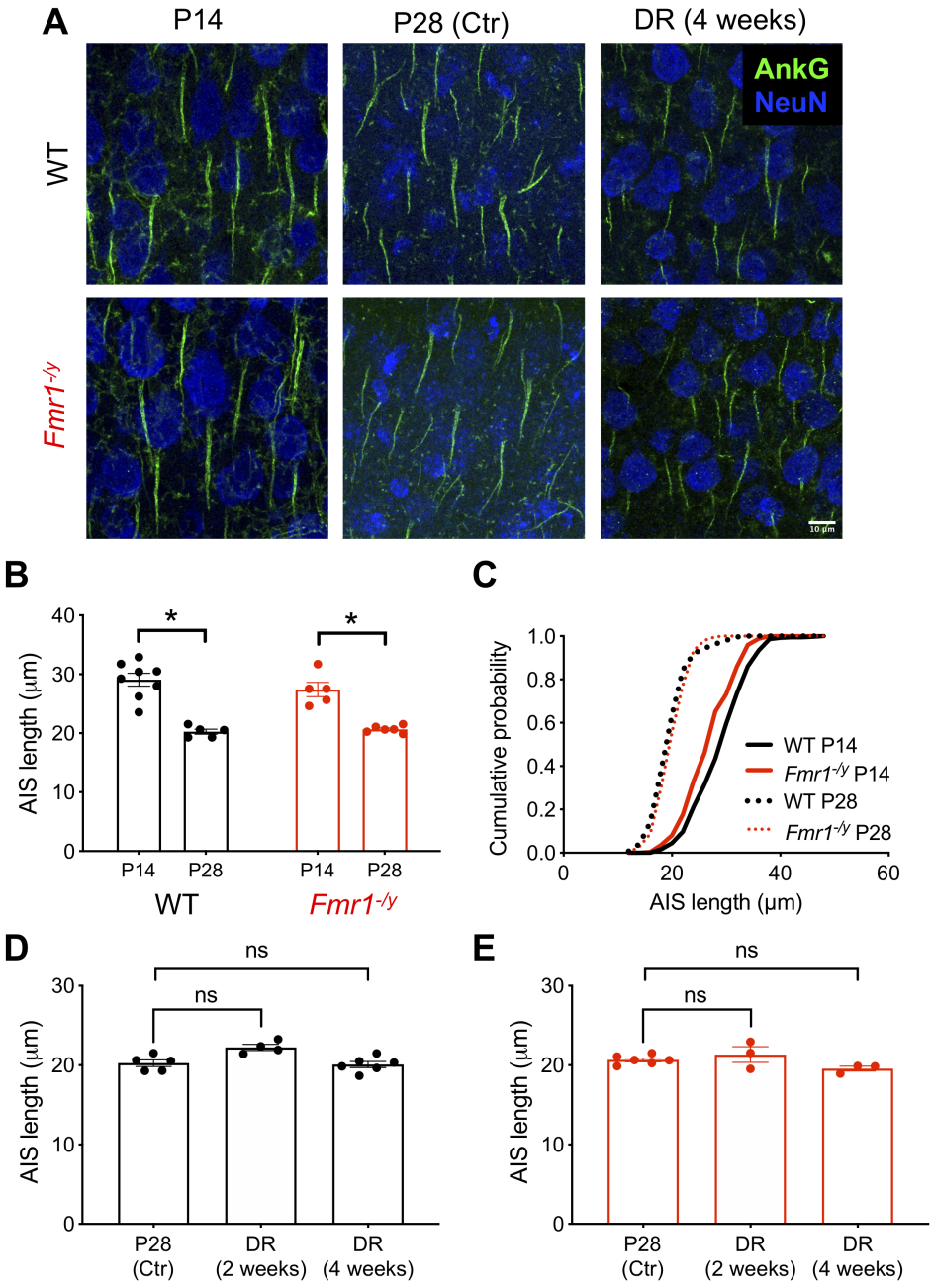

Figure 5.2: AIS length over development and following visual deprivation in L5 of primary visual cortex A - Flattened confocal stacks of L5 of the primary visual cortex from P14 and P28 mice as well as P28 mice dark reared (DR) for 4 weeks, labelled for the AIS scaffolding protein Ankyrin G (green) and the neuronal marker NeuN (blue). Average AIS length (B) and respective cumulative distribution (C) in control P14 and P28 WT and *Fmr1*$^{-/y}$ mice. Average AIS length following 2 or 4 weeks of visual deprivation (DR) compared to control AIS length in P28 WT (D) and *Fmr1*$^{-/y}$ (E) mice. All bar chart data shown as animal averages, dots represent individual animals. (P14 WT: n= 361 / 8 mice *Fmr1*$^{-/y}$: n= 250 AISs / 5 mice; P28 (ctr) WT: n= 250 AISs/5 mice *Fmr1*$^{-/y}$: n= 300 AISs / 6 mice; DR 2 weeks WT: n= 400 / 4 mice *Fmr1*$^{-/y}$: n= 283 / 3 mice; DR 4 weeks WT: n= 300 AISs / 6 mice *Fmr1*$^{-/y}$: n= 150 AISs / 3 mice). Statistics shown: * $p<0.05$, ns $p>0.05$, LMM

rearing. AIS length after 2 or 4 weeks of dark rearing was comparable to that of control P28 mice in WT (DR 2 weeks: p=0.75, DR 4 weeks: p>0.99, LMM, Figure 5.2 D) and *Fmr1*$^{-/y}$ mice (DR 2 weeks: p>0.99, DR 4 weeks: p>0.99, LMM, Figure 5.2 E).

Layer 4 is the main input layer in the visual cortex, receiving visual information via thalamic inputs (Olivas et al., 2012; da Costa and Martin, 2011). Thus, I hypothesised that loss of visual input during early postnatal development would have a greater impact in L4. To test this I assessed AIS length in P14 and P28 mice under control conditions compared to AIS length in mice dark reared for 4 weeks from birth.

Interestingly, the developmental trajectory of AIS length appears to be altered in *Fmr1*$^{-/y}$ mice in L4, in contrast to my observations in L2/3 and L5. WT mice exhibit longer AISs at P14 (27.1 ± 0.8 μm) relative to P28 (20.8 ± 0.6 μm, p<0.0001, LMM), as has been observed in L2/3 and 5. However, AIS length at P14 is reduced in *Fmr1*$^{-/y}$ (23.3 ± 0.8 μm) mice relative to WT at the same age (27.1 ± 0.8 μm, p=0.01, LMM) and not significantly different to that at of P28 *Fmr1*$^{-/y}$ mice (21.0 ± 0.6 μm, p=0.2, LMM, Figure 5.3 B, C). I did not find an effect of dark rearing on AIS length in L4 in either genotype, with AIS length following dark rearing (WT: 18.9 ± 0.6 μm, *Fmr1*$^{-/y}$: 19.8 ± 0.8 μm) being comparable to that of P28 control mice (WT: 20.8 ± 0.6 μm *Fmr1*$^{-/y}$: 21.0 ± 0.6 μm, p=0.2 and p=0.8, respectively, LMM, Figure 5.3 B).

These data confirm the findings of Gutzmann et al. (2014), showing a developmental regulation of AIS length in WT mice and extend this observation to *Fmr1*$^{-/y}$ mice. Whilst the developmental trajectory of AIS length appears to be unaltered in *Fmr1*$^{-/y}$ mice in L2/3 and L5 of the primary visual cortex, this is not the case in L4. In contrast to what has previously been reported, I did not observe an effect of visual deprivation on AIS length across all cortical layers examined.

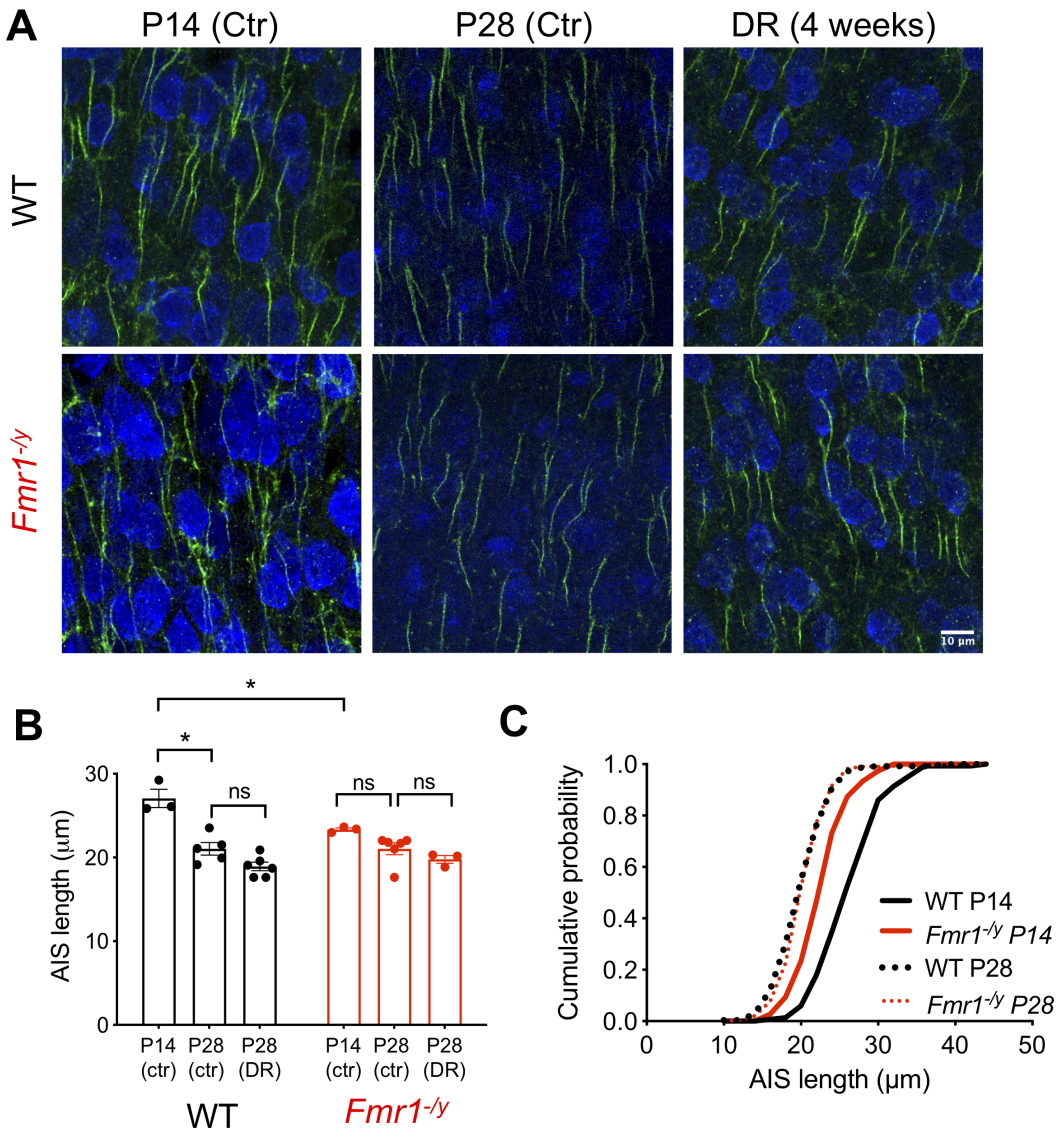

Figure 5.3: AIS length over development and following visual deprivation in L4 of primary visual cortex A - Flattened confocal stacks of L4 of the primary visual cortex from P14 and P28 mice under control conditions (Ctr) as well as P28 mice dark reared (DR) for 4 weeks, labelled for the AIS scaffolding protein Ankyrin G (green) and the neuronal marker NeuN (blue). B - Average AIS length in control P14 and P28 WT and dark reared mice from both genotypes. C - Cumulative distribution in control P14 and P28 WT and *Fmr1*$^{-/y}$ mice. All bar chart data shown as animal averages, dots represent individual animals. (P14 WT: n= 150 / 3 mice *Fmr1*$^{-/y}$: n= 150 AISs / 3 mice; P28 (ctr) WT: n= 248 AISs/5 mice *Fmr1*$^{-/y}$: n= 300 AISs / 6 mice; DR WT: n= 300 AISs / 6 mice *Fmr1*$^{-/y}$: n= 150 AISs / 3 mice). Statistics shown: * $p<0.05$, ns $p>0.05$, LMM

5.2.2 Intrinsic physiology of L2/3 pyramidal cells of the visual cortex following visual deprivation

A recent study by Brown et al. (2019) reported increased cellular excitability in L2/3 pyramidal neuron in the mouse visual cortex following visual deprivation. Even though I did not observe AIS plasticity, examining intrinsic excitability following visual deprivation provides valuable information about homeostatic response to loss of visual input. In the previous chapter I show compensatory changes in intrinsic excitability that are independent of AIS remodelling, and exacerbated in *Fmr1*$^{-/y}$ neurons. Therefore, I hypothesised that following visual deprivation L2/3 pyramidal cells would exhibit enhanced excitability to compensate for loss of sensory input, and this effect would be more pronounced in *Fmr1*$^{-/y}$ mice. To address this hypothesis, I performed whole-cell patch clamp recordings from L2/3 pyramidal neurons in acute slices of primary visual cortex from control mice and mice that had been dark reared for 4 weeks (from birth), at P28 to 35.

Firstly, I assessed the intrinsic excitability of L2/3 pyramidal neurons under control conditions in *Fmr1*$^{-/y}$ and WT mice. WT neurons exhibited a hyperpolarised resting membrane potential of -78.2 ± 2.0 mV, which was unaltered in *Fmr1*$^{-/y}$ neurons (-79.5 ± 1.7 mV, p=0.96, LMM). *Fmr1*$^{-/y}$ neurons appeared to be slightly more excitable than those of WT mice (Two-way RM ANOVA interaction: $F_{16,160}$=1.7 p=0.0008, main genotype effect p=0.03), as seen by the IF plot in Figure 5.4 C. Despite the significant current step∗genotype interaction and significant main effect of genotype, post hoc multiple comparisons do not show a significant difference between genotypes at any of the current steps tested (p>0.05 for all current steps, Holm-Sidak post-hoc test, Figure 5.4 C). Furthermore, this was not accompanied by a significant change in input resistance (WT Ctr: 123 ± 14 MΩ, *Fmr1*$^{-/y}$ Ctr: 109 ± 7 MΩ, p=0.87, GLMM) or rheobase current (WT Ctr: 120 ± 8 pA, *Fmr1*$^{-/y}$ Ctr: 106± 9 pA, p=0.09, GLMM). I examined AP properties including voltage threshold, amplitude and rise and decay rates, all of which were unaltered in *Fmr1*$^{-/y}$ mice relative to WT (Table 5.1). The AP adaptation ratio in response to the highest current injection step was also unaltered in *Fmr1*$^{-/y}$ mice relative to WT (Table 5.1).

Next, I examined the effect of visual deprivation in the excitability of WT neurons. Resting membrane potential was not altered following dark rearing (p=0.43, LMM, Figure 5.4 F). I found excitability of L2/3 pyramidal cells from dark reared mice to be

Table 5.1: Comparison of action potential properties of primary visual cortex L2/3 pyramidal cells in control WT and *Fmr1*$^{-/y}$ mice

Physiological property	**WT**	***Fmr1*$^{-/y}$**	**Stats test**	**p value**
Voltage threshold (mV)	-38.0 ± 0.9	-38.3 ± 0.3	GLMM	0.68
Half height duration (ms)	0.76 ± 0.04	0.76 ± 0.03	LMM	0.95
Amplitude (mV)	82.5 ± 1.7	81.7 ± 1.1	LMM	0.85
Max rise rate (mV.ms^{-1})	436 ± 23	433 ± 19	LMM	0.86
Max decay rate (mV.ms^{-1})	96.4 ± 5.1	96.2 ± 2.4	LMM	0.88
Adaptation ratio	3.03 ± 0.24	3.09 ± 0.25	T-test	0.85

comparable to that of control mice, as these show similar AP discharge in response to depolarising current steps (Figure 5.4 D, Two-way RM ANOVA $F_{16,144}$=0.14, main DR effect p=0.85). This was accompanied by no change in input resistance (p=1, GLMM) or rheobase current (p=0.35, GLMM) following dark rearing (Figure 5.4 G, H). All AP kinetic properties were also unchanged relative to control recordings (Table 5.2). The data I collected for DR *Fmr1*$^{-/y}$ mice is minimal at this stage, however I found no evidence of an effect of visual deprivation on the excitability of *Fmr1*$^{-/y}$ neurons. AP discharge in response to current steps was unaltered following visual deprivation (Two-way RM ANOVA $F_{16,112}$=0.63, main DR effect p=0.88), as was rheobase current (p=0.99, GLMM) and input resistance (p=0.13, GLMM). AP kinetic parameters were also comparable between dark reared and control *Fmr1*$^{-/y}$ mice (Table 5.3).

Table 5.2: Comparison of action potential properties in primary visual cortex L2/3 pyramidal cells in dark reared WT mice relative to control

Physiological property	**Ctr**	**DR**	**Stats test**	**p value**
Voltage threshold (mV)	-38.0 ± 0.9	-37.9 ± 0.6	GLMM	0.66
Half height duration (ms)	0.76 ± 0.04	0.91 ± 0.04	LMM	0.06
Amplitude (mV)	82.5 ± 1.7	80.1 ± 1.6	LMM	0.98
Max rise rate (mV.ms^{-1})	436 ± 23	385 ± 21	LMM	0.94
Max decay rate (mV.ms^{-1})	96.4 ± 5.1	78.2 ± 4.5	LMM	0.18

Table 5.3: Comparison of action potential properties in primary visual cortex L2/3 pyramidal cells in dark reared *Fmr1*$^{-/y}$ mice relative to control

Physiological property	**Ctr**	**DR**	**Stats test**	**p value**
Voltage threshold (mV)	-38.3 ± 0.3	-39.9 ± 0.1	GLMM	0.46
Half height duration (ms)	0.76 ± 0.03	0.86 ± 0.07	LMM	0.40
Amplitude (mV)	81.7 ± 1.1	82.0 ± 2.8	LMM	1.00
Max rise rate (mV.ms^{-1})	433 ± 19	393 ± 21	LMM	0.77
Max decay rate (mV.ms^{-1})	96.2 ± 2.4	84.4 ± 9.9	LMM	0.53

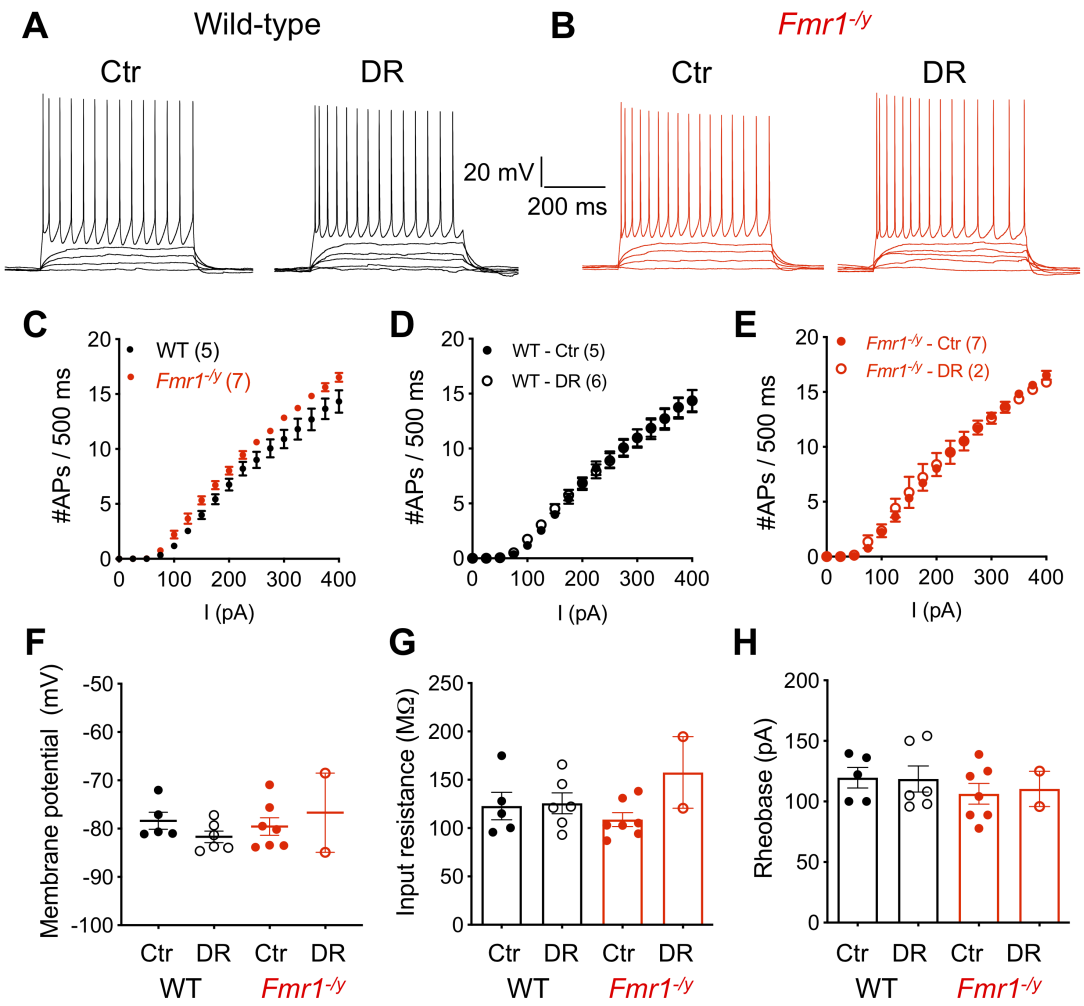

Figure 5.4: Intrinsic excitability of V1 L2/3 pyramidal cells following visual deprivation Example traces of voltage responses to 500 ms long depolarising current steps (0 to +400 pA, in 25 pA steps) from control (Ctr) and dark rearing (DR) conditions from WT (A) and *Fmr1*$^{-/y}$ (B) cells. C - Comparison of AP discharge in response to depolarising current steps in control WT and *Fmr1*$^{-/y}$ cells. Comparison of AP discharge in response to depolarising current steps in control (filled circles) and dark reared (open circles) conditions for WT (D) and *Fmr1*$^{-/y}$ (E) mice. Quantification of resting membrane potential (F), input resistance (G) and rheobase current (H) for control and dark reared mice of both genotypes (WT Ctr n= 14 cells / 5 mice, WT DR n= 19 cells / 6 mice; *Fmr1*$^{-/y}$ Ctr n= 22 cells / 7 mice *Fmr1*$^{-/y}$ DR: n= 6 cells / 2 mice) All data shown as averages of individual mice (dots), with total mice analysed in parenthesis (all p values > 0.05 GLMM (F-H)).

5.3 Discussion

5.3.1 Developmental trajectory of AIS is affected in a layer specific manner the visual cortex of *Fmr1*$^{-/y}$ mice

In this chapter, I show that there is a developmental regulation of the AIS in the mouse visual cortex. In particular, I observed a decrease in AIS length after eye opening in L2/3 and L5 in WT mice, as described by Gutzmann et al. (2014). I extended these findings to *Fmr1*$^{-/y}$ mice, which followed a similar developmental trajectory. However, examining AISs in L4 revealed disruption of the AIS developmental profile in *Fmr1*$^{-/y}$ mice. At odds with previous studies (Gutzmann et al., 2014), I found no effect of visual deprivation on AIS length in any of the cortical layers examined.

Altered critical periods over development have been described in other sensory areas in the *Fmr1*$^{-/y}$ mice, namely the somatosensory cortex (Harlow et al., 2010) and the auditory cortex (Kim et al., 2013). These are thought to contribute to abnormal circuit function (Doll et al., 2017) and the sensory hypersensitivities seen in the *Fmr1*$^{-/y}$ mouse and characteristic of the disorder in patients. Given the findings in other cortical areas, its perhaps not surprising that, in the visual cortex, AISs diverge from the typical developmental trajectory. Indeed, abnormal function of the brain circuitry involved in visual processing has been reported both in *Fmr1*$^{-/y}$ mice (Berzhanskaya et al., 2016; Haberl et al., 2015) and FXS infants (Farzin and Rivera, 2010; Farzin et al., 2008).

AIS development in L4 had not yet been examined. In this chapter, I show that in L4 AISs decrease in length from P14 to P28 in WT mice, following a similar pattern to that observed in other cortical layers. However, in *Fmr1*$^{-/y}$ mice this developmental shift is disrupted. Two possible scenarios might account for the reduced AIS length at P14 in *Fmr1*$^{-/y}$ mice: either AIS length does not increase post-natally until P14 as has been reported in other cortical layers (Gutzmann et al., 2014), or the shortening of the AIS that typically occurs after P14 happens earlier in development in the mouse model of FXS. A more in depth analysis of AIS length during early post-natal development would be required to establish the onset of this phenotype. Moreover, the layer specificity of this phenotype might be a consequence of different critical periods across cortical layers, making L4 more susceptible to early post-natal life disruptions. Indeed, layer specific plasticity windows have previously been described in the mouse visual cortex (Maffei et al., 2004; Jiang et al., 2007; Goel and Lee, 2007).

L4 is the main input layer of the cortex. It receives visual information via thalamic inputs from the lateral geniculate nucleus (LGN), and projects to L2/3 (Gilbert, 1993). Thus abnormal AIS development in this layer can have wider implications in circuit function. Given the role of the AIS as site of AP initiation, altered AIS length is predicted to result in altered L4 cellular excitability, and consequently affect the way information is passed on to superficial layers of the cortex. Reduced AIS length in L4 at P14 is expected to correlate with reduced cellular excitability, therefore I would predict reduced output from L4 to L2/3. Whilst many other factors would influence strength of synaptic transmission across cortical layers, this is in line with evidence showing reduced response to visual input in superficial layers of the cortex in *Fmr1*$^{-/y}$ mice prior to eye opening (Berzhanskaya et al., 2016). Moreover, Berzhanskaya et al. (2016) have shown that hyperexcitability arises later in life, indicating that early circuit dysfunction has consequences that remain into adulthood. On the other hand, as suggested in the hippocampus of *Fmr1*$^{-/y}$ mice, the altered AIS length I observe in L4 in early development could result from a compensatory response to altered inputs in order to normalise neuronal output. Indeed, there is anatomical evidence suggesting abnormal LGN inputs to the visual cortex in FXS patients (Kogan et al., 2004b,a). Furthermore, thalamic inputs to L4 contribute to the orientation tuning in V1 (Sun et al., 2016), which is known to be altered in *Fmr1*$^{-/y}$ mice (Goel et al., 2018).

The data presented in this chapter shows abnormal AIS development in *Fmr1*$^{-/y}$ mice in a layer specific manner, indicating that the AIS might contribute to altered circuit function in V1. Examining L4 cellular excitability correlated with AIS length over development would be crucial to understand the impact of the altered AIS developmental trajectory here described. Furthermore, an in depth characterisation of thalamic inputs to V1 and connectivity between cortical layers in *Fmr1*$^{-/y}$ mice would be important to understand circuit dysfunction in the visual cortex and the mechanisms underlying visual processing deficits in FXS.

5.3.2 Absence of plasticity following visual deprivation - experimental considerations

In this chapter I was unable to replicate the findings of Gutzmann et al. (2014) regarding AIS plasticity following visual deprivation, as I observed no effect of dark rearing (2 or 4 weeks) on AIS length in any of the cortical layers tested in WT or

Fmr1$^{-/y}$ mice. One immediate consideration is that I failed to maintain adequate dark conditions. This is unlikely, given that I controlled for light exposure in my experiments by regularly checking the photographic film placed inside the dark cabinet for the duration of the experiments. Furthermore, the ages that the animals were tested at, as well as the duration of the visual deprivation followed the same conditions previously described to induce AIS plasticity (Schlüter et al., 2018; Gutzmann et al., 2014). Indeed, personal communication with lab responsible for these reports confirmed the similarity of experimental conditions. Therefore, other discrepancies in the experimental design must contribute to this outcome.

One major consideration is the strain of mouse used in the current study. Even though differences across inbred mouse lines present a concern when it comes to reproducibility of experimental findings, these are often overlooked. Sub-strains of C57/BL6 mice are known to differ in genetic (Watkins-Chow and Pavan, 2008; Mekada et al., 2009; Zurita et al., 2011), behavioural (Bryant et al., 2008) and metabolic profiles (Fontaine and Davis, 2016). The *Fmr1* mouse line I used is bred on the C57BL6J(JAX^{TM}) background while the mice used by Gutzmann et al. (2014) are C57/BL6J/Rj. Both of these lines originate from the C57/BL6J strain from Jackson Laboratories, however C57BL6J(JAX^{TM}) has been maintained by Charles River in the UK since 2004, while C57/BL6J/Rj has been maintained by Janvier Labs in France since 1993. Further differences might exist, as the C57/BL6J colony used to maintain the *Fmr1* mouse line used in this study has been maintained in house for a minimum of 10 years, during which genetic drift is possible. Whilst both of these sub-strains originate from the same C57/BL6J from Jackson Laboratories, Åhlgren and Voikar (2019) have recently shown that, even within the same strain of C57/BL6J mice, behavioural differences arise in sub-strains depending on the specific vendor. So it is possible that strain differences account for the lack of effect I observe. AIS plasticity might still be present, as I observe a similar developmental profile to that previously reported, however the critical period for visual deprivation to have an effect might be different in different mouse sub-strains.

Differences in housing conditions such as environmental enrichment (EE) and litter size contribute to the discrepancies between my data and what is reported in the literature. Standard laboratory housing can differ across institutions; the specific details such as cage size, number of animals in a cage or presence of some form of EE (e.g. tube, wood stick, nesting material) are subject to local guidelines and are not typically

reported in research publications, making it hard to perform a detailed comparison across experimental setups. EE is known to affect different forms of plasticity (Baroncelli et al., 2010), including ocular dominance plasticity in the visual cortex (Greifzu et al., 2014). Interestingly, there is also some evidence of EE affecting AIS plasticity and development in the mPFC (Nozari et al., 2016), the dentate gyrus (DG) (Bolos et al., 2019) and somatosensory cortex (Jamann et al., 2020). However, it is hard to estimate how EE would affect AIS plasticity in the visual cortex as it appears to have a brain region specific effect, as it results in shorter AISs in mPFC but longer in DG. It is clear that environmental conditions affect mouse behaviour and physiology, however a recent metanalysis has shown that EE results in changes in mean values of physiological parameters which do not necessarily put at risk the reproducibility of results (André et al., 2018). Taking this into account, I believe that whilst differences in standard housing conditions might be a possible confound when comparing my data to the literature, they are unlikely to solely explain the absence of plasticity I observe.

Another environmental factor that might contribute to my results is the use of transgenic animals in my experiments. As I only tested mice in cages with mixed genotype litters (i.e. both WT and *Fmr1*$^{-/y}$ mice), it is possible that plasticity in WT is being affected by the presence of transgenic littermates. In other transgenic mouse lines, co-housing with transgenic mice can have a significant effect on WT behaviour (Kalbassi et al., 2017). To my knowledge the effect of *Fmr1*$^{-/y}$ mice on WT behaviour has not been assessed. However, there is evidence of hyperactivity in *Fmr1*$^{-/y}$ mice (Pietropaolo et al., 2011; Kramvis et al., 2013), which in turn could result in enhanced motor activity in WT littermates. Behavioural states, and motor activity in particular, are known to modulate neuronal activity in the mouse visual cortex (Attinger et al., 2017; Pakan et al., 2016). In fact, locomotion alone can drive neuronal activity in V1 independently from visual input (Keller et al., 2012). As such, it is plausible that enhanced motor activity in mixed genotype cages would result in a less pronounced effect of visual deprivation on neuronal activity, not sufficient to induce AIS plasticity. Home cage monitoring in WT only and mixed genotype cages during visual deprivation experiments would be necessary to test this hypothesis. In the future it would be relevant to test WT-only cages in our experimental setup to address some of the confounds here highlighted. Furthermore, a comparison of AIS developmental trajectory and plasticity across different mouse strains or even in outbred rat strains

would be valuable, especially if this paradigm is to be used in studying circuit function in other models of neurodevelopmental disorders.

My data regarding the effect of visual deprivation on cellular excitability is still preliminary, not allowing for a definite conclusion about the effect of DR on *Fmr1*$^{-/y}$ mice, with only 2 DR mice tested. However, my WT data set does not show any evidence of homeostatic compensation of intrinsic excitability in DR mice. Whilst the environmental factors mentioned above can also contribute to the absence of plasticity when assessing intrinsic excitability following dark rearing, there are several differences easy to identify between my data and that published by Brown et al. (2019). Firstly, my recordings were performed in *ex vivo* brain tissue, while the data from Brown et al. (2019) is from *in vivo* recordings. Secondly, my recordings were performed following dark rearing from birth, whilst Brown et al. (2019) deprived mice from visual input for up to 5 weeks after eye opening. Interestingly, different paradigms used to reduce visual input can result in distinct homeostatic responses to maintain circuit function. For instance, lid suture results in enhanced cellular excitability of L2/3 PCs, while blocking visual input with TTX for the same amount of time leads to enhanced AMPAR/NMDAR ratio without affecting cellular excitability (Maffei and Turrigiano, 2008). Therefore a more thorough assessment of different aspects of circuit function would be necessary in order to identify which elements of neuronal function are homeostatically regulated in the visual deprivation paradigm I used, to then test whether the homeostatic response is altered in *Fmr1*$^{-/y}$ mice. Indeed, preliminary data from our lab shows that dark rearing for 4 weeks (P0-P28) or for 7 days (P21-P28) results in longer NMDAR-mediated EPSC decay times (Booker and Aaltonen, unpublished), in line with published data (Philpot et al., 2001; Yashiro et al., 2005). It is also possible the 4 week visual deprivation paradigm I used induces transient changes in cellular excitability that return to normal during that period, as previous studies have shown changes in cellular excitability and/or synaptic transmission within 2 days of visual deprivation (Maffei et al., 2004; Maffei and Turrigiano, 2008). With my current experimental design I would miss such changes, therefore testing cellar excitability at different timepoints of visual deprivation, might provide valuable insight on the timescale of such homeostatic responses. In summary, whilst I did not observe plasticity of the AIS or intrinsic excitability, I highlight a number of possible confounds that must be addressed in future studies examining homeostatic responses in the visual cortex of rodent models of ASD/ID.

Chapter 6

Concluding remarks

Individuals with monogenic forms of ASD/ID share common behavioural features and underlying neuronal dysfunction despite the diversity of their genetic causes. Synaptic dysfunction and altered cellular excitability in particular are presumed hallmarks of these disorders, leading to altered circuit function and ultimately to behavioural phenotypes (Zoghbi and Bear, 2012; Nelson and Valakh, 2015; Contractor et al., 2015). Importantly, in support of this view, pre-clinical studies that rescue aspects of cellular physiology and synaptic function also have a positive impact on behaviour (Asiminas et al., 2019; Okuda et al., 2017; Han et al., 2012; Michalon et al., 2012; Auerbach et al., 2011).

Although synaptic transmission and cellular excitability are linked to multiple forms of ASD/ID, the way these processes are altered may be inherently specific to different forms of ASD/ID. Therefore it is important to study a diversity of pre-clinical models of ASD/ID to build a better picture of convergent and divergent phenotypes across the different genetic causes of ASD/ID. Only by examining how synaptic and cellular phenotypes converge and diverge across models, brain areas, and developmental stages can we develop a picture of how these diverse genetic causes of ASD/ID produce apparently similar endophenotypes and develop targeted therapeutic approaches. As such, the work presented in this thesis provided insights into cellular excitability and synaptic physiology in two rodent models of monogenic ASD/ID, with particular focus on hippocampal function.

In Chapter 3. I presented a characterisation of synaptic physiology and intrinsic excitability in the hippocampus and mPFC of a novel rat model of CDD. The data in this chapter revealed enhanced synaptic plasticity and altered synaptic transmission in the

hippocampus of *Cdkl5*$^{-/y}$ rats. Whilst cellular excitability and synaptic transmission was unaltered in mPFC. In Chapter 4. I suggested the AIS as a key contributor to cellular hyperexcitability in the mouse model of FXS, representing a compensatory mechanism for reduced EC synaptic input. In Chapter 5. I reveal altered AIS developmental trajectory in the visual cortex of *Fmr1*$^{-/y}$ mice, potentially reflecting a compensatory mechanism as seen in the hippocampus.

6.1 Compensation in ASD/ID

Altered synaptic plasticity has been suggested as a cellular correlate for cognitive impairment in ASD/ID. This includes not only reduced synaptic plasticity (Asiminas et al., 2019; Komiyama et al., 2002; Won et al., 2012) but also enhanced plasticity of neural circuits (Pilpel et al., 2009; Till et al., 2015; Okuda et al., 2017). The work presented in this thesis shows that hippocampal LTP is enhanced in the rat model of CDD, in line with previous studies in mouse models (Okuda et al., 2017; Yennawar et al., 2019). Since threshold for LTP induction can be modulated by experience and prior activity states of the post-synaptic neurons (Kirkwood et al., 1996; Abraham et al., 2001), it is therefore plausible that enhanced LTP in ASD/ID arises as a compensatory mechanism for altered circuit activity. The direction of the alterations in synaptic plasticity are dependent not only on different genetic models of ASD/ID (Auerbach et al., 2011), but also on the specific brain regions and ages examined (Pilpel et al., 2009; Asiminas et al., 2019). Therefore compensatory changes through meta-plasticity mechanisms could explain why many of the synaptic plasticity phenotypes observed in ASD/ID are brain region and/or age dependent., as these could arise as compensation for altered connectivity (Haberl et al., 2015; Zerbi et al., 2018) or altered activity states during development (Gibson et al., 2008; Harlow et al., 2010).

Alternatively, enhanced plasticity could be a consequence of the neurodevelopmental nature of ASD/ID, thus reflecting a developmental delay that can leave circuits more vulnerable to subsequent insults. As such, the altered timing of critical periods of plasticity could present an opportunity for abnormal neuronal function to develop. Work in the somatosensory cortex, supports this idea and highlights the importance of examining cellular properties at a range of different ages when trying to understand circuit function. Harlow et al. (2010) show that the critical period for synapse development is

delayed in the barrel cortex of *Fmr1*$^{-/y}$ mice. In the hippocampus, Pilpel et al. (2009) report that enhanced LTP in a mouse model of FXS is restricted to early postnatal development. Additionally, the altered developmental trajectory of AIS I observe in the visual cortex (Chapter 5.) could be explained either by a shift in the critical period for AIS plasticity of by homeostatic compensation in response to altered thalamic inputs.

Whilst altered Hebbian plasticity has long been suggested as a cellular correlate for impaired cognition in ASD/ID, the role of homeostatic plasticity in ASD/ID is much less clear. Recent studies have raised the possibility of homeostatic mechanisms contributing to many of the cellular phenotypes observed in ASD/ID. Antoine et al. (2019) suggest enhanced E/I balance as homeostatic compensation to normalise spiking in the somatosensory cortex across four different models of genetic forms of ASD/ID, including FXS. Domanski et al. (2019) suggest that synaptic and cellular mechanisms can act in opposition to normalise circuit activity, at the expense of precision of neuronal responses to sensory input. The work presented in this thesis suggests hyperexcitability of CA1 pyramidal cells, as an additional phenotype resulting from homeostatic compensation (Chapter 4). I propose regulation of AIS morphology as an additional compensatory mechanism at play in ASD/ID. Indeed beyond the ASD/ID field, homeostatic response of neurons is critical in modulating their response to emergent activity patterns (O'Leary et al., 2010; Turrigiano et al., 1994; Golowasch et al., 1999).

It appears that neuronal circuits in ASD/ID are capable of compensation. Nonetheless, homeostatic mechanisms are not sufficient to fully restore behaviour. Studies by Soden and Chen (2010) suggest homeostatic scaling is impaired in the absence of FMRP. On the other hand compensatory changes in intrinsic excitability are enhanced in *Fmr1*$^{-/y}$ neurons (Bülow et al. (2019) and Chapter 4 of this thesis), whilst the ability of the AIS to respond to changes in activity appears unaltered and sufficient to compensate for reduced EC input. Therefore, whilst homeostatic mechanisms can restore some aspects of circuit function it is possible that imbalance of different forms of synaptic and intrinsic homeostatic plasticity during development may explain disturbed circuit function later in life. A better understanding of compensatory mechanisms at play in ASD/ID, and in particular how synaptic and cellular excitability phenotypes interact to shape circuit function, might provide further insight into how manipulating aspects of neuronal activity through therapeutic intervention influences behavioural output.

Compensatory mechanisms are relevant to the human condition and are believed to contribute to the progression of neurodevelopmental disorders and amelioration or worsening of symptoms with age (Livingston and Happé, 2017). Neuroimaging studies have shown that autistic individuals that perform well in Theory of Mind tasks still exhibit enhanced activation of brain networks involved in the task, thus expending greater effort to achieve the same outcome as typically developing individuals (White et al., 2014). This indicates that altered function of brain networks in ASD/ID might reflect a compensatory mechanism that allows for typical behavioural outcomes, nonetheless this compensation results in less efficient network function that limits the ability to perform more complex cognitive tasks. Thus, it is plausible that the variability in severity of symptoms between individuals with the same genetic cause of ASD/ID reflects differences in compensatory changes throughout development (Bourgeron, 2015).

6.2 Future directions

The work presented in this thesis provided a snapshot of synaptic function and cellular excitability in rodent models of CDD and FXS, however the developmental nature of these disorders makes it difficult to disentangle core deficits from a sequence of compensatory changes occurring during development that contribute to the adult phenotype. Therefore it is essential to perform a thorough characterisation of the developmental profile of these phenotypes in order to understand whether these arise from core deficits or as transitory states resulting from compensatory mechanisms. This would also be useful when comparing results to the published literature, as some of the cellular phenotypes can be transient it is hard to judge if divergent reports from different labs arise due to different models and experimental conditions or if they reflect age-dependent alterations instead.

The complex contribution of compensatory responses to ASD/ID phenotypes also hinders a full interpretation of the potential impact that isolated cellular phenotypes might have on circuit function. Therefore, future studies should turn to *in vivo* recording approaches to build a more complete picture of how the cellular phenotypes highlighted in this thesis contribute to circuit function and *vice versa* how circuit function during development result in compensatory changes at the cellular level.

Appendix A

A.1 Behaviour phenotypes in *Cdkl5*$^{-/y}$ rats

The behaviour data in this section was collected by Vijay Kumar, Shashank Tiwari under the supervision of Prof Shona Chattarji, Prof Peter Kind, Dr Emma Wood and Dr Oliver Hardt, as part of a collaboration between Edinburgh University and the National Centre for Biological Sciences (NCBS) in Bangalore.

Cdkl5$^{-/y}$ rats exhibited typical fear-learning (Figure A.1B) and increased freezing during recall (Figure A.1C, D).

Cdkl5$^{-/y}$ rats impaired learning when tested in the active place avoidance task, as seen by the higher number of entries in the shock zone during training sessions 1 and 2, and increased number of entries when the shock zone position is altered during the conflict session (Figure A.2C).

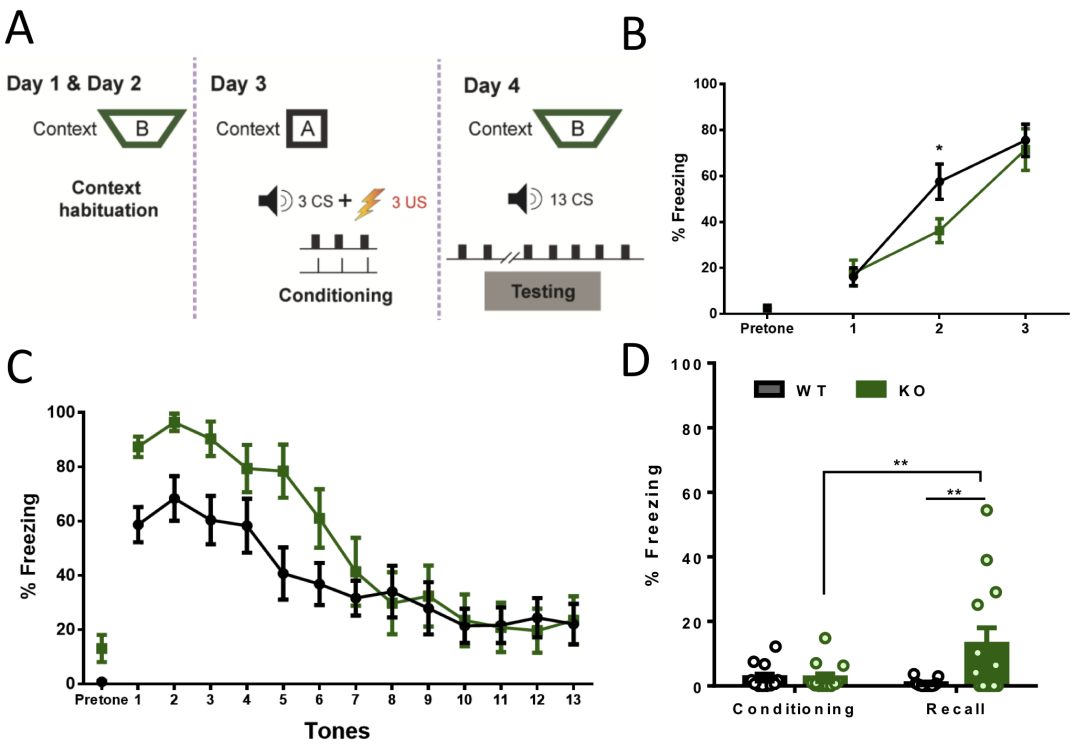

Figure A.1: Auditory fear conditioning in *Cdkl5*$^{-/y}$ rats.% of time spent freezing in response to subsequent tone presentations during conditioning (day 3, B) and recall (day 4, C). D - Average % freezing prior to tone presentation (pre-tone) during the conditioning (Day 3) and Recall (Day 4) sessions. (WT: n=11 rats, *Cdkl5*$^{-/y}$: n=12 rats, **p<0.01, 2-way ANOVA, Holm Sidak post-hoc)

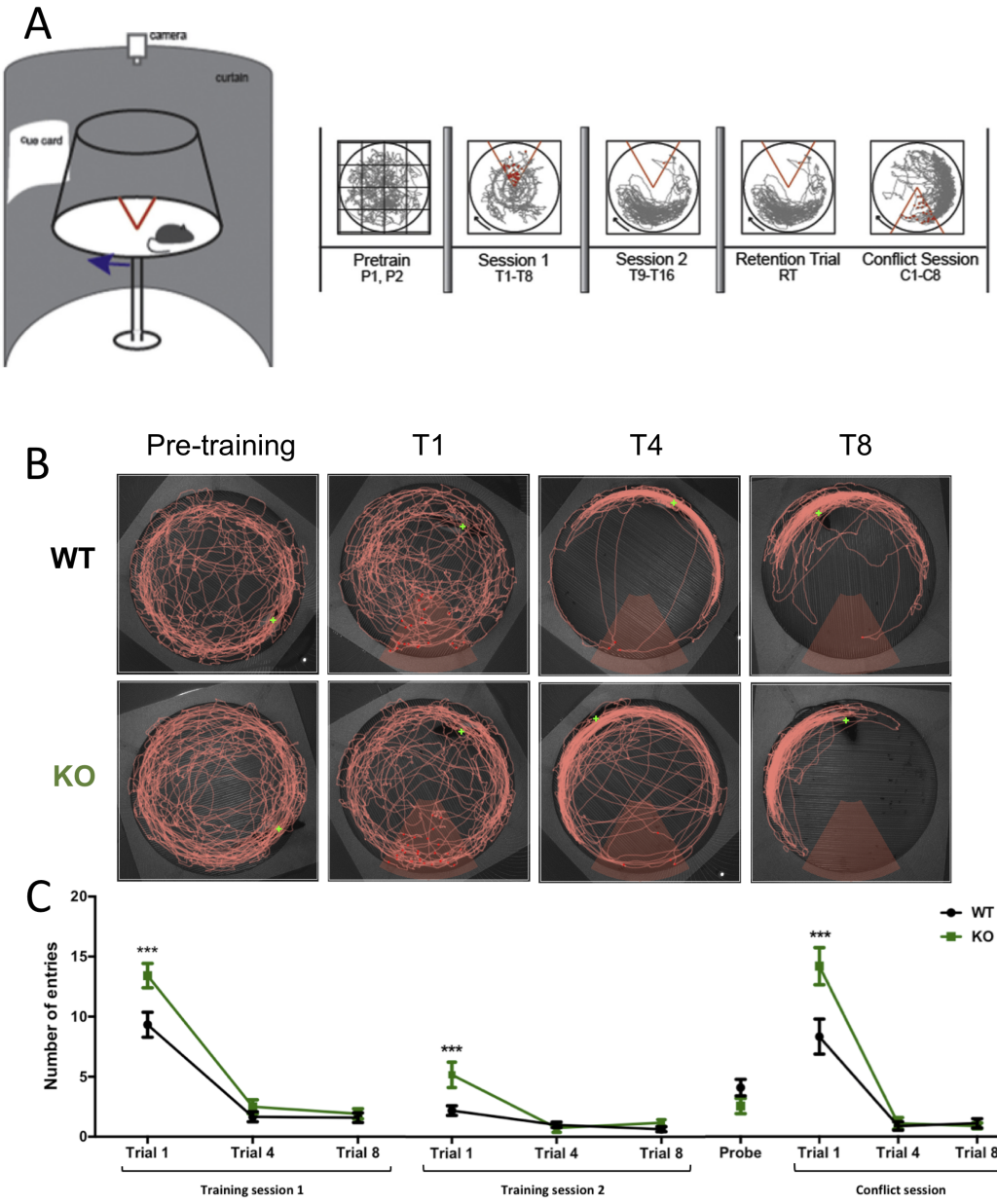

Figure A.2: Active place avoidance task in WT and *Cdkl5*$^{-/y}$ rats. A - Schematic representation of testing arena (left) and experimental paradigm (right). B - Example trajectories (red lines) of WT (top) and *Cdkl5*$^{-/y}$ rats (bottom) over trials in the first training session. Red zone represented by red shading. C - Number of entries in the shock zone over training sessions (WT: n=10 rats, *Cdkl5*$^{-/y}$: n=11 rats, ***p<0.001 2-way ANOVA, Holm Sidak post-hoc test)

Appendix B

B.1 Statistical analysis of CA1 mEPSC data

This appendix provides a detailed description of the statistical analysis used to assess the effect of genotype on mEPCS frequency in CA1 and relates to the data presented in Figure 3.8. A similar approach was used for the remaining datasets where GLMM/LMM was used to carry our statistical analysis.

1. Testing the distribution that best fits CA1 mEPSC frequency data:

"Fitdist" function in R was used to check which distribution best fitted the data. Normal, log-normal and gamma distribution were tested. Goodness of fit statistics (lower values indicating better fit) and Q-Q plots (overlapping of experimental data points with straight line indicating better fit) were examined to determine what distribution was more appropriate.

```
Goodness-of-fit statistics
                           1-mle-norm 2-mle-lnorm 3-mle-gamma
Kolmogorov-Smirnov statistic 0.10562065  0.07191821  0.05661703
Cramer-von Mises statistic   0.08204239  0.02988433  0.01847263
Anderson-Darling statistic   0.57947274  0.18763505  0.13968521
```

Values for goodness of fit statistics and Q-Q plots are very similar for log-normal distribution and gamma distribution, so tested both cases.

2. GLMM based on gamma distribution using genotype as fixed effect and Animal as random effect (p=0.06):

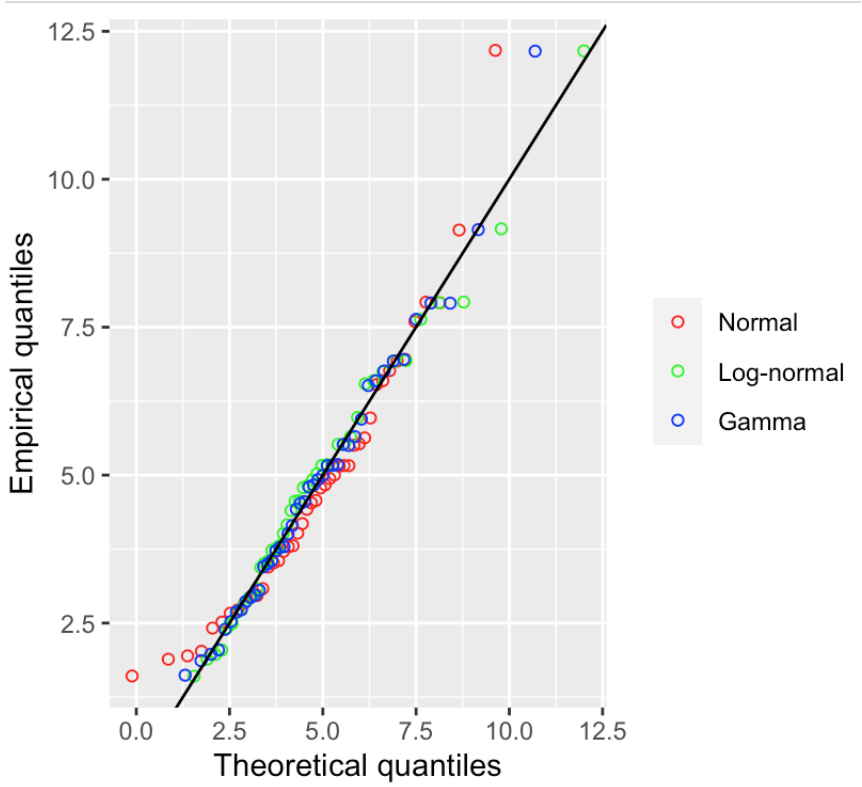

Figure B.1: Q-Q plot of CA1 mEPSC frequency data showing empirical quantiles in the y axis relative to theoretical quantiles for normal (red), log-normal(green) and gamma (blue) -distributed data.

```
Generalized linear mixed model fit by maximum likelihood (Laplace
Approximation) ['glmerMod']
 Family: Gamma  ( log )
Formula: mEPSC.frequency ~ Genotype + (1 | Animal)
   Data: data
Control: glmerControl(optimizer = "bobyqa")

     AIC      BIC   logLik deviance df.resid
   187.2    194.3    -89.6    179.2       40

Scaled residuals:
     Min       1Q   Median       3Q      Max
-1.47068 -0.69650 -0.02476  0.42234  2.72610

Random effects:
 Groups   Name        Variance Std.Dev.
 Animal   (Intercept) 0.02154  0.1468
 Residual             0.16446  0.4055
Number of obs: 44, groups:  Animal, 17

Fixed effects:
            Estimate Std. Error t value Pr(>|z|)
(Intercept)   1.6579     0.1061  15.626   <2e-16 ***
Genotype-/y  -0.3002     0.1575  -1.905   0.0568 .
---
Signif. codes:  0 ‘***’ 0.001 ‘**’ 0.01 ‘*’ 0.05 ‘.’ 0.1 ‘ ’ 1
```

3. LMM based on log-normal distribution using genotype as fixed effect and Animal as random effect:

```
Linear mixed model fit by REML ['lmerMod']
Formula: log(mEPSC.frequency) ~ Genotype + (1 | Animal)
   Data: data
Control: lmerControl(optimizer = "bobyqa")

REML criterion at convergence: 54.9

Scaled residuals:
     Min       1Q   Median       3Q      Max
-1.90295 -0.68429  0.05728  0.65576  2.07912

Random effects:
 Groups   Name        Variance Std.Dev.
 Animal   (Intercept) 0.000    0.0000
 Residual             0.187    0.4324
Number of obs: 44, groups:  Animal, 17

Fixed effects:
            Estimate Std. Error t value
(Intercept)  1.60109    0.08826  18.141
Genotype-/y -0.30828    0.13091  -2.355

Correlation of Fixed Effects:
            (Intr)
Genotype-/y -0.674
convergence code: 0
boundary (singular) fit: see ?isSingular
```

The fit is singular: when using the log-normal distribution the variances assigned at animal level is zero or practically zero. I tried a simple linear model (without any random effects).

4. Linear model using log-normal distribution with no random effects (p=0.02):

```
lm(formula = log(mEPSC.frequency) ~ Genotype, data = data)

Residuals:
     Min       1Q   Median       3Q      Max
-0.82281 -0.29588  0.02477  0.28354  0.89898

Coefficients:
            Estimate Std. Error t value Pr(>|t|)
(Intercept)  1.60109    0.08826  18.141   <2e-16 ***
Genotype-/y -0.30828    0.13091  -2.355   0.0233 *
---
Signif. codes:  0 ‘***’ 0.001 ‘**’ 0.01 ‘*’ 0.05 ‘.’ 0.1 ‘ ’ 1

Residual standard error: 0.4324 on 42 degrees of freedom
Multiple R-squared:  0.1166,      Adjusted R-squared:  0.0956
F-statistic: 5.546 on 1 and 42 DF,  p-value: 0.02328
```

5. Given that the GLMM analysis described above resulted in a non-significant difference between genotypes when using the gamma distribution (p=0.06) but significant when using the log-normal distribution (p=0.02). I used a Two tailed T test using animal averages as replicates to test the difference between genotypes (average data was normally distributed). Test output for genotype comparison: T_{15}=2.695, p=0.0166

Bibliography

Abidi A, Devaux JJ, Molinari F, Alcaraz G, Michon FX, Sutera-Sardo J, Becq H, Lacoste C, Altuzarra C, Afenjar A, Mignot C, Doummar D, Isidor B, Guyen SN, Colin E, De La Vaissière S, Haye D, Trauffler A, Badens C, Prieur F, Lesca G, Villard L, Milh M, Aniksztejn L (2015) A recurrent KCNQ2 pore mutation causing early onset epileptic encephalopathy has a moderate effect on M current but alters subcellular localization of Kv7 channels. *Neurobiology of Disease* 80:80–92.

Abraham WC, Bear MF (1996) Metaplasticity : plasticity of synaptic plasticity. *Trends in neurosciences* 19:126–130.

Abraham WC, Mason-Parker SE, Bear MF, Webb S, Tate WP (2001) Heterosynaptic metaplasticity in the hippocampus in vivo: A BCM-like modifiable threshold for LTP. *Proceedings of the National Academy of Sciences of the United States of America* 98:10924–10929.

Adhikari A, Topiwala MA, Gordon JA (2010) Synchronized Activity between the Ventral Hippocampus and the Medial Prefrontal Cortex during Anxiety. *Neuron* 65:257–269.

Aerde KIV, Feldmeyer D (2015) Morphological and Physiological Characterization of Pyramidal Neuron Subtypes in Rat Medial Prefrontal Cortex. *Cerebral Cortex* pp. 788–805.

Åhlgren J, Voikar V (2019) Experiments done in Black-6 mice: what does it mean? *Lab Animal* 48:171–180.

Amaral D, Witter M (1989) The three-dimensional organization of the hippocampal formation: A review of anatomical data. *Neuroscience* 31:571–591.

Amendola E, Zhan Y, Mattucci C, Castroflorio E, Calcagno E, Fuchs C, Lonetti G, Silingardi D, Vyssotski AL, Farley D, Ciani E, Pizzorusso T, Giustetto M, Gross CT (2014) Mapping pathological phenotypes in a mouse model of CDKL5 disorder. *PLoS ONE* 9:5–16.

Andersen P, Raastad M, Storm JF (1990) Excitatory synaptic integration in hippocampal pyramids and dentate granule cells. *Cold Spring Harbor Symposia on Quantitative Biology* 55:81–86.

Andersen P, Sundberg SH, Sveen O, Swann JW, Wigström H (1980) Possible mechanisms for long-lasting potentiation of synaptic transmission in hippocampal slices from guinea-pigs. *The Journal of Physiology* 302:463–482.

André V, Gau C, Scheideler A, Aguilar-Pimentel JA, Amarie OV, Becker L, Garrett L, Hans W, Hölter SM, Janik D, Moreth K, Neff F, Östereicher M, Racz I, Rathkolb B, Rozman J, Bekeredjian R, Graw J, Klingenspor M, Klopstock T, Ollert M, Schmidt-

Weber C, Wolf E, Wurst W, Gailus-Durner V, Brielmeier M, Fuchs H, Hrabé de Angelis M (2018) Laboratory mouse housing conditions can be improved using common environmental enrichment without compromising data. *PLoS Biology* 16:1–24.

Antoine MW, Langberg T, Schnepel P, Feldman DE (2019) Increased Excitation-Inhibition Ratio Stabilizes Synapse and Circuit Excitability in Four Autism Mouse Models. *Neuron* 101:648–661.e4.

Appleby VJ, Corrêa SAL, Duckworth JK, Nash JE, Noël J, Fitzjohn SM, Collingridge GL, Molnár E (2011) LTP in hippocampal neurons is associated with a CaMKII-mediated increase in GluA1 surface expression. *Journal of Neurochemistry* 116:530–543.

Arbab T, Pennartz CM, Battaglia FP (2018) Impaired hippocampal representation of place in the Fmr1-knockout mouse model of fragile X syndrome. *Scientific Reports* 8:1–9.

Arrigoni E, Greene RW (2004) Schaffer collateral and perforant path inputs activate different subtypes of NMDA receptors on the same CA1 pyramidal cell. *British Journal of Pharmacology* 142:317–322.

Asiminas A, Jackson AD, Louros SR, Till SM, Spano T, Dando O, Bear MF, Chattarji S, Hardingham GE, Osterweil EK, Wyllie DJA, Wood ER, Kind PC (2019) Sustained correction of associative learning deficits after brief, early treatment in a rat model of Fragile X Syndrome. *Science Translational Medicine* 11:eaao0498.

Attinger A, Wang B, Keller GB (2017) Visuomotor Coupling Shapes the Functional Development of Mouse Visual Cortex. *Cell* 169:1291–1302.e14.

Auerbach BD, Osterweil EK, Bear MF (2011) Mutations causing syndromic autism define an axis of synaptic pathophysiology. *Nature* 480:63–68.

Backus AR, Schoffelen JM, Szebényi S, Hanslmayr S, Doeller CF (2016) Hippocampal-Prefrontal Theta Oscillations Support Memory Integration. *Current Biology* 26:450–457.

Bahi-Buisson N, Bienvenu T (2012) CDKL5-related disorders: From clinical description to molecular genetics. *Molecular Syndromology* 2:137–152.

Bailey A, Phillips W, Rutter M (1996) Autism: Towards an Integration of Clinical, Genetic, Neuropsychological, and Neurobiological Perspectives. *Journal of Child Psychology and Psychiatry* 37:89–126.

Baltussen LL, Negraes PD, Silvestre M, Claxton S, Moeskops M, Christodoulou E, Flynn HR, Snijders AP, Muotri AR, Ultanir SK (2018) Chemical genetic identification of CDKL 5 substrates reveals its role in neuronal microtubule dynamics . *The EMBO Journal* 37:1–18.

Bannister AP (2005) Inter- and intra-laminar connections of pyramidal cells in the neocortex. *Neuroscience Research* 53:95–103.

Bannister NJ, Larkman AU (1995) Dendritic morphology of CA1 pyramidal neurones from the rat hippocampus: II. Spine distributions. *Journal of Comparative Neurology* 360:150–160.

Barnes SA, Wijetunge LS, Jackson AD, Katsanevaki D, Osterweil EK, Komiyama NH, Grant SGN, Bear MF, Näger UV, Kind PC, Wyllie DJA (2015) Convergence of hippocampal pathophysiology in syngap+/- and fmr1-/y mice. *Journal of Neuroscience* 35:15073–15081.

Baroncelli L, Braschi C, Spolidoro M, Begenisic T, Sale A, Maffei L (2010) Nurturing brain plasticity: Impact of environmental enrichment. *Cell Death and Differentiation* 17:1092–1103.

Bates D, Mächler M, Bolker B, Walker S (2014) Fitting Linear Mixed-Effects Models using lme4 .

Baxter PS, Bell KFS, Hasel P, Kaindl AM, Fricker M, Thomson D, Cregan SP, Gillingwater TH, Hardingham GE (2015) Synaptic NMDA receptor activity is coupled to the transcriptional control of the glutathione system. *Nature Communications* 6:6761.

Bear MF, Huber KM, Warren ST (2004) The mGluR theory of fragile X mental retardation. *Trends in Neurosciences* 27:370–377.

Bell MV, Hirst MC, Nakahori Y, MacKinnon RN, Roche A, Flint TJ, Jacobs PA, Tommerup N, Tranebjaerg L, Froster-Iskenius U, Kerr B, Turner G, Lindenbaum RH, Winter R, Prembrey M, Thibodeau S, Davies KE (1991) Physical mapping across the fragile X: Hypermethylation and clinical expression of the fragile X syndrome. *Cell* 64:861–866.

Ben-Shalom R, Keeshen CM, Berrios KN, An JY, Sanders SJ, Bender KJ (2017) Opposing Effects on NaV1.2 Function Underlie Differences Between SCN2A Variants Observed in Individuals With Autism Spectrum Disorder or Infantile Seizures. *Biological Psychiatry* 82:224–232.

Bender KJ, Trussell LO (2009) Axon Initial Segment Ca2+ Channels Influence Action Potential Generation and Timing. *Neuron* 61:259–271.

Berry-Kravis E (2002) Epilepsy in fragile X syndrome. *Developmental Medicine & Child Neurology* 44:724–728.

Berzhanskaya J, Phillips MA, Shen J, Colonnese MT (2016) Sensory hypo-excitability in a rat model of fetal development in Fragile X Syndrome. *Scientific Reports* 6:1–12.

Betancur C (2011) Etiological heterogeneity in autism spectrum disorders: More than 100 genetic and genomic disorders and still counting. *Brain Research* 1380:42–77.

Biane JS, Scanziani M, Tuszynski MH, Conner JM (2015) Motor Cortex Maturation Is Associated with Reductions in Recurrent Connectivity among Functional Subpopulations and Increases in Intrinsic Excitability. *The Journal of Neuroscience* 35:4719 – 4728.

Bienenstock EL, Cooper LN, Munro PW (1982) Theory for the development of neuron selectivity: orientation specificity and binocular interaction in visual cortex. *The Journal of Neuroscience* 2:32 – 48.

Binder S, Mölle M, Lippert M, Bruder R, Aksamaz S, Ohl F, Wiegert JS, Marshall L (2019) Monosynaptic Hippocampal-Prefrontal Projections Contribute to Spatial Memory Consolidation in Mice. *The Journal of Neuroscience* 39:6978 – 6991.

Blackstad TW (1956) Commissural connections of the hippocampal region in the rat, with special reference to their mode of termination. *Journal of Comparative Neurology* 105:417–537.

Bliss TVP, Lømo T (1973) Long-lasting potentiation of synaptic transmission in the dentate area of the anaesthetized rabbit following stimulation of the perforant path. *The Journal of Physiology* 232:331–356.

Bliss TVP, Collingridge GL (2013) Expression of NMDA receptor-dependent LTP in the hippocampus: bridging the divide. *Molecular Brain* 6:5.

Blumenfeld H, Lampert A, Klein JP, Mission J, Chen MC, Rivera M, Dib-Hajj S, Brennan AR, Hains BC, Waxman SG (2009) Role of hippocampal sodium channel Nav1.6 in kindling epileptogenesis. *Epilepsia* 50:44–55.

Bolos M, Terreros-Roncal J, Perea JR, Pallas-Bazarra N, Avila J, Llorens-Martin M (2019) Maturation Dynamics of the Axon Initial Segment (AIS) of Newborn Dentate Granule Cells in Young Adult C57BL / 6J. *The Journal of Neuroscience* 39:1605–1620.

Booker SA, Domanski AP, Dando OR, Jackson AD, Isaac JT, Hardingham GE, Wyllie DJ, Kind PC (2019) Altered dendritic spine function and integration in a mouse model of fragile X syndrome. *Nature Communications* 10.

Booker SA, Vida I (2018) Morphological diversity and connectivity of hippocampal interneurons. *Cell and Tissue Research* 373:619–641.

Bourgeron T (2015) From the genetic architecture to synaptic plasticity in autism spectrum disorder. *Nature Reviews Neuroscience* 16:551–563.

Brager D, Akhavan A, Johnston D (2012) Impaired Dendritic Expression and Plasticity of h-Channels in the fmr1/y Mouse Model of Fragile X Syndrome. *Cell Reports* 1:225–233.

Branco T, Häusser M (2011) Synaptic Integration Gradients in Single Cortical Pyramidal Cell Dendrites. *Neuron* 69:885–892.

Brennan FX, Albeck DS, Paylor R (2006) Fmr1 knockout mice are impaired in a leverpress escape/avoidance task. *Genes, Brain and Behavior* 5:467–471.

Breton JD, Stuart GJ (2009) Loss of sensory input increases the intrinsic excitability of layer 5 pyramidal neurons in rat barrel cortex. *The Journal of Physiology* 587:5107–5119.

Brock LG, Coombs JS, Eccles JC (1953) Intracellular recording from antidromically activated motoneurones. *The Journal of Physiology* 122:429–461.

Brown APY, Cossell L, Margrie TW, Brown APY, Cossell L, Margrie TW (2019) Visual Experience Regulates the Intrinsic Excitability of Visual Cortical Neurons to Maintain Sensory Report Visual Experience Regulates the Intrinsic Excitability of Visual Cortical Neurons to Maintain Sensory Function. *CellReports* 27:685–689.e4.

Brown MR, Kronengold J, Gazula VR, Chen Y, Strumbos JG, Sigworth FJ, Navaratnam D, Kaczmarek LK (2010) Fragile X mental retardation protein controls gating of the sodium-activated potassium channel Slack. *Nature Neuroscience* 13:819–821.

Brown SP, Hestrin S (2009) Intracortical circuits of pyramidal neurons reflect their long-range axonal targets. *Nature* 457:1133–1136.

Brown V, Jin P, Ceman S, Darnell JC, O'Donnell WT, Tenenbaum SA, Jin X, Feng Y, Wilkinson KD, Keene JD, Darnell RB, Warren ST (2001) Microarray Identification of FMRP-Associated Brain mRNAs and Altered mRNA Translational Profiles in Fragile X Syndrome. *Cell* 107:477–487.

Brun VH, Leutgeb S, Wu HQ, Schwarcz R, Witter MP, Moser EI, Moser MB (2008) Impaired Spatial Representation in CA1 after Lesion of Direct Input from Entorhinal Cortex. *Neuron* 57:290–302.

Bryant CD, Zhang NN, Sokoloff G, Fanselow MS, Ennes HS, Palmer AA, McRoberts JA (2008) Behavioral differences among C57BL/6 substrains: Implications for transgenic and knockout studies. *Journal of Neurogenetics* 22:315–331.

Buffington SA, Rasband MN (2011) The axon initial segment in nervous system disease and injury. *European Journal of Neuroscience* 34:1609–1619.

Bülow P, Murphy T, Bassell GJ, Wenner P (2019) Homeostatic Intrinsic Plasticity Is Functionally Altered in Fmr1 KO Cortical Neurons. *Cell Reports* 26:1378–1388.e3.

Bureau I, Shepherd GMG, Svoboda K (2008) Circuit and Plasticity Defects in the Developing Somatosensory Cortex of Fmr1 Knock-Out Mice. *The Journal of Neuroscience* 28:5178 – 5188.

Burgess N, Maguire EA, O'Keefe J (2002) The Human Hippocampus and Spatial and Episodic Memory. *Neuron* 35:625–641.

Burke KJ, Keeshen CM, Bender KJ (2018) Two Forms of Synaptic Depression Produced by Differential Neuromodulation of Presynaptic Calcium Channels. *Neuron* 99:969–984.e7.

Burrone J, Murthy VN (2003) Synaptic gain control and homeostasis. *Current Opinion in Neurobiology* 13:560–567.

Cammalleri M, Lütjens R, Berton F, King AR, Simpson C, Francesconi W, Sanna PP (2003) Time-restricted role for dendritic activation of the mTOR-p70 S6K pathway in the induction of late-phase long-term potentiation in the CA1. *Proceedings of the National Academy of Sciences* 100:14368 – 14373.

Caporale N, Dan Y (2008) Spike Timing–Dependent Plasticity: A Hebbian Learning Rule. *Annual Review of Neuroscience* 31:25–46.

Caroni P (1997) Overexpression of growth-associated proteins in the neurons of adult transgenic mice. *Journal of Neuroscience Methods* 71:3–9.

Catterall WA, Kalume F, Oakley JC (2010) NaV1.1 channels and epilepsy. *The Journal of Physiology* 588:1849–1859.

Cendes F, Andermann F, Gloor P, Evans A, Jones-Gotman M, Watson C, Melanson D, Olivier A, Peters T, Lopes-Cendes I, Leroux G (1993) MRI volumetric measurement of amygdala and hippocampus in temporal lobe epilepsy. *Neurology* 43:719 –725.

Cervantes PE, Matson JL (2015) Comorbid Symptomology in Adults with Autism

Spectrum Disorder and Intellectual Disability. *Journal of Autism and Developmental Disorders* 45:3961–3970.

Chen L, Toth M (2001) Fragile X mice develop sensory hyperreactivity to auditory stimuli. *Neuroscience* 103:1043–1050.

Cimadevilla JM, Fenton AA, Bures J (2000) Functional inactivation of dorsal hippocampus impairs active place avoidance in rats. *Neuroscience Letters* 285:53–56.

Clement J, Aceti M, Creson T, Ozkan E, Shi Y, Reish N, Almonte A, Miller B, Wiltgen B, Miller C, Xu X, Rumbaugh G (2012) Pathogenic SYNGAP1 Mutations Impair Cognitive Development by Disrupting Maturation of Dendritic Spine Synapses. *Cell* 151:709–723.

Clements JD, Bekkers JM (1997) Detection of spontaneous synaptic events with an optimally scaled template. *Biophysical journal* 73:220–9.

Coffee B, Keith K, Albizua I, Malone T, Mowrey J, Sherman SL, Warren ST (2009) Incidence of Fragile X Syndrome by Newborn Screening for Methylated FMR1 DNA. *The American Journal of Human Genetics* 85:503–514.

Collingridge GL, Isaac JT, Yu TW (2004) Receptor trafficking and synaptic plasticity. *Nature Reviews Neuroscience* 5:952–962.

Connors BW, Gutnick MJ (1990) Intrinsic firing patterns of diverse neocortical neurons. *Trends in Neurosciences* 13:99–104.

Contractor A, Klyachko V, Portera-Cailliau C (2015) Altered Neuronal and Circuit Excitability in Fragile X Syndrome. *Neuron* 87:699–715.

Cook MJ, Fish DR, Shorvon SD, Straughan K, Stevens JM (1992) Hippocampal volumetric and morphometric studies in frontal and temporal lobe epilepsy. *Brain* 115:1001–1015.

Cordeiro L, Ballinger E, Hagerman R, Hessl D (2011) Clinical assessment of DSM-IV anxiety disorders in fragile X syndrome: prevalence and characterization. *Journal of Neurodevelopmental Disorders* 3:57–67.

Cornish KM, Munir F, Cross G (1999) Spatial Cognition in Males With Fragile-X Syndrome: Evidence for a Neuropsychological Phenotype. *Cortex* 35:263–271.

Crair MC, Malenka RC (1995) A critical period for long-term potentiation at thalamocortical synapses. *Nature* 375:325–328.

Crandall SR, Patrick SL, Cruikshank SJ, Connors BW (2017) Infrabarrels Are Layer 6 Circuit Modules in the Barrel Cortex that Link Long-Range Inputs and Outputs. *Cell Reports* 21:3065–3078.

Crawford DC, Acuña JM, Sherman SL (2001) FMR1 and the fragile X syndrome: Human genome epidemiology review. *Genetics in Medicine* 3:359–371.

Crocker-Buque A, Brown SM, Kind PC, Isaac JTR, Daw MI (2014) Experience-Dependent, Layer-Specific Development of Divergent Thalamocortical Connectivity. *Cerebral Cortex* 25:2255–2266.

Curia G, Papouin T, Séguéla P, Avoli M (2009) Downregulation of tonic GABAergic inhibition in a mouse model of fragile X syndrome. *Cerebral Cortex* 19:1515–1520.

da Costa NM, Martin KAC (2011) How Thalamus Connects to Spiny Stellate Cells in the Cat's Visual Cortex. *The Journal of Neuroscience* 31:2925 – 2937.

Dager SR, Wang L, Friedman SD, Shaw DW, Constantino JN, Artru AA, Dawson G, Csernansky JG (2007) Shape mapping of the hippocampus in young children with autism spectrum disorder. *American Journal of Neuroradiology* 28:672–677.

Dam AM (1980) Epilepsy and Neuron Loss in the Hippocampus. *Epilepsia* 21:617–629.

Darnell J, Van Driesche S, Zhang C, Hung K, Mele A, Fraser C, Stone E, Chen C, Fak J, Chi S, Licatalosi D, Richter J, Darnell R (2011) FMRP Stalls Ribosomal Translocation on mRNAs Linked to Synaptic Function and Autism. *Cell* 146:247–261.

Debanne D, Guérineau NC, Gähwiler BH, Thompson SM (1996) Paired-pulse facilitation and depression at unitary synapses in rat hippocampus: quantal fluctuation affects subsequent release. *The Journal of Physiology* 491:163–176.

Debanne D, Inglebert Y, Russier M (2019) Plasticity of intrinsic neuronal excitability. *Current Opinion in Neurobiology* 54:73–82.

Della Sala G, Putignano E, Chelini G, Melani R, Calcagno E, Michele Ratto G, Amendola E, Gross CT, Giustetto M, Pizzorusso T (2016) Dendritic Spine Instability in a Mouse Model of CDKL5 Disorder Is Rescued by Insulin-like Growth Factor 1. *Biological Psychiatry* 80:302–311.

Dembrow NC, Chitwood RA, Johnston D (2010) Projection-Specific Neuromodulation of Medial Prefrontal Cortex Neurons. *Journal of Neuroscience* 30:16922–16937.

Deng PY, Klyachko VA (2016) Increased Persistent Sodium Current Causes Neuronal Hyperexcitability in the Entorhinal Cortex of Fmr1 Knockout Mice. *Cell Reports* 16:3157–3166.

Deng PY, Rotman Z, Blundon J, Cho Y, Cui J, Cavalli V, Zakharenko S, Klyachko V (2013) FMRP Regulates Neurotransmitter Release and Synaptic Information Transmission by Modulating Action Potential Duration via BK Channels. *Neuron* 77:696–711.

Desai NS, Cudmore RH, Nelson SB, Turrigiano GG (2002) Critical periods for experience- dependent synaptic scaling in visual cortex. *Nature Neuroscience* 23:783–790.

Devaux J, Abidi A, Roubertie A, Molinari F, Becq H, Lacoste C, Villard L, Milh M, Anikstejn L (2016) A Kv7.2 mutation associated with early onset epileptic encephalopathy with suppression-burst enhances Kv7/M channel activity. *Epilepsia* 57:e87–e93.

D'Hooge R, Nagels G, Franck F, Bakker CE, Reyniers E, Storm K, Kooy RF, Oostra BA, Willems PJ, De Deyn PP (1997) Mildly impaired water maze performance in maleFmr1 knockout mice. *Neuroscience* 76:367–376.

Di Martino A, Yan CG, Li Q, Denio E, Castellanos FX, Alaerts K, Anderson JS, Assaf M, Bookheimer SY, Dapretto M, Deen B, Delmonte S, Dinstein I, Ertl-Wagner B, Fair DA, Gallagher L, Kennedy DP, Keown CL, Keysers C, Lainhart JE, Lord C,

Luna B, Menon V, Minshew NJ, Monk CS, Mueller S, Müller RA, Nebel MB, Nigg JT, O'Hearn K, Pelphrey KA, Peltier SJ, Rudie JD, Sunaert S, Thioux M, Tyszka JM, Uddin LQ, Verhoeven JS, Wenderoth N, Wiggins JL, Mostofsky SH, Milham MP (2014) The autism brain imaging data exchange: Towards a large-scale evaluation of the intrinsic brain architecture in autism. *Molecular Psychiatry* 19:659–667.

Dobrunz LE, Huang EP, Stevens CF (1997) Very short-term plasticity in hippocampal synapses. *Proceedings of the National Academy of Sciences of the United States of America* 94:14843–7.

Dobrunz LE, Stevens CF (1997) Heterogeneity of Release Probability, Facilitation, and Depletion at Central Synapses. *Neuron* 18:995–1008.

Dölen G, Osterweil E, Rao BS, Smith GB, Auerbach BD, Chattarji S, Bear MF (2007) Correction of Fragile X Syndrome in Mice. *Neuron* 56:955–962.

Doll CA, Vita DJ, Broadie K (2017) Fragile X Mental Retardation Protein Requirements in Activity-Dependent Critical Period Neural Circuit Refinement. *Current Biology* 27:2318–2330.e3.

Domanski APF, Booker SA, Wyllie DJA, Isaac JTR, Kind PC (2019) Cellular and synaptic phenotypes lead to disrupted information processing in Fmr1-KO mouse layer 4 barrel cortex. *Nature Communications* 10:4814.

Doyle-Thomas KAR, Lee W, Foster NEV, Tryfon A, Ouimet T, Hyde KL, Evans AC, Lewis J, Zwaigenbaum L, Anagnostou E, Group ftNASDI (2015) Atypical functional brain connectivity during rest in autism spectrum disorders. *Annals of Neurology* 77:866–876.

Du J, Haak LL, Phillips-Tansey E, Russell JT, McBain CJ (2000) Frequency-dependent regulation of rat hippocampal somato-dendritic excitability by the K+ channel subunit Kv2.1. *The Journal of Physiology* 522:19–31.

Durand GM, Kovalchuk Y, Konnerth A (1996) Long-term potentiation and functional synapse induction in developing hippocampus. *Nature* 381:71–75.

Eichenbaum H, Dudchenko P, Wood E, Shapiro M, Tanila H (1999) The Hippocampus, Memory, and Place Cells: Is It Spatial Memory or a Memory Space? *Neuron* 23:209–226.

Espinosa JS, Stryker MP (2012) Development and Plasticity of the Primary Visual Cortex. *Neuron* 75:230–249.

Estacion M, O'Brien JE, Conravey A, Hammer MF, Waxman SG, Dib-Hajj SD, Meisler MH (2014) A novel de novo mutation of SCN8A (Nav1.6) with enhanced channel activation in a child with epileptic encephalopathy. *Neurobiology of Disease* 69:117–123.

Ethridge LE, White SP, Mosconi MW, Wang J, Pedapati EV, Erickson CA, Byerly MJ, Sweeney JA (2017) Neural synchronization deficits linked to cortical hyper-excitability and auditory hypersensitivity in fragile X syndrome. *Molecular Autism* 8:1–11.

Euston DR, Gruber AJ, McNaughton BL (2012) The Role of Medial Prefrontal Cortex in Memory and Decision Making.

Evans MD, Dumitrescu AS, Kruijssen DLH, Taylor SE, Grubb MS (2015) Rapid

Modulation of Axon Initial Segment Length Influences Repetitive Spike Firing. *Cell Reports* 13:1233–1245.

Evans MD, Sammons RP, Lebron S, Dumitrescu AS, Watkins TBK, Uebele VN, Renger JJ, Grubb MS (2013) Calcineurin Signaling Mediates Activity-Dependent Relocation of the Axon Initial Segment. *The Journal of Neuroscience* 33:6950 – 6963.

Fagiolini M, Leblanc JJ (2011) Autism: A critical period disorder? *Neural Plasticity* 2011.

Fan Y, Fricker D, Brager DH, Chen X, Lu HC, Chitwood RA, Johnston D (2005) Activity-dependent decrease of excitability in rat hippocampal neurons through increases in Ih. *Nature Neuroscience* 8:1542–1551.

Farzin F, Whitney D, Hagerman RJ, Rivera SM (2008) Contrast detection in infants with fragile X syndrome. *Vision Research* 48:1471–1478.

Farzin F, Rivera SM (2010) Dynamic object representations in infants with and without fragile X syndrome. *Frontiers in Human Neuroscience* 4:1–9.

Fehr S, Wilson M, Downs J, Williams S, Murgia A, Sartori S, Vecchi M, Ho G, Polli R, Psoni S, Bao X, De Klerk N, Leonard H, Christodoulou J (2013) The CDKL5 disorder is an independent clinical entity associated with early-onset encephalopathy. *European Journal of Human Genetics* 21:266–273.

Fehr S, Wong K, Chin R, Williams S, De Klerk N, Forbes D, Krishnaraj R, Christodoulou J, Downs J, Leonard H (2016) Seizure variables and their relationship to genotype and functional abilities in the CDKL5 disorder. *Neurology* 87:2206–2213.

Ferreira TA, Blackman AV, Oyrer J, Jayabal S, Chung AJ, Watt AJ, Sjöström PJ, van Meyel DJ (2014) Neuronal morphometry directly from bitmap images. *Nature Methods* 11:982–984.

Fleidervish IA, Lasser-Ross N, Gutnick MJ, Ross WN (2010) Na+ imaging reveals little difference in action potential-evoked Na+ influx between axon and soma. *Nature Neuroscience* 13:852–860.

Fontaine DA, Davis DB (2016) Attention to Background Strain Is Essential for Metabolic Research: C57BL/6 and the International Knockout Mouse Consortium. *Diabetes* 65:25 – 33.

Fox K (1992) A critical period for experience-dependent synaptic plasticity in rat barrel cortex. *The Journal of Neuroscience* 12:1826 – 1838.

Fuchs C, Trazzi S, Torricella R, Viggiano R, De Franceschi M, Amendola E, Gross C, Calzà L, Bartesaghi R, Ciani E (2014) Loss of CDKL5 impairs survival and dendritic growth of newborn neurons by altering AKT/GSK-3β signaling. *Neurobiology of Disease* 70:53–68.

Fyhn M, Molden S, Witter MP, Moser EI, Moser MB (2004) Spatial Representation in the Entorhinal Cortex. *Science* 305:1258 – 1264.

Gabel LA, Won S, Kawai H, McKinney M, Tartakoff AM, Fallon JR (2004) Visual Experience Regulates Transient Expression and Dendritic Localization of Fragile X Mental Retardation Protein. *The Journal of Neuroscience* 24:10579 – 10583.

Gallagher MJ, Huang H, Pritchett DB, Lynch DR (1996) Interactions between ifenprodil and the NR2B subunit of the N-methyl-D-aspartate receptor. *The Journal of biological chemistry* 271:9603–11.

Gantois I, Pop AS, de Esch CEF, Buijsen RAM, Pooters T, Gomez-Mancilla B, Gasparini F, Oostra BA, D'Hooge R, Willemsen R (2013) Chronic administration of AFQ056/Mavoglurant restores social behaviour in Fmr1 knockout mice. *Behavioural Brain Research* 239:72–79.

Garber KB, Visootsak J, Warren ST (2008) Fragile X syndrome. *European Journal of Human Genetics* 16:666–672.

Gaudissard J, Ginger M, Premoli M, Memo M, Frick A, Pietropaolo S (2017) Behavioral abnormalities in the Fmr1-KO2 mouse model of fragile X syndrome: The relevance of early life phases. *Autism Research* 10:1584–1596.

Gibson JR, Bartley AF, Hays SA, Huber KM (2008) Imbalance of Neocortical Excitation and Inhibition and Altered UP States Reflect Network Hyperexcitability in the Mouse Model of Fragile X Syndrome. *Journal of Neurophysiology* 100:2615–2626.

Gilbert CD (1993) Circuitry, Architecture, and Functional Dynamics of Visual Cortex. *Cerebral Cortex* 3:373–386.

Gilling M, Rasmussen H, Calloe K, Sequeira A, Baretto M, Oliveira G, Almeida J, Lauritsen M, Ullmann R, Boonen S, Brøndum-Nielsen K, Kalscheuer V, Tümer Z, Vicente A, Schmitt N, Tommerup N (2013) Dysfunction of the Heteromeric KV7.3/KV7.5 Potassium Channel is Associated with Autism Spectrum Disorders .

Goddard GV, McIntyre DC, Leech CK (1969) A permanent change in brain function resulting from daily electrical stimulation. *Experimental Neurology* 25:295–330.

Godfraind JM, Reyniers E, De Boulle K, D'Hooge R, De Deyn PP, Bakker CE, Oostra BA, Kooy RF, Willems PJ (1996) Long-term potentiation in the hippocampus of fragile X knockout mice. *American Journal of Medical Genetics* 64:246–251.

Goel A, Lee HK (2007) Persistence of Experience-Induced Homeostatic Synaptic Plasticity through Adulthood in Superficial Layers of Mouse Visual Cortex. *Journal of Neuroscience* 27:6692–6700.

Goel A, Cantu DA, Guilfoyle J, Chaudhari GR, Newadkar A, Todisco B, de Alba D, Kourdougli N, Schmitt LM, Pedapati E, Erickson CA, Portera-Cailliau C (2018) Impaired perceptual learning in a mouse model of Fragile X syndrome is mediated by parvalbumin neuron dysfunction and is reversible. *Nature Neuroscience* 21:1404–1411.

Golowasch J, Casey M, Abbott LF, Marder E (1999) Network Stability from Activity-Dependent Regulation of Neuronal Conductances. *Neural Computation* 11:1079–1096.

Gordon JA, Stryker MP (1996) Experience-Dependent Plasticity of Binocular Responses in the Primary Visual Cortex of the Mouse. *The Journal of Neuroscience* 16:3274 – 3286.

Green JD (1964) The Hippocampus. *Physiological Reviews* 44:561–608.

Greifzu F, Pielecka-Fortuna J, Kalogeraki E, Krempler K, Favaro PD, Schlüter OM, Löwel S (2014) Environmental enrichment extends ocular dominance plasticity into

adulthood and protects from stroke-induced impairments of plasticity. *Proceedings of the National Academy of Sciences* 111:1150–1155.

Grubb MS, Burrone J (2010) Activity-dependent relocation of the axon initial segment fine-tunes neuronal excitability. *Nature* 465:1070–1074.

Grubb MS, Shu Y, Kuba H, Rasband MN, Wimmer VC, Bender KJ (2011) Short- and Long-Term Plasticity at the Axon Initial Segment. *The Journal of Neuroscience* 31:16049 – 16055.

Guire ES, Oh MC, Soderling TR, Derkach VA (2008) Recruitment of calcium-permeable AMPA receptors during synaptic potentiation is regulated by CaM-kinase I. *Journal of Neuroscience* 28:6000–6009.

Gulledge AT, Bravo JJ (2016) Neuron Morphology Influences Axon Initial Segment Plasticity. *eNeuro* 3:1–24.

Guo Y, Su Zj, Chen Yk, Chai Z (2017) Brain-derived neurotrophic factor/neurotrophin 3 regulate axon initial segment location and affect neuronal excitability in cultured hippocampal neurons. *Journal of Neurochemistry* 142:260–271.

Gutzmann A, Ergül N, Grossmann R, Schultz C, Wahle P, Engelhardt M, Erguel N, Grossmann R, Schultz C, Wahle P, Engelhardt M (2014) A period of structural plasticity at the axon initial segment in developing visual cortex. *Frontiers in Neuroanatomy* 8:11.

Haberl MG, Zerbi V, Veltien A, Ginger M, Heerschap A, Frick A (2015) Structural-functional connectivity deficits of neocortical circuits in the Fmr1/y mouse model of autism. *Science Advances* 1:e1500775.

Han S, Tai C, Westenbroek RE, Yu FH, Cheah CS, Potter GB, Rubenstein JL, Scheuer T, de la Iglesia HO, Catterall WA (2012) Autistic-like behaviour in Scn1a+/ mice and rescue by enhanced GABA-mediated neurotransmission. *Nature* 489:385–390.

Hanse E, Gustafsson B (2001a) Paired-Pulse Plasticity at the Single Release Site Level: An Experimental and Computational Study. *The Journal of Neuroscience* 21:8362 – 8369.

Hanse E, Gustafsson B (2001b) Vesicle release probability and pre-primed pool at glutamatergic synapses in area CA1 of the rat neonatal hippocampus. *Journal of Physiology* 531:481–493.

Hargus NJ, Nigam A, Bertram EH, Patel MK (2013) Evidence for a role of Nav1.6 in facilitating increases in neuronal hyperexcitability during epileptogenesis. *Journal of Neurophysiology* 110:1144–1157.

Harlow EG, Till SM, Russell TA, Wijetunge LS, Kind P, Contractor A (2010) Critical Period Plasticity Is Disrupted in the Barrel Cortex of Fmr1 Knockout Mice. *Neuron* 65:385–398.

Harris KD, Mrsic-flogel TD (2013) Cortical connectivity and sensory coding. *Nature* 503:51–58.

Harty RC, Kim TH, Thomas EA, Cardamone L, Jones NC, Petrou S, Wimmer VC (2013) Axon initial segment structural plasticity in animal models of genetic and acquired epilepsy. *Epilepsy Research* 105:272–279.

He Y, Janssen WG, Morrison JH (1998) Synaptic coexistence of AMPA and NMDA receptors in the rat hippocampus: A postembedding immunogold study. *Journal of Neuroscience Research* 54:444–449.

Hebb DO (1949) *The organisation of behaviour: a neuropsychological theory* Wiley.

Hector RD, Dando O, Landsberger N, Kilstrup-Nielsen C, Kind PC, Bailey MES, Cobb SR (2016) Characterisation of CDKL5 Transcript Isoforms in Human and Mouse. *PLoS ONE* 11:1–22.

Hector RD, Dando O, Ritakari TE, Kind PC, Bailey MES, Cobb SR (2017a) Characterisation of Cdkl5 transcript isoforms in rat. *Gene* 603:21–26.

Hector RD, Kalscheuer VM, Hennig F, Leonard H, Downs J, Clarke A, Benke TA, Armstrong J, Pineda M, Bailey MES, Cobb SR (2017b) CDKL5 variants . *Neurology Genetics* 3:e200.

Henley JM, Wilkinson KA (2016) Synaptic AMPA receptor composition in development, plasticity and disease. *Nature Reviews Neuroscience* 17:337–350.

Hensch TK (2005) Critical period plasticity in local cortical circuits. *Nature Reviews Neuroscience* 6:877–888.

Hill AS, Nishino A, Nakajo K, Zhang G, Fineman JR, Selzer ME, Okamura Y, Cooper EC (2008) Ion Channel Clustering at the Axon Initial Segment and Node of Ranvier Evolved Sequentially in Early Chordates. *PLOS Genetics* 4:e1000317.

Hodgkin AL, Huxley AF (1952) The components of membrane conductance in the giant axon of Loligo. *The Journal of Physiology* 116:473–496.

Hoeffer CA, Klann E (2010) mTOR signaling: At the crossroads of plasticity, memory and disease. *Trends in Neurosciences* 33:67–75.

Hsia AY, Malenka RC, Nicoll RA (1998) Development of excitatory circuitry in the hippocampus. *Journal of Neurophysiology* 79:2013–2024.

Hu W, Tian C, Li T, Yang M, Hou H, Shu Y (2009) Distinct contributions of Nav1.6 and Nav1.2 in action potential initiation and backpropagation. *Nature Neuroscience* 12:996–1002.

Hubel DH, Wiesel TN (1970) The period of susceptibility to the physiological effects of unilateral eye closure in kittens. *The Journal of Physiology* 206:419–436.

Huber KM, Gallagher SM, Warren ST, Bear MF (2002) Altered synaptic plasticity in a mouse model of fragile X mental retardation. *Proceedings of the National Academy of Sciences of the United States of America* 99:7746–50.

Huganir RL, Nicoll RA (2013) AMPARs and synaptic plasticity: The last 25 years. *Neuron* 80:704–717.

Isaac JT (2003) Postsynaptic silent synapses: Evidence and mechanisms. *Neuropharmacology* 45:450–460.

Isaac JT, Crair MC, Nicoll RA, Malenka RC (1997) Silent synapses during development of thalamocortical inputs. *Neuron* 18:269–280.

Isaac JT, Nicoll RA, Malenka RC (1995) Evidence for silent synapses: Implications for the expression of LTP. *Neuron* 15:427–434.

Ishizuka N, Cowan WM, Amaral DG (1995) A quantitative analysis of the dendritic organization of pyramidal cells in the rat hippocampus. *Journal of Comparative Neurology* 362:17–45.

Ishizuka N, Weber J, Amaral DG (1990) Organization of intrahippocampal projections originating from CA3 pyramidal cells in the rat. *Journal of Comparative Neurology* 295:580–623.

Jackson A (2016) Cellular and synaptic pathophysiology in a rat model of Fragile X syndrome Phd thesis, The University of Edinburgh.

Jamann N, Dannehl D, Wagener R, Corcelli C, Schultz C, Staiger J, Kole MHP, Engelhardt M (2020) Sensory input drives rapid homeostatic scaling of the axon initial segment in mouse barrel cortex. *bioRxiv* .

Jhang CL, Huang TN, Hsueh YP, Liao W (2017) Mice lacking cyclin-dependent kinase-like 5 manifest autistic and ADHD-like behaviors. *Human Molecular Genetics* 26:3922–3934.

Jia Z, Agopyan N, Miu P, Xiong Z, Henderson J, Gerlai R, Taverna FA, Velumian A, MacDonald J, Carlen P, Abramow-Newerly W, Roder J (1996) Enhanced LTP in Mice Deficient in the AMPA Receptor GluR2. *Neuron* 17:945–956.

Jiang B, Treviño M, Kirkwood A (2007) Sequential development of long-term potentiation and depression in different layers of the mouse visual cortex. *Journal of Neuroscience* 27:9648–9652.

Johnston, Daniel and Wu SMS (1994) *Foundations of cellular neurophysiology* MIT Press.

Jonas P, Racca C, Sakmann B, Seeburg P, Monyer H (1994) Differences in Ca2+ permeability of AMPA-type glutamate receptor channels in neocortical neurons caused by differential GluR-B subunit expression. *Neuron* 12:1281–1289.

Jonas P, Sakmann B (1992) Glutamate receptor channels in isolated patches from CA1 and CA3 pyramidal cells of rat hippocampal slices. *The Journal of Physiology* 455:143–171.

Jung S, Warner LN, Pitsch J, Becker AJ, Poolos NP (2011) Rapid Loss of Dendritic HCN Channel Expression in Hippocampal Pyramidal Neurons following Status Epilepticus. *The Journal of Neuroscience* 31:14291 – 14295.

Kalbassi S, Bachmann SO, Cross E, Roberton VH, Baudouin SJ (2017) Male and Female Mice Lacking Neuroligin-3 Modify the Behavior of Their Wild-Type Littermates. *eneuro* 4:ENEURO.0145–17.2017.

Kalmbach BE, Johnston D, Brager DH (2015) Cell-Type Specific Channelopathies in the Prefrontal Cortex of the fmr1-/y Mouse Model of Fragile X Syndrome. *eneuro* 2:ENEURO.0114–15.2015.

Kalscheuer VM, Tao J, Donnelly A, Hollway G, Schwinger E, Kübart S, Menzel C, Hoeltzenbein M, Tommerup N, Eyre H, Harbord M, Haan E, Sutherland GR, Ropers HH, Gécz J (2003) Disruption of the Serine/Threonine Kinase 9 Gene Causes Severe

X-Linked Infantile Spasms and Mental Retardation. *The American Journal of Human Genetics* 72:1401–1411.

Kamboj SK, Swanson GT, Cull-Candy SG (1995) Intracellular spermine confers rectification on rat calcium-permeable AMPA and kainate receptors. *The Journal of Physiology* 486:297–303.

Kaphzan H, Buffington Sa, Jung JII, Rasband MN, Klann E (2011) Alterations in Intrinsic Membrane Properties and the Axon Initial Segment in a Mouse Model of Angelman Syndrome. *Journal of Neuroscience* 31:17637–17648.

Kazdoba TM, Leach PT, Silverman JL, Crawley JN (2014) Modeling fragile X syndrome in the Fmr1 knockout mouse. *Intractable & rare diseases research* 3:118–33.

Keck T, Keller G, Jacobsen R, Eysel U, Bonhoeffer T, Hübener M (2013) Synaptic Scaling and Homeostatic Plasticity in the Mouse Visual Cortex In Vivo. *Neuron* 80:327–334.

Keller G, Bonhoeffer T, Hübener M (2012) Sensorimotor Mismatch Signals in Primary Visual Cortex of the Behaving Mouse. *Neuron* 74:809–815.

Kemper MB, Hagerman RJ, Altshul-Stark D (1988) Cognitive profiles of boys with the fragile X syndrome. *American Journal of Medical Genetics* 30:191–200.

Kerns CM, Kendall PC, Zickgraf H, Franklin ME, Miller J, Herrington J (2015) Not to Be Overshadowed or Overlooked: Functional Impairments Associated With Comorbid Anxiety Disorders in Youth With ASD. *Behavior Therapy* 46:29–39.

Kerti K, Lorincz A, Nusser Z (2012) Unique somato-dendritic distribution pattern of Kv4.2 channels on hippocampal CA1 pyramidal cells. *European Journal of Neuroscience* 35:66–75.

Kim EC, Patel J, Zhang J, Soh H, Rhodes JS, Tzingounis AV, Chung HJ (2020) Heterozygous loss of epilepsy gene KCNQ2 alters social, repetitive and exploratory behaviors. *Genes, Brain and Behavior* 19:e12599.

Kim H, Gibboni R, Kirkhart C, Bao S (2013) Impaired Critical Period Plasticity in Primary Auditory Cortex of Fragile X Model Mice. *The Journal of Neuroscience* 33:15686 – 15692.

Kirkwood A, Rioult MG, Bear MF (1996) Experience-dependent modification of synaptic plasticity in visual cortex. *Nature* 381:526–528.

Kirson ED, Schirra C, Konnerth A, Yaari Y (1999) Early postnatal switch in magnesium sensitivity of NMDA receptors in rat CA1 pyramidal cells. *The Journal of Physiology* 521:99–111.

Klausberger T (2009) GABAergic interneurons targeting dendrites of pyramidal cells in the CA1 area of the hippocampus. *European Journal of Neuroscience* 30:947–957.

Klemmer P, Meredith RM, Holmgren CD, Klychnikov OI, Stahl-Zeng J, Loos M, van der Schors RC, Wortel J, de Wit H, Spijker S, Rotaru DC, Mansvelder HD, Smit AB, Li KW (2011) Proteomics, ultrastructure, and physiology of hippocampal synapses in a fragile X syndrome mouse model reveal presynaptic phenotype. *The Journal of biological chemistry* 286:25495–504.

Knapska E, Macias M, Mikosz M, Nowak A, Owczarek D, Wawrzyniak M, Pieprzyk M, Cymerman IA, Werka T, Sheng M, Maren S, Jaworski J, Kaczmarek L (2012) Functional anatomy of neural circuits regulating fear and extinction. *Proceedings of the National Academy of Sciences of the United States of America* 109:17093–17098.

Koester HJ, Sakmann B (1998) Calcium dynamics in single spines during coincident pre- and postsynaptic activity depend on relative timing of back-propagating action potentials and subthreshold excitatory postsynaptic potentials. *Proceedings of the National Academy of Sciences* 95:9596–9601.

Kogan CS, Bertone A, Cornish K, Boutet I, Der Kaloustian VM, Andermann E, Faubert J, Chaudhuri A (2004a) Integrative cortical dysfunction and pervasive motion perception deficit in fragile X syndrome. *Neurology* 63:1634–1639.

Kogan CS, Boutet I, Cornish K, Zangenehpour S, Mullen KT, Holden JJ, Der Kaloustian VM, Andermann E, Chaudhuri A (2004b) Differential impact of the FMR1 gene on visual processing in fragile X syndrome. *Brain* 127:591–601.

Kole MHP, Ilschner SU, Kampa BM, Williams SR, Ruben PC, Stuart GJ (2008) Action potential generation requires a high sodium channel density in the axon initial segment. *Nature neuroscience* 11:178–86.

Kole MHP, Letzkus JJ, Stuart GJ (2007) Axon Initial Segment Kv1 Channels Control Axonal Action Potential Waveform and Synaptic Efficacy. *Neuron* 55:633–647.

Kole M, Stuart G (2012) Signal Processing in the Axon Initial Segment. *Neuron* 73:235–247.

Komiyama NH, Watabe AM, Carlisle HJ, Porter K, Charlesworth P, Monti J, Strathdee DJC, Carroll CM, Martin SJ, Morris RGM, Dell TJ, Grant SGN (2002) SynGAP Regulates ERK/MAPK Signaling, Synaptic Plasticity, and Learning in the Complex with Postsynaptic Density 95 and NMDA Receptor. *The Journal of Neuroscience* 22:9721 – 9732.

Kramvis I, Mansvelder HD, Loos M, Meredith R (2013) Hyperactivity , perseveration and increased responding during attentional rule acquisition in the Fragile X mouse model. *Frontiers in Behavioral Neuroscience* 7:1–13.

Krueger DD, Osterweil EK, Chen SP, Tye LD, Bear MF (2011) Cognitive dysfunction and prefrontal synaptic abnormalities in a mouse model of fragile X syndrome. *Proceedings of the National Academy of Sciences* 108:2587–2592.

Kuba H, Adachi R, Ohmori H (2014) Activity-Dependent and Activity-Independent Development of the Axon Initial Segment. *The Journal of Neuroscience* 34:3443–3453.

Kuba H, Ishii TM, Ohmori H (2006) Axonal site of spike initiation enhances auditory coincidence detection. *Nature* 444:1069–1072.

Kuba H, Oichi Y, Ohmori H (2010) Presynaptic activity regulates Na+ channel distribution at the axon initial segment. *Nature* 465:1075–1078.

Kullmann DM, Nicoll RA (1992) Long term potentiation is associated with increases in quantal content and quantal amplitude. *Nature* 357:243–244.

Kumar SS, Bacci A, Kharazia V, Huguenard JR (2002) A developmental switch of

AMPA receptor subunits in neocortical pyramidal neurons. *Journal of Neuroscience* 22:3005–3015.

La Fata G, Gärtner A, Domínguez-Iturza N, Dresselaers T, Dawitz J, Poorthuis RB, Averna M, Himmelreich U, Meredith RM, Achsel T, Dotti CG, Bagni C (2014) FMRP regulates multipolar to bipolar transition affecting neuronal migration and cortical circuitry. *Nature Neuroscience* 17:1693–1700.

Larson J, Jessen RE, Kim D, Fine AKS, du Hoffmann J (2005) Age-Dependent and Selective Impairment of Long-Term Potentiation in the Anterior Piriform Cortex of Mice Lacking the Fragile X Mental Retardation Protein. *The Journal of Neuroscience* 25:9460 – 9469.

Lauterborn JC, Rex CS, Kramár E, Chen LY, Pandyarajan V, Lynch G, Gall CM (2007) Brain-Derived Neurotrophic Factor Rescues Synaptic Plasticity in a Mouse Model of Fragile X Syndrome. *The Journal of Neuroscience* 27:10685 – 10694.

Leterrier C (2018) The Axon Initial Segment: An Updated Viewpoint. *The Journal of Neuroscience* 38:2135 – 2145.

Leterrier C, Dargent B (2014) No Pasaran! Role of the axon initial segment in the regulation of protein transport and the maintenance of axonal identity. *Seminars in Cell & Developmental Biology* 27:44–51.

Leterrier C, Potier J, Caillol G, Debarnot C, Rueda Boroni F, Dargent B (2015) Nanoscale Architecture of the Axon Initial Segment Reveals an Organized and Robust Scaffold. *Cell Reports* 13:2781–2793.

Lezmy J, Lipinsky M, Khrapunsky Y, Patrich E, Shalom L, Peretz A, Fleidervish IA, Attali B (2017) M-current inhibition rapidly induces a unique CK2-dependent plasticity of the axon initial segment. *Proceedings of the National Academy of Sciences* 114:E10234–E10243.

Liao D, Hessler NA, Malinow R (1995) Activation of postsynaptically silent synapses during pairing-induced LTP in CA1 region of hippocampal slice. *Nature* 375:400–404.

Liao W, Lee KZ, Chen JC, Su SH, Luo Y (2020) Deficiency of cyclin-dependent kinase-like 5 causes spontaneous seizures in neonatal mice. *bioRxiv* p. 2020.03.09.983981.

Livingston LA, Happé F (2017) Conceptualising compensation in neurodevelopmental disorders: Reflections from autism spectrum disorder. *Neuroscience & Biobehavioral Reviews* 80:729–742.

Lledo PM, Zhang X, Südhof TC, Malenka RC, Nicoll RA (1998) Postsynaptic Membrane Fusion and Long-Term Potentiation. *Science* 279:399 – 403.

Longair MH, Baker DA, Armstrong JD (2011) Simple Neurite Tracer: open source software for reconstruction, visualization and analysis of neuronal processes. *Bioinformatics* 27:2453–2454.

Lopantsev V, Tempel BL, Schwartzkroin PA (2003) Hyperexcitability of CA3 Pyramidal Cells in Mice Lacking the Potassium Channel Subunit Kv1.1. *Epilepsia* 44:1506–1512.

Lorente De Nó R (1934) Studies on the structure of the cerebral cortex. II. Continuation of the study of the ammonic system. *Journal für Psychologie und Neurologie* 46:113–177.

Lorincz A, Nusser Z (2008) Cell-Type-Dependent Molecular Composition of the Axon Initial Segment. *The Journal of Neuroscience* 28:14329 – 14340.

Lorincz A, Nusser Z (2010) Molecular Identity of Dendritic Voltage-Gated Sodium Channels. *Science* 328:906 – 909.

LoVullo SV, Matson JL (2009) Comorbid psychopathology in adults with Autism Spectrum Disorders and intellectual disabilities. *Research in Developmental Disabilities* 30:1288–1296.

Luque MA, Beltran-Matas P, Marin MC, Torres B, Herrero L (2017) Excitability is increased in hippocampal CA1 pyramidal cells of Fmr1 knockout mice. *PLOS ONE* 12:1–18.

Luscher C, Malenka RC (2012) NMDA Receptor-Dependent Long-Term Potentiation and Long-Term Depression (LTP / LTD). *Cold Spring Harbor perspectives in biology* .

Lüscher C, Xia H, Beattie EC, Carroll RC, von Zastrow M, Malenka RC, Nicoll RA (1999) Role of AMPA Receptor Cycling in Synaptic Transmission and Plasticity. *Neuron* 24:649–658.

Maffei A, Nelson SB, Turrigiano GG (2004) Selective reconfiguration of layer 4 visual cortical circuitry by visual deprivation. *Nature Neuroscience* 7:1353–1359.

Maffei A, Turrigiano GG (2008) Multiple modes of network homeostasis in visual cortical layer 2/3. *Journal of Neuroscience* 28:4377–4384.

Magee J, Hoffman D, Colbert C, Johnston D (1998) Electrical and Calcium Signaling in Dendrites of Hippocampal Pyramidal Neurons. *Annual Review of Physiology* 60:327–346.

Magee JC (2000) Dendritic integration of excitatory synaptic input. *Nature Reviews Neuroscience* 1:181–190.

Maguire EA, Frackowiak RSJ, Frith CD (1996) Learning to find your way: a role for the human hippocampal formation. *Proceedings of the Royal Society of London. Series B: Biological Sciences* 263:1745–1750.

Maguire EA, Burgess N, Donnett JG, Frackowiak RSJ, Frith CD, O'Keefe J (1998) Knowing Where and Getting There: A Human Navigation Network. *Science* 280:921 – 924.

Mainen ZF, Sejnowski TJ (1996) Influence of dendritic structure on firing pattern in model neocortical neurons. *Nature* 382:363–366.

Malenka RC, Bear MF (2004) LTP and LTD: An Embarrassment of Riches. *Neuron* 44:5–21.

Manita S, Suzuki T, Inoue M, Kudo Y, Miyakawa H (2007) Paired-pulse ratio of synaptically induced transporter currents at hippocampal CA1 synapses is not related to release probability. *Brain Research* 1154:71–79.

Mantegazza M, Gambardella A, Rusconi R, Schiavon E, Annesi F, Cassulini RR, Labate A, Carrideo S, Chifari R, Canevini MP, Canger R, Franceschetti S, Annesi G, Wanke E, Quattrone A (2005) Identification of an Nav1.1 sodium channel

(SCN1A) loss-of-function mutation associated with familial simple febrile seizures. *PNAS* 81:3443–3446.

Marder E, Goaillard JM (2006) Variability, compensation and homeostasis in neuron and network function. *Nature Reviews Neuroscience* 7:563–574.

Mari F, Azimonti S, Bertani I, Bolognese F, Colombo E, Caselli R, Scala E, Longo I, Grosso S, Pescucci C, Ariani F, Hayek G, Balestri P, Bergo A, Badaracco G, Zappella M, Broccoli V, Renieri A, Kilstrup-Nielsen C, Landsberger N (2005) CDKL5 belongs to the same molecular pathway of MeCP2 and it is responsible for the early-onset seizure variant of Rett syndrome. *Human Molecular Genetics* 14:1935–1946.

Martin HGS, Lassalle O, Brown JT, Manzoni OJ (2015) Age-Dependent Long-Term Potentiation Deficits in the Prefrontal Cortex of the Fmr1 Knockout Mouse Model of Fragile X Syndrome. *Cerebral Cortex* 26:2084–2092.

Martin JP, Bell J (1943) A pedigree of mental defect showing sex-linkage. *Journal of Neurology and Psychiatry* 6:154–157.

Martin MS, Tang B, Papale LA, Yu FH, Catterall WA, Escayg A (2007) The voltage-gated sodium channel Scn8a is a genetic modifier of severe myoclonic epilepsy of infancy. *Human Molecular Genetics* 16:2892–2899.

Mazziotti R, Lupori L, Sagona G, Gennaro M, Della Sala G, Putignano E, Pizzorusso T (2017) Searching for biomarkers of CDKL5 disorder: early-onset visual impairment in CDKL5 mutant mice. *Human molecular genetics* 26:2290–2298.

McEwen DP, Chen C, Meadows LS, Lopez-Santiago L, Isom LL (2009) The voltage-gated Na+ channel β3 subunit does not mediate trans homophilic cell adhesion or associate with the cell adhesion molecule contactin. *Neuroscience Letters* 462:272–275.

McRae JF, Clayton S, Fitzgerald TW, Kaplanis J, Prigmore E, Rajan D, Sifrim A, Aitken S, Akawi N, Alvi M, Ambridge K, Barrett DM, Bayzetinova T, Jones P, Jones WD, King D, Krishnappa N, Mason LE, Singh T, Tivey AR, Ahmed M, Anjum U, Archer H, Armstrong R, Awada J, Balasubramanian M, Banka S, Baralle D, Barnicoat A, Batstone P, Baty D, Bennett C, Berg J, Bernhard B, Bevan AP, Bitner-Glindzicz M, Blair E, Blyth M, Bohanna D, Bourdon L, Bourn D, Bradley L, Brady A, Brent S, Brewer C, Brunstrom K, Bunyan DJ, Burn J, Canham N, Castle B, Chandler K, Chatzimichali E, Cilliers D, Clarke A, Clasper S, Clayton-Smith J, Clowes V, Coates A, Cole T, Colgiu I, Collins A, Collinson MN, Connell F, Cooper N, Cox H, Cresswell L, Cross G, Crow Y, D'Alessandro M, Dabir T, Davidson R, Davies S, De Vries D, Dean J, Deshpande C, Devlin G, Dixit A, Dobbie A, Donaldson A, Donnai D, Donnelly D, Donnelly C, Douglas A, Douzgou S, Duncan A, Eason J, Ellard S, Ellis I, Elmslie F, Evans K, Everest S, Fendick T, Fisher R, Flinter F, Foulds N, Fry A, Fryer A, Gardiner C, Gaunt L, Ghali N, Gibbons R, Gill H, Goodship J, Goudie D, Gray E, Green A, Greene P, Greenhalgh L, Gribble S, Harrison R, Harrison L, Harrison V, Hawkins R, He L, Hellens S, Henderson A, Hewitt S, Hildyard L, Hobson E, Holden S, Holder M, Holder S, Hollingsworth G, Homfray T, Humphreys M, Hurst J, Hutton B, Ingram S, Irving M, Islam L, Jackson A, Jarvis J, Jenkins L, Johnson D, Jones E, Josifova D, Joss S, Kaemba B, Kazembe S, Kelsell R, Kerr B, Kingston H, Kini U, Kinning E, Kirby G, Kirk C, Kivuva E, Kraus A, Kumar D, Ajith Kumar VK, Lachlan K, Lam W, Lampe A, Langman C, Lees M, Lim D, Longman C, Lowther G, Lynch SA, Magee A, Maher E, Male A, Mansour S, Marks K, Martin K, Maye U, McCann

E, McConnell V, McEntagart M, McGowan R, McKay K, McKee S, McMullan DJ, McNerlan S, McWilliam C, Mehta S, Metcalfe K, Middleton A, Miedzybrodzka Z, Miles E, Mohammed S, Montgomery T, Moore D, Morgan S, Morton J, Mugalaasi H, Murday V, Murphy H, Naik S, Nemeth A, Nevitt L, Newbury-Ecob R, Norman A, O'Shea R, Ogilvie C, Ong KR, Park SM, Parker MJ, Patel C, Paterson J, Payne S, Perrett D, Phipps J, Pilz DT, Pollard M, Pottinger C, Poulton J, Pratt N, Prescott K, Price S, Pridham A, Procter A, Purnell H, Quarrell O, Ragge N, Rahbari R, Randall J, Rankin J, Raymond L, Rice D, Robert L, Roberts E, Roberts J, Roberts P, Roberts G, Ross A, Rosser E, Saggar A, Samant S, Sampson J, Sandford R, Sarkar A, Schweiger S, Scott R, Scurr I, Selby A, Seller A, Sequeira C, Shannon N, Sharif S, Shaw-Smith C, Shearing E, Shears D, Sheridan E, Simonic I, Singzon R, Skitt Z, Smith A, Smith K, Smithson S, Sneddon L, Splitt M, Squires M, Stewart F, Stewart H, Straub V, Suri M, Sutton V, Swaminathan GJ, Sweeney E, Tatton-Brown K, Taylor C, Taylor R, Tein M, Temple IK, Thomson J, Tischkowitz M, Tomkins S, Torokwa A, Treacy B, Turner C, Turnpenny P, Tysoe C, Vandersteen A, Varghese V, Vasudevan P, Vijayarangakannan P, Vogt J, Wakeling E, Wallwark S, Waters J, Weber A, Wellesley D, Whiteford M, Widaa S, Wilcox S, Wilkinson E, Williams D, Williams N, Wilson L, Woods G, Wragg C, Wright M, Yates L, Yau M, Nellåker C, Firth HV, Wright CF, FitzPatrick DR, Barrett JC, Hurles ME (2017) Prevalence and architecture of de novo mutations in developmental disorders. *Nature* 542:433–438.

Megıas M, Emri Z, Freund T, Gulyás A (2001) Total number and distribution of inhibitory and excitatory synapses on hippocampal CA1 pyramidal cells. *Neuroscience* 102:527–540.

Mekada K, Abe K, Murakami A, Nakamura S, Nakata H, Moriwaki K, Obata Y, Yoshiki A (2009) Genetic differences among C57BL/6 substrains. *Experimental Animals* 58:141–149.

Meredith RM, de Jong R, Mansvelder HD (2011) Functional rescue of excitatory synaptic transmission in the developing hippocampus in Fmr1-KO mouse. *Neurobiology of Disease* 41:104–110.

Meredith RM, Holmgren CD, Weidum M, Burnashev N, Mansvelder HD (2007) Increased Threshold for Spike-Timing-Dependent Plasticity Is Caused by Unreliable Calcium Signaling in Mice Lacking Fragile X Gene Fmr1. *Neuron* 54:627–638.

Miceli F, Soldovieri MV, Ambrosino P, De Maria M, Migliore M, Migliore R, Taglialatela M (2015) Early-Onset Epileptic Encephalopathy Caused by Gain-of-Function Mutations in the Voltage Sensor of Kv7.2 and Kv7.3 Potassium Channel Subunits. *The Journal of Neuroscience* 35:3782 – 3793.

Michalon A, Sidorov M, Ballard TM, Ozmen L, Spooren W, Wettstein JG, Jaeschke G, Bear MF, Lindemann L (2012) Chronic Pharmacological mGlu5 Inhibition Corrects Fragile X in Adult Mice. *Neuron* 74:49–56.

Mientjes EJ, Nieuwenhuizen I, Kirkpatrick L, Zu T, Hoogeveen-Westerveld M, Severijnen L, Rifé M, Willemsen R, Nelson DL, Oostra BA (2006) The generation of a conditional Fmr1 knock out mouse model to study Fmrp function in vivo. *Neurobiology of Disease* 21:549–555.

Millar AG, Bradacs H, Charlton MP, Atwood HL (2002) Inverse Relationship between

Release Probability and Readily Releasable Vesicles in Depressing and Facilitating Synapses. *The Journal of Neuroscience* 22:9661 – 9667.

Miller KD, Pinto DJ, Simons DJ (2001) Processing in layer 4 of the neocortical circuit: new insights from visual and somatosensory cortex. *Current Opinion in Neurobiology* 11:488–497.

Miller VM, Best PJ (1980) Spatial correlates of hippocampal unit activity are altered by lesions of the fornix and entorhinal cortex. *Brain Research* 194:311–323.

Mohapatra DP, Misonou H, Sheng-Jun P, Held JE, Surmeier DJ, Trimmer JS (2009) Regulation of intrinsic excitability in hippocampal neurons by activity-dependent modulation of the KV2.1 potassium channel. *Channels* 3:46–56.

Molnár Z, Cheung AFP (2006) Towards the classification of subpopulations of layer V pyramidal projection neurons. *Neuroscience Research* 55:105–115.

Moyer Jr. JR, Thompson LT, Disterhoft JF (1996) Trace Eyeblink Conditioning Increases CA1 Excitability in a Transient and Learning-Specific Manner. *The Journal of Neuroscience* 16:5536 – 5546.

Muddashetty RS, Kelić S, Gross C, Xu M, Bassell GJ (2007) Dysregulated metabotropic glutamate receptor-dependent translation of AMPA receptor and postsynaptic density-95 mRNAs at synapses in a mouse model of fragile X syndrome. *Journal of Neuroscience* 27:5338–5348.

Muñoz IM, Morgan ME, Peltier J, Weiland F, Gregorczyk M, Brown FCM, Macartney T, Toth R, Trost M, Rouse J (2018) Phosphoproteomic screening identifies physiological substrates of the CDKL 5 kinase . *The EMBO Journal* 37:1–19.

Murthy VN, Camilli PD (2003) Cell Biology of the Presynaptic Terminal. *Annual Review of Neuroscience* 26:701–728.

Musumeci SA, Hagerman RJ, Ferri R, Bosco P, Bernardina BD, Tassinari CA, De Sarro GB, Elia M (1999) Epilepsy and EEG Findings in Males with Fragile X Syndrome. *Epilepsia* 40:1092–1099.

Musumeci SA, Bosco P, Calabrese G, Bakker C, De Sarro GB, Elia M, Ferri R, Oostra BA (2000) Audiogenic Seizures Susceptibility in Transgenic Mice with Fragile X Syndrome. *Epilepsia* 41:19–23.

Nakamoto M, Nalavadi V, Epstein MP, Narayanan U, Bassell GJ, Warren ST (2007) Fragile X mental retardation protein deficiency leads to excessive mGluR5-dependent internalization of AMPA receptors. *Proceedings of the National Academy of Sciences of the United States of America* 104:15537–15542.

Nelson SB, Valakh V (2015) Excitatory/Inhibitory Balance and Circuit Homeostasis in Autism Spectrum Disorders. *Neuron* 87:684–698.

Nozari M, Suzuki T, Rosa, Marcello G, Ymamkawa K, Atapour N (2016) The impact of early environmental interventions on structural plasticity of the axon initial segment in neocortex. *Developmental Psychobiology* 59:39–47.

O'Brien J, Meisler M (2013) Sodium channel SCN8A (Nav1.6): properties and de novo mutations in epileptic encephalopathy and intellectual disability .

Ogiwara I, Miyamoto H, Morita N, Atapour N, Mazaki E, Inoue I, Takeuchi T, Itohara S, Yanagawa Y, Obata K, Furuichi T, Hensch TK, Yamakawa K (2007) Nav1.1 Localizes to Axons of Parvalbumin-Positive Inhibitory Interneurons: A Circuit Basis for Epileptic Seizures in Mice Carrying an Scn1a Gene Mutation. *The Journal of Neuroscience* 27:5903 – 5914.

Oh MM, Kuo AG, Wu WW, Sametsky EA, Disterhoft JF (2003) Watermaze Learning Enhances Excitability of CA1 Pyramidal Neurons. *Journal of Neurophysiology* 90:2171–2179.

O'Keefe J, Dostrovsky J (1971) The hippocampus as a spatial map. Preliminary evidence from unit activity in the freely-moving rat. *Brain Research* 34:171–175.

O'Keefe J, Nadel L (1978) *The hippocampus as a cognitive map* Clarendon Press, Oxford.

Okuda K, Kobayashi S, Fukaya M, Watanabe A, Murakami T, Hagiwara M, Sato T, Ueno H, Ogonuki N, Komano-Inoue S, Manabe H, Yamaguchi M, Ogura A, Asahara H, Sakagami H, Mizuguchi M, Manabe T, Tanaka T (2017) CDKL5 controls postsynaptic localization of GluN2B-containing NMDA receptors in the hippocampus and regulates seizure susceptibility. *Neurobiology of Disease* 106:158–170.

Okuda K, Takao K, Watanabe A, Miyakawa T, Mizuguchi M, Tanaka T (2018) Comprehensive behavioral analysis of the Cdkl5 knockout mice revealed significant enhancement in anxiety- and fear-related behaviors and impairment in both acquisition and long-term retention of spatial reference memory. *Plos One* 13.

O'Leary T, van Rossum MCW, Wyllie DJA (2010) Homeostasis of intrinsic excitability in hippocampal neurones: dynamics and mechanism of the response to chronic depolarization. *The Journal of Physiology* 588:157–70.

Olivas ND, Quintanar-Zilinskas V, Nenadic Z, Xu X (2012) Laminar circuit organization and response modulation in mouse visual cortex. *Frontiers in Neural Circuits* 6:1–21.

Olson HE, Demarest ST, Pestana-Knight EM, Swanson LC, Iqbal S, Lal D, Leonard H, Cross JH, Devinsky O, Benke TA (2019) Cyclin-Dependent Kinase-Like 5 Deficiency Disorder: Clinical Review. *Pediatric Neurology* 97:18–25.

Orsini CA, Kim JH, Knapska E, Maren S (2011) Hippocampal and prefrontal projections to the basal amygdala mediate contextual regulation of fear after extinction. *Journal of Neuroscience* 31:17269–17277.

Osterweil EK, Krueger DD, Reinhold K, Bear MF (2010) Hypersensitivity to mGluR5 and ERK1/2 Leads to Excessive Protein Synthesis in the Hippocampus of a Mouse Model of Fragile X Syndrome. *The Journal of Neuroscience* 30:15616 – 15627.

Otmakhova NA, Otmakhov N, Lisman JE (2002) Pathway-Specific Properties of AMPA and NMDA-Mediated Transmission in CA1 Hippocampal Pyramidal Cells. *The Journal of Neuroscience* 22:1199 – 1207.

Padamsey Z, Tong R, Emptage N (2019) Optical Quantal Analysis Using Ca^{2+} Indicators: A Robust Method for Assessing Transmitter Release Probability at Excitatory Synapses by Imaging Single Glutamate Release Events. *Frontiers in Synaptic Neuroscience* 11:5.

Padilla-Coreano N, Bolkan SS, Pierce GM, Blackman DR, Hardin WD, Garcia-Garcia AL, Spellman TJ, Gordon JA (2016) Direct Ventral Hippocampal-Prefrontal Input Is Required for Anxiety-Related Neural Activity and Behavior. *Neuron* 89:857–866.

Pakan JM, Lowe SC, Dylda E, Keemink SW, Currie SP, Coutts CA, Rochefort NL (2016) Behavioral-state modulation of inhibition is context-dependent and cell type specific in mouse visual cortex. *eLife* 5.

Palay SL, Sotelo C, Peters A, Orkand PM (1968) The axon hillock and the initial segment. *Journal of Cell Biology* 38:193–201.

Pan Z, Kao T, Horvath Z, Lemos J, Sul JY, Cranstoun SD, Bennett V, Scherer SS, Cooper EC (2006) A Common Ankyrin-G-Based Mechanism Retains KCNQ and NaV Channels at Electrically Active Domains of the Axon. *The Journal of Neuroscience* 26:2599 – 2613.

Peters A, Proskauer CC, Kaiserman-Abramof IR (1968) The Small Pyramidal Neuron of the Rat Cerebral Cortex: The Axon Hillock and Initial Segment. *Journal of Cell Biology* 39:604–619.

Petralia RS, Esteban JA, Wang YX, Partridge JG, Zhao HM, Wenthold RJ, Malinow R (1999) Selective acquisition of AMPA receptors over postnatal development suggests a molecular basis for silent synapses. *Nature Neuroscience* 2:31–36.

Philpot BD, Sekhar AK, Shouval HZ, Bear MF (2001) Visual Experience and Deprivation Bidirectionally Modify the Composition and Function of NMDA Receptors in Visual Cortex. *Neuron* 29:157–169.

Pieretti M, Zhang F, Fu YH, Warren ST, Oostra BA, Caskey C, Nelson DL (1991) Absence of expression of the FMR-1 gene in fragile X syndrome. *Cell* 66:817–822.

Pietropaolo S, Guilleminot A, Martin B, D'Amato FR, Crusio WE (2011) Genetic-Background Modulation of Core and Variable Autistic-Like Symptoms in Fmr1 Knock-Out Mice. *PLOS ONE* 6:e17073.

Pilpel Y, Kolleker A, Berberich S, Ginger M, Frick A, Mientjes E, Oostra BA, Seeburg PH (2009) Synaptic ionotropic glutamate receptors and plasticity are developmentally altered in the CA1 field of Fmr1 knockout mice. *The Journal of Physiology* 587:787–804.

Pizzo R, Lamarca A, Sassoè-Pognetto M, Giustetto M (2019) Structural Bases of Atypical Whisker Responses in a Mouse Model of CDKL5 Deficiency Disorder. *Neuroscience* .

Pizzo R, Gurgone A, Castroflorio E, Amendola E, Gross C, Sassoè-Pognetto M, Giustetto M, Wang H, Tropea D, Maffei A, Katz DM, Fagiolini M (2016) Lack of Cdkl5 disrupts the organization of excitatory and inhibitory synapses and parvalbumin interneurons in the primary visual cortex. *Frontiers in Cellular Neuroscience* 10:1–16.

Plant K, Pelkey KA, Bortolotto ZA, Morita D, Terashima A, McBain CJ, Collingridge GL, Isaac JT (2006) Transient incorporation of native GluR2-lacking AMPA receptors during hippocampal long-term potentiation. *Nature Neuroscience* 9:602–604.

Preibisch S, Saalfeld S, Tomancak P (2009) Globally optimal stitching of tiled 3D microscopic image acquisitions. *Bioinformatics* 25:1463–1465.

Racca C, Stephenson FA, Streit P, Roberts JDB, Somogyi P (2000) NMDA receptor content of synapses in stratum radiatum of the hippocampal CA1 area. *Journal of Neuroscience* 20:2512–2522.

Rama S, Zbili M, Fékété A, Tapia M, Benitez MJ, Boumedine N, Garrido JJ, Debanne D (2017) The role of axonal Kv1 channels in CA3 pyramidal cell excitability. *Scientific Reports* 7:315.

Ramon y Cajal S (1911) *Histologie du systeme nerveux de l'Homme & des Vertebres Tome II: Cervelet,Cerveau moyen, Retine, Couche optique, Corps strie, Ecorce cerebrale generale & regionale grand Sympathique*, Vol. 2 A. Maloine, Paris.

Richichi C, Brewster AL, Bender RA, Simeone TA, Zha Q, Yin HZ, Weiss JH, Baram TZ (2008) Mechanisms of seizure-induced 'transcriptional channelopathy' of hyperpolarization-activated cyclic nucleotide gated (HCN) channels. *Neurobiology of Disease* 29:297–305.

Routh BN, Johnston D, Brager DH (2013) Loss of Functional A-Type Potassium Channels in the Dendrites of CA1 Pyramidal Neurons from a Mouse Model of Fragile X Syndrome. *The Journal of Neuroscience* 33:19442 – 19450.

Routh BN, Rathour RK, Baumgardner ME, Kalmbach BE, Johnston D, Brager DH (2017) Increased transient Na+ conductance and action potential output in layer 2/3 prefrontal cortex neurons of the fmr1/y mouse. *Journal of Physiology* 595:4431–4448.

Rush AM, Dib-Hajj SD, Waxman SG (2005) Electrophysiological properties of two axonal sodium channels, Nav1.2 and Nav1.6, expressed in mouse spinal sensory neurones. *The Journal of Physiology* 564:803–815.

Sang Jo Y, Hye Park E, Hwan Kim I, Kwon Park S, Kim H, Taek Kim H, Choi JS (2007) The Medial Prefrontal Cortex Is Involved in Spatial Memory Retrieval under Partial-Cue Conditions. *The Journal of Neuroscience* 27:13567–13578.

Sanz-Clemente A, Nicoll RA, Roche KW (2013) Diversity in NMDA receptor composition: Many regulators, many consequences. *Neuroscientist* 19:62–75.

Scalmani P, Rusconi R, Armatura E, Zara F, Avanzini G, Franceschetti S, Mantegazza M (2006) Effects in Neocortical Neurons of Mutations of the Nav1.2 Na+ Channel causing Benign Familial Neonatal-Infantile Seizures. *The Journal of Neuroscience* 26:10100 – 10109.

Schindelin J, Arganda-Carreras I, Frise E, Kaynig V, Longair M, Pietzsch T, Preibisch S, Rueden C, Saalfeld S, Schmid B, Tinevez JY, White DJ, Hartenstein V, Eliceiri K, Tomancak P, Cardona A (2012) Fiji: an open-source platform for biological-image analysis. *Nature Methods* 9:676–682.

Schlüter A, Turco DD, Deller T, Gutzmann A, Schultz C, Engelhardt M, Del Turco D, Deller T, Gutzmann A, Schultz C, Engelhardt M (2018) Structural Plasticity of Synaptopodin in the Axon Initial Segment during Visual Cortex Development. *Cerebral Cortex* 27:4662–4675.

Schroeder E, Yuan L, Seong E, Ligon C, DeKorver N, Gurumurthy CB, Arikkath J (2019) Neuron-Type Specific Loss of CDKL5 Leads to Alterations in mTOR Signaling and Synaptic Markers. *Molecular Neurobiology* 56:4151–4162.

Schubert D, Staiger JF, Cho N, Kötter R, Zilles K, Luhmann HJ (2001) Layer-Specific Intracolumnar and Transcolumnar Functional Connectivity of Layer V Pyramidal Cells in Rat Barrel Cortex. *The Journal of Neuroscience* 21:3580 – 3592.

Scoville WB, Milner B (1957) Loss of Recent Memory After Bilateral Hippocampal Lesions. *Journal of Neurology, Neurosurgery and Psychiatry* 20:11 – 21.

Sekiguchi M, Katayama S, Hatano N, Shigeri Y, Sueyoshi N, Kameshita I (2013) Identification of amphiphysin 1 as an endogenous substrate for CDKL5, a protein kinase associated with X-linked neurodevelopmental disorder. *Archives of Biochemistry and Biophysics* 535:257–267.

Sengpiel F, Kind PC (2002) The Role of Activity in Development of the Visual System. *Current Biology* 12:R818–R826.

Shah MM (2014) Cortical HCN channels: Function, trafficking and plasticity. *Journal of Physiology* 592:2711–2719.

Shah MM, Migliore M, Valencia I, Cooper EC, Brown DA (2008) Functional significance of axonal Kv7 channels in hippocampal pyramidal neurons. *Proceedings of the National Academy of Sciences* 105:7869–7874.

Sheng M, Hoogenraad CC (2007) The Postsynaptic Architecture of Excitatory Synapses: A More Quantitative View. *Annual Review of Biochemistry* 76:823–847.

Shepherd GMG, Svoboda K (2005) Laminar and Columnar Organization of Ascending Excitatory Projections to Layer 2/3 Pyramidal Neurons in Rat Barrel Cortex. *The Journal of Neuroscience* 25:5670 – 5679.

Sherman DL, Brophy PJ (2000) A tripartite nuclear localization signal in the PDZ-domain protein L-periaxin. *The Journal of biological chemistry* 275:4537–40.

Sidorov MS, Krueger DD, Taylor M, Gisin E, Osterweil EK, Bear MF (2014) Extinction of an instrumental response: a cognitive behavioral assay in Fmr1 knockout mice. *Genes, Brain and Behavior* 13:451–458.

Sidorov MS, Auerbach BD, Bear MF (2013) Fragile X mental retardation protein and synaptic plasticity. *Molecular Brain* 6:1.

Sierra-Mercado D, Padilla-Coreano N, Quirk GJ (2011) Dissociable roles of prelimbic and infralimbic cortices, ventral hippocampus, and basolateral amygdala in the expression and extinction of conditioned fear. *Neuropsychopharmacology* 36:529–538.

Sivilia S, Mangano C, Beggiato S, Giuliani A, Torricella R, Baldassarro VA, Fernandez M, Lorenzini L, Giardino L, Borelli AC, Ferraro L, Calzà L (2016) CDKL5 knockout leads to altered inhibitory transmission in the cerebellum of adult mice. *Genes, Brain and Behavior* 15:491–502.

Smart SL, Lopantsev V, Zhang CL, Robbins CA, Wang H, Chiu SY, Schwartzkroin PA, Messing A, Tempel BL (1998) Deletion of the KV1.1 Potassium Channel Causes Epilepsy in Mice. *Neuron* 20:809–819.

Soden ME, Chen L (2010) Fragile X Protein FMRP Is Required for Homeostatic Plasticity and Regulation of Synaptic Strength by Retinoic Acid. *The Journal of Neuroscience* 30:16910 – 16921.

Sotres-Bayon F, Quirk GJ (2010) Prefrontal control of fear: more than just extinction. *Current Opinion in Neurobiology* 20:231–235.

Spratt PW, Ben-Shalom R, Keeshen CM, Burke KJ, Clarkson RL, Sanders SJ, Bender KJ (2019) The Autism-Associated Gene Scn2a Contributes to Dendritic Excitability and Synaptic Function in the Prefrontal Cortex. *Neuron* 103:673–685.e5.

Spruston N, Johnston D (1992) Perforated patch-clamp analysis of the passive membrane properties of three classes of hippocampal neurons. *Journal of Neurophysiology* 67:508–529.

Srivastava AK, Schwartz CE (2014) Intellectual disability and autism spectrum disorders: Causal genes and molecular mechanisms. *Neuroscience and Biobehavioral Reviews* 46:161–174.

Staff NP, Jung HY, Thiagarajan T, Yao M, Spruston N (2000) Resting and Active Properties of Pyramidal Neurons in Subiculum and CA1 of Rat Hippocampus. *Journal of Neurophysiology* 84:2398–2408.

Stent GS (1973) A physiological mechanism for Hebb's postulate of learning. *Proceedings of the National Academy of Sciences of the United States of America* 70:997–1001.

Stern EA, Maravall M, Svoboda K (2001) Rapid Development and Plasticity of Layer 2/3 Maps in Rat Barrel Cortex In Vivo. *Neuron* 31:305–315.

Sugawara T, Mazaki–Miyazaki E, Ito M, Nagafuji H, Fukuma G, Mitsudome A, Wada K, Kaneko S, Hirose S, Yamakawa K (2001) Nav1.1 mutations cause febrile seizures associated with afebrile partial seizures. *Neurology* 57:703 – 705.

Sun W, Tan Z, Mensh BD, Ji N (2016) Thalamus provides layer 4 of primary visual cortex with orientation- and direction-tuned inputs. *Nature Neuroscience* 19:308–315.

Sutcliffe JS, Nelson DL, Zhang F, Pieretti M, Caskey CT, Saxe D, Warren ST (1992) DNA methylation represses FMR-1 transcription in fragile X syndrome. *Human Molecular Genetics* 1:397–400.

Symonds JD, Zuberi SM, Stewart K, McLellan A, O'Regan M, MacLeod S, Jollands A, Joss S, Kirkpatrick M, Brunklaus A, Pilz DT, Shetty J, Dorris L, Abu-Arafeh I, Andrew J, Brink P, Callaghan M, Cruden J, Diver LA, Findlay C, Gardiner S, Grattan R, Lang B, MacDonnell J, McKnight J, Morrison CA, Nairn L, Slean MM, Stephen E, Webb A, Vincent A, Wilson M (2019) Incidence and phenotypes of childhood-onset genetic epilepsies: a prospective population-based national cohort. *Brain* 142:2303–2318.

Sztainberg Y, Zoghbi HY (2016) Lessons learned from studying syndromic autism spectrum disorders. *Nature Neuroscience* 19:1408–1418.

Talbot ZN, Sparks FT, Dvorak D, Curran BM, Alarcon JM, Fenton AA (2018) Normal CA1 Place Fields but Discoordinated Network Discharge in a Fmr1-Null Mouse Model of Fragile X Syndrome. *Neuron* 97:684–697.e4.

Tang SJ, Reis G, Kang H, Gingras AC, Sonenberg N, Schuman EM (2002) A rapamycin-sensitive signaling pathway contributes to long-term synaptic plasticity in the hippocampus. *Proceedings of the National Academy of Sciences* 99:467–472.

Tang S, Terzic B, Wang ITJTJ, Sarmiento N, Sizov K, Cui Y, Takano H, Marsh ED, Zhou Z, Coulter DA (2019) Altered NMDAR signaling underlies autistic-like features in mouse models of CDKL5 deficiency disorder. *Nature Communications* 10:1–14.

Tang S, Wang ITJ, Yue C, Takano H, Terzic B, Pance K, Lee JY, Cui Y, Coulter DA, Zhou Z (2017) Loss of CDKL5 in glutamatergic neurons disrupts hippocampal microcircuitry and leads to memory impairment in mice. *Journal of Neuroscience* 37:7420–7437.

The Dutch-Belgian Fragile X Consorthium, Bakker CE, Verheij C, Willemsen R, van der Helm R, Oerlemans F, Vermey M, Bygrave A, Hoogeveen A, Oostra BA, Reyniers E, De Boule K, D'Hooge R, Cras P, van Velzen D, Nagels G, Martin JJ, De Deyn PP, Darby JK, Willems PJ (1994) Fmr1 knockout mice: A model to study fragile X mental retardation. *Cell* 78:23–33.

Till SM (2010) The developmental roles of FMRP. *Biochemical Society Transactions* 38:507–510.

Till SM, Asiminas A, Jackson AD, Katsanevaki D, Barnes SA, Osterweil EK, Bear MF, Chattarji S, Wood ER, Wyllie DJA, Kind PC (2015) Conserved hippocampal cellular pathophysiology but distinct behavioural deficits in a new rat model of FXS. *Human Molecular Genetics* 24:5977–5984.

Till SM, Wijetunge LS, Seidel VG, Harlow E, Wright AK, Bagni C, Contractor A, Gillingwater TH, Kind PC (2012) Altered maturation of the primary somatosensory cortex in a mouse model of fragile X syndrome. *Human Molecular Genetics* 21:2143–2156.

Tovote P, Fadok JP, Lüthi A (2015) Neuronal circuits for fear and anxiety. *Nature Reviews Neuroscience* 16:317–331.

Turner G, Webb T, Wake S, Robinson H (1996) Prevalence of fragile X syndrome. *American Journal of Medical Genetics* 64:196–197.

Turrigiano G, Abbott LF, Marder E (1994) Activity-dependent changes in the intrinsic properties of cultured neurons. *Science* 264:974 – 977.

Turrigiano G, LeMasson G, Marder E (1995) Selective regulation of current densities underlies spontaneous changes in the activity of cultured neurons. *The Journal of Neuroscience* 15:3640 – 3652.

Turrigiano GG (2008) The Self-Tuning Neuron: Synaptic Scaling of Excitatory Synapses. *Cell* 135:422–435.

Turrigiano GG (2017) The dialectic of Hebb and homeostasis. *Philosophical Transactions of the Royal Society B: Biological Sciences* 372:20160258.

Turrigiano GG, Leslie KR, Desai NS, Rutherford LC, Nelson SB (1998) Activity-dependent scaling of quantal amplitude in neocortical neurons. *Nature* 391.

Turrigiano GG, Nelson SB (2004) Homeostatic plasticity in the developing nervous system. *Nature Reviews Neuroscience* 5:97–107.

van Bokhoven H (2011) Genetic and Epigenetic Networks in Intellectual Disabilities. *Annual Review of Genetics* 45:81–104.

Van Dam D, D'Hooge R, Hauben E, Reyniers E, Gantois I, Bakker CE, Oostra BA, Kooy R, De Deyn PP (2000) Spatial learning, contextual fear conditioning and conditioned emotional response in Fmr1 knockout mice. *Behavioural Brain Research* 117:127–136.

van der Molen MJW, Stam CJ, van der Molen MW (2014) Resting-State EEG Oscillatory Dynamics in Fragile X Syndrome: Abnormal Functional Connectivity and Brain Network Organization. *PLOS ONE* 9:e88451.

Veeramah K, O'Brien J, Meisler M, Cheng X, Dib-Hajj S, Waxman S, Talwar D, Girirajan S, Eichler E, Restifo L, Erickson R, Hammer M (2012) De Novo Pathogenic SCN8A Mutation Identified by Whole-Genome Sequencing of a Family Quartet Affected by Infantile Epileptic Encephalopathy and SUDEP. *The American Journal of Human Genetics* 90:502–510.

Vetter P, Roth A, Häusser M (2001) Propagation of Action Potentials in Dendrites Depends on Dendritic Morphology. *Journal of Neurophysiology* 85:926–937.

Vickers CA, Dickson KS, Wyllie DJA (2005) Induction and maintenance of late-phase long-term potentiation in isolated dendrites of rat hippocampal CA1 pyramidal neurones. *The Journal of Physiology* 568:803–813.

Vitureira N, Goda Y (2013) The interplay between hebbian and homeostatic synaptic plasticity. *Journal of Cell Biology* 203:175–186.

Volk L, Chiu SL, Sharma K, Huganir RL (2015) Glutamate Synapses in Human Cognitive Disorders. *Annual Review of Neuroscience* 38:127–149.

Wahlstrom-Helgren S, Klyachko VA (2015) GABAB receptor-mediated feed-forward circuit dysfunction in the mouse model of fragile X syndrome. *The Journal of Physiology* 593:5009–5024.

Wang ITJ, Allen M, Goffin D, Zhu X, Fairless AH, Brodkin ES, Siegel SJ, Marsh ED, Blendy JA, Zhou Z (2012) Loss of CDKL5 disrupts kinome profile and event-related potentials leading to autistic-like phenotypes in mice. *Proceedings of the National Academy of Sciences of the United States of America* 109:21516–21521.

Wang J, Ethridge LE, Mosconi MW, White SP, Binder DK, Pedapati EV, Erickson CA, Byerly MJ, Sweeney JA (2017) A resting EEG study of neocortical hyperexcitability and altered functional connectivity in fragile X syndrome Refining translational treatment development in fragile X syndrome. *Journal of Neurodevelopmental Disorders* 9:1–12.

Washington SD, Gordon EM, Brar J, Warburton S, Sawyer AT, Wolfe A, Mease-Ference ER, Girton L, Hailu A, Mbwana J, Gaillard WD, Kalbfleisch ML, VanMeter JW (2014) Dysmaturation of the default mode network in autism. *Human Brain Mapping* 35:1284–1296.

Watkins-Chow DE, Pavan WJ (2008) Genomic copy number and expression variation within the C57BL/6J inbred mouse strain. *Genome Research* 18:60–66.

Weiler IJ, Greenough WT (1999) Synaptic synthesis of the fragile X protein: Possible involvement in synapse maturation and elimination. *American Journal of Medical Genetics* 83:248–252.

White SJ, Frith U, Rellecke J, Al-Noor Z, Gilbert SJ (2014) Autistic adolescents show

atypical activation of the brains mentalizing system even without a prior history of mentalizing problems. *Neuropsychologia* 56:17–25.

Wiesel TN, Hubel DH (1965) Extent of recovery from the effects of visual deprivation in kittens. *Journal of Neurophysiology* 28:1060–1072.

Williams K (1993) Ifenprodil discriminates subtypes of the N-methyl-D-aspartate receptor: selectivity and mechanisms at recombinant heteromeric receptors. *Molecular Pharmacology* 44:851 – 859.

Wimmer VC, Reid CA, Mitchell S, Richards KL, Scaf BB, Leaw BT, Hill EL, Royeck M, Horstmann Mt, Cromer BA, Davies PJ, Xu R, Lerche H, Berkovic SF, Beck H, Petrou S (2010) Axon initial segment dysfunction in a mouse model of genetic epilepsy with febrile seizures plus. *The Journal of Clinical Investigation* 120:2661–2671.

Winden KD, Ebrahimi-Fakhari D, Sahin M (2018) Abnormal mTOR Activation in Autism. *Annual Review of Neuroscience* 41:1–23.

Won H, Lee HR, Gee HY, Mah W, Kim JI, Lee J, Ha S, Chung C, Jung ES, Cho YS, Park SG, Lee JS, Lee K, Kim D, Bae YC, Kaang BK, Lee MG, Kim E (2012) Autistic-like social behaviour in Shank2-mutant mice improved by restoring NMDA receptor function. *Nature* 486:261–265.

Wyllie DJ, Manabe T, Nicoll RA (1994) A rise in postsynaptic Ca 2+ potentiates miniature excitatory postsynaptic currents and AMPA responses in hippocampal neurons. *Neuron* 12:127–138.

Xu J, Kang N, Jiang L, Nedergaard M, Kang J (2005) Activity-Dependent Long-Term Potentiation of Intrinsic Excitability in Hippocampal CA1 Pyramidal Neurons. *The Journal of Neuroscience* 25:1750 – 1760.

Yamamuro K, Yoshino H, Ogawa Y, Makinodan M, Toritsuka M, Yamashita M, Corfas G, Kishimoto T (2018) Social Isolation During the Critical Period Reduces Synaptic and Intrinsic Excitability of a Subtype of Pyramidal Cell in Mouse Prefrontal Cortex. *Cerebral Cortex* 28:998–1010.

Yang SN, Tang YG, Zucker RS (1999) Selective Induction of LTP and LTD by Postsynaptic Ca^{2+} Elevation. *Journal of Neurophysiology* 81:781–787.

Yashiro K, Corlew R, Philpot BJ (2005) Visual Deprivation Modifies Both Presynaptic Glutamate Release and the Composition of Perisynaptic/Extrasynaptic NMDA Receptors in Adult Visual Cortex. *Journal of Neuroscience* 25:11684–11692.

Yennawar M, White RS, Jensen FE (2019) AMPA receptor dysregulation and therapeutic interventions in a mouse model of CDKL5 deficiency disorder. *Journal of Neuroscience* 39:4814–4828.

Yerys BE, Gordon EM, Abrams DN, Satterthwaite TD, Weinblatt R, Jankowski KF, Strang J, Kenworthy L, Gaillard WD, Vaidya CJ (2015) Default mode network segregation and social deficits in autism spectrum disorder: Evidence from non-medicated children. *NeuroImage: Clinical* 9:223–232.

Yu Y, Maureira C, Liu X, McCormick D (2010) P/Q and N Channels Control Baseline and Spike-Triggered Calcium Levels in Neocortical Axons and Synaptic Boutons. *The Journal of Neuroscience* 30:11858 – 11869.

Yue C, Yaari Y (2006) Axo-somatic and apical dendritic Kv7/M channels differentially regulate the intrinsic excitability of adult rat CA1 pyramidal cells. *Journal of Neurophysiology* 95:3480–3495.

Yun SH, Trommer BL (2011) Fragile X mice: Reduced long-term potentiation and N-Methyl-D-Aspartate receptor-mediated neurotransmission in dentate gyrus. *Journal of Neuroscience Research* 89:176–182.

Zerbi V, Ielacqua GD, Markicevic M, Haberl MG, Ellisman MH, Bhaskaran AA, Frick A, Rudin M, Wenderoth N (2018) Dysfunctional autism risk genes cause circuit-specific connectivity deficits with distinct developmental trajectories. *Cerebral Cortex* 28:2495–2506.

Zhang W, Peterson M, Beyer B, Frankel WN, Zhang ZW (2014) Loss of MeCP2 from forebrain excitatory neurons leads to cortical hyperexcitation and seizures. *Journal of Neuroscience* 34:2754–2763.

Zhang Y, Brown MR, Hyland C, Chen Y, Kronengold J, Fleming MR, Kohn AB, Moroz LL, Kaczmarek LK (2012) Regulation of Neuronal Excitability by Interaction of Fragile X Mental Retardation Protein with Slack Potassium Channels. *Journal of Neuroscience* 32:15318–15327.

Zhang Y, Bonnan A, Bony G, Ferezou I, Pietropaolo S, Ginger M, Sans N, Rossier J, Oostra B, LeMasson G, Frick A (2014) Dendritic channelopathies contribute to neocortical and sensory hyperexcitability in Fmr1-/y mice. *Nature Neuroscience* 17:1701–1709.

Zhou D, Lambert S, Malen PL, Carpenter S, Boland LM, Bennett V (1998) Ankyrin(G) is required for clustering of voltage-gated Na channels at axon initial segments and for normal action potential firing. *Journal of Cell Biology* 143:1295–1304.

Zoghbi HY, Bear MF (2012) Synaptic dysfunction in neurodevelopmental disorders associated with autism and intellectual disabilities. *Cold Spring Harbor Perspectives in Biology* 4.

Zonta B, Desmazieres A, Rinaldi A, Tait S, Sherman D, Nolan M, Brophy P (2011) A Critical Role for Neurofascin in Regulating Action Potential Initiation through Maintenance of the Axon Initial Segment. *Neuron* 69:945–956.

Zuberi SM, Eunson LH, Spauschus A, De Silva R, Tolmie J, Wood NW, McWilliam RC, Stephenson JPB, Kullmann DM, Hanna MG (1999) A novel mutation in the human voltage-gated potassium channel gene (Kv1.1) associates with episodic ataxia type 1 and sometimes with partial epilepsy. *Brain* 122:817–825.

Zucker RS, Regehr WG (2002) Short-Term Synaptic Plasticity. *Annual Review of Physiology* pp. 355–405.

Zurita E, Chagoyen M, Cantero M, Alonso R, González-Neira A, López-Jiménez A, López-Moreno JA, Landel CP, Benítez J, Pazos F, Montoliu L (2011) Genetic polymorphisms among C57BL/6 mouse inbred strains. *Transgenic Research* 20:481–489.